Investigating the role of ciliary localisation of the TRPP Channel, Polycystin2 (PKD2), on development and progression of Polycystic Kidney Disease

A thesis presented for the degree of Doctor of Philosophy (DPhil)

St Peters College, University of Oxford

Rebecca Violet Walker

Mammalian Genetic Unit, MRC Harwell

Department of Physiology, Anatomy and Genetics, University of Oxford

Supervisors: Dr Dominic Norris (MGU, MRC Harwell)

Professor Helen Christian (DPAG, Oxford)

Trinity Term 2016

Word count: 41663

Abstract

Autosomal Dominant Polycystic Kidney Disease (ADPKD) is a common inherited disease, affecting 1:400-1000 people worldwide and leads to end-stage renal failure in most patients before their 6th decade. ADPKD is characterised by abnormal persistent cellular proliferation combined with luminal fluid secretion in the kidneys leading to bilateral development of cysts. There are two causative genes associated with the development of ADPKD; *PKD1* and *PKD2*. PKD2 is an essential Ca^{2+} permeable cation channel which localises to the primary cilium in renal tubules as well as other locations within the cell.

Here we investigate the effects of aberrant cellular localisation of PKD2, specifically the loss of ciliary localisation. We used a non-ciliary localising mutant allele (*Pkd2*^{lrm4}) which retains channel function, for *in vitro* and *in vivo* mouse studies to show that there is an absolute requirement for the protein within the cilium. Embryonically, *Pkd2*$^{lrm4/lrm4}$ kidneys exhibit gross cystic development, beginning at E15.5. Heterozygotes develop a mild cystic phenotype in combination with polycystic liver disease. When expressed in combination with an inducible null allele in the proximal tubule of the adult kidney, a progressive development of cysts is observed. In vitro studies using *Pkd2*$^{lrm4/lrm4}$ MEFs show specific accumulation of the protein at the mother centriole. In addition to protein glycosylation studies, this indicates that PKD2 is able to traffic normally to the ciliary base, but cannot enter the cilium.

This work indicates an essential role for PKD2 in the cilium and that non-ciliary function alone is not sufficient to prevent cyst formation. In addition, this work provides a viable genetic model for the study of progression in Polycystic Kidney Disease.

Acknowledgements

I would like to thank my supervisor Dr Dominic Norris for the excellent opportunity to work in his lab. His knowledge, enthusiasm, support and guidance has been invaluable. I am grateful that he has been such a knowledgeable and approachable supervisor, for his willingness to read the drafts of this thesis, in many cases going out of his way to ensure that I submitted on time. I am thankful for his patience. I am also thankful for the help of members of the lab; Jennifer Keynton, David Asante, Dragoș Leordean, Dan Grimes and Hannah Farley, for their valuable advice and friendship. I am especially thankful for the guidance of Jennifer Keynton whose practical advice, reading of this thesis, support and friendship has been greatly appreciated. I extend my thanks to the rest of the development family, the Sexual Development lab, who join us for lab meetings and whose advise and discussion has been much appreciated.

My sincere thanks go to many members of the core facility at Harwell especially to members of the Mary Lyon centre. Thanks to Jackie Harrison, Sara Wells and the whole of ward five for excellent knowledge and care of my mice. Special thanks to Jackie for injecting so many bite-y mice. Thanks to the histology and necropsy teams for relentless yet exceptional work, Jeremy Sanderson for excellent microscopy advice, the clinical chemistry team for processing samples, team LacZ for help with staining and to many others.

I am ever grateful for my husband, Andrew Walker for his continued support, level-headedness, wisdom, patience and encouragement throughout my studies, without which I would not be where I am today. I am thankful for the sacrifices he has made to be the husband of a scientist. He has taught me how to be patient, to be disciplined and to persevere. His encouragement has enabled me to continue.

I am thankful to my family; my parents, in laws and siblings for their support and care. They have taught me a great deal and supported me along the way.

Finally, I thank the Medical research council for funding this research.

Abbreviations

aa	Amino acid
ADPKD	Autosomal Dominant Polycystic Kidney Disease
ANOVA	Analysis of Variance
ARE	Androgen response element
ARPKD	Autosomal recessive Polycystic Kidney Disease
ASP	Asparagine
B6J	C57BL/6J mice
bp	base pairs
BSA	Bovine serum albumin
bsw	Black swiss mice
BUN	Blood Urea Nitrogen
C3H	C3H/HeH mice
CD	Collecting duct
cDNA	Complementary DNA
CKD	Chronic kidney disease
CM	Cap mesenchyme
CTS	Ciliary targeting signal
CTT	C-terminal tail
DHT	Dihydrotestosterone
DMF	Dimethylformamide
DT	Distal tubule
E	Glutamic acid (Glu)
E 15.5	Embryonic day of development 15.5
EGF	Epidermal growth factor
eGFR	Estimated glomerular filtration rate
EGFR	Epidermal growth factor receptor
EndoH	Endoglycosidase H
ENU	N-ethyl-N-nitrosourea
ER	Endoplasmic reticulum

ERE	Oestrogen response element
ESRD	End-stage renal disease
ESRF	End-stage renal failure
EtOH	Ethanol
F1	Filial 1 hybrid, first generation from a parental cross
FEL	First extracellular loop
Flox	Flanked by LoxP
G	Glycine (Gly)
G0	Generation 0- the generation subjected to mutagenesis
GBM	Glomerular basement membrane
GCKD	Glomerulocystic kidney disease
gDNA	Genomic DNA
GFP	Green fluorescent protein
GOF	Gain of Function
H&E	Haematoxylin and Eosin
HPβCD	2-hydroxypropyl-β-cyclodextrin
HRE	Hormone response element
IFT	Intraflagellar Transport
IGEPAL	Octylphenoxy poly(ethyleneoxy)ethanol
IM	Inner medulla
ISOM	Inner stripe of outer medulla
IVF	*In vitro* fertilisation
LB	Left Bias
LI	left isomerism
LOF	Loss of function
LOH	Loss of heterozygosity
LoxP	Locus of crossing over from P1 bacteriophage
LPM	Lateral Plate Mesoderm
L-R	Left-Right
Lrm4	Left Right Mutant 4
MEF	Mouse embryonic fibroblast

MeOH	Methanol
miRNA	Micro RNA
MM	Metanephric mesenchyme
mRNA	Messenger RNA
mTOR	Mammalian target of rapamycin
ND	Nephric duct
NTT	N-Terminal tail
NVP	Node vesicular parcels
ORF	Open reading frame
OSOM	Outer stripe of outer medulla
PBS	Phosphate-buffered saline
PCP	Planar cell polarity
PCT	Proximal Convoluted Tubule
PFA	Paraformaldehyde
PI	partial isomerism
PKD	Polycystic kidney disease
PKD2	Polycystin 2
PLD	Polycystic liver Disease
PM	Plasma membrane
PNGaseF	Peptide N-glycosidase F
PT	Proximal tubule
QTL	Quantitative Trait Locus
RAAS	Renin Angiotensin Aldosterone system
RB	Right Bias
RI	right isomerism
SD	Standard Deviation
SEM	Standard Error of the Mean
SI	*situs inversus*
SNP	Single nucleotide polymorphism
SNP	Single nucleotide polymorphism
SS	*situs solitus*

Td	Tubule dilation (between 38.7-73.91µm)
Td2	Tubule dilation (between 73.91-116.1µm)
TM	Transmembrane
UB	Ureteric bud

Table of Contents

Notes for reading this thesis

The materials and methods section can be found in **Appendix 1**. Throughout this document, I have referred to the sections of the material and methods section in the following way: **MM:1.1.1**

Further items included in **Appendix 2** detail statistics tables and results tables.

1. Introduction

1.1 Overview

Polycystic kidney disease is a common yet devastating disease. It is a heritable disorder characterised by development of renal cysts which originate from the nephric tubules and overtake the kidney structure. These cysts destroy renal function, often resulting in end-stage renal failure. Two entities can be identified; the common form, autosomal dominant polycystic kidney disease (ADPKD), affects as many as 1:400 people worldwide and a rare form, autosomal recessive polycystic kidney disease (ARPKD), affects 1:20000 live births. The two can be distinguished by clinical presentation and are genetically distinct.

The first documented case of ADPKD dates back to the 16th century when Ştefan Báthory (1533-1586) the king of Poland, was autopsied (Torres and Watson, 1998). The autopsy report described his kidneys to be "large like those of bull, with uneven and bumpy surface." Centuries later in 1839, Pierre Rayer described cystic degeneration of the kidneys as a cause of renal failure. "There are cases where both kidneys are affected by a true generalised cyst degeneration of the cortical substance, which in some cases may be of such a degree that only traces of renal substance are left" (Rayer, 1839, Torres and Watson, 1998).

Despite being first reported five centuries ago, this disease is still considered untreatable, the mechanisms behind the development of cysts are relatively poorly understood and the clinical outcome is poor. In recent years, significant research has been undertaken identifying causative genes, first PKD1 (Harris et al., 1995, Ward, 1994, Hughes et al., 1995) and then PKD2 (Mochizuki et al., 1996, Peters et al., 1993, Schneider et al., 1996), and possible mechanisms that underlie the pathogenesis of the disease. The field has progressed significantly since the two genes were identified and mapped in the early 90s. The gene associated with ARPKD, *PKHD1*, was identified in 2002 (Ward et al., 2002).

Exciting progress has been made recently with a number of clinical trials for drugs which alter the course of the disease. The first clinical trials involved the mTOR inhibitors Sirolimus (Serra et al., 2010) and Everolimus (Walz et al., 2010) which were unsuccessful in halting the progression of the disease. Following this Tolvaptan (Torres et al., 2012), a drug found in clinical trials to decrease polycystic kidney volume and lessen signs and symptoms of the

disease, has been developed and approved for treatment of ADPKD. Tolvaptan is a selective vasopressin antagonist which reduces cell proliferation, cyst formation and fluid secretion, slowing the progression of kidney growth and the decline of filtration rate.

Despite recent progress in the field, there are still a number of areas underlying the pathogenesis of the disease which remain unclear. Studies such as this one will provide insight into the mechanism and development of the disease. We set out to characterise a murine model of the disease associated with the causative gene, PKD2, to increase insight into the mechanisms behind the progression of the disease and to deepen understanding of the molecular characteristics governing the development of ADPKD.

1.2 The kidney

The mammalian kidney is an essential organ which comprises a complex network of epithelial tubules, known as nephrons. The nephron is the functional unit of the kidney and acts in a highly specialised manner to filter the blood; removing waste and selectively recovering solutes and water in order to keep the body in homeostasis. Constituting the majority of the renal structure; the nephron consists of the glomerulus, proximal tubule, loop of Henle, distal tubule and collecting duct (see **Fig 4.1a**). Situated in the cortex, the glomerulus is the site of initiation of filtration. At the glomerular tuft, or capillary bundle, small molecules pass from the blood of the afferent arteriole, into the Bowman's capsule of the glomerulus, the beginning of the tubular component of the nephron. Each portion of the nephron is composed of highly adapted cells which reabsorb particular components of the filtrate and concentrate the filtrate to produce urine. The proximal convoluted tubule is characterised by its brush border of microvilli that provides a large surface area which concentrates the filtrate; reabsorbing 60-70% of its H_20 and NaCl content and a high proportion of the nutrient content back into the blood (Curthoys and Moe, 2014). Each nephron is connected to the collecting duct network through which the urine drains from the kidney into the ureter, then into the bladder.

The human kidney contains 1-2 million nephrons (Murawski et al., 2010a, Cain et al., 2010); however this number may vary with age, sex, ethnicity and birth weight (Bertram et al., 2011). The average glomerular count from a number of studies is similar, yet large studies

report high variation between individuals; 2- to 12-fold differences are observed (Bertram et al., 2011). The mouse kidney contains about 20000 nephrons (Murawski et al., 2010a).

1.2.1 Development of the mammalian kidney

In vertebrates, three excretory organs form throughout development as an outshoot from the nephric duct; these have different levels of function across vertebrate species. Some anamniotes such as Zebrafish and Xenopus, only form the first of these primitive kidneys which serve them throughout development into adult life, this is the pronephros (Naylor and Davidson, 2016). The pronephros is comprised of one large nephron connected to the unbranched nephric duct. In mammalian embryos, the pronephros is considered a non-functioning organ since the pronephric duct is not linked to the cloaca and cannot facilitate excretion outside the embryo.

In more advanced vertebrates, the pronephros rapidly degenerates and the mesonephros takes its place as the excretory organ. The mesonephros develops from the nephric duct posteriorly to the pronephros and consists of a linear array of nephrons. The mesonephros is the final excretory system to develop in most fish and amphibia, however, amniote classes such as birds, mammals and reptiles go on to form a third pair of renal apparatus, the metanephros.

The metanephric kidneys begin to develop at E9.5-10.5 in the mouse when the ureteric bud (UB) protrudes from the nephric duct into a region of metanephric mesenchyme (MM), a specialised region of intermediate mesoderm (Boivin et al., 2015) (**Fig 1.1**). As the UB expands and branches, it begins to form a treelike structure of tubules throughout the kidney, responding to signals from the MM. MM cells closest to the UB tip condense and become the cap mesenchyme (CM); a self-renewing population of cells which undergoes mesenchymal to epithelial transition (MET) and also donates cells into the branching UB. The CM at each UB tip undergoes cycles of elongation, branching and differentiation to give rise to the tubular network of the kidney. The epithelial cells of the UB condense to form the renal vesicle which then invaginates to form the comma shaped body. This invaginates once more to form the S-shaped body which contacts a distal portion of the developing nephron, forming the glomerulus (Takasato and Little, 2015). As the tubules branch and elongate, a developmental gradient becomes evident; the more central nephrons develop first with the

later nephron-forming branches, in the cortex, lagging behind. The topography of the developing kidney is such that position reflects age. The rest of the surrounding MM gives rise to the stroma and vasculature such as the glomerular tuft and associated capillaries (Little and McMahon, 2012).

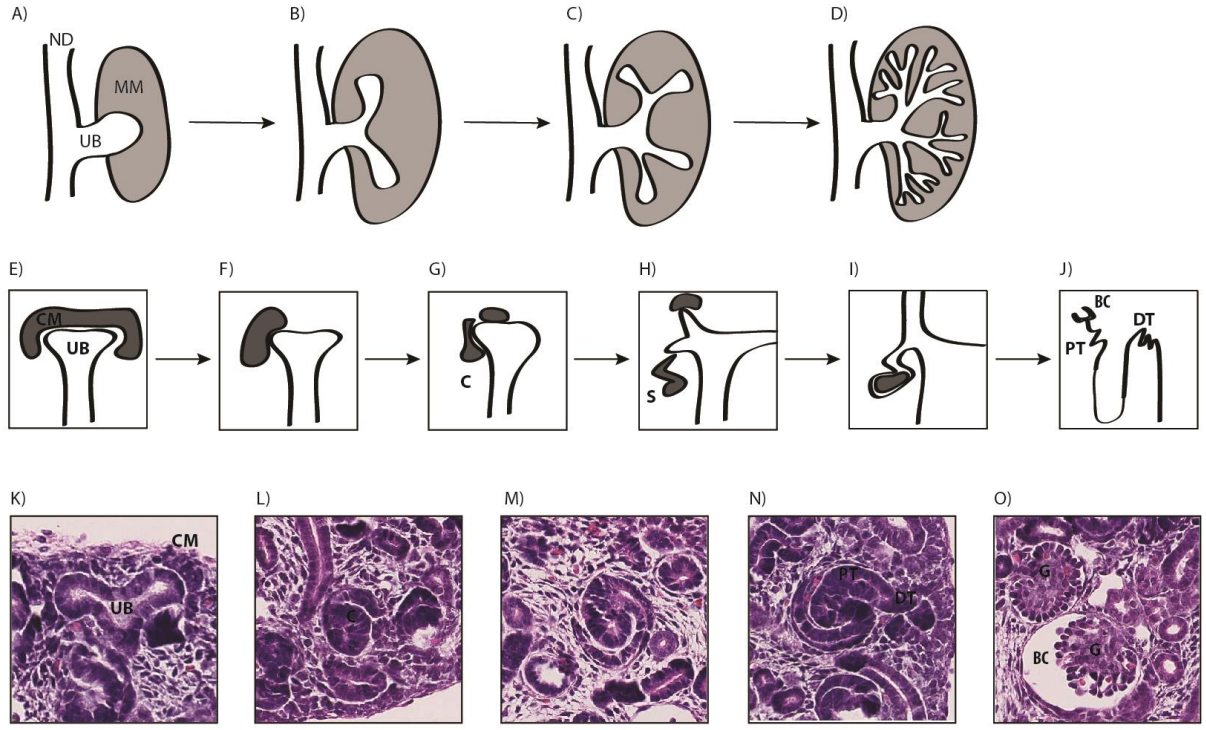

Figure 1.1: Nephrogenesis of the metanephric kidney

A) The metanephric kidney develops as the ureteric bud [UB] emerges from the nephric duct [ND]. The UB invades the metanephric mesenchyme [MM] where interactions between the two cause bifurcation of the UB B), branching of which continues C) to form the mature collecting duct system of the developed kidney D). E) The UB signals to the surrounding MM to condense and undergo MET to become the cap mesenchyme [CM] K) which goes on to form the comma shaped [C] G) and L) and S-shaped [S] H) and M-N) bodies. I) The S-shaped body differentiates further to form the proximal [PT] and distal tubules [DT] N) and the Bowman's capsule [BC] (O) of the nephron J). K)-O) show H&E stained sections of these developing stages in mouse embryonic kidneys from K) bifurcating tubule to O) glomerulus [G].

Ten cycles of branching and elongation (Cebrian et al., 2004) of the UB continue after birth until the third postnatal day (P3) in the mouse since the CM is retained (Hartman et al., 2007). During this time, the CM cell population ceases to be replenished and is exhausted as new nephrons form. When the population is depleted, existing nephrons continue to mature but no further nephrons can form (Hartman et al., 2007). The development of the

kidney in the first 4 postnatal weeks of the mouse resembles that seen in the later stages of human kidney development, at 36weeks (Zhong et al., 2012).

Human metanephros development begins at 5-6 weeks of gestation with the first signs of filtration becoming evident at ~10 weeks. Human nephrogenesis is complete by gestational week 36 when the stem cell population is exhausted and no further nephrons form. However, tubules continue to mature after birth. The difference in nephron number between the human and mouse kidney is the result of an extra round of branching in humans (Cain et al., 2010). In addition to UB bifurcation to form nephrogenic bud tips, the human kidney also goes through rounds of lateral and arcade branching. Arcades advance as several nephrons simultaneously develop along one branch of the UB. In the mouse, a bud would cease to branch when a glomerulus develops at the end, but human arcade branching allows an off-shoot of several nephrons to develop while the branch continues to elongate. This allows a greater number of nephrons to form. During lateral branching, the elongating UB induces branches of nephron development while it continues to elongate. Instead of bifurcating, this budding off of nephrons allows more nephrons to form in the more distal region of the cortex (al-Awqati and Goldberg, 1998)

1.2.2 Chronic kidney disease (CKD)

Chronic kidney disease (CKD) is an umbrella term which is used to describe a number of renal conditions and describes the gradual loss of kidney function. CKD is split into 5 stages which are specified by measured (m) or estimated (e) glomerular filtration rate (GFR) and which provide a useful structure to classify the progression of kidney disease. GFR is an estimation of the number of ml of waste that the kidneys can filter per min and is given in ml/min. Although difficult to measure, GFR is estimated by testing the level of creatinine in the blood and taking into account factors such as age and sex, the result is roughly equivalent to remaining kidney function. At Stage 1, kidney function is normal despite there being genetic or structural indicators of kidney disease such as specific gene mutation or kidney cysts. By stage 2, kidney function is beginning to decline and there may be issues with blood pressure control, proteinuria or other urine markers such as increased creatinine levels. Progression to Stages 3 and 4 are defined by moderately and severely reduced kidney function whereas Stage 5 indicates that end-stage renal failure has been reached, this may

not occur until 10-20 years after CKD diagnosis. End-stage renal disease can only be treated with dialysis or transplant.

1.2.3 The Juxtaglomerular apparatus and RAAS

The juxtaglomerular apparatus can be found next the glomerulus, as the name suggests. It is a specialised structure formed from the distal convoluted tubule and the afferent arteriole which is filled with unfiltered blood as it enters the glomerular tuft (**Fig 1.2**). The macula densa, a region of specialised epithelial cells of the distal convoluted tubule, detects the sodium concentration in the filtrate in the tubule. At high sodium concentration, these cells trigger the afferent arteriole to contract, reducing glomerular filtration. This sets up a feedback mechanism, monitoring the filtrate and adjusting the filtration rate of the glomerulus. The juxtaglomerular cells of the afferent arteriole secrete renin when blood pressure in the afferent arteriole falls. This increases blood pressure via the renin-angiotensin-aldosterone system (RAAS).

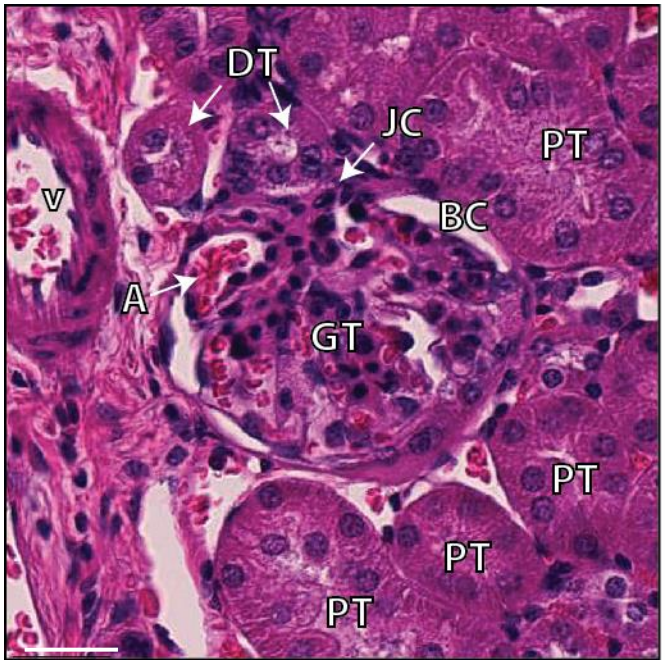

Figure 1.2: The Juxtaglomerular apparatus from an adult mouse kidney

In the centre of the image lies the glomerulus. The glomerular tuft (GT) is a bundle of capillaries filled by the afferent arteriole (A). The juxtaglomerular cells (JC) secrete renin. Surrounding the glomerulus are proximal tubules (PT) and distal tubules (DT) which are likely associated with the nephron emanating from this glomerulus. To the left of this glomerulus, a blood vessel can be seen (V). Scale bar 30um.

In response to low blood pressure, the liver and kidneys release angiotensinogen (Urushihara and Kagami, 2016). Renin, produced in the juxtaglomerular cells of the kidney in response to low plasma sodium concentration, cleaves angiotensinogen to produce Angiotensin-I. Angiotensin-converting-enzyme (ACE), found in high levels in the lung vascular system and in the kidney, cleaves Angiotensin-I to produce activated Angiotensin-II. ACE also degrades Bradykinin which is required to synthesise nitric oxide (NO). NO is a vasodilator. Angiotensin-II binds to angiotensin receptors, impairing NO synthesis. These two mechanisms inhibiting NO production lead to vasoconstriction. Angiotensin-II stimulates the adrenal glands to release aldosterone which increases sodium retention, contributing towards increased blood pressure (Paul et al., 2006).

Ace inhibitors and Angiotensin-II receptor blockers are therefore used to treat hypertension in ADPKD (Torres et al., 2014). Hypertension is one of the earliest signs of renal dysfunction. ACE inhibitors (ACEi) stop the conversion of Angiotensin-I to Angiotensin-II, preventing Angiotensin-II mediated vasoconstriction. Lowered Angiotensin-II also lowers the

production of Aldosterone, leading to sodium release into the urine, less water retention and lowered blood pressure. ACEi may also slow the progression of renal dysfunction in ADPKD (Torres et al., 2014) although recently this has been questioned in the HALT-PKD trial which found no significant improvement in renal function with ACEi (Chapman et al., 2010).

1.3 Polycystic kidney disease

Polycystic kidney disease (PKD) is a chronic inherited kidney disease which progresses and worsens over decades of life. PKD is characterised by the development of cysts in the kidneys, throughout the medulla and renal cortex and commonly also in the liver and pancreas. Cysts are non-cancerous, fluid filled sacs which can grow to a diameter of 10cm as fluid accumulates (Simms, 2016). The most severe and rapidly progressing forms of PKD arise in childhood but this form is far less common than the slower progressing adult form. The disease was previously characterised by the age of onset, yet recent research allows the two forms of the disease, ARPKD and ADPKD to be distinguished genetically.

1.3.1 ARPKD

Fibrocystin/*Polyductin* (*PKHD1*) is the causative gene of ARPKD and leads to polycystic kidney and hepatic disease in childhood. It is a very rare, recessively inherited form of PKD, affecting 1:20000 live births in the UK. Mutations in *PKHD1* cause cysts to develop from the bile ducts of the liver and collecting ducts of the kidneys. Kidney cysts develop by expanding from the collecting duct, but maintain contact with the nephron of origin (Wilson, 2004). This suggests that Fibrocystin is involved in mediating the terminal differentiation of the collecting duct. Fibrosis of the parenchyma is a prominent factor in the destruction of the liver and kidney function. *In utero*, the reduced renal function leads to oligohydramnios, i.e. extremely low amniotic fluid levels, which in turn affects lung development (Sweeney WE, 2016). These factors contribute to a once uniformly fatal disease however, with neonate respiratory support and renal replacement therapy, survival has increased to greater than 80% and the majority of these patients go on to survive beyond ten years of age (Roy et al., 1997).

PKHD1 is not well characterised. The gene is composed of 76 exons containing 16282bp, spread out over a ~472Kb genomic region. Fibrocystin is a large (4074aa) membrane

associated protein but the cellular function remains unknown. Fibrocystin is reportedly expressed in ductal structures during vascular development of the liver and kidneys and localises to the basal bodies of primary cilia (Zhang et al., 2004). Fibrocystin co-localises with PKD2 in complexes mediated by KIF3B (Wu et al., 2006) and may regulate calcium response in renal epithelial cells (Wang et al., 2007). This suggests that *PKD2*, *PKD1* and *PKHD1* function in the same cellular pathway.

1.3.2 ADPKD

ADPKD is the most common inherited kidney disease, one of the most common monogenic dominant disorders and a commonly life threatening genetic disease (Ong et al., 2015). The disease is dominantly inherited and affects both sexes equally. ADPKD is the common form of PKD and was once known as the adult form. However, in some cases ADPKD is diagnosed *in utero* and during infancy (Dell, 2011, Cole et al., 1987). Children are diagnosed by ultrasound and are generally asymptomatic but those with symptoms present with haematuria or hypertension. Genetic testing is not generally offered to children at risk of the disease but within affected families, members are monitored for high blood pressure and presence of protein in the urine (Dell, 2011). Very early onset ADPKD is rare and can be confused with ARPKD, in this case genetic testing is recommended.

ADPKD is characterised by the massive, cystic enlargement of the kidneys. The normal architecture of the network of nephrons is overtaken by progressively developing and enlarging cysts over several decades and 50% of cases result in end-stage renal failure (Gabow 1993). However, renal function remains relatively normal due to the ability of the kidney to increase filtration rates in other areas to compensate for regions of compromised function. A rapid precipitant drop in renal function is often observed in patients who have reached a critical threshold of cyst development. Cysts develop from every segment of the nephron; the tubule epithelium expands and pinches off, eventually becoming isolated from the tubule (Wilson, 2004). Cysts commonly develop in other epithelial organs such as the liver and pancreas. Increased cellular proliferation and apoptosis has been reported in ADPKD kidneys. Regulation of cell growth is an essential part of kidney development. Apoptosis destroys the renal parenchyma, contributing to the decline in renal function (Woo, 1995). Cysts may expand through prolonged renal cell proliferation, disrupted planar

cell polarity, increased fluid secretion and separation from the original nephron (Paul and Vanden Heuvel, 2014).

ADPKD is caused by mutations in either *PKD1* (85%) or *PKD2* (15%) (**Fig 1.3**). Mutations in PKD1, particularly PKD1 truncating mutations, are more severe and lead to a more rapid decline to ESRD than mutations in PKD2. There are some reports where patients have no family history of the disease suggesting that *de novo* mutations occur. However, a number of these could be caused by combinations of hypomorphic mutations. These lead to presentation of the disease in families where ADPKD would otherwise have gone undetected. The proteins encoded by *PKD1* and *PKD2*, Polycystin 1 (PKD1) and Polycystin 2 (PKD2), interact and localise to the cell-matrix interface, cell-cell contacts and primary cilium of renal tubule epithelial cells. In the cilium, they are thought to sense the extracellular environment, such as the flow of urine through the tubules, and signal to the cell (Wilson, 2004). The exact mechanisms of how they work are still debated.

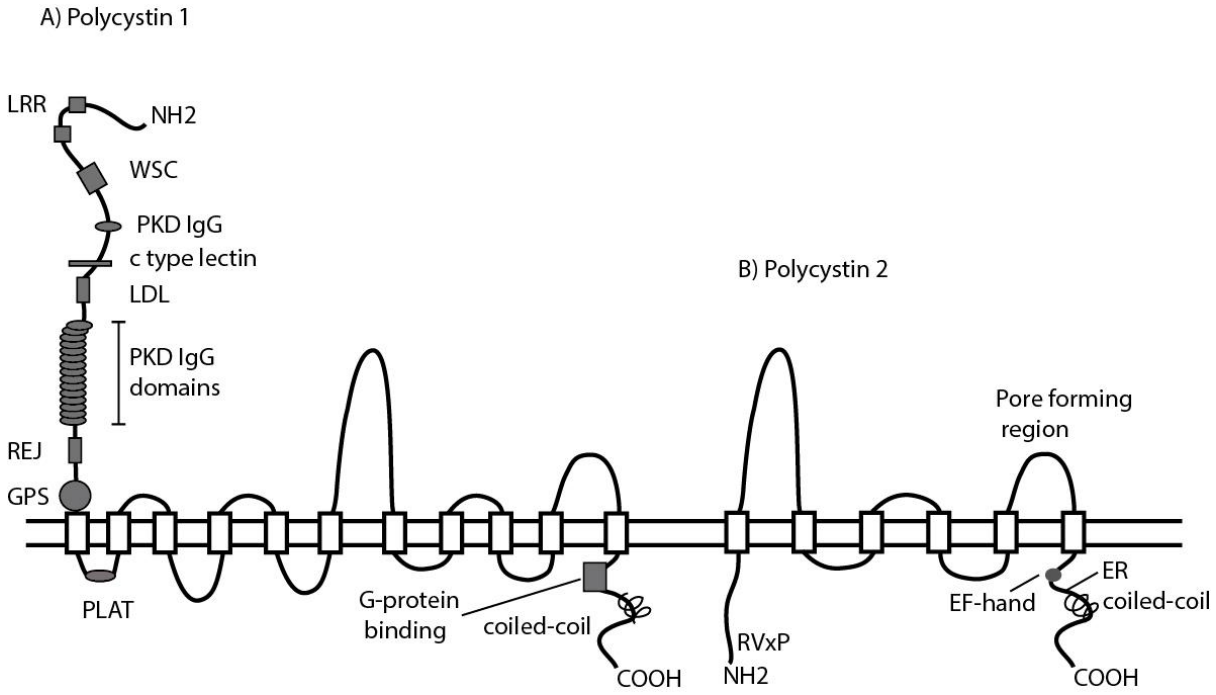

Figure 1.3: structural domains of Polycystin 1 and Polycystin 2

A) Polycystin 1 has 11 transmembrane domains, a cytoplasmic C-terminal and a large extracellular N-terminal. Many putative protein domains are detectable, including two leucine rich repeats (LRR), a cell wall integrity and stress response component (WSC), a PKD domain which binds receptor tyrosine phosphatases, a C-type lectin domain, a low density lipoprotein A related domain (LDL) and 15 more PKD IgG domains which have β-folded sheets and may bind protein ligands. There is a receptor for egg jelly (REJ) domain and a GPS cleavage site (GPS). On the cytoplasmic side there is a PLAT domain which has lipoxygenase homology. At the C-terminus, there is a site for G-Protein binding which may be surrounded by cleavage sites and a coiled-coil domain. B) Polycystin 2 is a smaller transmembrane protein with 6 transmembrane domains, a putative pore forming region between transmembrane domains 5 and 6, and cytoplasmic C- and N-termini. At the N-terminus there is a ciliary retention signal (RVxP). At the C-terminal tail there is an EF-hand which binds Ca^{2+}, an ER retention signal (ER) and a coiled coil-domain.

Adapted from (Torres and Harris, 2009) and (Wilson, 2004)

1.3.3 Genetics PKD1 and PKD2

PKD1 is a multi-domain, integral membrane protein with 11 transmembrane domains and a large extracellular N-terminus which contains many putative functional domains (**Fig 1.3**). Among these are 16 PKD domains which have beta-sandwich folds and may be linked to a mechano-sensory or ligand binding function, as well as a number of potential cleavage and phosphorylation sites.

PKD1 encodes a 460kDa, 4303aa transmembrane protein. Covering a genomic region of just 50Kb, *PKD1* is a large yet compact gene; 46 exons contain 12909bp of genomic sequence (Harris and Rossetti, 2010). Exons 1-33 are repeated in a cluster of 6 pseudogenes proximal to the *PKD1* locus on chromosome 16 (Ward, 1994). These have 97-99% sequence identity with the first 33 exons of *PKD1* (Tan et al., 2011b). They are transcribed yet contain sub-optimal start codons rendering them untranslatable. These pseudogenes are substantially homologous to *PKD1* in their structure, making genetic analysis of the mutated protein more complex.

PKD2 is a member of the transient receptor potential channel (TRP) family of proteins and is thought to function as a non-selective calcium permeable cation channel. The 15 exon long gene at human chromosome 4q21 encodes a 110KDa, 968aa protein; PKD2 (Mochizuki et al., 1996). PKD2 is likely to act as a homo- or hetero-polymer to form a channel (Ferreira et al., 2011, Feng et al., 2008, Tsiokas et al., 1997) and has dimerization domains at both N- and C-termini (Chapin and Caplan, 2010). PKD2 contains six transmembrane domains, cytoplasmic C- and N-termini, an EF-hand that binds Ca^{2+}, coiled-coil domains and structural motifs such as ER retention and ciliary localisation signals at the C- and N-termini. PKD2 is structurally similar to the C-terminal half of PKD1 (Tsiokas et al., 1997).

PKD2 is a calcium-activated channel. The EF-hand binds calcium enabling PKD2 to sense and potentially buffer changes in calcium (Gifford et al., 2007). Homotetramers of PKD2 molecules (Ferreira et al., 2011, Feng et al., 2008, Tsiokas et al., 1997) are thought to form a barrel shaped channel with the final extracellular loop contributing to the calcium conducting pore forming region. A missense mutation D511V in the third transmembrane domain disrupts the channel, therefore indicating that the third membrane domain is also essential for channel function (Koulen et al., 2002). PKD2 also interacts with ryanodine receptors and inositol 1,4,5-triphosphate receptor (IP_3R) to mediate calcium signalling (Chapin and Caplan, 2010).

PKD1 and PKD2 interact, possibly by their intracellular coiled-coil domain (Ferreira, 2015). PKD2 may be required for the maturation of PKD1 (Gainullin et al., 2015) and PKD2 has been described as a chaperone of PKD1, targeting PKD1 to the plasma membrane and ciliary membrane (Chapin et al., 2010).

1.3.4 A spectrum of mutations is seen in human ADPKD

ADPKD is a heterologous disease caused by mutations in either *Pkd1* or *Pkd2*. It is well established that homozygous inactivation of either gene causes rapid development of cysts in mice with lethality before birth (Lu et al., 1997, Wu et al., 2000). In general, human homozygous mutations in *PKD1* or *PKD2* are non-viable (Igarashi and Somlo, 2002), presenting in utero with severe cyst development. The spectrum of ADPKD cyst development and progression is variable and this is mostly attributed to the high allelic heterogeneity associated with *PKD1* and *PKD2*. At one end of the spectrum, patients live to old age developing only a few cysts and evade renal insufficiency; at the other end, neonates die postpartum with greatly enlarged cystic kidneys. The typical presentation lies in the middle with a slow progression towards ESRD by about 60yrs of age. The majority of patients have *PKD1* mutations and these generally cause a more severe form of the disease with an earlier onset of ESRD at around 54.3yrs compared to *PKD2* patients who reach ESRD at around 74yrs (Hateboer et al., 1999). Early onset, infantile disease is most associated with PKD1 mutations (Birewar and Zawada, 2003).

Table 1.1 summarises the mutations reported in the ADPKD human mutation database (PKDb, 2016). Reported mutations include those that disrupt splice sites, cause frameshifts, indels, nonsense mutations and amino acid substitutions as well as more neutral synonymous mutations and mutations in UTRs. Being a patient database, the majority of reported mutations are pathogenic. A large number of these cause truncations of the protein due to frameshifts, deletion or nonsense mutations. A small number of *PKD1* and *PKD2* mutations are hypomorphic indicating a role for gene dosage within the disease.

Table 1.1: ADPKD mutations recorded in PKD-database

The ADPKD database (PKDb, 2016) details mutations found in ADPKD patients. The database divides mutations into pathogenic, intermediate and neutral mutations. Neutral mutations include SNVs encoding synonymous amino acids, mutations in the 3' or 5' UTR or synonymous amino acid substitutions. The majority of mutations in the database are pathogenic, reflecting the nature of the database which records disease causing variants. The row detailing pathogenic mutations in this table includes mutations that are classed as definitely-, highly likely- and likely-pathogenic in the database (PKDb, 2016). However, non-pathogenic mutations are also included in the database and these are likely to be variants which arise coincidently in individuals who also carry pathogenic mutations. The columns of the table describe *PKD1* and *PKD2* mutations. Of the reported mutations, 54.8% of *PKD1* and 72.6% of *PKD2* mutations are pathogenic, a small number are hypomorphic, neutral or indeterminate. A large proportion of pathogenic mutations, in both *PKD1* and *PKD2*, are caused by truncations.

	PKD1	**PKD2**
Total mutations recorded	2323	278
Any Pathogenic mutation	1273 (54.8%)	202 (72.6%)
Hypomorphic	9 (0.39%)	1 (0.36%)
Likely neutral	856 (36.8%)	59 (21.2%)
Indeterminate	185 (8.0%)	16 (5.8%)
Truncations	724 (56.9% of pathogenic mutations)	122 (30.4% of pathogenic mutations)

1.4 Mechanisms of cyst development

The extent of intra-familial variation in ADPKD families indicates that other genetic as well as environmental modifiers may be involved in disease severity (Rossetti and Harris, 2007). This raises the question of the mechanism involved in modifying pathogenesis, such that the same mutation inherited throughout a family can result in drastically different clinical course and disease progression.

Research that has focused on the cellular mechanisms behind cyst development has shown that abnormal cellular proliferation and aberrant regulation of the extracellular matrix in combination with increased secretion into the cysts contribute to the progression of the disease. A plethora of research has unearthed details of cyst development, indicating that cysts may progress by a cellular recessive mechanism, that cysts may expand clonally and that specific timing of cyst development is key to progression.

1.4.1 The Two-hit hypothesis

Genetic analysis of cyst lining cells extracted from affected kidneys of ADPKD patients indicated that cysts developed by clonal expansion from a single cell. This founder cell may have undergone somatic inactivation of the Wt copy of either *PKD1* or *PKD2* leading to progressive cyst development (Qian et al., 1996, Wu et al., 2002).

ADPKD is dominantly inherited yet tubules become cystic progressively over decades. In mice, aged heterozygotes for either *Pkd1* (Lu et al., 1997, Lu et al., 1999, Boulter et al., 2001) or *Pkd2* mutations (Wu et al., 2000, Wu et al., 1998) develop small numbers of microcysts over time but do not display the rapid development of cysts seen in homozygotes. Perhaps this is due to species differences between mouse and human or perhaps low level phenotypes do not manifest in these mice because the mouse life span is short and does not allow for cyst progression. This inconsistency between a human dominantly inherited disorder and a seemingly recessive phenotype in mice may be partially explained by the two-hit hypothesis. The two-hit hypothesis suggests that ADPKD is recessive at a cellular level and that a second, somatic mutation is required in renal tubule cells before they begin to expand clonally to form cysts. This loss of heterozygosity (LOH) at a cellular level has been observed in a proportion of cysts from human patients. Watnick and colleagues compared somatic and germline *PKD2* mutations in cysts from two patients and found that 71% of the cysts examined exhibited somatic *PKD2* mutations (Watnick et al., 2000). These somatic mutations were randomly distributed through *PKD2* and no two mutations were the same, suggesting that there is no hot-spot within *PKD2* for somatic mutation. In another study from the same lab, 11/12 cysts exhibited a somatic mutation in the otherwise Wt *PKD2* allele. The probability of this non-random segregation pattern is <1 in 2000, indicating that the acquisition of the somatic mutation is linked to the cyst development process (Pei et al., 1999). For the two hit hypothesis to be working, a modifier of the random mutation process must be in place which causes a specific accumulation of mutations targeting these genes, currently no such mechanism has been suggested.

Somatic mutations of both *PKD1* in *PKD1*-germline-mutation containing cysts (Brasier and Henske, 1997) and *PKD2* in *PKD2*-germline-mutation containing cysts have been noted. This indicates that the mechanism causing additional mutation acquisition is part of the ADPKD

cyst development process, irrespective of whether the causative gene mutation is in *PKD1* or *PKD2*.

Assessment of PKD1 patients revealed that PKD1 somatic mutations occur in a percentage of PKD1 cysts, yet LOH was not reported in all cysts (Brasier and Henske, 1997). However, this could relate to the difficulty of genotyping for *PKD1* caused by the Pkd1-pseudogenes. Somatic *PKD1* mutations have also been observed in *PKD2*-germline mutated cysts (Watnick et al., 2000, Koptides et al., 2000), indicating that a transheterozygous mutation may be sufficient to drive cyst formation in the renal cells. The mechanism of how this comes about and how this is related to cyst formation is unclear. It seems that somatic loss of either a *PKD1* Wt allele or a *PKD2* Wt allele in either *PKD1*- or *PKD2*-germline-mutated cysts is sufficient to cause cyst formation. Wu et al. presented data supporting this idea; $Pkd1^{+/-}$;$Pkd2^{+/-}$ mice were compared to mice with a single deleted allele of either *Pkd1* or *Pkd2* (Wu et al., 2002). All mice exhibited a mild, slow growth of cysts which affected a small proportion of tubules at 12 months. This suggested that transheterozygous mutations alone were not sufficient to cause significant renal disease. However, the $Pkd1^{-/+}$;$Pkd2^{-/+}$ kidneys were found to exhibit more cysts than would be expected from additive effects of the two mutations alone (Wu et al., 2002). Therefore suggesting that PKD1 and PKD2 work together to maintain the Wt phenotype.

Further evidence supporting the two-hit hypothesis comes from analysis of an unstable *Pkd2* allele in the mouse (Wu et al., 1998, Wu et al., 2000). These mice carry one copy of the $Pkd2^{WS25}$ allele which is prone to genomic rearrangement causing gene inactivation. When in combination with a Wt allele of *Pkd2*, microcysts began to develop between 6-14 weeks of age (Wu et al., 1998). Mice with two copies of the unstable allele present a more severe yet varied phenotype. When in combination with a $Pkd2^{-}$ allele, these mice developed progressive cystic disease similar to affected patients, exhibiting renal and pancreatic cysts as well as cardiac defects and early mortality (Wu et al., 2000). The variation in phenotype modelled by $Pkd2^{WS25}$ is likely to be linked to when the allele stopped producing Wt protein. This therefore reflects some of the variety of phenotype and cyst development that could be explained by the two-hit hypothesis.

The two-hit hypothesis can go some way into explaining how patients with a familial inherited disease have different presentation severity to other family members. Assuming that loss of the Wt allele is required for cyst formation, LOH must occur early, before cysts start to develop. When observing cysts with LOH, it is difficult to differentiate cause from effect; perhaps LOH is required for progression of established cysts or dilated tubules rather than being the first event which initiates cyst development (Ong and Harris, 1997). It is possible that, although the germline mutation is required, the somatic mutation is the rate limiting step of the disease and it is this second mutation that causes a tubule to become cystic. On the other hand, perhaps cysts form and develop slowly until a second mutation is acquired, at which point the cells proliferate more rapidly.

1.4.2 Some inconsistencies with the two-hit hypothesis

Studies have highlighted incomplete penetrance in some cases of ADPKD which are inconsistent with the two-hit hypothesis. Rosetti et al (Rossetti et al., 2009) describe two families with homozygous carriers of hypomorphic alleles of *Pkd1* (*Pkd1*^{R3277C} *and Pkd1*^{N3188S}) caused by a substitution of a single amino acid. Surprisingly, these homozygous patients were viable and had a slowly progressing form of ADPKD. Family members who were heterozygotes developed fewer cysts. Another family exhibited *in utero* disease; a child carrying a hypomorphic allele in trans to a truncation of *PKD1* which inactivated the gene, developed gross cystic disease. This atypical presentation of the disease suggests a role of gene dosage in the development of ADPKD, consistent with the level of *PKD1* protein being critical in preventing cyst development. The PKD-database (PKDb, 2016) records nine more hypomorphic *PKD1* alleles and a hypomorphic *PKD2* allele which are reported to work in a similar way. There are likely to be more patients carrying hypomorphic alleles which are thus far undiscovered due to their mild phenotype.

A study of the *Pkd1*^{R3277C} hypomorphic allele in mice found that it induced a strongly progressive disease when combined with a null allele, whereas *Pkd1*$^{R3277C/R3277C}$ mice developed cysts more gradually (Hopp et al., 2012). Another study assessed an allele of *Pkd1* in the mouse which only produced 13-20% of correctly spliced transcripts. Homozygous mice developed cystic kidneys with mild fibrosis suggesting that reducing the level of *Pkd1* protein can lead to cyst development (Lantinga-van Leeuwen et al., 2004).

Wilm's tumour, an infantile disease of the kidney, progresses by LOH after acquiring second mutations in a Wt allele (Dome and Huff, 1993). The number of tumours does not equate to the number of cysts acquired in ADPKD during development, indicating that the rate of somatic mutation is not the same between the two diseases. Another mechanism must be acting to modify ADPKD in addition to the two-hit hypothesis. If a second hit is required for cyst progression, the mutation rate would have to be significantly higher in the kidney than other organs to allow for such a great accumulation of mutations. It is possible that the mutation rate is raised in the kidney due to the kidney's role of concentrating toxins; however, the rate of cyst development in the kidney does not fit with the mutation rate of other diseases of the kidney.

Despite every cell in the kidney carrying the same mutation, cysts are intermittent and only affect a proportion of possible tubules. Often, the Wt copy of *PKD1* or *PKD2* remains in cyst epithelia, this indicates that a second hit has not occurred (Wu et al., 2002). Assessment of human cysts shows that there is not always a fully penetrant somatic mutation causing loss of the Wt allele. Neither mouse nor human studies explain the higher mutation rate required in the kidney to cause somatic second hits in the correct genes. There are conflicting views as to whether there exists a hotspot for mutation in either *PKD1* or *PKD2* (Liu et al., 2015, Koptides et al., 1999, Pei et al., 1999, Tan et al., 2011a); it seems that there are no particular areas within the genes which are more susceptible to mutation, however it is unclear whether the genes themselves are targeted more often than other areas of the genome.

The evidence of gene dosage effects and hypomorphic alleles indicates that the two-hit hypothesis alone is too simple to explain the development of cysts in ADPKD. Two copies of a hypomorphic allele can be inherited and only lead to a mild phenotype. A great deal of research has been conducted to untangle this subject. Although the two-hit hypothesis is attractive, it is likely too simple to entirely explain the mechanism of cyst development. It is probable that other modifiers are involved which specifically target PKD1 or PKD2 and catalyse cyst development.

1.4.3 Developmental switch

A number of studies suggest that the timing of gene inactivation plays an important role in disease progression. From observing human ADPKD, we know that large numbers of cysts developing in utero leads to a severe and progressive form of the disease whilst cysts developing later in life tend to follow a slower and milder progression pattern. A similar variability in size and number of cysts is exhibited by mice homozygous for the unstable *Pkd2*^{WS25} allele (Wu et al., 1998). It is proposed that mice with a larger number of cysts have undergone the recombination of *Pkd2*^{WS25} early, possibly even during embryonic development, whereas those with fewer cysts have experienced more recent recombination events. This suggests that the timing of the initiation of LOH plays an important role in cyst development. The developmental switch model argues that there is a specific time point at which susceptibility to rapid cyst progression switches off in favour of a slower, more progressive development of cysts. This point has been argued to correspond to a time where the rapid growth and expansion of the developing kidney begins to slow (Piontek et al., 2007). Shortly after birth, the cap mesenchyme population is depleted and nephrogenesis ceases (Takasato and Little, 2015). Substantial elongation continues in the proximal tubules, loop of Henle and collecting ducts during the first 1-2 postnatal weeks (Little and McMahon, 2012) and significant changes occur with respect to gene expression, including down-regulation of growth and embryonic development related pathways at P5-7. At P14-21, DNA-replication, protein trafficking and cell cycle regulating pathways are amongst those that are down-regulated (Wu et al., 2013).

Piontek et al. undertook a study using a tamoxifen inducible-Cre to delete *Pkd1* in the kidney (Piontek et al., 2007). *Pkd1* was inactivated in mice at six weeks old and kidney structure was assessed three months and six months later. After three months, no cysts had developed and kidneys were indistinguishable from Wt. However, after six months, kidneys were grossly cystic. In contrast, deletion at P2 caused the development of a severe cystic phenotype evident when observed a month later. This revealed that the crucial time point of the developmental switch was between P2 and 4 weeks. To further pinpoint the interval of switchover, Piontek et al assessed a number of points of inactivation between P2 and P21. All mice inactivating *Pkd1* at P12 or earlier developed a rapid, progressive cystic disease within three weeks of inactivation. Mice induced between P14 and P21 exhibited normal

appearing kidneys until six months after inactivation when cysts were observed. Interestingly, P13 inactivation caused an intermediate phenotype with all mice developing renal cysts by three weeks but with fewer cysts than those activated earlier (Piontek et al., 2007). A similar study used a kidney epithelium-specific, tamoxifen inducible cre to delete *Pkd1* specifically in renal tubules and the results confirmed the Piontek findings (Lantinga-van Leeuwen et al., 2007). The time of transgene induction in this kind of study can be variable, depending on the time required to activate the delivered compound, e.g. Tamoxifen, to delete the gene and for existing gene products to be degraded (**Fig 1.4**).

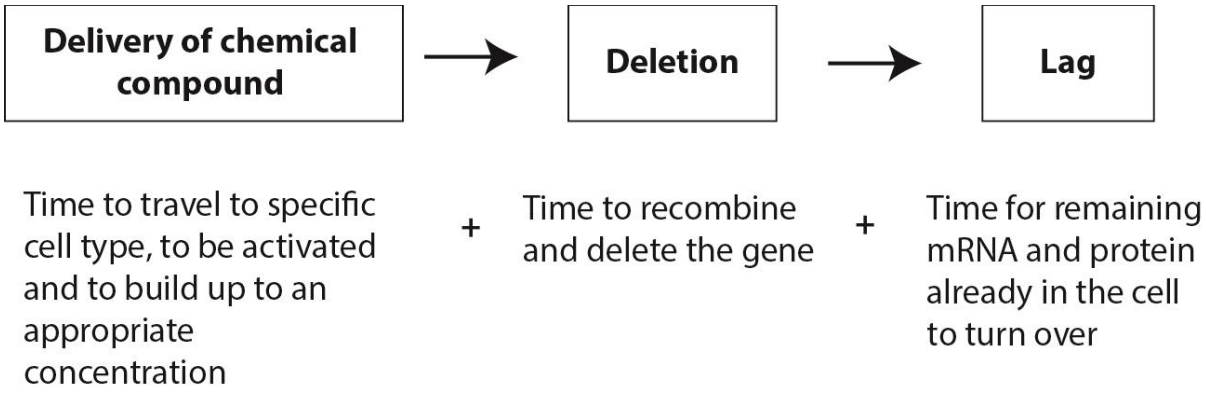

Figure 1.4: Timings associated with the deletion of a protein after induction of a transgene.

Chemical compounds such as Tamoxifen or Androgens must be delivered in a way that allows safe delivery of the compound to the site of deletion in the animal. The compound may be delivered in an active form or be activated *en route*. The recombination may not happen immediately, depending on the stage of the cell cycle and the chromatin state. After the sequence is deleted, there is likely to be protein and mRNA still present in the cell, the half-life of these will determine how quickly the cells become free of Wt protein.

A recent study showed that timing of deletion of *Pkd1* also altered the origin of cyst development indicating that different regions of the kidney are sensitive to loss of *Pkd1* at different times. Deletion at P1 or P2 led to cyst development in the corticomedullary region whereas deletion at P3-8 resulted in medullary cysts (Rogers et al., 2016), leading to a slight drop in phenotypic severity. Since regions of the kidney are demarcated by the presence of specific sections of the nephron, it is possible that different cell types are involved in cyst development at these different time points. This suggests that the developmental switch does not occur uniformly throughout the kidney, rather that different cell types are

sensitive to the loss of *Pkd1* at different times and that the developmental switch washes over the kidney as a wave. Considering the complexity of the kidney and the different cell populations, it is not surprising that subtle changes in *Pkd1* expression cause diverse responses throughout the nephron segments (Rogers et al., 2016).

This raises the question of what is happening at P12-14, around the time of the developmental switch. Rodgers et al suggest that changes in mTOR, Wnt and TGFβ signalling are occurring at this stage and that these changes are delayed in cystic kidneys (Rogers et al., 2016). The presentation of renal cysts in mice which lose *Pkd1* expression later in life indicates that *Pkd1* is required to maintain tubule structure in the adult kidney, yet inactivation at different stages causes a different disease progression. The rapid and severe progression of cysts following inactivation in the first two weeks after birth has been linked to the continuing growth and development of the kidney. At this stage, the population of stem-like cells in the cap mesenchyme are being used up and the nephrons are continuing to mature. The development of cysts after this stage could be explained by the maturation arrest hypothesis (Calvet, 1994). This suggests that tubule cells are suspended in an immature state and the normal developmental process cannot proceed, or that tubules are unable to regenerate following injury. Development of incipient cysts in the adult kidney may reflect this immature state. These adult cysts develop due to aberrant repair following renal injury which could be caused by tubule blockages, bacterial infection, inflammation or kidney stones (Lantinga-van Leeuwen et al., 2007).

1.4.5 Polarity, apoptosis and proliferation

The progression of cyst development requires altered cellular organisation and fluid secretion. Tubular cells must reorganise to produce circular structures rather than tubular structures and then fill with fluid as they expand. Cyst expansion is primarily due to cell proliferation rather than stretching of the epithelial layer (Chapin and Caplan, 2010). Defects in planar cell polarity (PCP) have been reported to contribute to cyst development. PCP refers to the coordination of cells along an axis, communicating by cell signalling pathways and global directional cues to orientate cells division (Devenport, 2014). Ciliary signalling may provide important cues about the extracellular environment to orientate cell division (Fischer et al., 2006). Disruption of PCP pathways may cause cells to stop dividing along the

tubular lumen axis and instead form a spherical cyst structure (Happé et al., 2011). However, this may not be the causative step in cyst development. Nishio et al. show that cells only lose polarised division after the initiation of cyst development (Nishio et al., 2010). They also note that *Pkhd1*$^{-/-}$ mice lose cellular polarisation but do not develop cysts as cells are able to reintegrate into the tubule structure. This indicates that defective PCP is not sufficient for cyst development.

Epidermal growth factor (EGF) is a mitogenic peptide which stimulates proliferation in normal cells and may contribute to the development of cysts (Du and Wilson, 1995). EGF is secreted into cyst lumens and has been found at high concentrations within cysts of ADPKD patients. EGF receptors (EGFR) are overexpressed and abnormally localised to the tubular lumen facing membrane of cystic tubules in ADPKD kidneys. EGFR in the cyst lining binds EGF secreted into the cyst fluid and induces cellular proliferation (Zheleznova et al., 2011).

Cyclic adenosine monophosphate (cAMP) is proposed to be a mediator of cellular proliferation and fluid secretion in cystic epithelia (Hanaoka and Guggino, 2000). The exact mechanism governing cAMP induced cell proliferation remains undetermined; however cAMP may stimulate EGF related expansion of cysts. cAMP also stimulates fluid secretion. The normally ion-absorbing tubule cells transition into ion-secreting cells, this then drives water movement into the cyst. The cystic fibrosis transmembrane regulator (CFTR) may be involved in transporting Cl^- ions into the cyst lumen (Chapin and Caplan, 2010) which appears to be important but not essential for cyst growth.

After cyst expansion begins to slow, cells stop dividing and apoptosis begins (Woo, 1995), the area surrounding cysts begins to become inflamed and interstitial fibrosis starts to damage significant portions of the kidney (Happé et al., 2011). Elevated levels of apoptosis have been reported in mouse (Lin et al., 2003) and human kidney cysts (Murcia et al., 1999, Woo, 1995). Apoptosis may be involved in removing uninduced mesenchyme in the developing nephrogenic zone and disruption of apoptotic/proliferative balance appears to be associated with increased cystic growth (Murcia et al., 1999).

1.5 Sensing

The Polycystins appear to participate in a substantial number of cellular pathways involving cell signalling and regulatory processes. Their sub-cellular localisation is vast and complex. Frequently, the PKD1 C-terminal tail (CTT) binds and negatively regulates the activity of signalling molecules (Chapin and Caplan, 2010), sequestering them from the nucleus. The cleaved CTT can itself travel to the nucleus, influencing transcription.

1.5.1 Cilia

Like many other renal cystic diseases, ADPKD is a ciliopathy; a disease that involves the aberrant function or formation of cilia. Many cyst causing genes reside within or interact with, the primary cilium. The polycystins play a highly important and essential role in signalling from the primary cilium.

The primary cilium is a single projection from the apical cell membrane. In renal epithelial cells, the cilium projects into the lumen of renal tubules and may sense flow of fluid through them (Lee and Somlo, 2014). The primary cilium consists of a ring of nine microtubule pairs making up the axonemal scaffolding. The axoneme is encased in membrane which is contiguous with the plasma membrane. The cilium is anchored into the cytoplasm by the basal body. The basal body is a structure that forms from the centriole and patterns the ciliary axoneme (Kim and Dynlacht, 2013). Early stages of ciliogenesis involve the basal body docking to membrane components of the ciliary vesicle or plasma membrane. Structures attached to the basal body anchor the base of the cilium to the plasma membrane and microtubule skeleton of the cell (**Fig 5.1**).

Proteins and axonemal components move into the cilium by Intraflagellar transport (IFT), the transport system of the cilium. IFT provides bidirectional movement of non-membrane bounded particles along the ciliary axoneme and is essential for ciliogenesis and maintenance. IFT trains form 2 complexes, A and B. Movement of cargo is either anterograde (complex B) powered by kinesin-2 or retrograde (complex A) powered by cytoplasmic dynein 2 (Rosenbaum and Witman, 2002). After initiation of ciliogenesis, the ciliary axoneme is maintained by addition of subunits to the distal tip, this requires tubulin subunits to be carried along the axoneme to the tip of the cilium (Kim and Dynlacht, 2013).

Inactivating IFT components required for ciliogenesis in renal epithelial cells prevents cilia growth and causes severe cyst development which progresses to renal failure rapidly (Lin et al., 2003). Indeed, cilia and Polycystin function appear to be linked; ablation of cilia or Polycystins from ciliated cells causes cyst development, whereas concomitant ablation of both leads to a less severe development of cysts (Ma et al., 2013). This strengthens the link between Polycystins and cilia in regulation of normal tubule development.

1.5.2 Calcium signalling

It is generally accepted that PKD1 and PKD2 form a complex which acts as a mechanosensitive channel on the ciliary membrane (Nauli et al., 2003, Ma et al., 2013, Harris and Torres, 2009). The PKD1-PKD2 complex is thought to regulate calcium influx in the ciliary membrane as well as the plasma membrane and ER (Mangolini et al., 2016). In the ER, PKD2 is thought to trigger calcium induced calcium release from ER stores by modulating IP_3R and ryanodine receptors (Ferreira, 2015). PKD1 inhibits the interaction with IP_3Rs and counterbalances PKD2 activation (Mangolini et al., 2016).

The specific positioning of the cilium jutting into the tubule lumen and the localisation of PKD1 and PKD2 to the ciliary membrane, allows for the attractive hypothesis that flow through the tubule causes the bending of the cilium, which is sensed by the PKD1-PKD2 mechanosensing complex. PKD2 then allows Ca^{2+} influx into the cilium. This model has also been argued in the development of left-right patterning (see **Chapter 2**); the mechanical force of flow generated in the node bends the cilia positioned around the node, the PKD2 Ca^{2+} channel then responds to this flow by allowing Ca^{2+} influx (McGrath et al., 2003, Yoshiba et al., 2012). The mechanism of how this signal is translated into the cell is hotly debated.

Recently, the Clapham lab argued that primary cilia are not calcium responsive mechanosensors. They state that if mechanosensation does originate in the cilium, that it is not due to calcium influx. They used a genetically encoded ratiometric calcium indicator in the cilium of several cell types. After verifying that their Ca^{2+} indicator can reliably report Ca^{2+} signals, the researchers applied flow across an embryonic mouse node and found that no Ca^{2+} influx into the cilium could be seen. This suggested that calcium did not enter the cilium in response to ciliary bending (Delling et al., 2016). The authors suggest that previous work that reports calcium influx in response to cilium bending may be due to cilium rupture

or reflux of calcium from the cell body. This work, being a finding that contradicts a major hypothesis that is the foundation of many studies, has been under fierce debate (Norris and Jackson, 2016).

Several studies support the model of cilia as specialised calcium responsive organelles. Notably, work from the Clapham lab previously stated that cilia are specialised calcium signalling organelles (Delling et al., 2013). They state that calcium channels alter ciliary Ca^{2+} levels without causing a substantial change in cytoplasmic calcium. They report that Ca^{2+} can move from the cytoplasm into the cilium but that, due to the massive difference in volume between the cilium and cytoplasm, calcium moving from the cilium into the cytoplasm is rapidly diluted and therefore unlikely to elicit a response. Both these studies used elegant genetically encoded calcium indicators and high speed microscopy to assess the calcium levels in the cilium. Further studies are likely to test these methods and further elucidate the question over calcium signalling within the cilium.

The fact that PKD2 is essential in cilia around the node to detect flow and within cells of the renal tubules to prevent cyst development remains. If this work proves to be rigorous, alternative explanations of a number of the functions, pathways and signalling mechanisms need to be formed.

1.5.3 mTOR signalling

The mammalian target of rapamycin (mTOR) regulates cell growth, proliferation, protein synthesis and survival. mTOR is negatively regulated by *TSC1* and *TSC2*, the genes associated with tuberous sclerosis. *PKD1* lies genetically end to end with *TSC2* in the genome therefore large contiguous deletion of PKD1 and TSC2 cause ADPKD-TSC disease, a form of PKD which combines severely cystic kidneys with factors of tuberous sclerosis such as benign tumours (Ferreira, 2015).

PKD1 inhibits mTOR activity by stabilising the TSC1-TSC2 complex, maintaining inhibition of mTOR. mTOR regulates cell size possibly through cilia under flow conditions (Boehlke et al., 2010). Boelhke et al. investigated the physiological stimulus of flow and found that, grown in the presence of flow, ciliated MDCK cells were smaller than their non-flow counterparts. However, cells without cilia, after *Kif3a* knockdown, were enlarged. Boelhke et al. suggest

that bending of the cilium is essential for mTOR downregulation and cell size control and that this is independent of flow induced Ca^{2+} influx.

In ADPKD cells, PKD1 dysfunction may ablate TSC1/TSC2 mediated inhibition of mTOR, leading to upregulation of the mTOR pathway and increased cell growth. Rapamycin has been shown to slow cyst growth in rodent models of PKD by reducing cell proliferation (Tao et al., 2005, Shillingford et al., 2006). The mTOR inhibitors sirolimus and everolimus were the first drugs to be trialed against ADPKD. These drugs were effective against rodent models of the disease; mice can tolerate higher blood levels of mTOR inhibitors than humans and the acceptable human level appears to be too low to inhibit mTOR in the kidney (Harris and Torres, 2014).

1.5.4 TGF-β signalling

Transforming growth factor-β (TGF-β) is also involved in cell proliferation, differentiation and apoptosis and may have a role in cyst progression in ADPKD. TGF-β ligands bind the type II TGF-β receptor on the plasma membrane which recruits and phosphorylates the type I TGF-β receptor. Type I receptors then go on to recruit and phosphorylate receptor SMADs in the cytoplasm. These bind to SMAD4, move into the nucleus and act as transcription factors (Leonhard et al., 2016). Since the TGF-β pathway is involved in a wide range of cellular processes, an array of mechanisms exist to modify and regulate the signalling. Several members of the Nodal cascade, for instance, are TGF-β family members (e.g *Nodal* and *Lefty1/2*).

Altered TGF-β signalling is evident in a number of mouse models of PKD (Hassane et al., 2010) and in studies of human ADPKD kidneys (Chea and Lee, 2009). Hassane et al. assessed TGF-β signalling in mouse and human samples with *Pkd1* mutations. They found that TGF-β signalling is not increased until late stages of cyst expansion in both mouse and human samples. TGF-β is a major fibrogenic cytokine and may be involved in implementing interstitial fibrosis in the progressively cystic kidney rather than being involved in the initial stages of cyst development (Hassane et al., 2010).

1.6 Aims of this thesis

PKD2 is a causative gene of ADPKD and is essential to prevent cyst development within the kidney. PKD2, along with PKD1, is involved in a many signalling pathways within the cell and functions in a number of sub-cellular compartments. The relationship between the cilium and the Polycystins has been extensively studied. However, there remains a great deal of confusion surrounding the roles that *PKD2* plays. Recent work stating that the cilium is not a calcium-responsive mechanosensor has added to this confusion. This thesis aims to provide insight into the role of *PKD2* in the cilium and to deepen understanding of the molecular characteristics governing the development of ADPKD.

Chapter 2: The *lrm4* allele of *Pkd2* induces renal cyst growth during embryonic development in the mouse

2.1 Introduction

2.1.1. Gene expression at the node governs left right patterning

Unlike human embryos, mouse embryos develop as a cup shape with their ectoderm on the inside and endoderm layer facing outside (**Fig 2.1 A**); this later resolves in a process of embryonic turning which rearranges the germ layers at around 8-12 somite stage. After turning, the final stages of gastrulation are still occurring and the mouse embryo lies in a concave shape with the mesoderm inside, forming a simple structure surrounded by extraembryonic tissues. The primitive streak lies at the posterior of the embryo (**Fig 2.1 B**). As cells migrate and pass through the primitive streak, they delaminate and form the three germ layers. The anterior portion contributes cells to the somites (which give rise to muscle) and gut endoderm, and the middle portion contributes to the lateral plate mesoderm (LPM). The LPM later gives rise to the mesenchyme of many visceral organs, including the heart and kidneys. The posterior end of the primitive streak gives rise to the allantois and extraembryonic tissues. The node, a transient structure in the developing embryo present between ~E7.5-9, lies at the anterior end of the primitive streak. As the embryo develops, the node regresses and leaves behind cells which later contribute to the notochord.

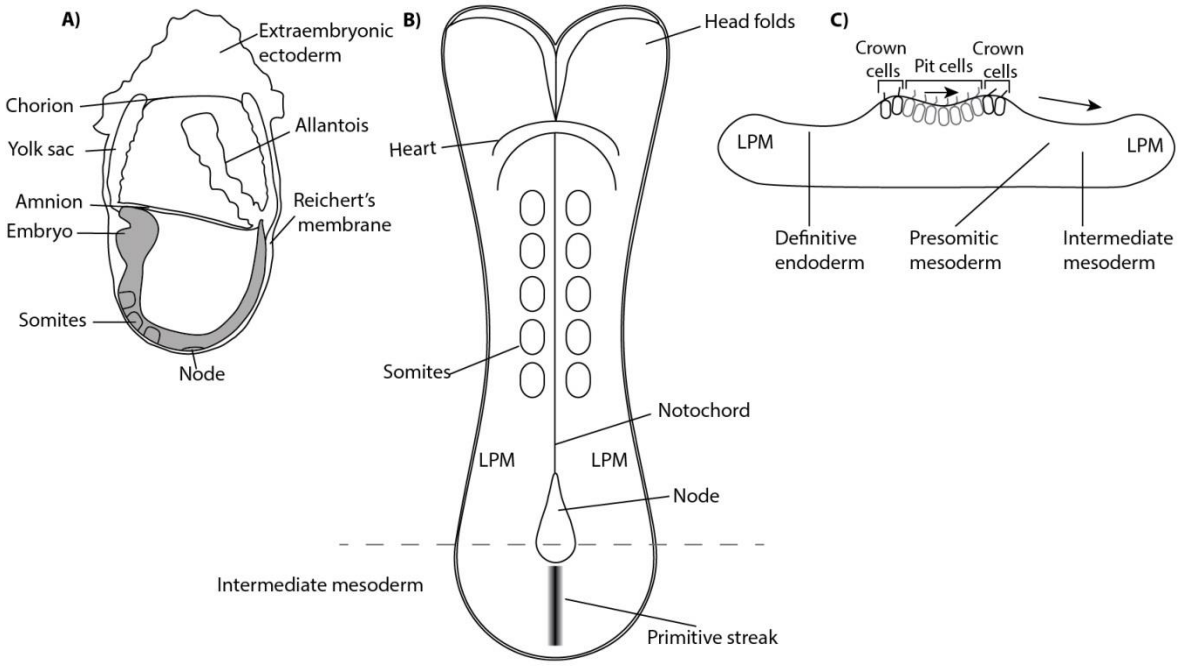

Figure 2.1: Structure of the developing embryo

A) Sagittal slice of mouse embryo at E8.25. The embryo forms a cup-shaped structure, surrounded by supporting extraembryonic membranes. B) Ventral view of an E8.5 embryo. When dissected and laid flat, the headfolds, heart and somites can be clearly observed. The grey dotted line through B) indicates the position of the section in C). A transverse section through the embryo C) reveals the tissues through which an asymmetric signal must travel, from the pit cells at the node where the signal is generated, to the L-LPM where the Nodal cascade is initiated. The intermediate mesoderm goes on to form the kidneys.

The vertebrate body plan is externally bilaterally symmetrical however; internal organ placement is consistently asymmetric. This asymmetry is the result of a complex cascade of asymmetric events, involving mechanical force, cell polarity changes and asymmetric gene expression (Blum et al., 2014a). These events can be broken down into two steps; the breaking of symmetry and the initiation of asymmetric gene expression in the LPM, known as the *Nodal* cascade. The initial breaking of symmetry originates in the node; a cilia lined pit at the anterior end of the primitive streak. From here, the signal is transferred across the primitive endoderm to the LPM resulting in the second step; the induction of the *Nodal* cascade. (**Fig 2.2)**

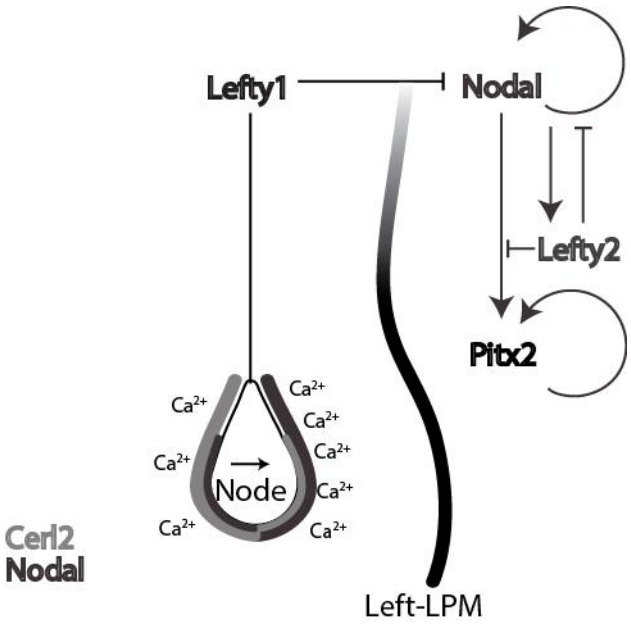

Figure 2.2: Asymmetric gene expression around the node

Cilia in the node rotate, causing a leftward flow across the node. This flow establishes asymmetric Cerl2 (Grey), calcium (Ca^{2+}) and Nodal (black) expression around the node. This left-sided biased signal is communicated through the endoderm to the left lateral plate mesoderm (LPM) where the Nodal cascade initiates. Left sided Pitx2 eventually leads to asymmetric organ morphogenesis.

The cilia in the pit of the node are motile but unlike most motile cilia, pit cilia lack a central microtubule pair (9+0). Consequently, these cilia rotate in a clockwise direction instead of having the whip-like beating pattern of 9+2 motile cilia, such as those in the trachea or lungs. Rotation alone is not sufficient to produce a leftward flow across the node; in fact this would create a windmill effect with non-directional flow (Cartwright et al., 2008). At the genesis of the node, these cilia are relatively sparse and short. As the node matures, the pit cilia lengthen, gain a posterior tilt and begin to become motile (Santos and Reiter, 2010, Okada et al., 2005). The elliptical axis of rotation caused by the posterior tilt produces a leftward efficient sweep away from the surface of the cell and a rightward inefficient sweep closer to the surface. It is the tilt, in combination with the clockwise rotation, which generates the leftward flow across the node (Hirokawa et al., 2006, Okada et al., 2005). This flow, which begins at E7.5-8 in the mouse embryo, is the first asymmetric event in the genesis of the left-right axis of the embryo (Nonaka et al., 1998, Blum et al., 2014a, Blum et al., 2014b).

A second population of ciliated cells at the edge of the node is thought to be involved in sensing the fluid flow emanating from the node (Tabin and Vogan, 2003, McGrath et al., 2003). These cells are known as crown cells. There are three main hypothesised mechanisms by which leftward flow is detected. Two of these explain how flow could be sensed from a chemosensory perspective, the third from a mechanosensory perspective. In the Morphogen Gradient model, morphogens travel across the node in the cilia-generated-leftward-flow. This establishes a L-R concentration gradient of the morphogen leading to asymmetric signalling around the node. A similar model proposes that the morphogens are bounded in nodal vesicular parcels (NVPs) rather than being free moving (Tanaka et al., 2005). As the parcels open, either by mechanically crashing against the node wall or by chemical lysis, the morphogen cargo is released. The final model, the two cilia hypothesis, suggests that two groups of node cilia, the motile pit cilia and the immotile crown cilia work together to establish laterality (McGrath et al., 2003). The pit cilia generate flow across the node and the mechanical force produced is sensed at the periphery by the left sided crown cilia (Okada et al., 2005, Chen et al., 2014). No single theory has been completely ruled out; indeed it is even possible that a combination of 2 or more of these could be involved in establishing laterality.

Following the onset of leftward flow, asymmetric expression of *Cerberus-like-2* (*Cerl2*) is established at the node (Inacio et al., 2013, Marques et al., 2004). *Cerl2* accumulates in the cells on either side of the node before expression becomes biased to the right. *Cerl2* is an antagonist of *Nodal,* a secreted TGF-β superfamily member. Nodal is a morphogen which is expressed bilaterally at the perinodal crown cells but becomes biased to the left, downstream of *Cerl2* asymmetry. Following this, its expression expands to the left but not right-LPM. *Cerl2* is required to maintain the asymmetric expression pattern of *Nodal* around the node and to prevent *Nodal* expression on the right of the embryo by directly binding and inactivating Nodal. *Nodal* is the left side determinant which induces a cascade of gene expression on the left of the embryo (**Fig 2.2**). Known as the *Nodal* cascade, this pattern of gene expression leads to the eventual specification of left-sided fate. Indeed, the left sided expression pattern of *Nodal* is conserved across vertebrates and beyond.

Around the node, Ca^{2+} accumulates in the endodermal cells with a left asymmetric bias, at the immediate margin of the node, extending into the left-LPM (McGrath et al., 2003).

McGrath et al found that calcium was not observed in this asymmetric pattern around the node until after the leftward laminar flow is established, implying a link between calcium signalling and node flow (McGrath et al., 2003). In the absence of flow, Ca^{2+} at the node became randomised, indicating that leftward flow is required to set up consistent leftward Ca^{2+} asymmetry at the node. PKD2, a calcium channel expressed throughout the node, has been proposed to initiate calcium induced calcium release in response to elevated Ca^{2+} concentration around the node. In *Pkd2*$^{-/-}$ embryos, the perinodal Ca^{2+} signal was lost. This indicates that PKD2 is required to relay leftward nodal flow to a leftward asymmetric Ca^{2+} signal at the node (McGrath et al., 2003).

Having been established at the node, the asymmetric *Nodal* signal is propagated across the definitive endoderm, to the L-LPM. The cells of the left and right LPM are competent to respond to *Nodal* signalling but a midline barrier exists, consisting of Lefty1, which inhibits Nodal activity (**Fig 2.2**). This prevents Nodal activation on the right of the embryo.

In the left-LPM, as well as reinforcing its own expression, Nodal activates *Pitx2*, a bicoid-like homeobox transcription factor. Expression of *Pitx2* spreads along the LPM and subsequently establishes the asymmetric development of the heart, lung, spleen, liver and looping of the gut in the growing embryo. It remains to be determined how *Pitx2* regulates the asymmetric development of such a vast array of organs. Whilst *Nodal*, *Lefty1* and *Lefty2* have a short-lived, dynamic expression pattern which ceases after 6-8 hours, *Pitx2* expression persists after Nodal expression is over. At this time, *Pitx2* expression is maintained by Nkx2.5 (Shiratori et al., 2001). This upregulates *Pitx2* expression during organogenesis.

2.1.2. *lrm4* is an ENU-induced allele of *Pkd2*

Ermakov and colleagues carried out a G3 ENU-based recessive genetic screen to identify novel genes involved in L-R patterning (Ermakov et al., 2009). A G3 screen is designed to identify recessive mutations. G0 BALB/c male mice were subjected to ENU mutagenesis. These males were crossed to Wt C3H/HeH (C3H) females. Their offspring, the G1 carriers, were outcrossed to C3H females to give G2 mice and these were finally backcrossed to G1 males (Gondo et al., 2010, Acevedo-Arozena et al., 2008). This breeding scheme segregates mutations and mice are selected by virtue of their phenotype. This forward genetics

approach produces a wide variety of mutations so that novel genes of interest can be detected.

During the screen, G3 embryos were examined at E9.5 or E13.5 for gross developmental and situs defects. At these stages, the L-R axis has been established and organ situs can be assessed. A proportion of the lines studied at these stages exhibited consistent mutant phenotypes over several litters, indicating heritable mutations. Overall, 135 pedigrees were analysed of which 11 were identified with L-R patterning defects. These fell into two categories; a group with classical L-R defects and a second group with more complex traits. The classical group were designated left-right-mutant-1 to 5 (lrm1-5) and presented with simple organ situs defects affecting the lungs, stomach, heart and vasculature. The second group presented with ciliopathy related defects (Gpg1-6).

Left-right-mutant-4 (lrm4) presented with marked oedema, situs defects and cardiac patterning defects (Ermakov et al., 2009) and was selected for further analysis. Initial phenotyping was carried out on a mixed genetic background. The mice were also likely to incorporate additional mutations from the ENU mutagenesis. Since ENU mutagenesis is not targeted, it is possible that the phenotype seen in the original screen could be interwoven with phenotypes caused by other mutations throughout the genome. In order to segregate the causative *lrm4* phenotypic mutation, mice were backcrossed until congenic on a C3H background for over 10 generations (Field et al., 2011). These congenic mice were then used for further study.

lrm4 was mapped to a 38Mb region on mouse chromosome 5. Candidate gene sequencing revealed that lrm4 is a mutation in the *Pkd2* locus. $Pkd2^{lrm4}$ is a point mutation at a conserved residue in the first extracellular loop of PKD2. The mutation causes a single amino acid substitution at residue 442; replacing a negatively charged glutamic acid with the smallest amino acid glycine. At the DNA level, an Adenine to Guanine transition occurs at base 1331, which is the third base of the codon (GGA>GGG) in exon 5. More detail about the molecular phenotyping of *lrm4* can be found in **chapter 5**.

The initial screening of the *lrm4* phenotype is summarised in the first column of **Table 2.1**. These mice were on a mixed genetic background. Characterisation of $Pkd2^{lrm4}$ on a congenic C3H-HeH background is detailed in column 2 of **Table 2.1** (Field et al., 2011).

Table 2.1: Characterisation of *Pkd2*^{lrm4} mouse line

Column 1 summarises the initial phenotyping of *Pkd2*^{lrm4} on a mixed genetic background. Column 2 summarises the same organ phenotyping panel in addition to a panel of molecular expression patterns on a congenic C3H background. For each aspect assessed, the age at which the assessment was undertaken is in brackets.

	***Pkd2*$^{lrm4/\ lrm4}$** (Ermakov et al., 2009)	***Pkd2*$^{lrm4/\ lrm4}$** (Field et al., 2011)
Turning (E9.5)	Not analysed	Random (36% SS, 64% SI)
Heart apex (E13.5)	Random (46% SS, 50% SI, 4% mid)	Random (52% SS, 41% SI, 7% mid)
Stomach situs (E13.5)	Random (46% SS, 50% SI, 4% mid)	Random (63% SS, 26% SI, 11% mid)
Lung (E13.5)	RI (71% RI, 11% PI, 7% SS, 7% SI, 4% LI)	RI (97% RI, 3% SS)
Oedema (E13.5)	64%	94%
Node *Cerl2* (E9.5)	Not assessed	Lost bias (75% Sym, 16% RB, 8% LB)
Node *Nodal* (E9.5)		Symmetric (100%)
LPM *Nodal* (E9.5)		Absent (100%)
Lefty1 &2		Absent (100%)
LPM *Pitx2*		Absent (100%)
Survival	Significant survival at 13.5, later stages not assessed	Failed to survive significantly beyond E14.5
Background	Mixed	C3H/HeH

SS= situs solitus; SI=situs inversus; mid=midline; RI=right isomerism; LI=left isomerism; RB=Right Bias; LB= Left Bias, PI= partial isomerism, Sym= symmetric

The *lrm4* line exhibited randomisation of stomach and cardiac positioning, and right isomerism of the lungs. This indicates a failure to initiate the *Nodal* cascade in the L-LPM. After crossing onto a congenic background, heart and stomach patterning remained consistently randomised. Oedema markedly increased from 64% to 94% and right pulmonary isomerism increased from 71% to 97% penetrance. However, oedema is difficult to score at E13.5 and it is likely that oedema would be seen at a higher rate in older embryos.

Pkd2 is expressed ubiquitously during the establishment of L-R development. The situs defects of *Pkd2*$^{lrm4/lrm4}$ are strikingly similar to those of engineered *Pkd2*$^{-/-}$ mice (Pennekamp

et al., 2002, Wu et al., 2000, Yoshiba et al., 2012). Molecularly, normal left-biased asymmetry of *Nodal* at the node is lost and this disrupts the rest of the downstream Nodal cascade members. This leads to the supposition that *Pkd2*^{lrm4} is a null allele (Ermakov et al., 2009). In each case, when *Pkd2* is disrupted, a portion of resultant embryos exhibit oedema, situs and organ structure defects much like those seen in the *Pkd2*^{lrm4} line (Wu et al., 2000, Garcia-Gonzalez et al., 2010).

Nodal and *Cerl2* require a specific balance to initiate the *Nodal* cascade in the L-LPM. This loss of *Nodal* cascade initiation in *Pkd2*$^{lrm4/lrm4}$ embryos indicates that *Pkd2* is involved in the communication of the asymmetric signal from the node to the LPM. This mechanism possibly also involves calcium signalling at the node. However, calcium asymmetry was not scored in these embryos. Node and cilium structure assessed by SEM was normal (Field et al., 2011). Ciliary motility was also found to be normal (Grimes et al., 2016). This argues that *Pkd2* acts downstream of cilia motility yet upstream of the *Nodal* cascade. Embryos did not survive to birth in either cohort, likely as a result of cardiac defects.

2.1.3 PKD2^{lrm4} mislocalises in the node and retains channel function

PKD2 localises to the crown and pit cell cilia in the node (McGrath et al., 2003, Yoshiba et al., 2012). Yoshiba et al examined *Pkd2* expression using a PKD2::Venus fusion protein. Transgenic expression of PKD2::Venus in the crown cells of *Pkd2*$^{-/-}$ mice rescued the laterality defects. They next analysed a number of mutant alleles of *Pkd2*, including *Pkd2*^{lrm4}. The exogenously expressed *Pkd2*^{lrm4}::Venus construct was unable to localise to cilia at the node in *Pkd2*$^{-/-}$ embryos and LLC-PK1 cells (Yoshiba et al., 2012). When assessed endogenously at the node of *Pkd2*$^{lrm4/lrm4}$ embryos, Grimes et al found that *PKD2*^{lrm4} could not localise to node cilia (Grimes et al., 2016). Nonetheless, when assessed for calcium channel activity, *Pkd2*^{lrm4} was found to retain calcium channel function (Yoshiba et al., 2012).

2.1.4 Cilia and the kidney

Due to the pleiotropic nature of the cilium, defective ciliary function or disruption of proteins associated with cilia have a broad affect throughout the body. A connection between laterality defects and renal cysts has arisen from several mouse lines, indicating a role for cilia in cystic kidney disease (Igarashi and Somlo, 2002).

In fact, the oak ridge polycystic kidney (orpk) mouse was the first mammalian model to establish a link between cystic kidney disease and cilia function (Moyer et al., 1994, Pazour et al., 2000, Taulman et al., 2001, Pazour et al., 2002) . The orpk mutation is a recessive mutation in *Ift88* (*polaris*), made by random transgenic insertion into an intron, creating a hypomorphic allele. *orpk* partially disrupts the expression of IFT88, which is required for cilium assembly and to carry non-membrane bounded proteins from the cell body along the cilium (Rosenbaum and Witman, 2002, Pazour et al., 2000). The hypomorphic nature of the $Ift88^{orpk}$ allele allowed homozygotes to survive to adulthood and therefore provided a useful model of renal disease (Lehman et al., 2008). $Itf88^{orpk/orpk}$ mice have short cilia with distal bulges which accumulate PKD2, in cystic and non-cystic renal tubules (Pazour et al., 2002). This suggests that development of renal cysts in the orpk mouse could be mechanistically linked to development of PKD2 associated renal cysts in Polycystic Kidney Disease, perhaps due to PKD2 being unable to localise along the full length of the cilium. Murcia et al engineered a null allele (Murcia et al., 2000) and $Ift88^{orpk/-}$ compound-heterozygotes were found to exhibit cystic lesions of the kidney, liver and pancreas. Mice also failed to establish a L-R axis and displayed polydactyly and neural tube defects. Cilia in the kidney and at the node were shortened or absent, and abnormalities of the structure of the node were observed. In addition, bilateral expression of *Lefty2* and *Nodal* was observed in the LPM. *Nodal* was symmetrically expressed around the node, with no left bias (Murcia et al., 2000). This further exposes the role of cilia in both L-R patterning and kidney development.

Another mouse model with L-R axis and kidney defects is Inversin (Invs). Like orpk, *Inversin* is also a random insertion mutant and exhibits renal cysts along with organ situs defects (Yokoyama et al., 1993). Embryos displayed consistent *situs inversus* of both organ patterning and molecular events during development. *Invs* was demonstrated to be upstream of the *Nodal* cascade as asymmetric *Nodal* (Lowe et al., 1996, Collignon et al., 1996) and *Lefty* (Meno et al., 1996) gene expression was reversed. In addition, abnormally slow flow across the node was observed despite cilia rotating at a similar speed to those of wildtype embryos (Okada et al., 1999). Flow across the node was more turbulent, similar to that seen at earlier stages of development before flow has matured, yet unexpectedly was found to be leftward. Deformation of the node and aberrant cell masses also disturbed the flow across the node. Artificial flow was able to rescue the L-R patterning defects of

cultured *Invs*/*Invs* embryos correcting heart looping and embryonic turning. This indicated that *Invs* affects flow rather than sensation of flow in the mutant embryos (Watanabe et al., 2003). *Inversin* was shown to localise to primary cilia of MEFs and in the cilia of the node (Watanabe et al., 2003). Upon examining other 9+0 primary cilia, Watanabe and colleagues found that *Inversin* also localises to cilia of epithelial cells of the renal collecting duct, the pituitary gland and retina. When 9+2 cilia were examined, *Inversin* was absent, being found only in the cytoplasm. The authors argue that *Inversin* preferentially localises to 9+0 cilia but not 9+2 cilia and that *Invs* may be involved in the motility of 9+0 node pit cilia and play a sensing role in 9+0 immotile primary cilia.

Homozygous *Invs/Invs* mice die within a few weeks after birth due to liver and renal failure (Yokoyama et al., 1993). The abundance of *Invs* expression in the renal proximal tubule cilia correlated with the severity of cysts seen in newborn kidneys of *Invs/Invs* mice indicating a role for *Invs* in these cilia (Watanabe et al., 2003). *Invs* has been identified as the gene mutated in infantile nephronophthisis (Otto et al., 2002) and has been shown to interact with nephrocystin in renal cilia (Otto et al., 2003).

Another model of cystic kidney disease which displays L-R patterning defects is the juvenile cystic kidneys (jck) mouse. This is associated with a missense mutation in *Nek8*, a ciliary kinase. To study *Nek8* function, a null allele was generated. *Nek8*$^{-/-}$ mice died at birth and exhibited laterality defects including randomised situs, cardiac defects, and glomerular kidney cysts (Manning et al., 2012). NEK8 localises at the base of renal epithelial cilia, but cilia morphology and function was normal in *Nek8*$^{-/-}$ mice, indicating that the function of NEK8 is downstream of ciliogenesis. Of embryos assessed, 61% exhibited right pulmonary isomerism along with randomised abdominal situs and mostly absent *Nodal* and *Pitx2* from the L-LPM. This is markedly similar to *Pkd2*^{tm1Dwo} (Pennekamp et al., 2002), in fact NEK8 and PKD2 have been shown to physically interact (Sohara et al., 2008). Manning et al indicated that the PKD2-associated calcium response in *Nek8* knockdown IMCD cells is diminished, indicating that NEK8 interactions could affect the PKD2 channel (Manning et al., 2012).

Clearly genetic links exist between cilia, situs and cystic kidney disease. Mutated genes have been shown to cause both renal cysts and L-R patterning phenotypes (Polaris (*Ift88*), Inversin (*Invs*), *Nek8* and the Polycystins). These links also strengthen the hypothesis that

cilia are highly important organelles during development, both in the establishment of the L-R axis and during renal development. It is clear that disruption of genes which localise to cilia in the kidney cause renal cyst development. PKD2^{lrm4} has been shown to lose ciliary localisation in the node when expressed both endogenously (Grimes et al., 2016) and exogenously (Yoshiba et al., 2012). *Pkd2$^{lrm4/lrm4}$* mice also exhibit situs defects yet the renal phenotype has not yet been reported. The *Pkd2^{lrm4}* allele is an interesting allele to study because it retains calcium channel function. The specific characteristics of *Pkd2^{lrm4}* allow interesting dissections of the requirement of function and localisation within the cell.

2.2 RESULTS

2.2.1 Embryonic lethality- assessing genetic background

Analysis of *Pkd2$^{-/-}$* (Wu et al., 2000) and *Pkd1$^{-/-}$* (Lu et al., 1997) mice indicate that embryonic kidney cysts first become evident at E15.5. Field et al report that *Pkd2$^{lrm4/lrm4}$* embryos on the C3H background fail to survive significantly past E14.5 (Field et al., 2011), preventing assessment of the kidney phenotype at an appropriate stage. Assessment of *Pkd2$^{lrm4/lrm4}$* embryos indicates that disrupted situs and cardiac defects, as indicated in **Table 2.1**, could be responsible for the embryonic lethality. It is clear that strain differences are a confounding factor when assessing phenotypes and that strain specific variation can be exploited to modify the survival of a line. Therefore, mice were crossed onto different genetic backgrounds to assess survival.

Firstly, the CD1 background was selected to assess whether the effect of a more outbred background would modify embryonic survival. CD1 mice originate from a non-inbred stock of Swiss mice and are larger in size and develop slightly faster than most inbred lines.

To assess embryonic phenotypes, timed mates were set up. Pregnant females were identified by the presence of the vaginal plug after mating. Since mating usually occurs at midnight, midday on the first day of gestation is considered to be E0.5. C3H males carrying *Pkd2^{lrm4}* were selected and matings were set up with CD1 mothers, to produce litters yielding CD1-Pkd2$^{lrm4/+}$ F1 mice. These mice were genotyped for the *Pkd2^{lrm4}* allele by the lrm4-genotyping method (**MM:1.1.2)**. *Pkd2$^{lrm4/+}$* mice were selected to perform intercrosses in sibling matings and subsequent litters were analysed. Twelve F2 and nine F3 litters of

embryos were harvested for analysis at E15.5 and assessed for survival, situs defects and external kidney appearance. Where dead embryos were recovered, time of death was estimated. Embryos were genotyped for the *Pkd2*^{lrm4} allele. No homozygotes survived to E15.5. The majority of embryos died between E12-13.5 as recorded in **Table 2.2** and **Fig 2.3**. Despite being more outbred, the CD1 background did not increase embryonic survival past E15.5. In fact, CD1-*Pkd2*$^{lrm4/lrm4}$ embryos died earlier than those on a C3H background. This may be because these embryos develop slightly quicker than other strains and therefore reach a point where heart complications become lethal sooner **(Fig 2.4).**

Table 2.2: Analysis of embryos analysed for survival

The top row corresponds to analysis of the CD1-*Pkd2*^{lrm4} mice. Of the 6 litters analysed, 20 homs were obtained. Each column details the number of homs that survived to that age and the % indicates the percentage of homs that were alive at that point. The second row details the 12 litters of B6J-Pkd2^{lrm4} mice. These were smaller litters, yielding 27 homs in total.

	Litters analysed	**Survived until E12.5**	**Survived until E13.5**	**Survived until E14.5**	**Survived until E15.5**
CD1-*Pkd2*^{lrm4}	6 (20 homs total)	7 (35%)	6 (30%)	0 (0%)	0 (0%)
B6J-*Pkd2*^{lrm4}	12 (27 homs total)	25 (93%)	21 (78%)	16 (59%)	12 (44%)

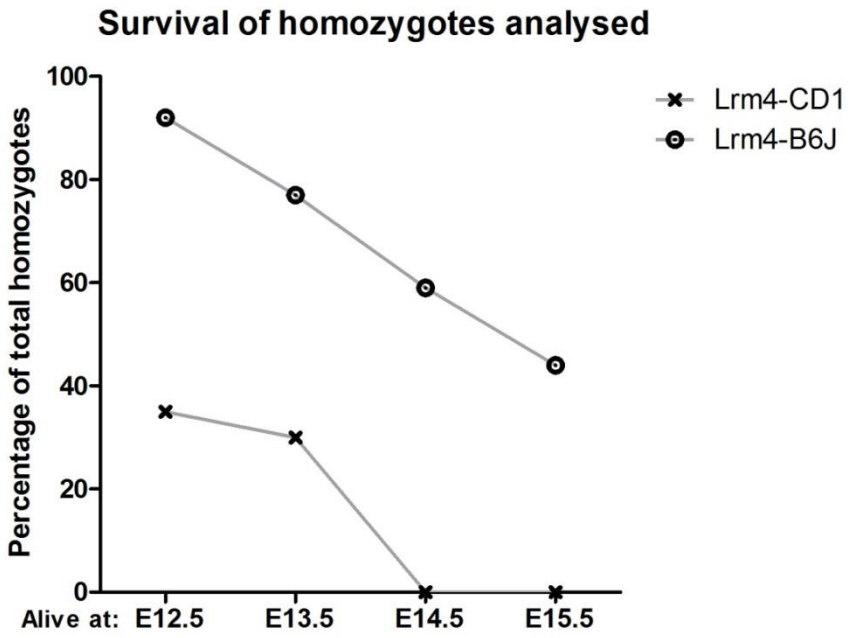

Chi-square	
Chi-square, df	35.46, 3
P value	< 0.0001
P value summary	****

Figure 2.3: Analysis of litters for embryonic survival

The table details the number of litters analysed at E15.5 for *Pkd2*$^{lrm4/lrm4}$ survival on a both backgrounds, the number of homozygous embryos recorded and the numbers of surviving embryos at each time point. The graph shows percentage of homozygous embryos surviving between E12.5 and E15.5.

Following analysis of CD1-*Pkd2*$^{lrm4/lrm4}$ embryos, another background was sought with the aim of modifying embryonic survival. Lu and colleagues report that background strain modified the craniofacial defects, heart defects and the associated embryonic lethality of *Fgf16* null mice (Lu et al., 2010). Their study compared *Fgf16*$^{-/-}$ mice on B6J and Black-Swiss (Bsw) backgrounds and found that the defects were severe on Bsw but were rescued after three backcrosses to B6J. In fact, the surviving *Fgf16*$^{-/-}$ mice survived to adulthood and did not display any morphological defects. This was further confirmed by crossing back to Bsw, which led to the reintroduction of the embryonic lethality, craniofacial and heart defects. Considering the power of genomic context and the possibility of increasing survival of embryos with cardiac defects, *Pkd2*^{lrm4} mice were crossed onto the B6J genetic background.

C3H-*Pkd2*$^{lrm4/+}$ males were selected and mated to B6J females. The resultant F1 males carrying the *Pkd2*^{lrm4} allele were used as studs to plug B6J-*Pkd2*$^{lrm4/+}$ females which were sacrificed for embryo harvest. Eight litters were analysed at G2 and 17 more after continued backcrossing. Litters were analysed at E14.5 and E15.5 for embryonic survival, situs defects and external renal morphology **(Fig 2.5)**. When analysed at E14.5, Mendelian ratios were observed and only 3 dead homozygotes were observed out of 65 embryos. At E15.5, a significant number of B6J-*Pkd2*$^{lrm4/lrm4}$ embryos had survived compared to other backgrounds **(Fig 2.4)**. Of the litters dissected at E15.5, only 30% of the homozygous embryos that were expected according to Mendelian ratios, survived. Nonetheless, this allowed the kidney phenotype to be assessed at an age where renal cysts are predicted to develop.

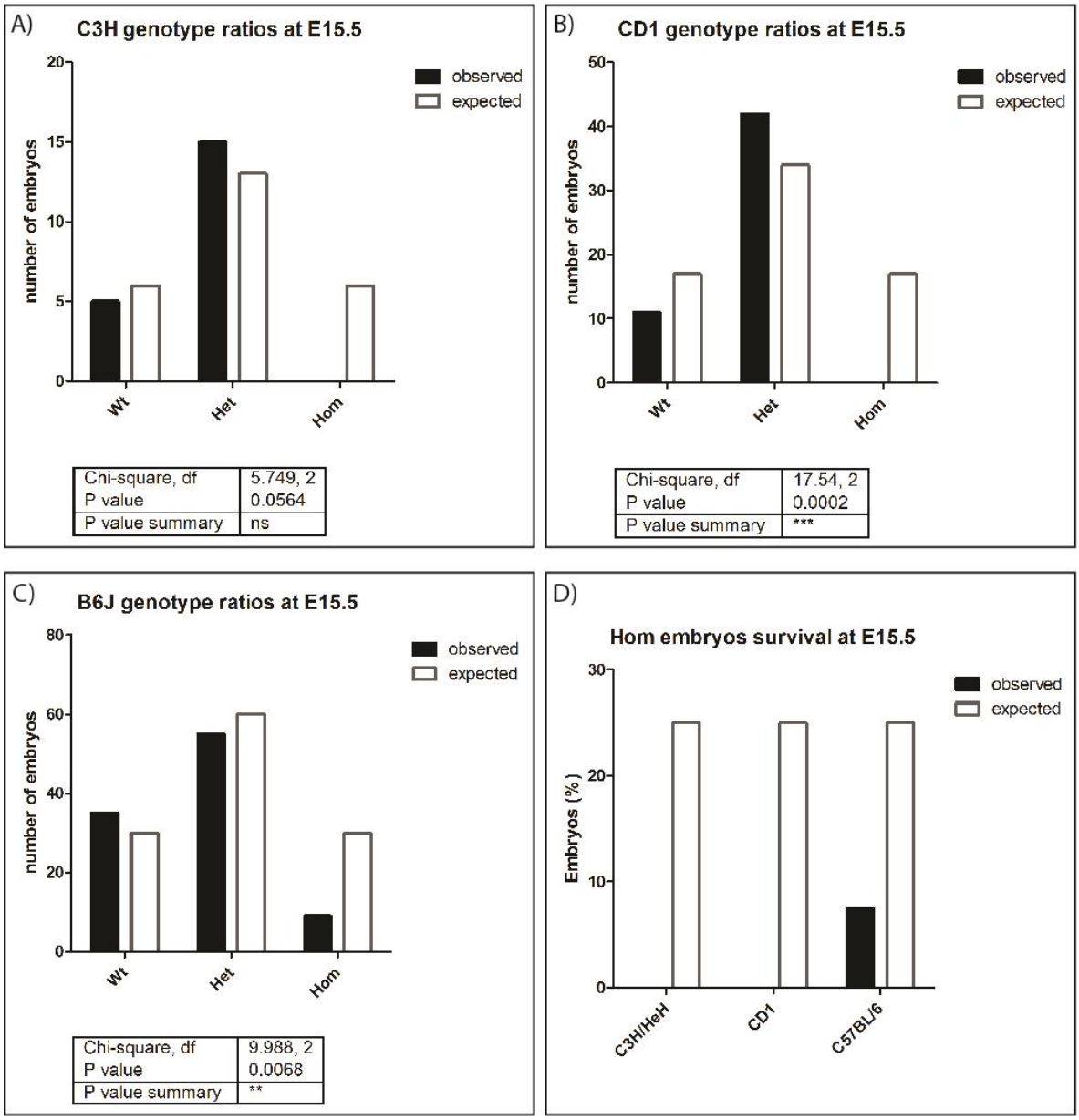

Figure 2.4: Survival of *Pkd2*$^{lrm4/lrm4}$ at E15.5 with different genetic backgrounds

Graphs showing survival of embryos comparing observed and expected ratios. The black column represents the observed surviving embryos at E15.5 and the white column in each graph represents the expected number of embryos. Graph A) details the survival of C3H-*Pkd2*$^{lrm4/lrm4}$ mice. No embryos were observed at E15.5. There mice were assessed in low numbers as they were the mice used for previous work that did not require later stages of embryonic development. It was clear from these numbers and previous studies (Field et al., 2011) that these mice did not survive significantly past E13.5. B) details the CD1-*Pkd2*$^{lrm4/lrm4}$ litters, again no homozygotes survived to E15.5. C) shows the ratios of B6J-*Pkd2*$^{lrm4/lrm4}$ embryos. A significant number of embryos survived to E15.5, yet this still departed from Mendelian ratios. Although a proportion of B6J-*Pkd2*$^{lrm4/lrm4}$ embryos were dying, 37.5% of homozygous embryos were observed with beating hearts indicating that they were still alive at E15.5.

Table 2.3: Analysis of situs in CD1- and B6J-Pkd2$^{lrm4/lrm4}$ mice

The table compares heart and lung situs between congenic *C3H-Pkd2*$^{lrm4/lrm4}$ embryos (Field et al., 2011) , *B6J-Pkd2*$^{lrm4/lrm4}$ embryos from early and late backcrosses. The *C3H-* embryos were scored at E13.5-E14.5 and the *B6J-* embryos were scored at E14.5-E15.5. Lungs which had an intermediate development of lung lobes e.g. 4:3 or 4:2, were marked as partial isomerisms.

	C3H-Pkd2$^{lrm4/lrm4}$ (Field et al., 2011)	***B6J-Pkd2***$^{Lrm4/lrm4}$ (backcrosses 1 and 2)	***B6J-Pkd2***$^{Lrm4/lrm4}$ (backcrosses 8 and 9)
Lung situs	RI (97% RI, 3% SS)	RI (100%)	RI (63% RI, 28% PI, 6% SI, 3% SS)
Heart situs	Random (52% SS, 41% SI, 7% mid)	Random (54%SI ,29% SS,17% mid)	SS (60% SS, 37% SI, 3% mid)
Oedema	100%	100%	100%
Homs scored	n=38 for lung =29 for heart	n=41	n=35
RI=Right Isomerism, PI=partial isomerism (e.g. lung lobes 4:2 or 4:3), SI=Situs Inversus, SS=Situs Solitus, mid=central			

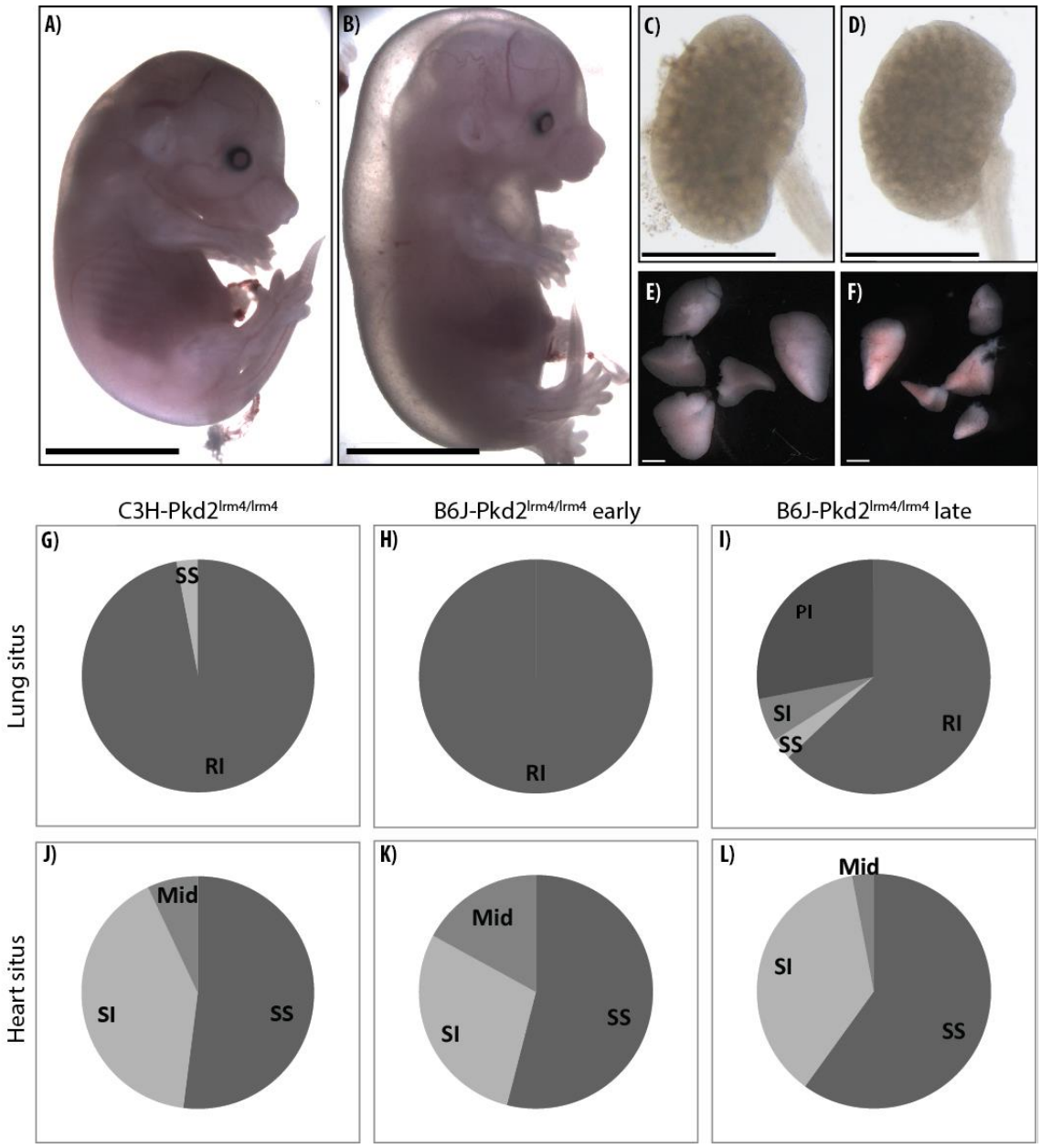

Figure 2.5: Embryo phenotypes at E15.5

B6J-Wt (A) and *B6J-Pkd2*$^{lrm4/lrm4}$ (B) littermates at E15.5, scale bar 5mm. *Pkd2*$^{lrm4/lrm4}$ embryos exhibit gross oedema (B). *Pkd2*$^{lrm4/lrm4}$ kidneys (D) appear externally indistinguishable from Wt (C). Scale bar 1mm. Lung situs is disrupted in *Pkd2*$^{lrm4/lrm4}$ embryos compared to Wt lungs (E). *Pkd2*$^{lrm4/lrm4}$ lungs exhibit situs defects, here showing situs inversus (F), scale bar 1mm. Pie charts G)-I) represent the lung situs scored in the first row of the table. J)-L) represent the heart situs scored in the second row of the table. "B6J-Pkd2$^{lrm4/lrm4}$ early" corresponds to the second column of **Table 2.3** which was scored at an early stage of backcrossing (backcross 1-2). "B6J-Pkd2$^{lrm4/lrm4}$ late" corresponds to the third column of **Table 2.3** detailing situs which was scored at a late stage of backcrossing (backcross 8-9). **RI=Right Isomerism, PI=partial isomerism (e.g. lung lobes 4:2 or 4:3), SI=Situs Inversus, SS=Situs Solitus, mid=central**

Dissections assessing organ situs were undertaken in parallel with embryonic survival assessment. Embryos were scored for the presence of oedema as well as lung and heart situs **(Fig 2.5)**. Right pulmonary isomerism was seen in 97% of C3H-*Pkd2*$^{lrm4/lrm4}$ embryos and this high proportion of right isomerism continued on the B6J background at early backcrosses before other lung situs arrangements started to appear. Since the B6J background conveyed survival to the line, *B6J-Pkd2*$^{lrm4/lrm4}$ mice were used in further experiments. Each embryo was assessed morphologically before being used for other experiments, therefore situs data was collected at various stages of backcrossing. Before the line was considered congenic, at early backcrosses, right pulmonary isomerism was fully penetrant. After continued backcrossing, the lung situs was modified and a higher proportion of partial isomerism was observed in the lung situs, possibly reflecting a higher proportion of the B6J genome.

2.2.2 Making a Pkd2^{-} allele

When assessing the renal phenotype of *Pkd2*$^{lrm4/lrm4}$ embryos and examining for the presence of cysts, a positive control for cyst development allows confirmation of cyst identification. Since *Pkd2*$^{-/-}$ kidneys are known to develop cysts at E15.5 (Wu et al., 2000), a *Pkd2*$^{-}$ allele was sought to provide a positive control for *Pkd2* induced cyst development.

To generate the *Pkd2*$^{-}$ allele, a floxed allele of *Pkd2* was imported as sperm from the Jackson Laboratory. The allele (**Fig 2.6**) was recovered by IVF at Harwell. Of the 47 founders, 22 pups were female and 21 were male (4 were dead). Homozygous *Pkd2*^{flox} mice are viable, fertile, normal in size and display no gross physical or behavioural abnormalities.

These mice were used to produce a deleted allele, detailed below, and in the conditional cross which is detailed in **Chapter 4**.

The *Pkd2*^{flox} allele carries LoxP sites flanking exons 11-13 (**Fig 2.6)**. Cre-mediated recombination deletes exons 11-13, causing a frameshift which produces a stop codon (UAG) in exon 14. Exons 11-13 encode part of the C-terminal cytoplasmic tail of PKD2. When deleted, the *Pkd2*$^{-}$ allele does not yield protein which could be detected by either an N- or C-terminal antibody by Western blot (Garcia-Gonzalez et al., 2010).

A deletion allele of *Pkd2* was made by crossing the *Pkd2*$^{fl/fl}$ mouse with an Actin-cre mouse line to delete the floxed allele. Actin-cre is a ubiquitous Cre-expressing line that is maintained on a C57BL/6Ntac background. After this cross, the Cre was segregated from the line by crossing to B6J. This line was maintained as a heterozygous colony on a congenic B6J background. These mice were viable, fertile and did not display any abnormalities. A het intercross of these mice resulted in *Pkd2*$^{-/-}$ embryos.

To assess deletion of the *Pkd2*^{flox} allele, E14.5 kidneys were dissected, dried and frozen in liquid nitrogen. After genotyping, 3 pairs of kidneys were pooled by genotype and lysed in RIPA buffer with added protease inhibitors. Protein levels were quantified by Bradford protein quantification assay and Western blotting for PKD2 was performed (outlined in **MM:1.3.4**). The membrane was imaged using the Odyssey SA image studio Licor system. Following this, densitometry of the bands was undertaken and each signal was normalised to the tubulin band for each sample. The *Pkd2*$^{-}$ allele produced no protein detectable by anti-PKD2 antibody whereas the floxed allele yielded a similar amount of protein as the wt. **Fig 2.6 C)**. Genotyping assays for the floxed allele and the deleted allele are detailed in **MM:1.1.4**.

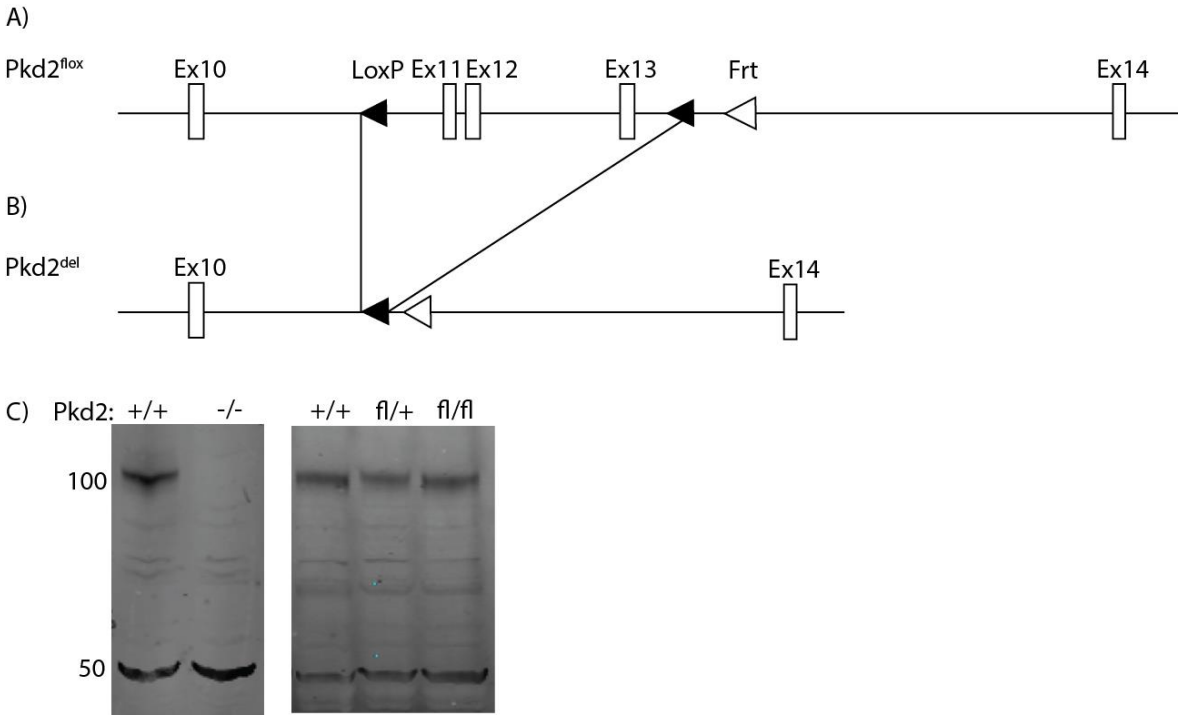

Figure 2.6: Schematic of Pkd2^{flox} allele and Pkd2^{-} allele

The *Pkd2^{flox}* allele A) has LoxP sites flanking exons 11-13 of *Pkd2*. After crossing to a line expressing cre recombinase, the floxed exons are deleted giving rise to the *Pkd2^{-}* allele B). C) Western blot analysis of E14.5 embryonic kidneys shows that the deleted allele (-/-) does not produce protein whereas the floxed allele (fl/fl) is indistinguishable from the Wt (+/+). The band at ~110 KDa corresponds to PKD2, the band at 50 corresponds to tubulin, the loading control.

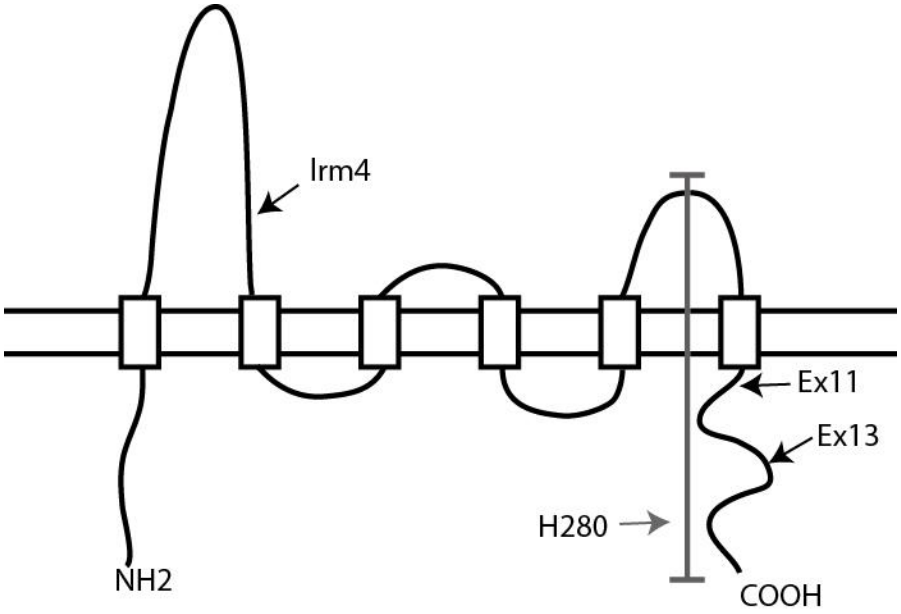

Figure 2.7: Schematic of PKD2 showing H280 epitope

lrm4 is a point mutation (E442G) in Exon 5 of *Pkd2,* in the first extracellular loop. The polyclonal H280 antibody recognises amino acids 689-968 of the human protein, to the right of the grey line. These constitute the whole of the cytoplasmic portion of the C-terminus and half of the final extracellular loop. Sequence corresponding to exons 11 (Ex11) and 13 (Ex13) is indicated (arrows).

All *Pkd2* alleles were assessed using the H280 antibody (sc25749), a rabbit polyclonal antibody raised against amino acids 689-968 of the C-terminus of human PKD2 (**Fig 2.7**). This corresponds to the entire cytoplasmic C-terminal tail of PKD2 and part of the final extracellular loop. The ability to detect PKD2 protein with H280 antibody does not appear to be disrupted in either $Pkd2^{fl}$ samples (**Fig 2.6 C**) or in $Pkd2^{lrm4}$ samples (**Fig 5.3 A**).

The loxP sites of the $Pkd2^{flox}$ allele flank exons 11-13. Cre-mediated recombination therefore deletes part of the sequence recognised by the H280 antibody. This may mean that $Pkd2^{-}$ protein is in fact produced but that it cannot be detected by this antibody. Garcia-Gonzalez et al. report that neither an N-terminal (Zymed-discontinued) nor a C-terminal (Sc2833) antibody could detect any protein produced by the deleted allele (Garcia-Gonzalez et al., 2010). However, both antibodies detected strong bands for $PKD2^{+}$ in total embryo lysate. The authors predict that Cre-mediated recombination produces a frameshift and STOP codon (UAG) in exon14 and no protein is detectable (Garcia-Gonzalez et al., 2010).

Since H280 is polyclonal, it is possible that it could still detect and bind to PKD2 where part of the recognition sequence had been deleted, and therefore could detect $PKD2^{-}$ if a

truncation had occurred from exon 11. Polyclonal antibodies are secreted from a mixed population of cell lineages and therefore within the collection of immunoglobins there exist specific antigens which react to different epitopes of the region to which they were raised. This means that within the population of immuoglobins raised against residues 689-968, it is likely that there are short antigens which can recognise sequences outside of the deleted exons.

Part of the immunogen against which the C-terminal antibody is raised flanks the deleted portion of *Pkd2*$^{-}$, it is therefore possible that H280 could pick up a portion of the remaining C-terminal tail.

Published work using our *Pkd2*$^{-}$ allele has not detected protein, using either C-terminal antibodies (Nie and Arend, 2014, Outeda et al., 2014, Ohata et al., 2015) or N-terminal antibodies (Garcia-Gonzalez et al., 2010). However, it remains possible that low levels of truncated protein could be made by the *Pkd2*$^{-}$ allele. To definitively ascertain whether *Pkd2*$^{-}$ completely ablated PKD2 protein production, further assessment is required. However, considering that the N-terminal antibody does not identify any protein, it is most likely that no protein is made.

2.2.3 Embryonic lrm4 kidneys develop cysts

Having established *Pkd2*^{lrm4} on a B6J background and achieved a significant survival rate for embryos at E15.5, dissections were undertaken to assess kidneys for the presence of cysts. At E15.5 the kidneys measure around 1mm in length, making dissection straightforward. First the head was removed and the thoracic cavity was opened, lungs and heart were removed for situs assessment. Next, the abdominal cavity was opened and the liver and intestines were removed. This provided a clear view of the kidneys which were extracted.
All of the B6J-*Pkd2*$^{lrm4/lrm4}$ embryos observed presented with oedema, and situs defects (**Fig 2.5)**. However when viewed externally with a light microscope, dissected kidneys appeared normal**.** Therefore, histological sectioning of the kidneys was necessary in order to assess their structure.

Embryonic kidneys were dissected, fixed in 4% PFA, dehydrated through a methanol series and washed through xylenes before being embedded in paraffin wax. Serial sections were

cut by microtome to a thickness of 4µm and stained with haemotoxylin and eosin (H&E). After H&E staining, clear structures within the kidney can be distinguished. Sections were imaged using a 20X lens on the Hamamatsu NanoZoomer whole slide imaging system.

Kidneys were assessed at E14.5 and E15.5 for the presence of cysts. At E14.5 three pairs of *Pkd2*$^{lrm4/lrm4}$ and six pairs of Wt kidneys were examined. At this stage, *Pkd2*$^{lrm4/lrm4}$ kidneys were indistinguishable from Wt littermates (**Fig 2.8**). These kidneys exhibit normal branching, a normal nephrogenic zone and are devoid of cysts.

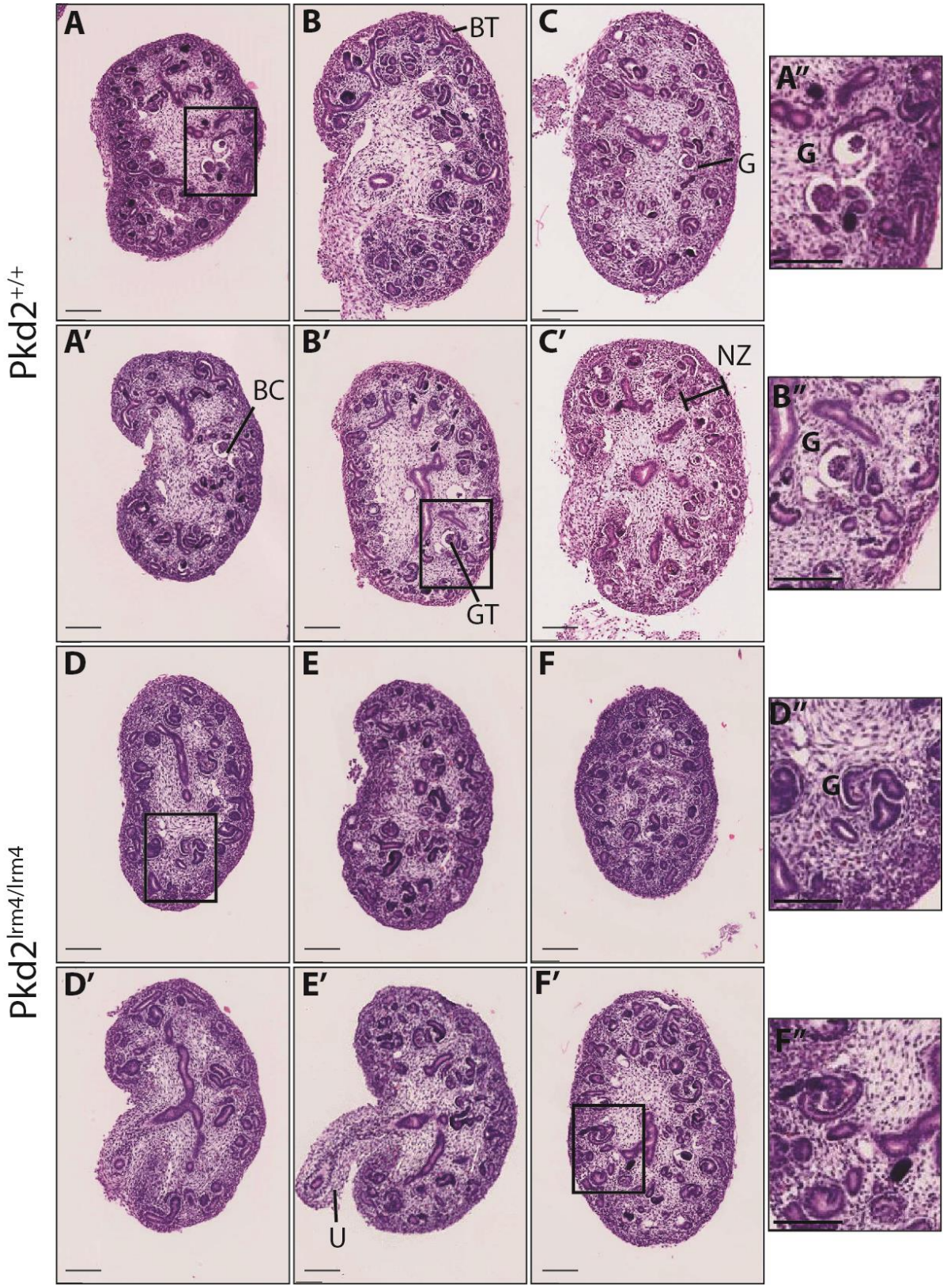

Figure 2.8: *Pkd2*$^{lrm4/lrm4}$ Embryonic kidneys at E14.5 are indistinguishable from Wt

At E14.5 Homozygous *lrm4* kidneys are indistinguishable from Wt kidneys. They have a normal branching pattern and normal nephrogenic zone and the medulla has yet to condense. No cysts are evident. A-C) show representative sections of the three pairs of Wt

kidneys examined. A) and A') show the pair of kidneys from the same embryo. A'') at the end of the row is an enlargement of the box in A). B'') is enlarged from B'). D-F) show three representative *Pkd2*$^{lrm4/lrm4}$ kidneys of the same age. D' is the kidney pair of D) and D'') is enlarged from the box in D). F'') is enlarged from the box in F'). BT=bifurcating tubule, G=glomerulus, BC=Bowman's capsule, GT=glomerular tuft, U=ureter, NZ=nephrogenic Zone. Both scale bars 100um.

In addition to *Pkd2*$^{lrm4/lrm4}$ kidneys, a number of controls were also assessed at E14.5. Kidneys from *Pkd2*$^{-/-}$ embryos were assessed as a positive control known to develop cysts at E15.5 (Wu et al., 2000). *Pkd2*$^{+/+}$ kidneys, that do not develop cysts at any stage, were used as negative controls. Indeed, at this stage kidneys of all genotypes examined were devoid of cysts (**Fig 2.9)**.

To assess kidney development, embryos were harvested at the same point each morning and assessed morphologically for indications of age. Kidneys were dissected, embedded and stained as previously described, before being scored. Estimated glomerular count was scored from a series of embryonic kidney sections and compared across genotypes. Obtaining an accurate estimate is not without challenge. Firstly, when scoring glomerular count histologically, care must be taken to count glomeruli in each section so that they are counted only once and so that none are overlooked. Estimates based on a subset of sections are inaccurate because glomeruli vary by size and shape; larger glomeruli will be over represented whereas smaller glomeruli will be missed (Bertram, 2013). Considering this, glomeruli were counted in every section from each kidney. Care was taken to count each glomerulus only once and to record the number of sections per kidney counted.

Ensuring that kidneys are at the same developmental stage reduces variation in glomerular count. Kidneys analysed at different stages may have gone through a different number of UB branching cycles which would lead to a different number of developed glomeruli. Apart from harvesting embryos from timed mates at the same time of day and assessing morphological aspects of embryos, it is difficult to guarantee that the embryos and thus the kidneys are at the same developmental stage. Five to ten kidneys (three to five pairs) were assessed per genotype at E14.5. Glomeruli were counted in an average of 63.6 sections per kidney. The length of each kidney was measure and it appeared that the number of glomeruli does not correlate with length suggesting that the kidney does not increase greatly in size at this stage while the glomeruli are maturing. The average kidney length was

918.6µm (733-1050 µm) and the average total glomerular count per kidney for *Pkd2*$^{lrm4/lrm4}$ was 19.3, for *Pkd2*$^{-/-}$ was 25.8, for *Pkd2*$^{+/+}$ was 21.5 and for *Pkd2*$^{-/+}$ was 25.1. The *Pkd2*$^{lrm4/lrm4}$ kidneys appeared slightly younger than other genotypes and this is reflected in glomerular count, one pair had yet to develop any glomeruli. Although the averages presented in the graph appear to be distinct and therefore significantly different, this is likely to reflect the unmatched developmental stage rather than a defect of *Pkd2*$^{lrm4/lrm4}$ development. The number of kidneys assessed would need to be greater to establish a correlation between glomerular count and developmental stage. The average number of glomeruli per section was indistinguishable from other genotypes when the pair of *Pkd2*$^{lrm4/lrm4}$ kidneys that had no glomeruli was ignored indicating that there is no difference in glomerular count across ages. However numbers were low.

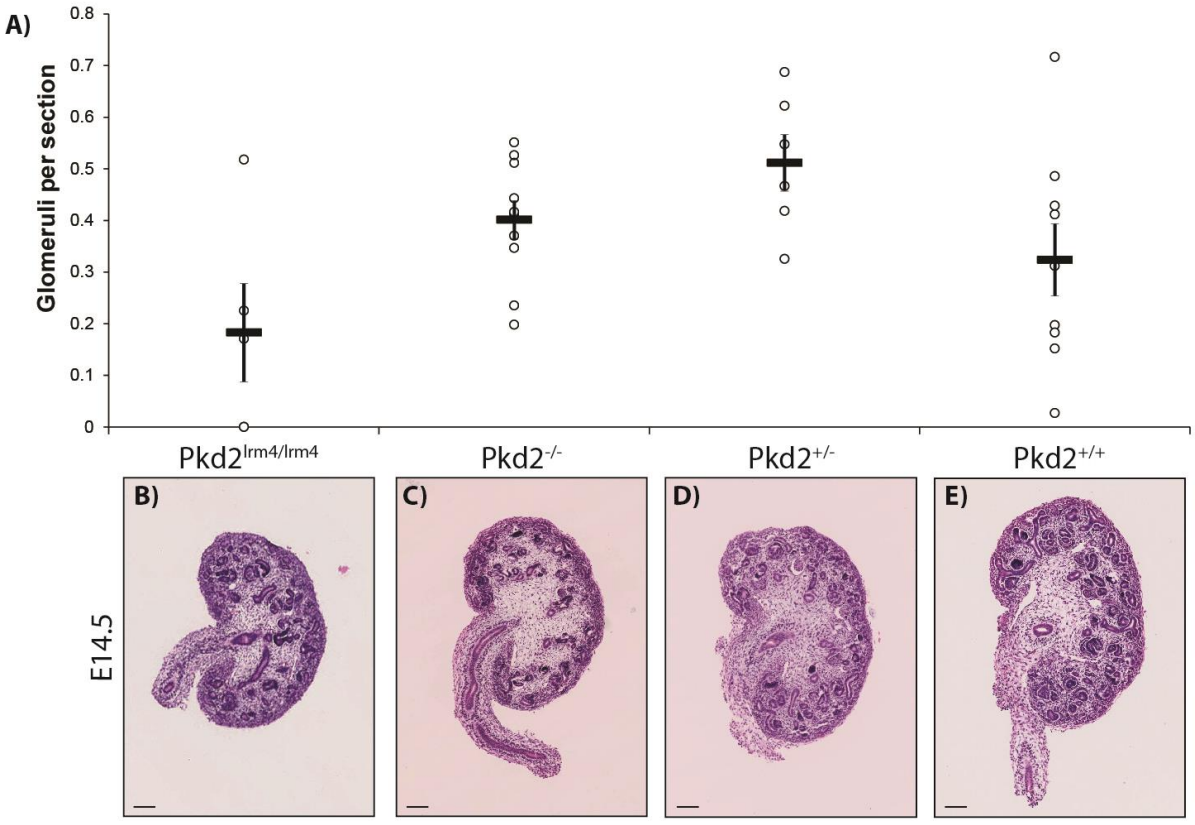

Figure 2.9: At E14.5 kidneys appear normal with a normal glomerular count and tubule architecture

For each genotype studied, normal development of the nephrons can be seen at E14.5. No cysts have developed. Speckles of mesenchymal cells can be seen on a matrix on connective fibres in the centre of the kidney, where the medulla has yet to form. The normal branching pattern of the UB and infolding of the tips to form the medulla can be seen. A) shows a

graph of glomerular count. For each genotype, between 3 and 5 pairs of kidneys were assessed. The graph shows the number of glomeruli per section counted, the average as a dark bar and error bars representing SEM. B) shows a representative image of *Pkd2*$^{lrm4/lrm4}$ kidney, C) *Pkd2*$^{-/-}$, D) *Pkd2*$^{+/-}$ and E) *Pkd2*$^{+/+}$ kidneys are shown. Scale bar 100um.

At E14.5, in the embryonic kidney, the future medullary region cannot be morphologically distinguished from the cortex. There is a sparse central area spotted with mesenchymal cells and the first glomeruli are beginning to form. However, as the kidney develops and more tubules are laid down a more complex picture emerges. The developing kidney represents an array of tubules of different maturities. The newest nephrons are induced at the periphery of the kidney with more mature tubules towards the centre. Therefore, multiple stages of nephron development can be observed throughout a single developing kidney (for example see **Fig 1.1**. detailing the development of the nephron, stages K)-O) were taken from the same E15.5 Wt kidney.)

By E15.5 the murine embryonic metanephros has gone through ~8-9 branching cycles (Cebrian et al., 2004). Cebrian et al report that the number of glomeruli has rapidly increased from ~80 at E14.5 to ~300 by E15.5 signifying an escalation of nephrons that have reached a mature state. This work was undertaken on Swiss Webster mice which are an albino outbred strain related to CD1. It is likely that these mice are slightly developmentally advanced, compared to B6J embryos, since we see fewer glomeruli at this point.

As tubules start to mature in the developing kidney, glomeruli begin to develop. The average glomerular count of E14.5 Wt kidneys was 21.5 per kidney which is vastly lower than ~80 observed in Swiss Webster embryos. This indicates that B6J kidneys develop later than Swiss Webster embryonic kidneys. Comparison of B6J-*Pkd2*$^{+/+}$ and *Pkd2*^{lrm4}/lrm4 kidneys indicates that kidney development is progressing normally in the mutant kidneys with a similar number of glomeruli forming at each stage; the average for Wt was 21.5 glomeruli compared to the two *Pkd2*^{lrm4}/lrm4 embryos which had developed glomeruli which averaged 19.3.

As the medulla starts to appear and condense, at around E15.5, the first stromal cells begin to develop. From this point to birth, the medullary volume rapidly increases (Cebrian et al., 2004). These features coincide with the sudden appearance of cysts in published *Pkd2*$^{-/-}$ and

Pkd1$^{-/-}$ kidneys at E15.5, possibly due to a sudden change in tension exerted on the tubules (Cebrian et al., 2004).

To assess E15.5 embryonic kidneys, dissections were carried out as with E14.5 kidneys. When examined for the presence of cysts, cysts were seen in *Pkd2*$^{lrm4/lrm4}$ kidneys at E15.5 (**Fig 2.10)**. This is a point which coincides with the development of glomeruli in the renal cortex. The number and maximum diameter of tubular dilations was measured in the central section. The central section gives a representation of all areas of the kidney and is the point where the kidney is at its longest. Dilations were counted if they exceeded 50µm since this is the average size of a glomerulus at this stage. The average dilation diameter in *Pkd2*$^{lrm4/lrm4}$ was 121.8µm (50.3-238µm). The largest cyst diameter (238µm) corresponds to 21.8% of its kidneys length. All *Pkd2*$^{lrm4/lrm4}$ cysts seen at this stage are glomerular. Each kidney had between 4-10 dilations.

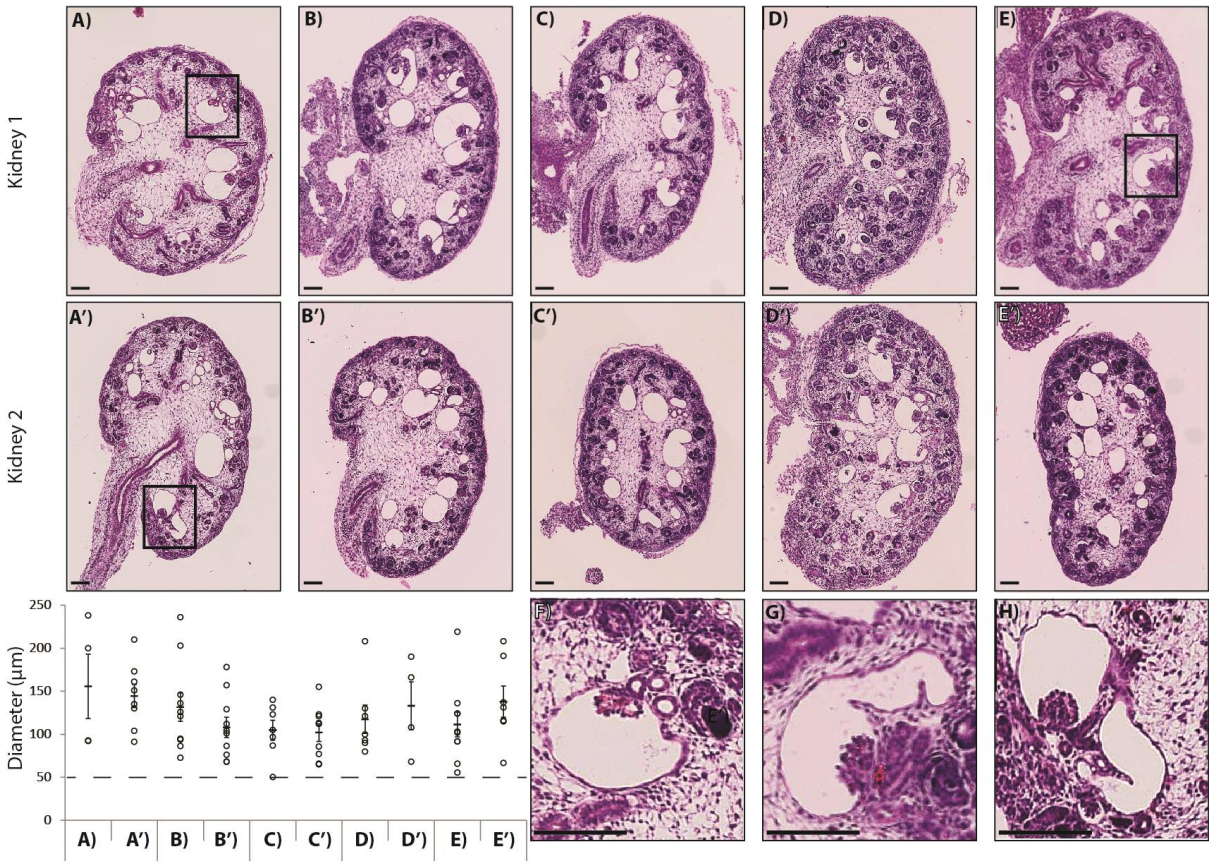

Figure 2.10: At E15.5 cyst develop in the *Pkd2*$^{lrm4/lrm4}$ embryonic kidney

All E15.5 *Pkd2*$^{lrm4/lrm4}$ embryonic kidneys examined developed a gross cystic phenotype. A)-E) are kidneys from 5 individual embryos. A')-E') are representative images from the other kidney in the pair. Bilateral renal cysts are evident in each case. F) is enlarged from the box

in A) and shows a glomerular cysts. On the irregular wall to the right of the cyst, the simple cuboidal epithelium of the proximal tubule can be seen. This portion would normally be adjacent to the glomerular tuft in Wt glomeruli. The smaller tubules near the vascular pole, close to the glomerular tuft are likely to be portions of the convoluted distal tubule which is associated with this glomerulus. G) is enlarged from the box in E) which shows an irregular shaped cyst which is associated with a glomerulus. H) is enlarged from the box in A'). H) shows a glomerular cysts with a thin cyst wall. An irregular shaped cyst can be seen to the right and a normal glomerulus to the bottom. The scale bar is 100um in each case. The graph shows the diameters of cysts seen in each kidney. The dotted line at 50µm shows the size of an average glomerulus. The error bars represent SEM.

2.3.4 Heterozygous kidney phenotype

Considering that ADPKD is a dominant condition, it seemed possible that kidney defects may be visible in *Pkd2*$^{lrm4/+}$ embryonic kidneys at this stage. When assessed at E15.5, renal cyst development was not observed. These kidneys have a normal nephrogenic zone devoid of cysts (**Fig 2.11**). *Pkd2*$^{lrm4/+}$ embryonic kidneys were indistinguishable from Wt kidneys in structure. Since *Pkd2*$^{lrm4/+}$ mice are viable, a cohort of these mice was observed through to adulthood and into old age and have been assessed in detail in **chapter 3.**

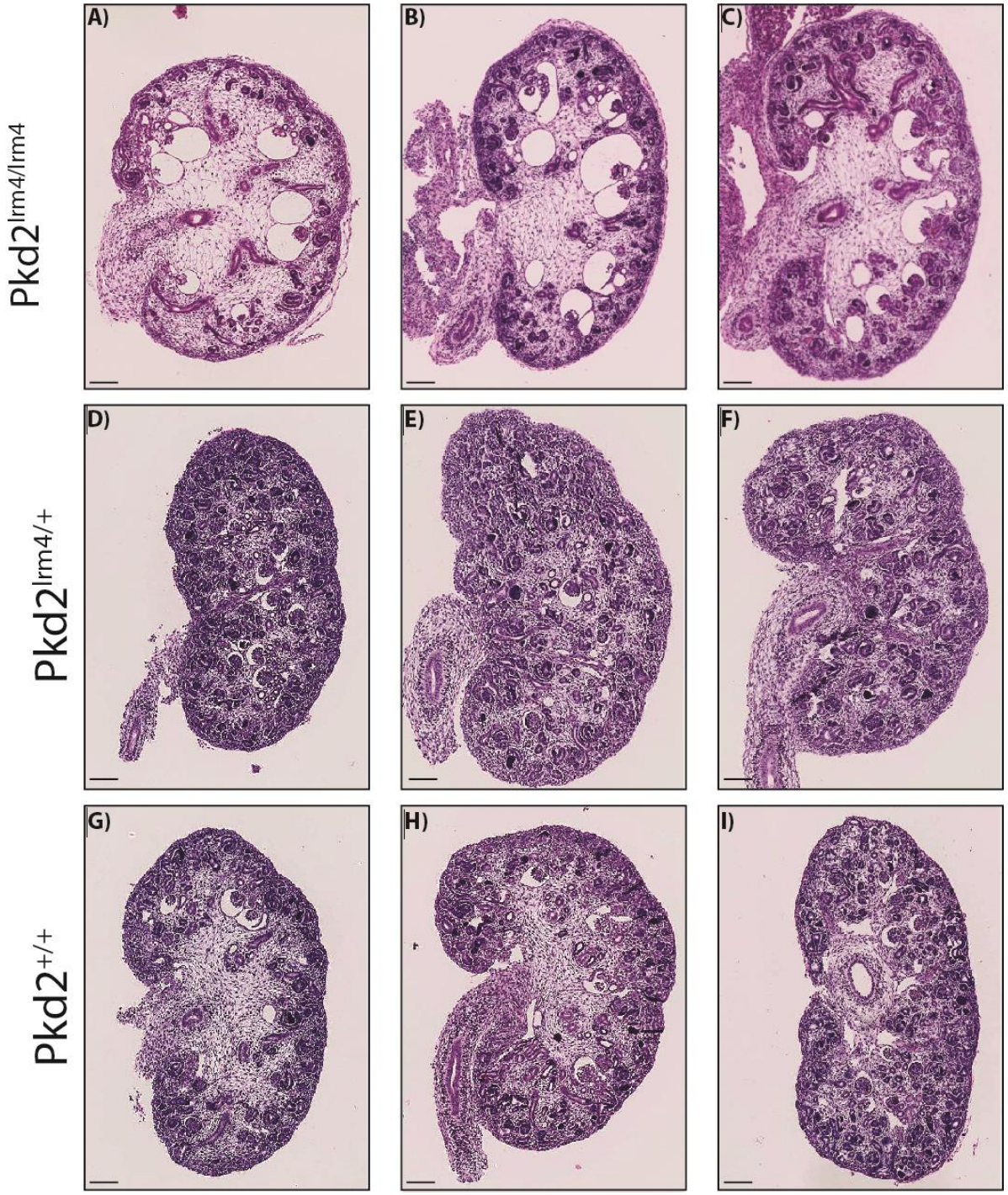

Figure 2.11: Heterozygous *lrm4* mice do not develop renal cysts at E15.5

A)-C) Cysts are evident in *Pkd2*$^{lrm4/lrm4}$ embryonic kidneys at E15.5 D)-F) *Pkd2*$^{lrm4/+}$ and G)-I) *Pkd2*$^{+/+}$ embryonic kidneys do not present with cysts at the same age. Scale bar 100um.

2.3.5 Comparison of Pkd2^{lrm4} to Pkd2^{-}

Pkd2$^{lrm4/lrm4}$ embryonic kidneys develop bilateral renal cysts which are visible at E15.5. To compare this cystic phenotype to an established null, embryos were harvested from pregnant mothers after intercrossing with male *Pkd2*$^{-}$ carriers. *Pkd2*$^{-/-}$ embryos were produced at a rate of 1:4 as per Mendelian ratios, although by E15.5 all embryos had significant oedema and were close to death.

Kidneys were harvested, fixed and processed for sectioning in the same way as *Pkd2*$^{lrm4/lrm4}$ kidneys, described earlier. *Pkd2*$^{-/-}$ embryonic kidneys were found to have significant bilateral cyst development throughout the kidney, (**Fig 2.12)**. A similar rate of glomerular cysts were seen in both *Pkd2*$^{lrm4/lrm4}$ and *Pkd2*$^{-/-}$ embryonic kidneys, indicating that the glomerulus is the first area to become cystic following Pkd2 disruption.

Cyst diameter was measured in *Pkd2*$^{-/-}$ kidneys and compared with *Pkd2*$^{lrm4/lrm4}$ diameters. Cysts were comparable in size and number. The average cyst diameters were 121.8µm in *Pkd2*$^{lrm4/lrm4}$ kidneys and 108.1µm in *Pkd2*$^{-/-}$, with largest diameters of 238 and 153µm respectively. Cyst diameters were not significantly different between the two sets of kidneys ($p=0.063$). The majority of *Pkd2*$^{lrm4/lrm4}$ cysts seen at this stage are glomerular. Glomerular cysts are also prominent in *Pkd2*$^{-/-}$ kidneys, both with our *Pkd2*$^{-}$ allele and others reported in the literature (Wu et al., 2000).

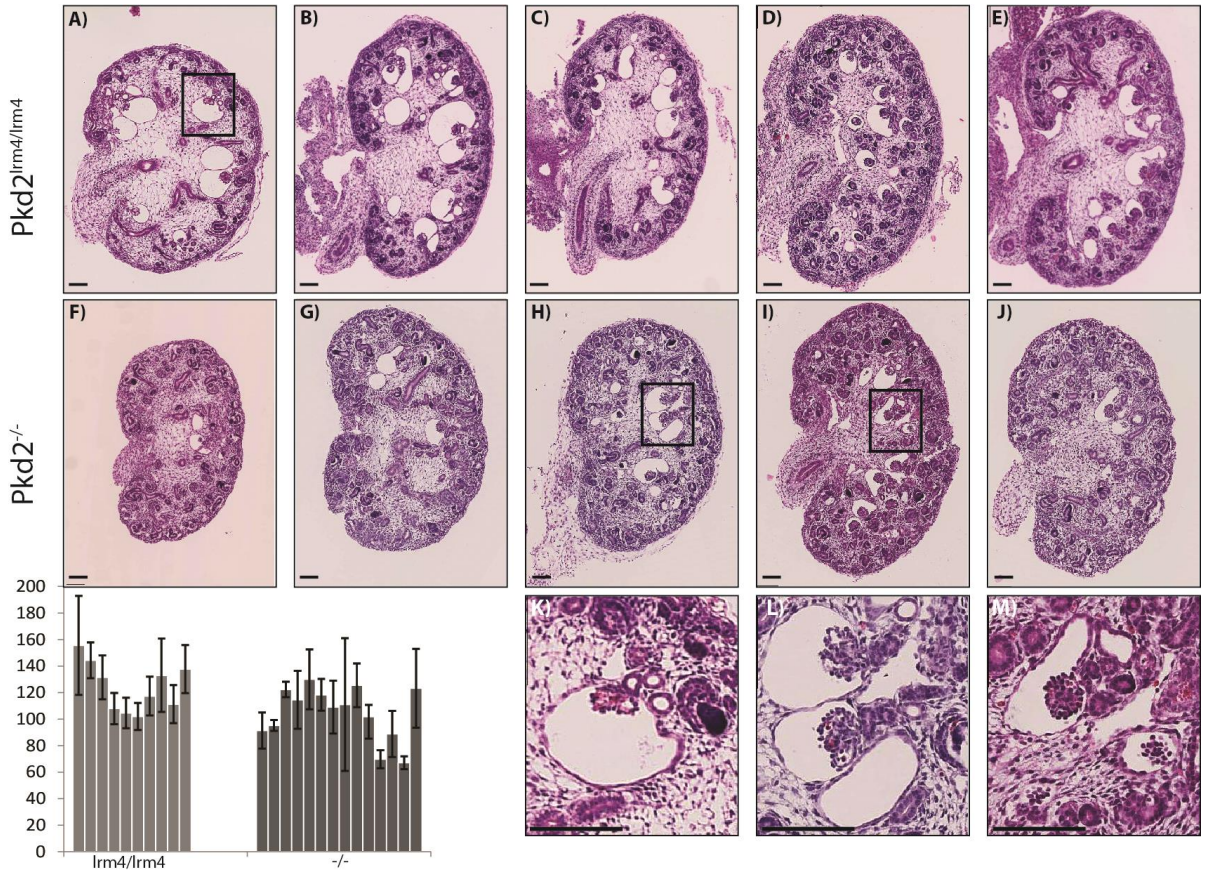

Figure 2.12: Both *Pkd2*$^{lrm4/lrm4}$ and *Pkd2*$^{-/-}$ embryonic kidneys develop cysts at E15.5

A)-E) are representative images of E15.5 embryonic kidneys from *Pkd2*$^{lrm4/lrm4}$ embryos. F)-J) are representative images of *Pkd2*$^{-/-}$ embryonic kidneys at the same stage. Both genotypes show bilateral renal cysts which are not evident at E14.5. K) is enlarged from the box in A). A cyst with a glomerular tuft can be seen, the irregular bulge to the right of the cyst is the beginning of the proximal tubule. L) is enlarged from the box in H). Two glomerular cysts can be seen along with a glomerular cyst which does not include a glomerular tuft. K) is enlarged from the box in I) and shows a cyst where the proximal tubule emanating from the glomerulus can also be seen to be dilated. The graph represents dilations measured in *Pkd2*$^{lrm4/lrm4}$ (light columns) and *Pkd2*$^{-/-}$ (dark columns) kidneys. Each column shows the average cyst size of each kidney and error bars representing SEM. Scale bars 100 µm.

A genetic non-complementation experiment was undertaken to further assess *Pkd2*^{lrm4}. A heterozygote intercross between mice carrying *Pkd2*^{lrm4} and mice carrying the *Pkd2*$^{-}$ allele was undertaken to produce compound heterozygotes. Ten litters of embryos were harvested at E15.5, resulting in 16 compound heterozygote embryos. These *Pkd2*$^{lrm4/-}$ embryos appeared externally similar to both *Pkd2*$^{lrm4/lrm4}$ and *Pkd2*$^{-/-}$ embryos of the same stage. All embryos had severe oedema as well as exhibiting situs defects such as pulmonary isomerism and cardiac patterning defects.

When kidneys were assessed, bilateral renal cysts were evident which appeared morphologically similar to those of *Pkd2*$^{lrm4/lrm4}$ and *Pkd2*$^{-/-}$ (**Fig 2.13)**. However, the cysts were significantly smaller (p= 0.00027), with an average size of 85.9µm (50-140 µm). The identification of cystic kidneys in *Pkd2*$^{lrm4/-}$ confirms that *lrm4* is an allele of *Pkd2*.

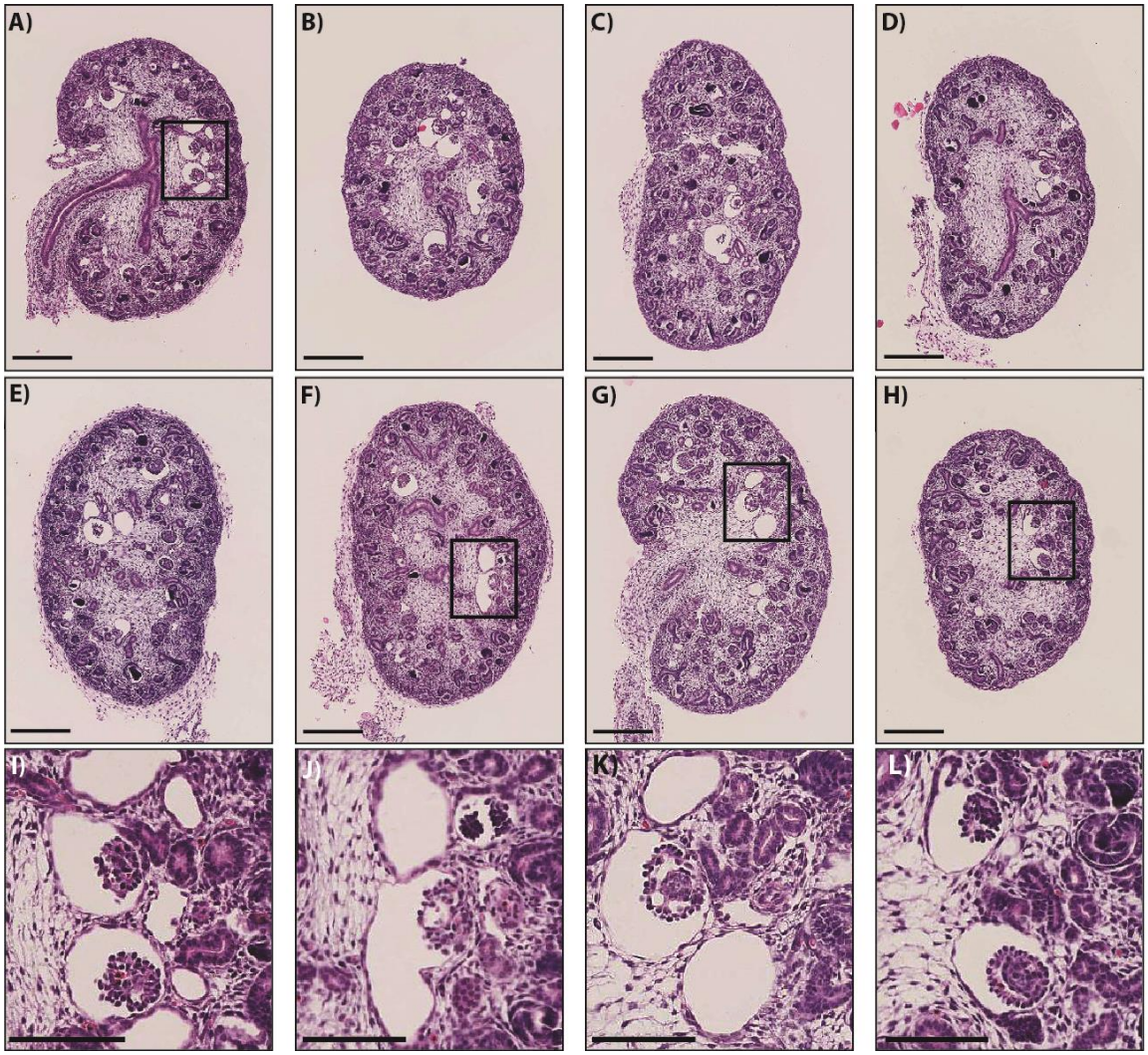

Figure 2.13: *Pkd2*$^{lrm4/-}$ kidneys develop renal cysts at E15.5

A)-D) are representative images of E15.5 embryonic kidneys from *Pkd2*$^{lrm4/-}$ embryos, E)-H) are the other kidney in the pair. Bilateral renal cysts are evident, confirming that *lrm4* is an allele of Pkd2. Scale bar 200µm. I) is enlarged from the box in A) and shows a pair of glomerular cysts. J) is enlarged from the box in F) and shows a glomerular cyst with an enlarged proximal tubule. K) is enlarged from the box in G) and shows a glomerular cysts and two other dilated tubules. L) is enlarged from the box in H) and shows two glomerular cysts, the uppermost exhibits a normal sized proximal tubule. Scale bar in I) is 100 µm.

2.3 Results Summary

In this chapter, the embryonic phenotype of *Pkd2*$^{lrm4/lrm4}$ has been discussed in detail and directly compared to *Pkd2*$^{-/-}$. At E15.5 *Pkd2*$^{lrm4/lrm4}$ embryos exhibit situs defects, gross oedema and organ patterning defects. When assessed at this stage, *Pkd2*$^{lrm4/lrm4}$ kidneys are shown for the first time to exhibit renal cysts. The development of the kidney is otherwise comparable to Wt, with a normal size and glomerular count. In corroboration with other *Pkd2* null alleles (Wu et al., 2000), B6J-*Pkd2*$^{-/-}$ kidneys develop cysts. The *Pkd2*$^{lrm4/lrm4}$ kidney cysts are comparable in size and number to the cysts seen in *Pkd2*$^{-/-}$ kidneys. Assessment of compound heterozygote *Pkd2*$^{lrm4/-}$ kidneys also revealed renal cysts, confirmed that *Pkd2*^{lrm4} is an allele of *Pkd2*.

These striking renal phenotypes indicate, for the first time, that *Pkd2*^{lrm4} is an allele that causes polycystic kidney disease, similar to the null allele. This work evaluating the allele of *Pkd2* has established an important cyst causing mutant which will provide insight into the mechanism behind cyst development in ADPKD.

2.4 Discussion

Pkd2 is a causative gene of ADPKD, mutations in which are evident in approximately 15% of patients (Cornec-Le Gall et al., 2014). A number of mutations in human *PKD2* are recorded in the PKD-database (PKDb, 2016), these range from neutral synonymous mutations to highly pathogenic deletions, frameshifts and nonsense mutations (PKDb, 2016). Single amino acid substitutions, like the *Pkd2*^{lrm4} mutation, range in severity from neutral to pathogenic, and are reported across almost every exon. The nature and location of these mutations throughout the gene leads to a spectrum of different phenotypes which range in severity. Therefore, analysis of specific mutations has the potential to provide significant insight into the mechanisms which control the disease and the specific domains which are required for PKD2 function. This provides insight into the pathogenesis of different disease causing variants.

The *Pkd2*^{lrm4} allele has been previously described (Field et al., 2011, Ermakov et al., 2009) in terms of the embryonic situs defects however, the kidney phenotype has not been characterised until now. It is clear from *Pkd2*$^{-/-}$ (Wu et al., 2000) and *Pkd1*$^{-/-}$ (Lu et al., 1997)

embryonic kidneys that renal cysts do not become visible until E15.5. The B6J genetic background extended embryonic survival of *Pkd2*$^{lrm4/lrm4}$ embryos to a point where the kidney phenotype could be analysed. Cysts were found to develop in the embryonic kidney at E15.5. The *Pkd2*$^{lrm4/lrm4}$ kidney phenotype was compared to that of *Pkd2*$^{-/-}$ and found to be striking similar. Both develop glomerular cysts yet present otherwise normal development of the surrounding renal structure. Both exhibit left right patterning defects with heart defects, oedema and a high proportion of right pulmonary isomerism. These similarities raise the question of whether *Pkd2*^{lrm4} is in fact a null allele, as suggested previously (Ermakov et al., 2009).

Kidney cysts develop after the complete inactivation of *Pkd1* (Lu et al., 1997) or *Pkd2* (Wu et al., 2000) throughout the kidney tubule cells or when cilia are ablated or unable to develop. The development of cysts and tubules, which are described as spherical or elongated monolayers of cells which enclose a central lumen, is proposed to be part of a normal epithelial monolayer development and contributes to branching of the developing kidney (O'Brien et al., 2002). Disruptions of the regulation of tubule formation, perhaps linked to planar cell polarity (PCP) (Fischer et al., 2006), Ca^{2+} signalling or cilia defects, lead to the cyst development which overtakes the ADPKD kidney. Mutations which cause shortened or absent cilia, such as those seen in the orpk mouse (Moyer et al., 1994, Pazour et al., 2002) , often cause a cystic renal phenotype. It is clear that ADPKD is a ciliopathy and that cilia are essential for the correct development and function of the kidneys (Patel et al., 2009). This strong link to the cilium compelled us to assess ciliary function, structure and development and this is presented in the following chapters.

It is possible that the *Pkd2*^{lrm4} mutation could affect ciliary development, function or signalling resulting in the cystic phenotype described here. Ciliary motility (Grimes et al., 2016) and structure (Field et al., 2011) have been previously found to be normal in *Pkd2*$^{lrm4/lrm4}$ node cilia. The specific localisation of the protein within the cell or to the cilium seems likely to be essential for its function. PKD2 is a ciliary localising protein which has been proposed to function as a mechanosensitive channel (Foggensteiner et al., 2000, AbouAlaiwi et al., 2009) along with PKD1 (Qian et al., 1997) within the ciliary membrane. Therefore, these elements of PKD2 function and localisation with respect to the mutant PKD2 protein could shed light on the mechanism causing the disease.

The embryonic development of cysts presented in this chapter is associated with a homozygous mutation in *Pkd2* which can be compared to the recessive form of polycystic kidney disease, ARPKD. Similar to ADPKD, ARPKD is characterised by a progressive increase in tubular diameter followed by cyst formation. *Fibrocystin* (*PKHD1*) is the causative gene of ARPKD, mutations in which cause dilation of collecting ducts which is distinct from cyst development along the whole nephron which is seen in ADPKD. Kidneys become enlarged and overtaken with cysts during development yet a once uniformly fatal disease has become survivable with the care of modern neonatal units; >70% of patients survive the newborn period and the majority of these go on to survive beyond ten years of age (Roy et al., 1997). Like ADPKD, the severity of ARPKD is also variable (Dell et al., 2016). Unlike ADPKD, heterozygous carriers of mutated *PKHD1* do not present with cystic kidneys.

Although disease presentation in ADPKD and ARPKD appears superficially different, similarities can be drawn between them (Kaimori and Germino, 2008). The Polycystins and Fibrocystin are all ciliary proteins: Fibrocystin is expressed on primary cilia and has been reported to interact with PKD2 (Wang et al., 2007). It is likely that they all function in a common pathway since disruption of PKD1, PKD2 or Fibrocystin results in disrupted mechanosensation of fluid flow in the kidneys and abnormal tubule morphology (Wang et al., 2007, Garcia-Gonzalez et al., 2007).

One difference between ADPKD and ARPKD is their associated laterality defects. While ADPKD patients sometimes exhibit situs defects (Bataille et al., 2011), patients with ARPKD do not. Unlike PKD1 and PKD2, Fibrocystin does not function in L-R axis development and does not localise to node cilia. It is likely that the spatial expression pattern of these genes contributes to the varied phenotype seen. Fibrocystin localises to cilia in the collecting ducts therefore mutant forms of *PKHD1* cause collecting duct cysts (Xiong et al., 2002). PKD1 and PKD2 localise to cilia along the length of the nephron and therefore in ADPKD cysts form in all parts of the nephron.

The majority of cysts in the $Pkd2^{lrm4/lrm4}$ embryonic kidney are glomerular. $Pkd2^{-/-}$ and $Pkd2^{lrm4/-}$ kidneys also exhibited glomerular cysts. This is in concordance with other *Pkd2* or *Pkd1* cyst causing mutations (Wu et al., 2000, Lu et al., 1997). The high proportion of glomerular cysts in rapidly developing embryonic kidneys has been noted in the literature,

although it is unclear why the glomerulus is the first portion of the kidney to display cysts. In ADPKD, cysts develop along the length of the nephron (Baert, 1978) and glomerular cysts are uncommon. ADPKD was previously thought to be the adult form of polycystic kidney disease, however presentation has been noted *in utero*, in infancy and in adolescence (Lennerz et al., 2010). Although embryonic cysts are not a common feature of ADPKD, when cysts are observed embryonically, glomerular cysts are the most common kind (Lennerz et al., 2010). ADPKD that is diagnosed *in utero,* or in the first year of infancy, is reported to manifest more severely than in affected family members diagnosed later in life (Guay-Woodford et al., 1998). Glomerulocystic kidney disease (GCKD) is a morphologically defined disease which describes a subset of individuals with ADPKD who develop cysts prenatally. GCKD is characterised by embryonic representation of cystic dilations of the Bowman's capsule and the nearby proximal tubule (Sharp et al., 1997, Bissler et al., 2010). Infants with GCKD who later present with ADPKD develop cysts in other parts of the nephron in addition to the glomerular cysts. It is possible that glomerular cysts are an indication of rapid renal cyst development and are therefore a sign of fast progressing disease. Slower forms of ADPKD which are noted in adult patients therefore do not present with glomerular cysts. Although cyst development in ARPKD is both rapid and severe, glomerular cysts are not observed. Fibrocystin is only localised to the collecting duct (Xiong et al., 2002) therefore it is unsurprising that mutations of *PKHD1* do not affect glomerular development in ARPKD.

In order to assess a slower progression of the disease associated with the $Pkd2^{lrm4}$ allele, a conditional allele has been utilised which circumvents the systemic effect of the mutation. This is described in the next chapter. This model allows $Pkd2^{lrm4/-}$ to be expressed specifically in the kidney, whilst the other tissues of the mouse retain a level of Wt *Pkd2* expression. This enables the assessment of cyst progression in adult mice and also provides a model of adult polycystic kidney disease.

The strong renal phenotype evident in the $Pkd2^{lrm4/lrm4}$ kidney is compelling, indicating that the $Pkd2^{lrm4}$ mutation provides an excellent avenue for insight into the disease. Yet this leads to a number of questions concerning several different aspects of the mutation, which will be addressed in the following chapters. For instance

1) How does the development of cysts progress into adulthood?

2) What is the nature of the mutation and how does it modify the function of the protein?
3) How does the *Pkd2*^{lrm4} allele differ, if at all, from the *Pkd2*$^{-}$ allele?

Understanding these aspects of the *Pkd2*^{lrm4} mutation will provide valuable insight into the mechanism behind the development and progression of polycystic kidney disease as well as understanding of how specific mutations can modify the function of PKD2 with respect to its function in cyst prevention.

Chapter 3: Adult *Pkd2*$^{lrm4/+}$ mice develop microcysts

3.1 Introduction

The previous chapter assessed the embryonic phenotype of *Pkd2*$^{lrm4/lrm4}$ embryos and revealed the development of grossly cystic kidneys in homozygous mutants. These mice die embryonically and therefore the adult phenotype cannot be assessed. In this chapter, adult phenotyping is undertaken in *Pkd2*$^{lrm4/+}$ mice to assess renal function after kidney development.

3.1.1 Extrarenal manifestations

ADPKD is pleiotropic, affecting multiple physiological systems, reflecting expression of *PKD1* and *PKD2* in multiple tissues. Although renal cyst development is the major clinical manifestation, the disease is complicated by other features including liver cysts, cerebral aneurysms, hypertension, mitral valve prolapse and cardiac structural defects. Both the renal and extrarenal manifestations vary between patients, due to variation in the specific mutation, genetic background and environmental factors.

Polycystic liver disease (PLD) is the most common extrarenal manifestation in ADPKD and has become more prominent with increasing survival associated with improved clinical care and renal replacement therapy (Hogan et al., 2015). Developing from biliary ducts and peribilary glands, liver cysts often remain asymptomatic but cyst development can lead to hepatomegaly which can cause pressure on the abdomen, intestine, stomach and diaphragm. Some patients may require cyst aspiration or liver resection in order to relieve this pressure. Pressure caused by cyst development can also cause obstructive jaundice. The frequency of cysts in the liver increases with age and is not a common feature of infantile ADPKD. PLD is more common in women than men and this is thought to be associated with oestrogen impacting the development of cysts (Reynolds et al., 2000). Although the majority of PLD cases are associated with ADPKD, PLD itself is a distinct autosomal dominantly inherited disease, caused by mutations in *PRKCSH* or *SEC63 (Wills et al., 2014)*.

Pancreatic cysts are present in 5% of patients and like other extrarenal manifestations, pancreatic cysts are diagnosed by MRI or ultrasound. In one study, pancreatic cysts were

found in 62% of patients who carried a mutation in PKD2 whereas only 25% of PKD1 mutated patients had pancreatic cysts. *PKD2* mutations also correlated with a higher number of cysts in the pancreas (Kim et al., 2016).

3.1.5 Markers of end-stage renal disease.

ESRD is characterised by a sudden or gradual drop in glomerular filtration rate (GFR) as the kidney fails to efficiently remove waste products from the blood and balance electrolytes and water. Kidney function is affected by defects in the vascular and tubular portions of the kidney. Reduced glomerular filtration pressure, vasoconstriction of the renal vessels, vascular congestion combined with tubular obstruction, tubular leakage and interstitial inflammation all contribute to the decline of renal function. Clinically, decline towards ESRD may present as low urinary output in combination with increased serum creatinine and blood urea nitrogen accumulation (Trof et al., 2006). A number of biomarkers are used to assess renal function and to estimate the impact of injury to the kidney.

Serum creatinine, a by-product of muscle metabolism excreted via the kidneys, is a routine marker used to assess renal function. Creatinine is produced when creatine, the energy source for the muscles, is broken down. Comparison of creatinine levels in the blood (serum creatinine) and urine allows for an estimate of kidney function (creatinine clearance). Creatinine levels remain constant from day to day since the muscle mass stays relatively constant. Elevated serum creatinine indicates a drop in creatinine clearance and thus a drop in renal filtration. In combination with patient age, sex, ethnicity and weight, creatinine clearance allows estimated GFR (eGFR) to be calculated. eGFR is a more accurate measure of kidney function because it gives a normalised measure to the patient's body size. A decrease in eGFR indicates a decline in kidney function.

Blood urea nitrogen (BUN) is another commonly used biomarker of renal function. Urea is a by-product of protein metabolism in the liver. As amino acids are deaminated through the urea cycle, ammonia is produced. Ammonia is extremely toxic and must therefore be converted to urea which is safely removed by the kidneys. BUN is calculated from blood urea and represents the mass of nitrogen in the blood urea. High BUN is an indicator of kidney dysfunction or obstruction of the urinary tract; the kidneys cannot filter the urea out

of the blood efficiently. Low BUN is an indication of liver disease as the liver becomes unable to metabolise protein.

Uric acid is another nitrogenous waste excreted via the kidneys. Uric acid is the end product of human purine metabolism; other mammals however, possess enzymes which catabolise uric acid to allantoin which is eliminated in the urine (Maiuolo et al., 2016). Produced mainly in the liver, almost all uric acid is filtered from the blood in the glomerulus then reabsorbed in the proximal tubule to regulate uric acid excretion. Increased urinary uric acid is an indicator of renal dysfunction, hypertension, diabetes and obesity (Maiuolo et al., 2016).

Urinary protein increases when the ability of the glomerulus to act as a macromolecular barrier is compromised. The glomerular tuft is lined by fenestrated endothelial cells which are in direct contact with the blood. Podocytes overlie this endothelium and make up the glomerular basement membrane. Proteins of 70 KDa and above are retained in the blood by the filtration barrier. Defects affecting the porosity of the barrier result in increased protein in the urine of a higher molecular weight (Frazier et al., 2012).

Increased urinary enzymes are a sign of tubular injury. Low level enzymuria may reflect a reversible mild injury, but higher levels are an indicator of declining renal function. Increased urinary N-acetyl-β-d-glucosaminidase (NAG) is used as a marker of renal injury. NAG is a lysosomal enzyme found in the proximal tubules and therefore increased urinary NAG may indicate injury to the proximal tubules. NAG has also been associated with increased lysosomal activity due to increased reabsorption by the proximal tubules (Bosomworth et al., 1999). The kidney is a common site for lesions due to its function in filtering and concentrating toxins. Markers which indicate injury of a specific region should be viewed with care as the nephron often responds to injury as a whole unit (Frazier et al., 2012).

Progression towards renal failure is associated with electrolyte imbalance. In this study, urinary potassium, chloride, calcium, inorganic phosphorus and sodium are measured. In humans, often only subtle changes are observed in electrolyte balance until later stages of kidney disease, when the kidney can no longer maintain the homeostatic balance of electrolytes. For instance, potassium excretion is maintained at normal levels until the renin-angiotensin-aldosterone system is compromised (Lascano, 2010).

3.1.6 Strain selection for kidney phenotyping

Mice are a useful tool in modelling kidney disease (Hewitson et al., 2009). However, renal lesions in Wt mice have been viewed in a number of mouse strains and several strains have particular susceptibility or resistance to certain aspects of renal disease (Frazier et al., 2012, Scudamore, 2014). The incidence of renal lesions varies between strains.

B6J mice are reported to show only mild generation of scar tissue in CKD models and are thought to be resistant to interstitial fibrosis (Huang et al., 2013, Walkin et al., 2013) and glomerulosclerosis (Ma and Fogo, 2003). In a sub-strain of B6 mice, C57BL/6CR, interstitial fibrosis has been reported to develop in untreated Wt mice after 12months of age (Yabuki et al., 2006). Interstitial fibrosis was reported at a higher rate in aged male mice and sex differences are also seen in glomerular hypertrophy with age. B6J mice are also reported to be less responsive to protein overload induced kidney failure than other strains (Ishola et al., 2006). C57BL/6J mice are reported to exhibit sexual dimorphism in response to albumin overload induced proteinuria. Whilst both sexes of 129S2/Sv mice exhibited significant proteinuria following 11 days of albumin overload, only male B6J mice showed a mild increase in proteinuria, female B6J mice remained unaffected. This indicates that functional differences in glomerular basement membrane permeability exist between mouse strains and sexes (Ishola et al., 2006).

Unilateral hydronephrosis is a relatively common pathology in laboratory rodents and presents as a dilation of the renal pelvis due to blockage of the urinary tract which leads to urine build-up. B6J mice are reported to have a spontaneous recessive mutation in *Aquaporin2* leading to congenital progressive hydronephrosis (McDill et al., 2006). Hydronephrosis is reported in both sexes (Taylor and Fraser, 1973) in 6-9% of mice (Brayton, 2009). B6J mice are also reported to exhibit glomerulonephritis and mild to moderate nephropathy in mice aged over 24 months (Brayton et al., 2012).

C3H mice are reported to display particular mineralization of renal arteries and tubules and also exhibit a high incidence of liver tumours (Brayton, 2009). C3H mice are renowned for developing renal complications and it is possible that these stem from a congenital defect of the ureter. From a screen of 12 inbred lines, 100% of C3H/HeJ mice were found to present with a shortened ureter at the uretero-vesical junction, inside the bladder (Murawski et al.,

2010b). This terminus of the ureter would normally close when the bladder empties; preventing reflux of urine into the kidneys. In C3H mice, the shortening of the ureter prevents the closure of the tube, allowing urinary reflux. If the urine carries infectious agents such as E.coli, inflammation and fibrosis can occur. Although C3H/HeH mice were not assessed, two substrains of C3H mice-HeN and HeJ were both found to develop reflux nephropathy following urinary tract infection (Bowen et al., 2013). However, the effects in C3H/HeJ were more severe which may be explained by their defect in innate immunity and bacterial clearance (Bowen et al., 2013).

Sexual dimorphism plays an important role in the pathogenesis and progression of kidney disease both in humans (Obialo et al., 2002, Chertow et al., 1998, Neugarten et al., 2002) and mice (Park et al., 2005). Structurally, the tubule arborisation of the mouse kidney appears to be comparable between B6J male and female embryonic kidneys (Short and Smyth, 2015). Overall kidney weight is generally higher in male than female mice but when normalised to body weight, this difference is lost (Sharma et al., 2015). Male urine production is generally higher than that of females, possibly reflecting the native behaviour of territory marking. Several studies report the effect of sex hormones on renal function; in particular oestrogen is proposed to have a protective effect on human renal function (Baylis, 2012, Elliot et al., 2003) whereas androgens are associated with increased blood pressure and reduced renal function (Reckelhoff et al., 2005).

Morphologically, the mouse kidney is sexually dimorphic (**Fig 3.1)**. The male parietal epithelium of a proportion of Bowman's capsules is made up of cuboidal cells whereas, the female glomerulus is lined by a flattened epithelium. This is unlikely to affect filtration or function in any way because it is the glomerular basement membrane rather than the parietal membrane which is the active area of the glomerulus.

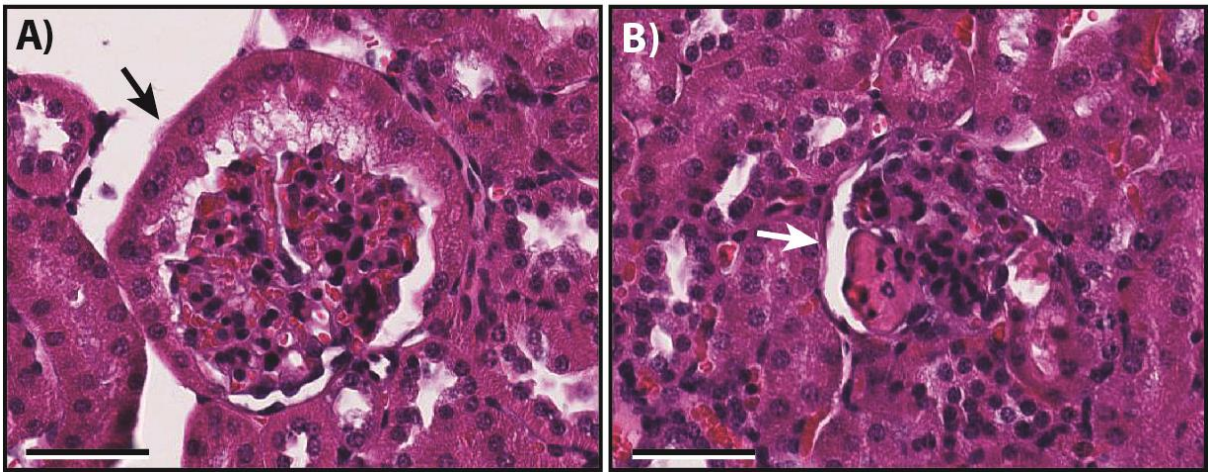

Figure 3.1: The mouse kidney is sexually dimorphic

A) The male glomeruli are lined by a cuboidal parietal epithelium (black arrow) whereas B) the female glomeruli are lined by flattened epithelial cells (white arrow). The parietal membrane is not involved in filtering the blood and this is therefore unlikely to cause a functional difference between the sexes. Scale bar 50um.

Background genetic susceptibility or resistance is likely to be an important factor in disease progression, therefore assessing mice with susceptibility to renal disease may reflect human disease pathogenesis more closely. Moreover, assessing the development of renal disease on several backgrounds allows us to discount strain differences and ascertain whether a consistent phenotype is seen. Whilst B6J mice are reported to exhibit some background renal dysfunction, this does not include cyst formation. Non-proliferative degenerative lesions of the kidney can be noted with age in many strains of mice. These background lesions can be exacerbated by disease, therefore it is essential to appropriately control for experimental genotype and background. Here C3H/HeH and C57BL/6J mice have been chosen for assessment of renal disease.

3.2 Results

3.2.1 Addressing the heterozygous phenotype in adult mice

In order to assess cyst development in *Pkd2*$^{lrm4/+}$ mice, two groups of adult heterozygous mice were aged and assessed for kidney cyst development. C3H-Pkd2$^{lrm4/+}$ and B6J-Pkd2$^{lrm4/+}$ mice, along with relevant age matched Wt controls were aged (4-8, 9-13 and 14-18 months) before samples were collected and assessed for evidence of kidney disease. Only male mice were assessed in order to avoid any possible variation from sex differences.

For each mouse, a urine sample was collected in metabolism cages over a 24 hour period. Since the mice were singly housed, the mice rested for a week before being sacrificed, then blood and kidney samples were collected at necropsy. **Fig 3.2** outlines the phenotyping pipeline and numbers of mice in each cohort studied.

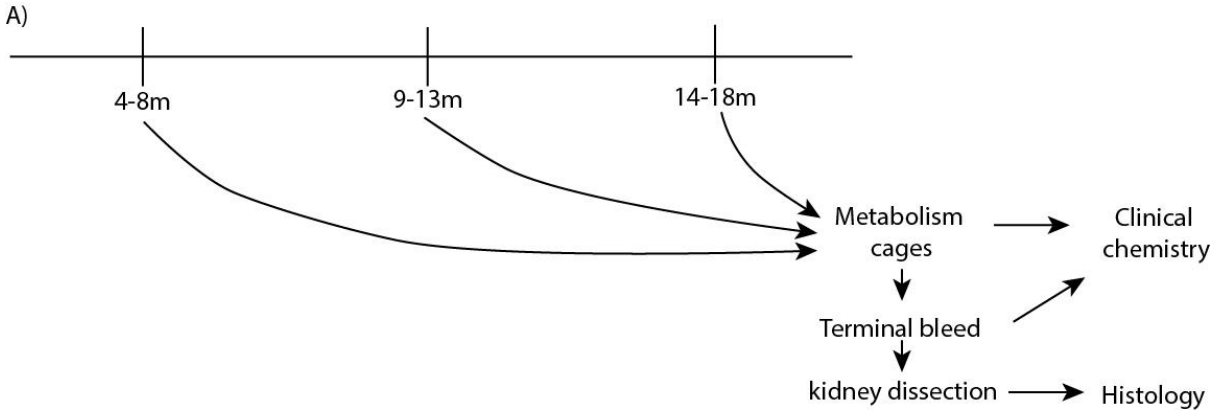

Age group	C3H/HeH-Pkd2$^{lrm4/+}$	C57BL/6J-Pkd2$^{lrm4/+}$
4-8 months	4 Wt males, 5 het males	5 Wt males, 4 het males
9-13 months	4 Wt males, 7 het males	4 Wt males, 4 het males
14-18 months	5 Wt males, 5 het males	4 Wt males, 4 het males

Figure 3.2: Phenotyping pipeline of work carried out on the Pkd2$^{lrm4/+}$ aging cohorts

A) Two cohorts of *Pkd2*$^{lrm4/+}$ mice, those on a C57BL/6J background and those on a C3H/HeH background were assessed at 3 different time points after ageing. Following this, the urine samples were collected in metabolism cages and blood and kidney samples were taken at necropsy. The table below details the number of mice assessed in each group.

Fig 3.3 shows the setup of the metabolism cages.

Figure 3.3: Setup of Metabolism cage apparatus.

Demonstrates the setup of the metabolism cage (Cat No. 3600M021, Tecniplast, Kettering, UK) designed to hold a single mouse. Food and water are supplied ad libitum at the side of the chamber. Water or food that is spilt is collected underneath the feeding areas so that none falls into the samples collected. Cages have a grated floor to allow urine to pass through into the separation funnel. Urine is collected at the bottom of the cage after having been separated from faeces and solid matter dropped from food; this provides a relatively clean sample. Our mice are supplied with a red transparent igloo which sits in the living space and provides housing and enrichment for the mouse.

Metabolism cages are commonly used to assess food and water consumption as well as the production of urine and faeces. However, the effect of housing the mice in metabolism cages can cause stress inducing physiological effects. These can alter many of the factors the cages are designed to study: Stressed mice may reduce food and water intake and produce less urine which may be chemically imbalanced. Reducing stress therefore reduces confounding factors. It is therefore also essential to maintain controls by assessing Wt mice in parallel.

A study conducted in our facility, using the same apparatus and conditions as this study, found that significant differences were observed between strains and genders of wildtype mice when assessing urinary and plasma components (Stechman et al., 2010). The study

assessed C3H/HeH, C57BL/6J and BALB/cAnNCrl mice; the first two are the backgrounds for this study, providing us with a useful reference point. During the first days in metabolism cages, mice experience a drop in body mass (Stechman et al., 2010), reduced food and water intake and an increase in body temperature (stress induced hyperthermia) due to an increased heart rate (Spani et al., 2003, Kalliokoski et al., 2013), indicating that metabolism cages are a stressful environment. Whilst some studies have shown that mice take 3-4 days to habituate to metabolism cages (Stechman et al., 2010), others indicate that habituation fails to occur (Kalliokoski et al., 2013). Nonetheless, a concern for animal welfare indicates that the mice should be housed in metabolism cages for the shortest period possible.

To increase mouse comfort, a number of adaptations have been undertaken. In the un-adapted system, the mouse is singly housed in a smaller area than the home cage, with a grated floor which often has no solid areas. There is no environmental enrichment and no area for bedding. To reduce stress, mice are supplied with an autoclavable red transparent igloo (Datesand Ltd, Manchester, UK) which provides a nesting area and a form of enrichment. Mice can be monitored through the plastic but they perceive it to be dark. Bedding and cardboard enrichment are not provided as these absorb urine and reduce the collection volume. Metabolism cages are set up in a Scantainer ventilated cabinet (Scanbar) which provides a clean air supply but also allows the singly housed mice to smell each other. The Scantainer accommodates 12 mice in metabolism cages at a time. Urine samples were frozen at -80°C until the full cohort was collected. Samples were then thawed and centrifuged at 3000rpm for 10mins at 4°C before being diluted 2-20 fold in distilled water to increase urinary volume. The resultant values were then multiplied to provide the actual value.

Following 24 hours in the metabolism cage, mice were left to recover for a week before terminal bleeds were taken. Whole blood samples were obtained by retro-orbital terminal bleed taken under isoflurane anaesthesia. Samples were collected by capillary action into lithium heparin-coated paediatric Microvette tubes (Sarstedt Ltd, Leicester, UK) and placed on ice. The blood collected was centrifuged at 3000rpm for 10mins at 4°C and the plasma was stored at -80°C until the full cohort had been collected.

Blood and urine samples were analysed on the same day at the end of collection for each cohort, in order to minimise difference in analysis conditions. Blood samples were analysed for a panel of components including urea, creatinine, total protein, albumin and amylase. The urine samples were analysed for sodium, potassium, chloride, urea, creatinine, calcium, inorganic phosphorus, glucose, uric acid and urinary protein. Samples were analysed using an Olympus AU680 bioanalyser (Olympus Diagnostic Systems, UK). The analyser probe was adjusted to minimise the dead sample volume to 40µl and the precision of the equipment was monitored with the use of internal quality control materials. Haemolysis of the samples was avoided by quick sample handling.

3.2.2 Plasma biochemistry

Assessment of Wt and *Pkd2*$^{lrm4/+}$ mice on C3H and B6J genetic backgrounds in 3 age groups; 4-8m, 9-13m and 14-18m is represented in the following graphs (**Fig 3.4)**. The average and standard deviation for each parameter is recorded in **Appendix2: Table 2.1.**

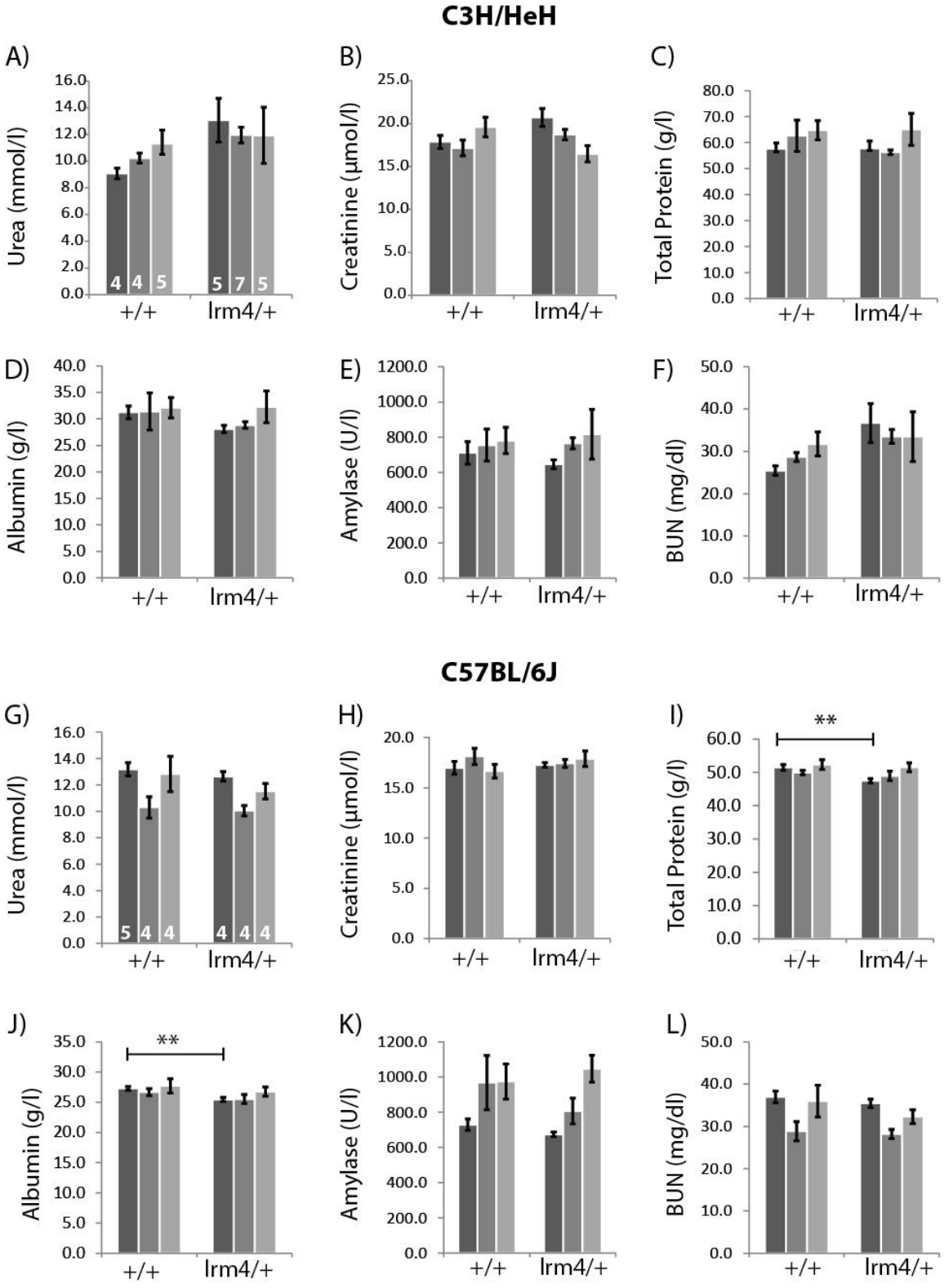

Figure 3.4: A comparison between plasma components from Wt and Pkd2$^{lrm4/+}$ mice on both C3H/HeH and C57BL/6J backgrounds.

Each graph is plotted with average values for each plasma component. In each graph the first cluster represents Wt values and the second cluster represents *Pkd2*$^{lrm4/+}$ mice. The first column in each cluster is the average at 4-8 months, the second column at 9-13 months and

the third at 14-18 months. Each column represents 4-7 mice, n numbers are recorded in panel A) and G) for each group of mice and also summarised in **Fig. 3.2**. A)-F) are the C3h cohort, graphs G)-L) are the B6J cohort. T-tests were performed to compare Wt and *Pkd2*$^{lrm4/+}$ mice in the same age group for both cohorts. Mice with a significant result are signified by **= significant P=<0.001 or *=significant P=<0.05. Error bars represent SEM.

For each plasma component analysed, average values were relatively similar, with no exceptional changes between *Pkd2*$^{lrm4/+}$ and Wt mice. There are no significant differences between Wt and *Pkd2*$^{lrm4/+}$ in the C3H cohort (graphs A)-F)). In the B6J cohort however, two components were significantly changed when compared to Wt. There is a significant difference when comparing total protein at 4-8 months (graph I), p=0.0108). The *Pkd2*$^{lrm4/+}$ value is significantly lower than the Wt value and the het continues to present lower values at each time point, although other ages are not significant. In the C3H cohort total protein, the same pattern is not observed. The general increase in total protein in the plasma is unlikely to be related to progressive renal disease since we see a similar increase in the Wt with age.

Serum albumin is also significantly lower in *Pkd2*$^{lrm4/+}$ mice in the B6J cohort at 4-8m (graph J), p=0.006) and the *Pkd2*$^{lrm4/+}$ values are consistently, although not significantly, lower than Wt in both cohorts. The significant drop in albumin seen in *Pkd2*$^{lrm4/+}$ when compared to Wt at 4-8 months does not continue to be significant at any other stage, indicating it is unlikely to be linked to a progressive reduction in kidney function. This suggests that the kidney function is likely to be normal and that any development of cysts is unlikely to be severe.

Although these backgrounds are noted to exhibit genetic sensitivity to renal disease, neither cohort of mice has shown a profound effect on plasma components. The mutation has not caused the renal phenotype to deteriorate in terms of plasma components more than the baseline Wt levels. No evidence of significant renal dysfunction in observed.

To clarify whether our Wt cohorts were normal, comparisons were made with mice from the Stechman study which were assessed in our facility (Stechman et al., 2010). Since both urine and plasma were analysed in the same clinical chemistry laboratory as our study, the Stechman study should give comparable results. Therefore it is reasonable to make comparisons between the two sets of results. **Table 3.1** compares the mean values of the analysed plasma components from 10-19 mice obtained after acclimatisation to the

metabolism cage environment (Stechman et al., 2010) with the 4 mice from this study that were the same age (4-8 months) but that were not acclimatised. It is clear from these results that there is a significant level of variation in Wt mice. The Stechman study compares higher numbers of mice and this in turn brings higher variation between samples than we see with the current study. Urea and Albumin measurements were comparable between studies. Plasma creatinine however was very different. The Stechman creatinine levels are much higher and have a higher standard deviation compared to our mice. Since creatinine reflects muscle mass, it is possible that the Stechman mice were larger than our cohort, however this is unlikely since they were the same age and fed the same diet.

Table 3.1: Comparison between plasma components from C3H and B6J mice of Stechman study and the present study

Average values (standard deviation) of plasma components assessed by Stechman et al from table 4 in (Stechman et al., 2010) in male Wt 24-30 week old mice compared to mice from the present study at an equivalent age. The results from this study are highlighted in grey

4-8 months	**C3H/HeH**		**C57BL/6**	
	Stechman study (n=10-15)	**Present study** (n=4)	**Stechman study** (n=19)	**Present study** (n=4)
Urea (mmol/l)	11.6 (1.7)	9.1 (0.80)	11.5 (2.8)	12.7 (0.72)
Creatinine (µmol/l)	36 (6)	17.9 (1.51)	35 (6)	17.3 (0.24)
Albumin (g/l)	30.5 (1.6)	31.2 (2.4)	28.2 (1.9)	25.5 (0.66)

Champy et al found there to be greater variation between strains than between ages of mice when they assessed plasma from fasted 3, 6 and 12 month old mice from four inbred strains (C57BL/6J, 129SvPas, C3HeB/FeJ, and Balb/cByJ) (Champy et al., 2008). They reported C57BL/6J mice to have significantly higher urea levels than the other strains. Thus, a comparison was made between Wt mice from the C57BL/6J and C3H/HeH cohorts of all ages in this study and these were compared to the Stechman study (Stechman et al., 2010) (**Table 3.2**.).

Table 3.2: A comparison between plasma components from all ages of Wt male mice from the Stechman study (Stechman et al., 2010) and the current study.

Columns 1 and 2 summarise results from the Stechman study, showing averages and (SD). Column 3 and 4 show results from this study (highlighted in grey). Average (Standard Deviation)

	Stechman study (Stechman et al., 2010)		**Present study**	
	C3H/HeH (n=10-15)	**C57BL/6** (n=19)	**C3H/HeH** (n=13)	**C57BL/6** (n=13)
Urea (mmol/l)	11.6 (1.7)	11.5 (2.8)	10.3 (1.71)	12.2 (2.14)
Creatinine (µmol/l)	36 (6.0)	35 (6.0)	18.3 (2.19)	17.2 (1.75)
Albumin (g/l)	30.5 (1.6)	28.2 (1.9)	31.6 (4.47)	27.2 (1.46)

When all ages of mice are compared, the standard deviations for this study are generally smaller indicating that our data are less spread. The urea and albumin are comparable across the studies but the creatinine is again much higher and exhibits greater variability in the Stechman study. Since our data is consistent across ages and has less variance than the Stechman data, it likely reflects normal functioning kidneys. These comparisons show that these Wt mice have consistent readings both between mice of the same age and across the ages in our study. Creatinine appears to be more variable between studies than either urea or albumin levels.

3.2.3 Urine biochemistry

Urine was assessed for indicators of compromised renal function. In order to control for animal size and creatinine clearance, the concentrations of urinary sodium, potassium, calcium and phosphate in mmol/L were expressed as a ratio to the concentration of urinary creatinine in mmol/L. The following sets of graphs represent urine component assessment for Wt and *Pkd2*$^{lrm4/+}$ mice on C3H and B6J genetic backgrounds (**Fig 3.5 and Fig 3.6)**. The average and standard deviation for each parameter and genotype is recorded in **Appendix2:Table 2.2-3.**

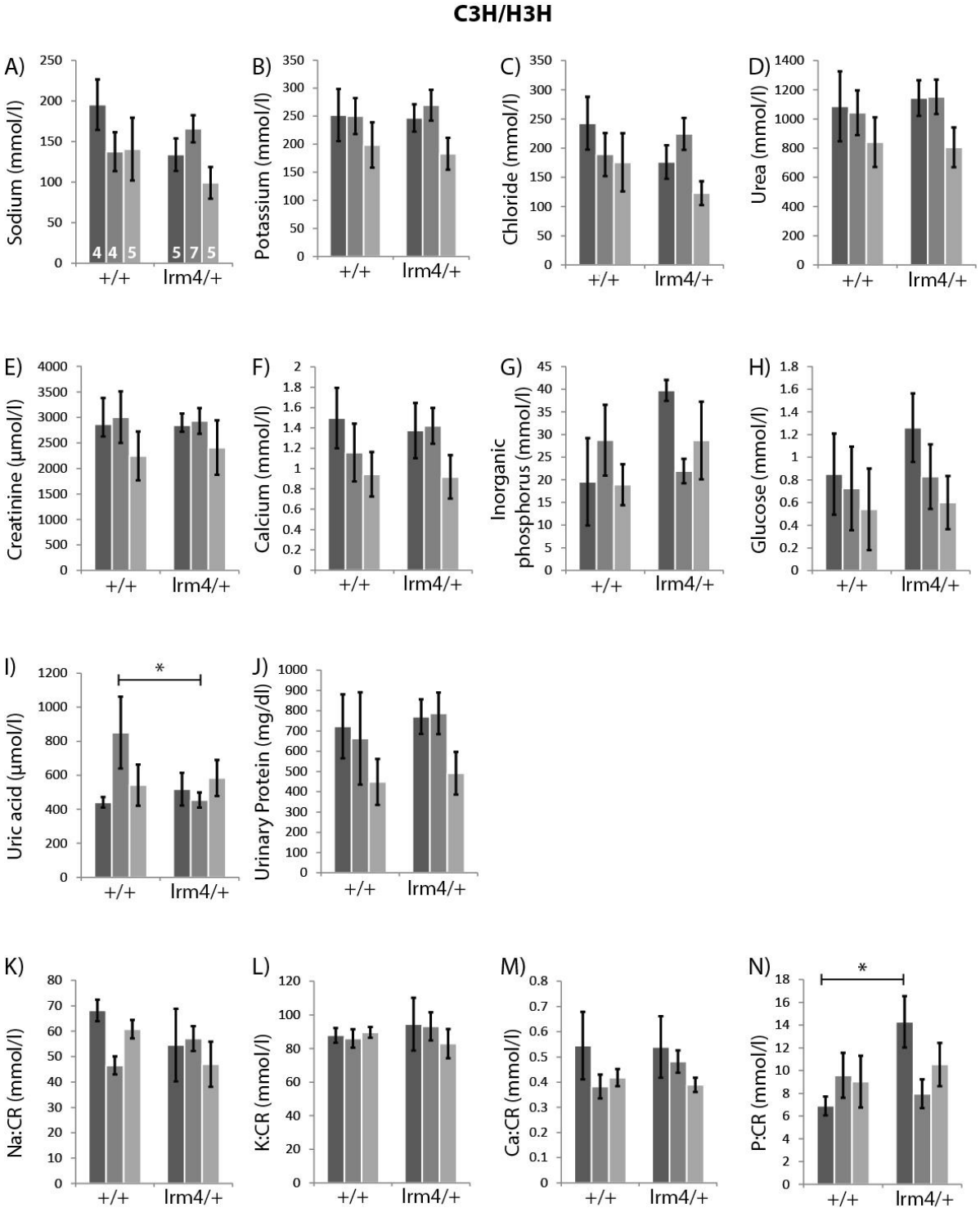

Figure 3.5: C3H urinalysis results

Average values of urine components of the Wt and *C3H-Pkd2*$^{lrm4/+}$ mice are compared for each age. In each graph, the first cluster represents Wt values and the second cluster represents *Pkd2*$^{lrm4/+}$ mice. The first column in each cluster is the average at 4-8 months, the second column at 9-13 months and the third at 14-18 months. Each column represents 4-7 mice. N numbers are recorded in white in A). T-tests were performed to compare Wt and

Pkd2$^{lrm4/+}$ mice in the same age group (in the same coloured column). Mice with a significant results are signified by *=significant P=<0.05, Error bars represent SEM.

For each urine component analysed, the general trend with age between Wt and *Pkd2*$^{lrm4/+}$ mice is similar. Graphs A)-F), H) and J) show a general descending trend overtime in their components for Wt and *Pkd2*$^{lrm4/+}$. Graph G) representing inorganic phosphorus seems to have no trend in either direction and none of the time-point assessed are significantly different between Wt and Pkd2$^{lrm4/+}$. Graphs K)-N) represent creatinine ratios.

Only one component of graphs A)-J) shows a significant difference. At 9-13m uric acid (I) is significantly higher in Wt mice than in *Pkd2*$^{lrm4/+}$ (p=0.039). This significant difference did not continue across the ages and therefore does not indicate a progressive loss of renal function. Of the creatinine ratio graphs (K-N), one component shows a significant different. Inorganic phosphate was raised in the 4-8m *Pkd2*$^{lrm4/+}$ mice (p=0.027). This value then drops by 9-13 months and 14-18 months. Since no trend is seen representing declining renal function across the ages assessed, it is likely that these mice do not present significant renal dysfunction with age.

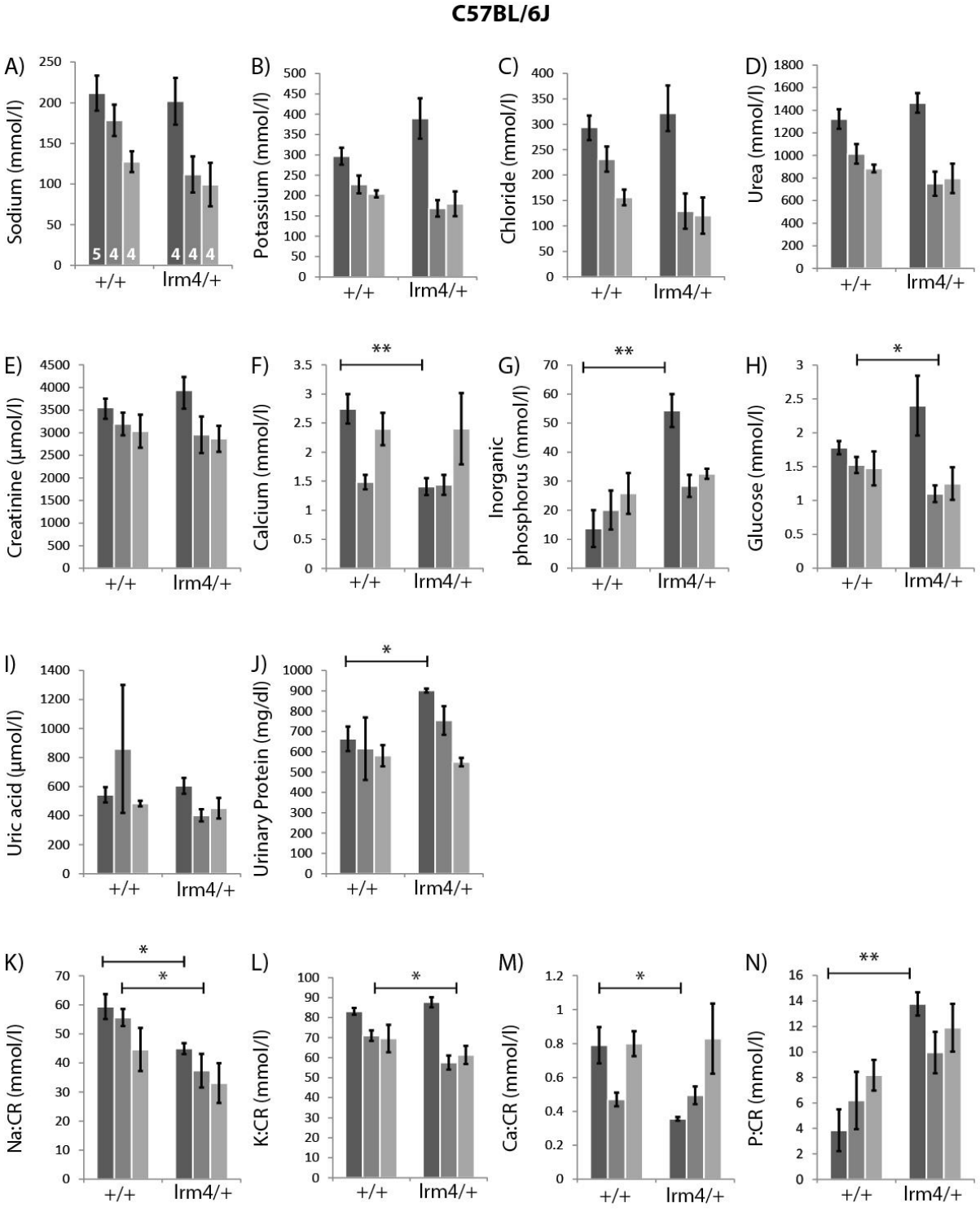

Figure 3.6: B6 urinalysis results

Average values of urine components of the Wt and *Pkd2*$^{lrm4/+}$ B6 mice are compared for each age. In each graph, the first cluster represents Wt values and the second cluster represents *Pkd2*$^{lrm4/+}$ mice. The first column in each cluster is the average at 4-8 months, the second column at 9-13 months and the third at 14-18 months. Each column represents 4-6 mice. T-tests were performed to compare Wt and *Pkd2*$^{lrm4/+}$ mice in the same age group (in

the same coloured column). Mice with a significant results are signified by *=significant P=<0.05, Error bars represent SEM.

For each urine component analysed in the B6J cohort, the general trend with age between Wt and *Pkd2*$^{lrm4/+}$ mice is similar. Graphs A)-E), H) and J) all represent a descending trend over time for each component analysed for both Wt and *Pkd2*$^{lrm4/+}$ mice. Although not significantly so, the average value at 4-8 months for *Pkd2*$^{lrm4/+}$ mice assessed for Potassium (B), Chloride (C), Urea (D) and creatinine (E) seemed raised when compared to Wt values. Inorganic phosphorus (G) (p=0.0058) and urinary protein (J) (p=0.025) were significantly higher in Pkd2$^{lrm4/+}$ at 4-8 months, and at 9-13 months, Glucose (H) (p=0.046) was significantly higher in *Pkd2*$^{lrm4/+}$ mice. Calcium was significantly lower at 4-8 months in *Pkd2*$^{lrm4/+}$ mice (p=0.009). Since none of these points remain significantly different over time, it is unlikely that they reflect a progression towards renal disease. In general, the *Pkd2*$^{lrm4/+}$ mice follow the same trend as the Wt mice but the 4-8 month group seems to be disrupted slightly. The same urine sample was used for each component assessed for each time point but since blood and kidneys were collected in a terminal procedure, samples were collected from different mice for each time-point. The values representing each age group therefore do not follow the same mice. The 4-8 month group of *Pkd2*$^{lrm4/+}$ mice have raised values for a number of components, which may reflect disruption of renal function in these particular mice.

When assessing creatinine ratios, which normalise the results to body size, Sodium:Creatinine (K) was significantly lower in *Pkd2*$^{lrm4/+}$ mice at 4-8m (p=0.049) and 9-13m (p=0.031) and remains lower than Wt mice, although not significantly so, at 14-18m. This could be an indication of renal tubular injury or reduced kidney function. All of the other creatinine-normalised components have one significantly different comparison between Wt and *Pkd2*$^{lrm4/+}$ but none follow a trend across several age groups. Potassium:Creatinine (L) was significantly lower in Pkd2$^{lrm4/+}$ at 9-13 months (p=0.023); Calcium:Creatinine (M) was significantly lower in *Pkd2*$^{lrm4/+}$ at 4-8 months (p=0.022); and Inorganic Phosphate:Creatinine (N) was significantly higher in *Pkd2*$^{lrm4/+}$ at 4-8 months (p=0.0049). Since none of the 14-18 months *Pkd2*$^{lrm4/+}$ mice were significantly different from the Wts, we can assume that the results do not reflect significant decline in renal function. The significant differences in some

components at earlier stages may reflect precocious compromised renal function similar to that which would normally be seen at later stages. I.e., we expect a decline in renal function with age, as we see in Wt mice, but this could be expedited in the *Pkd2*$^{lrm4/+}$ mice.

Although there were some significant differences between Wt and *Pkd2*$^{lrm4/+}$ mice at different time points, neither group exhibited a decline in renal function that continued throughout all three age groups. *Pkd2*$^{lrm4/+}$ total protein levels were significantly lowered in the B6J plasma analysis at 4-8 months, here we see the opposite trend in the urine results indicating that protein is being lost in the urine and levels are not retained in the blood at 4-8 months. This could indicate a decline in renal function in these mice, however the trend does not appear to continue when assessed at later stages, neither in plasma nor in urine samples.

Inorganic Phosphate:Creatinine (N) was significantly increased at 4-8 month in *Pkd2*$^{lrm4/+}$ mice of both C3H and B6J cohorts. Since this is consistent between cohorts, it could indicate that the disrupted Inorganic Phosphate in *Pkd2*$^{lrm4/+}$ mice reflects reduced renal function.

The B6J cohort appears to be more affected by the mutation than the C3H cohort. Alterations in both plasma and urine components are evident in the B6J cohort whereas no plasma components were significantly altered in the C3H cohort. Fewer urine components were significantly altered in the C3H cohort and lower levels of significance were noted between the C3H components that were affected. This suggests that the B6J-Pkd2$^{lrm4/+}$ mice were more sensitive to the effects of the mutation than the C3H cohort.

Although assessment of the urine and blood did not highlight any significant modification in kidney function which persisted throughout all three age groups, it remained possible that the mice could have developed renal cysts but not to a level which is associated with complete loss of kidney function. The kidney is an adaptable organ and is able to increase filtration to compensate for significant regions that have lost function. Therefore the kidney morphology was assessed.

3.2.4 *Pkd2*$^{lrm4/+}$ adult mice develop microcysts

During necropsy, kidneys from both cohorts were dissected and fixed in 10% neutral buffered formalin (3800810C, Surgipath Leica biosystems). The kidneys were dehydrated and washed through xylenes before being embedded in paraffin wax. Kidney sections were cut by microtome to a thickness of 7µm at 56µm intervals. Sections were mounted on slides and stained with H&E. Slides were imaged on the Hamamatsu NanoZoomer slide scanner using a 20X lens.

Studies assessing cystic kidneys mention dilated tubules, microcysts and macrocysts yet there is some ambiguity as to how these are defined (Park et al., 2009, Bastos et al., 2009, Lu et al., 1999). One technique for characterising cyst size involves measuring the lumen of a normal tubule and multiplying this measurement to define cyst sizes. Adaptions of this technique were used to measure cyst diameter in this study. Since the luminal diameter is difficult to accurately measure, the outer diameter of the proximal tubule was used. Ten proximal tubule cross-sectional diameters were averaged from the cortex of lateral section from a Wt adult kidney. This average value was compared to measurements of tubules in other kidneys and found to be representative.

For the purpose of this work, measurements were ascribed by the following criteria: The average outer diameter of a proximal tubule in the cortex is 38.7µm. The average glomerular tuft is 73.91µm therefore tubular dilations (Td) were defined in two ways; those larger than a normal tubule diameter but smaller than a glomerulus (73.91µm) were denoted Td, those larger than a glomerulus but smaller than three times the tubule diameter were denoted Td2. Microcysts were counted between three and five times the tubule diameter; up to 193.5µm. Cysts were defined as lesions in the kidney with a diameter greater than five times the regular tubule diameter (>193.5µm). The scale used is slightly conservative in comparison to the scale used by others (Lu et al., 1999, Bastos et al., 2009), designed to reduce falsely labelling smaller dilations as cysts (**Fig 3.7)**.

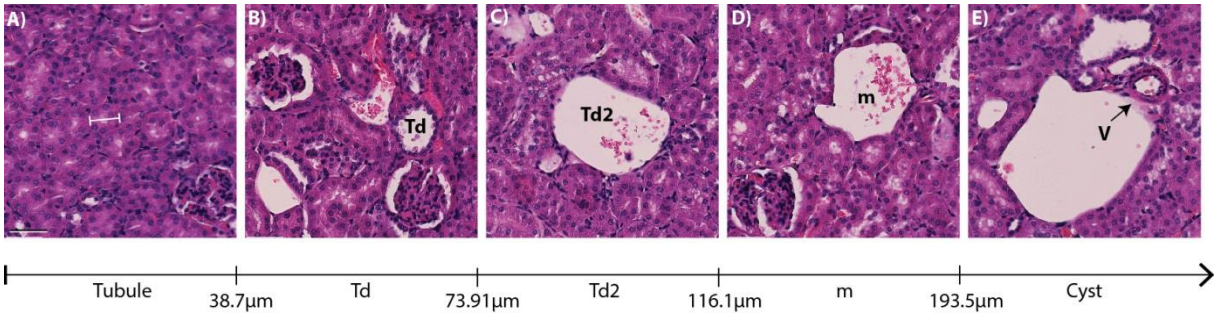

Figure 3.7: The scale and diameters characterising tubule dilations and cysts

A) shows proximal tubules in the cortex, the average diameter of which is 38.7µm. B) shows a tubule dilation (Td), the dilation pictured is 50.2µm. These are smaller than the average glomerular tufts, which can also be seen in the image. C) Larger tubular dilations (Td2), here pictured at 108µm are larger than glomeruli but smaller than 3x tubule diameters. D) microcysts (m) are between 3-5 times the tubule diameter, here the diameter is 122µm. E) shows a blood vessel (arrowed with V), dilations near blood vessels were not counted. Scale bar in a 50µm.

Kidneys were sectioned both sagittally and laterally. Sagittal sections provided a good overall representation of the renal architecture, but measuring tubular dilations was difficult due to the orientation of blood vessels. In many cases, blood vessels were surrounded by dilations and spaces which may be artefacts of the sectioning process due to blood tubules moving away from the kidney interstitium. Dilations in the kidneys were assessed morphologically as measurements were taken. Blood vessels were identified by their smooth muscle layer (**Fig 3.7 E**) and dilations in close proximity were not measured. Kidneys from mice at 9-18 months from the aging cohort were assessed.

Two pairs of B6J kidneys were randomly selected for assessment from the group of 18 month old mice. These were assessed blind to genotype, but both were *Pkd2*$^{lrm4/+}$ kidneys. These kidneys were assessed fully in both orientations, i.e. kidneys were cut both sagittally and laterally; 34 and 30 sagittal sections were assessed, and 26 and 36 lateral sections were assessed respectively (**Fig 3.8)**. This was extremely arduous and time consuming. An average of 143.5 dilations was measured per kidney. There were a high number of dilated tubules and the microcysts tended to cluster around the smaller size limit of the category, as can be seen from the graph in **Fig 3.8**. The largest cyst observed was 190µm in diameter. When all the sections were counted in each kidney, the microcysts seemed to be dispersed throughout the sections. Therefore it seemed likely that assessment of fewer sections would remain representative of the populations of dilations that could be viewed throughout the

kidney. Since step sections rather than serial sections were examined, smaller dilations may be under represented when measuring cysts since the "step" cannot be counted, however microcysts are likely to be large enough to span more than one section. Assessment of four lateral sections per mouse provided a representation of the dilations present in the kidneys.

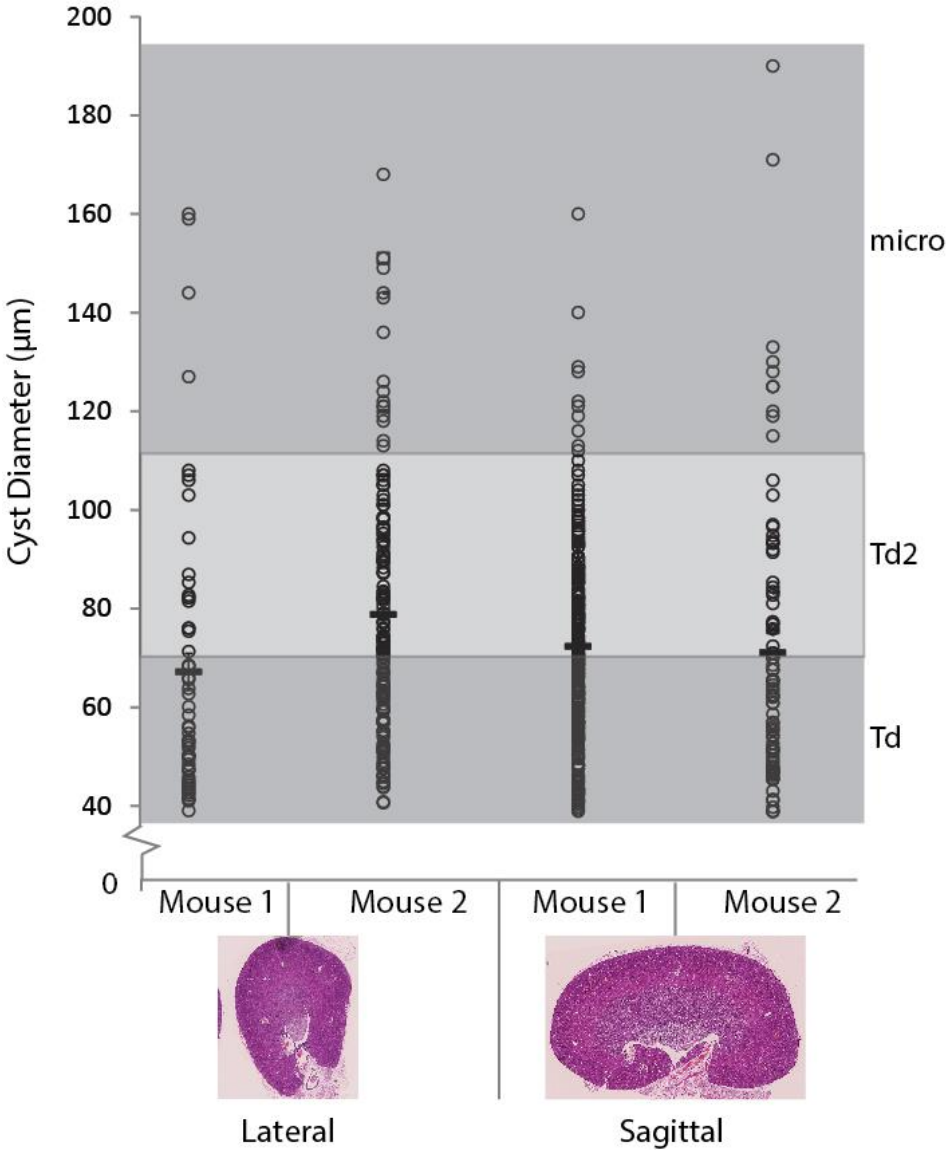

Figure 3.8: Representation of cyst diameters from two 18 month old B6J-Pkd2$^{lrm4/+}$ mice where kidneys were assessed in full

In total, 26 sections were scored from mouse 1's laterally cut kidney and 36 were scored for mouse 2; 34 sagittal sections were scored for the other kidney from mouse 1 and 30 were scored from the sagittal sectioned kidney of mouse 2. The shaded areas represent tubular dilations Td (38.7-73.91µm), Td2 (73.91-116.1µm) and microcysts (116.1-193.5µm). The black rectangular point for each set represents the average and SEM is also marked.

Both mice presented with bilateral renal microcysts. Mouse 1 exhibited four microcysts ranging between 127-160µm in the laterally cut kidney and eight microcysts between 116-160µm in the sagittally cut kidney. Mouse 2 exhibited slightly more microcysts; 17 ranging between 118-168µm in the laterally cut kidney and nine microcysts between 119-190µm in the sagittally cut kidney.

Following the assessment of the kidney sections in **Fig 3.8**, mice at 9-13 months and 14-18 months were assessed for tubule dilations. Four lateral sections were assessed per mouse. Three *Pkd2*$^{lrm4/+}$ and four *Pkd2*$^{+/+}$ mice were assessed 9-13 months. Four of each, *Pkd2*$^{lrm4/+}$ and *Pkd2*$^{+/+}$ mice were assessed 14-18 months. The dilations recorded are presented in the graph in **Fig 3.9**.

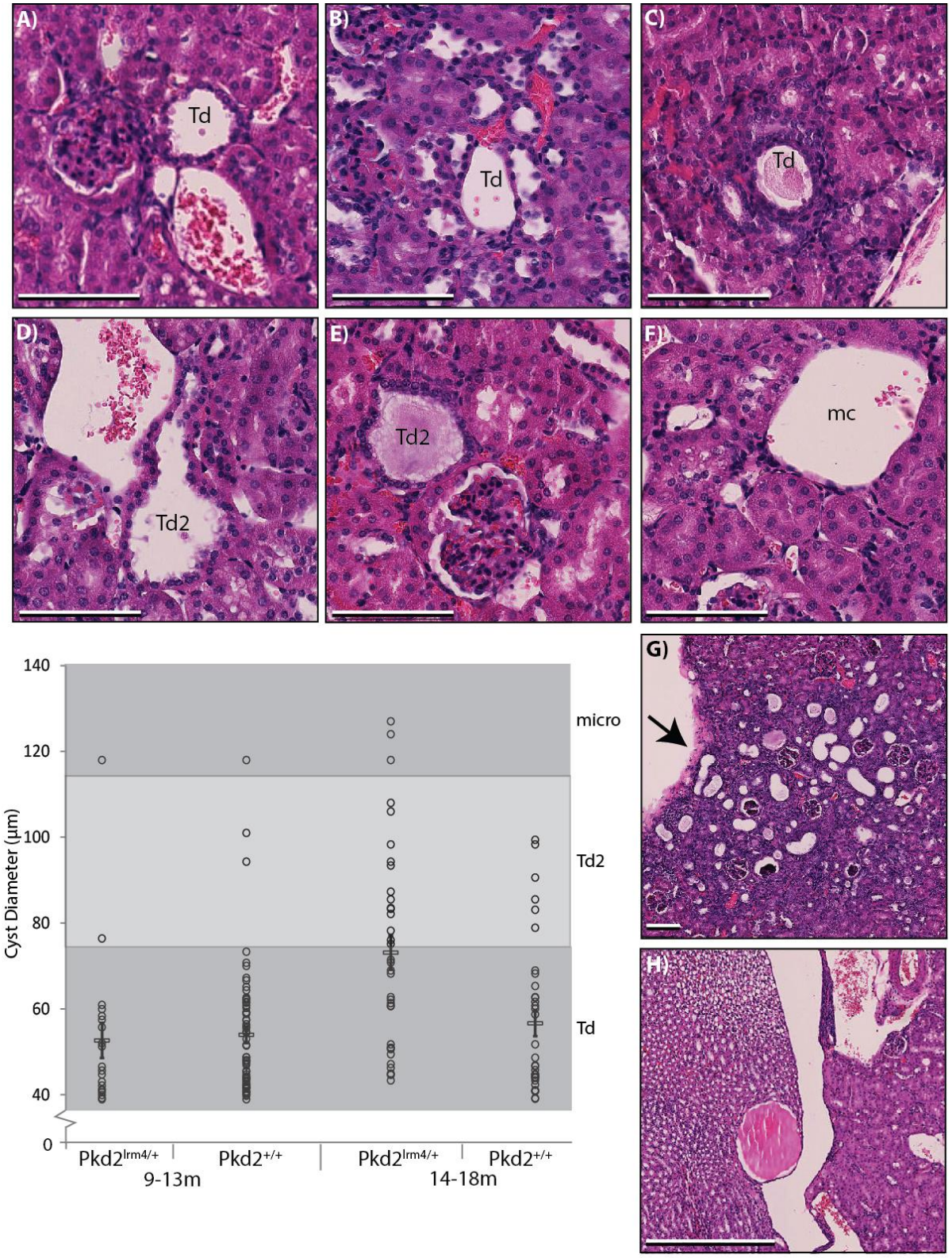

Figure 3.9: Cyst categories and examples of dilations observed in B6J-Pkd2$^{lrm4/+}$ mice.

Kidneys exhibit tubular dilations at 9-13m and 14-18m. A)-C) are examples of tubular dilations (Td). A) shows a dilation of 59.4µm diameter next to its associated glomerulus. B) dilated tubules can be seen in groups indicating that several nephrons are affected, the largest dilation here is 47.3 µm. C) A strong tubule border can be seen around this cortical

dilation. D) is a larger tubule dilation (Td2), larger than an average glomerulus. The dilation here is 81.7µm. E) is a Td2 which is filled with a proteinaceous cast, next to a larger than average glomerulus. F) shows a microcysts of 118µm. The tubule lining is stretched, becoming less visible. G) shows a point of injury to the kidney which could have been caused by a cyst. The area adjacent to the damage demonstrates dilated tubules. H) shows a cyst of 301µm which developed in the papilla. The scale bar in H) is 500 µm. All other scale bars are 100 µm. The graph shows measurements of dilated tubules in 4 sections per kidney, 4 kidneys per genotype (3 kidneys for *Pkd2*$^{lrm4/+}$ at 9-13 months). The top section of the graph represents the number of microcysts, the middle section shows the Td2s and the bottom section shows the dilated tubules (Td) of each genotype. Error bars represent SEM.

At 9-13 months the Wt and *Pkd2*$^{lrm4/+}$ sections were not significantly different (p=0.7470). When assessed at 14-18 months however, the Pkd2$^{lrm4/+}$ kidneys contained significantly larger dilations than the Wt kidneys (p=0.0016). Indeed, when the 9-13 month old *Pkd2*$^{lrm4/+}$ mice were compared to the 14-18 months old group of *Pkd2*$^{lrm4/+}$mice, the older group exhibited significantly larger cysts (p=0.0016). The same comparison between 9-13 month and 14-18 months old Wt mice was not significantly different (p=0.4269).

Assessment of these sections indicated that microcysts do develop in *Pkd2*$^{lrm4/+}$ kidneys. One macrocyst of 301µm diameter, was identified in the papilla of a *Pkd2*$^{lrm4/+}$ mouse at 14-18m (**Fig 3.9 H**), representing a cysts of collecting duct origin. Macrocysts were not noted in any other mice. At 14-18 months, one *Pkd2*$^{lrm4/+}$ mouse exhibited a single microcyst (in the 4 sections assessed) and another exhibited 2 microcysts. This indicates that microcysts are spread sparsely throughout the kidney. One microcyst was seen at 9-13 months in both *Pkd2*$^{lrm4/+}$ and *Pkd2*$^{+/+}$ mice. Two of the older *Pkd2*$^{lrm4/+}$ mice exhibited a region of renal injury which resulted in localised tubule damage (**Fig 3.9 G**). This resulted in a number of dilated tubules.

Although tubular dilations are evident in both Wt and *Pkd2*$^{lrm4/+}$ kidneys at 14-18 months of age, *Pkd2*$^{lrm4/+}$ have a higher incidence of microcysts. Mild unilateral hydronephrosis was noted in one *Pkd2*$^{lrm4/+}$ mouse at 14-18 months. This is a condition where a portion of the renal tubule can become blocked and the renal pelvis, the portion of the kidney where the collecting ducts filter into, then becomes enlarged and distended due to fluid build-up.

3.2.5 Extrarenal phenotypes

During dissections of these mice at necropsy, some extra-renal phenotypes were noticed. In B6J-Pkd2$^{lrm4/+}$ but not C3H-Pkd2$^{lrm4/+}$ mice, liver cysts were observed. Polycystic liver disease is a known extra-renal complication of PKD. However, liver cysts do not always arise in combination with kidney cysts. **Figure 3.10** details the liver cysts which were seen in the B6J-Pkd2$^{lrm4/+}$ cohort.

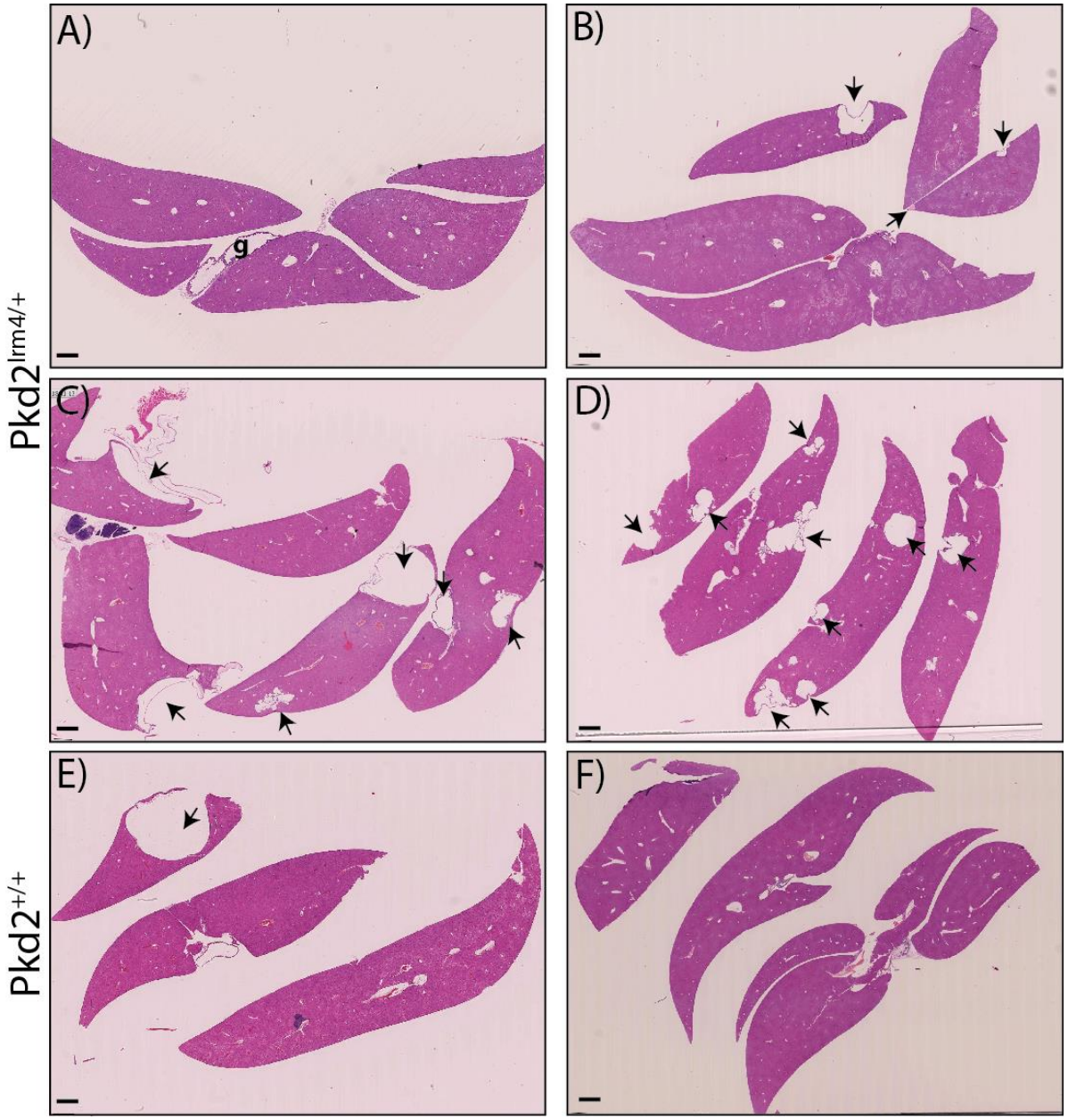

Figure 3.10: Liver sections of B6J cohort at 14-18m.

A)-D) represent single sections through *Pkd2*$^{lrm4/+}$ livers from mice aged 14-18m. Arrows point to cysts. Cyst phenotype ranges from absent A), mild B) to moderate D) in the *Pkd2*$^{lrm4/+}$ mice. In addition to cysts, B) also exhibits regions of fatty liver disease. One *Pkd2*$^{+/+}$ mouse exhibited a single hepatic cyst E). F) represents a normal *Pkd2*$^{+/+}$ liver with normal ducts. g= gall bladder. Scale bar 1mm.

Polycystic liver disease was noted in 3/4 of the *Pkd2*$^{lrm4/+}$ mice at 14-18 months. This phenotype was not noted in the four 4-8 month nor the four 9-13 month mice at necropsy. However, one of the 14-18 month old Wt mice presented with a single large liver cyst. The liver cysts did not appear to cause significant disruption of components in the urine such as urea, which would decrease with liver disease.

3.3 Results summary

In this chapter, the adult phenotype of *Pkd2*$^{lrm4/+}$ mice has been presented. Ageing these mice to 18 months resulted in the development of small numbers of microcysts on a B6J genetic background. Polycystic liver disease was also seen in a proportion of B6J-*Pkd2*$^{lrm4/+}$ aged mice. This models a known extrarenal phenotype which accompanies ADPKD and suggests that polycystic liver disease is due to genetic alterations related to ADPKD, rather than being a secondary phenotype caused by other alterations such as blood composition.

3.4 Discussion

3.4.1 Comparison to other models

ADPKD is a progressive disease where multiple fluid filled cysts initially develop in utero and expand in both size and number with age, overtaking the structure of the kidney and compromising renal function. At present, a number of models exist which reproduce aspects of the disease **Table 3.3** (reviewed by (Happe and Peters, 2014)). *Pkd1*$^{-/-}$ and *Pkd2*$^{-/-}$ mice demonstrate a rapid and severe development of cysts and are nearly always embryonic lethal, much like *Pkd2*$^{lrm4/lrm4}$ mice. Conditional alleles of *Pkd1 (Liu et al., 2014)* and *Pkd2 (Garcia-Gonzalez et al., 2010, Kim et al., 2009)* have been used to spatially restrict expression of mutant protein, and these have been useful in modelling the adult phenotype. Cystic development in these mice is often rapidly progressive. Inducible conditional alleles hold more potential for the development of a more slowly progressing model because they can be spatially and temporally restricted.

Table 3.3: Heterozygous mouse models of Pkd2 kidney disease.

Details of Pkd2 heterozygotes where renal phenotype has been studied in adult mice.

***Pkd2* allele (type)**	**Phenotype**
Pkd2^{-} (null) (Wu et al., 2000, Wu et al., 1998)	Unilateral 1-5 renal cysts in 20.7-28.6% mice n=21 and 29 6.9-53% had 1-2 liver cysts
Pkd2^{WS25} (unstable) (Wu et al., 1998)	Unilateral microcysts (2-5 clusters) in 6.5% mice at 6-14 weeks, n=46.
Pkd2^{lacZ} (null) **(Stypmann et al., 2007)**	A few cysts in adult >12 months. Do not affect renal function. Not extensively studied
Pkd2^{lrm4} (point mutation)	Bilateral Low numbers of microcysts and tubular dilations. 33-75% n=7 mice between 9-18 months

Although cysts are identified in other heterozygote models, in general these exhibit low numbers of micro cysts and in only a proportion of mice. Wu et al. observe small numbers of microcysts in 6.5% of their mice which have undergone a somatic rearrangement of one copy of Pkd2 (Wu et al., 1998). We note similar numbers of microcysts per kidney but found them to be bilateral and in a higher proportion of mice. We see an increase in numbers of microcysts with age. Our mice were aged for longer than the Wu cohorts therefore it is possible that they would have seen higher numbers of cysts or bilateral cysts if they assessed their mice at a later time point. Similar to Wu, we noted clusters of tubule dilation, although these were common in Wt mice too. The two mice where both kidneys were scored, presented with bilateral microcysts indicating that both kidneys were affected equally (**Fig 3.8**).

Pkd2$^{-/+}$ (Wu et al., 2000) mice do not develop cysts embryonically and only a small proportion (29%) of aged mice developed sparse unilateral renal cysts. Wu and colleagues (Wu et al., 2000) reported liver cysts in half (53%) of the *Pkd2*$^{-/+}$ mice studied yet a third did not develop cysts in either kidney or liver. None of the mice presented with decreased renal function nor did any have bilateral renal cysts. *Pkd1*$^{(del34)/+}$ adult mice (Lu et al., 1999), representing a more severe form of the disease, expectedly presented a more severe phenotype. The majority (80%) of aged mice developed a small number of renal cysts and 33% of the mice studied presented with bilateral cysts. Renal function was normal. A third (27%) of mice developed liver cysts and had reduced liver function. The *Irm4* result is comparable to the development of cysts seen in other published *Pkd2* heterozygote mouse mutants. It is reported that at least half the renal function must be compromised in order to detect biomarkers of renal disease (Scarfe et al., 2015) and this is not observed in the aged *Pkd2*$^{Irm4/+}$ mice.

3.4.2 Liver cysts

We see a more severe liver phenotype than others have noted. Cilia have been implicated in the development of polycystic liver disease and liver cysts are a feature of a number of ciliopathies. Liver cysts are evident in 83-94% of ADPKD patients (Wills et al., 2014). A drop in urinary urea would indicate liver dysfunction since urea is produced in the liver as a by-

product of protein metabolism. This was not noted in these mice indicating that liver function is not drastically compromised.

3.4.3 Interstitial fibrosis

Tubular interstitial fibrosis is reported to be a contributing factor to the progression towards ESRD (Norman, 2011) yet there is a widely varying degree of fibrosis seen in ADPKD patients. It is unclear whether interstitial fibrosis is mechanistically linked to the development of cysts or whether the cysts cause the fibrosis to develop. The B6J background has been reported to be resistant to fibrosis however, this aspect of the disease was not assessed here. In the future, crossing to a more susceptible genetic background may allow for the effect of interstitial fibrosis on the progression of PKD in *Pkd2*$^{lrm4/+}$ mice to be assessed.

3.4.4 The nature of the *Pkd2*^{lrm4} allele

The similarity between *Pkd2*$^{-/+}$ and *Pkd2*$^{lrm4/+}$ is further evidence indicating that *Pkd2*^{lrm4} is a null allele in terms of liver and renal phenotypes. Comparing *Pkd2*$^{-/+}$ and *Pkd2*$^{lrm4/+}$, the embryonic phenotypes and adult heterozygous phenotypes are remarkably similar. The question of the nature of the *Pkd2*^{lrm4} mutation and whether it acts as a functional null has still to be answered. The molecular characteristics and cellular interactions of the protein are still to be established. These questions are addressed in the following chapters.

Chapter 4: The deletion of the Wt copy of *Pkd2* in *Pkd2*$^{lrm4/+}$ is sufficient to induce renal cyst development in adult mice

4.1 Introduction

The previous chapter assessed the phenotype of adult *Pkd2*$^{lrm4/+}$ mice, revealing the development of cystic liver diseases and renal microcyst development in aged mice. To further assess *lrm4* associated kidney disease, the *lrm4* mutation was assessed over a null allele specifically in the kidney. The floxed allele of *Pkd2* was deleted specifically in the kidney and mice harbouring the *lrm4* allele were assessed for kidney function.

4.1.1 The regions of the adult kidney

Sectioning through the kidney transversely enables identification of regions of the kidney and permits visualisation of each portion of the nephron. The main body of the kidney is divided into three areas; the cortex to the outside; the outer medulla, which itself is divided into the outer stripe of the outer medulla (OSOM) and the inner stripe of the outer medulla (ISOM); and the inner medulla which leads into the papilla and renal pelvis (**Fig 4.1**). The cortex is the outer portion of the kidney where the glomeruli reside. The convoluted segments of the proximal and distal tubules also lie here. The OSOM is interdigitated with the cortex and devoid of glomeruli, it is made up of the straight portion (pars recta) of the proximal tubule and the thick ascending limb of the loop of Henle, this straightening of the tubules makes for a less compacted appearance. The OSOM and ISOM are demarcated where the thick pars recta of the proximal tubule transitions into the thin descending limb. The proximal tubule is divided up into three segments, S1, S2 and S3 (**Fig 4.1**). The pars convoluta or proximal convoluted tubule is situated in the cortex and is the first portion of the proximal tubule that filtrate enters after the glomerulus. S1 has high cellar complexity, with densely-packed elongated mitochondria and a brush border of microvilli. S2 is a transitional segment which begins in the cortex and has intermediate characteristics between S1 and S3. S2 has shorter microvilli than S1 and the fewer mitochondria. S3 lies in the OSOM and is the thinnest segment of the proximal tubule which has the lowest cellular complexity and no brush border. The S3 tubules are lined by flattened epithelia; while the outer diameter is markedly reduced compared to the thicker segments, the lumen is only

slightly smaller (Frazier et al., 2012). S3 transitions into the thin descending limb of the loop of Henle at the border between OSOM and ISOM, delineating the sections of the outer medulla. The thin descending limb projects through the ISOM into the inner medulla in a proportion of long loop nephrons. The inner medulla is otherwise filled with collecting tubules which funnel the urine into the renal pelvis. The loop of Henle is made up of the thin descending limb, as the loop turns back towards the medulla, the thin ascending limb transitions into the thick ascending limb or straight portion of the distal tubule. At the point where the distal tubule reaches the glomerulus, the juxtaglomerular apparatus can be found. The thick distal tubule then becomes convoluted and the nephron ends in the cortex near its own glomerulus.

The kidney is one of the most heterologous tissues in the body, made up of more than 26 different cell types (Al-Awqati and Oliver, 2002). The majority of the renal parenchyma is made up of tubular portions with interstitial tissue being sparse in the cortex and increasing gradually towards the papilla. The papilla is surrounded by the renal pelvis which is continuous with the ureter. The vascular system of the kidney is supplied by the renal artery and renal vein. The renal artery branches into interlobar arteries and arcuate arteries which then branch off to supply blood to the afferent arteriole which enters the glomerulus.

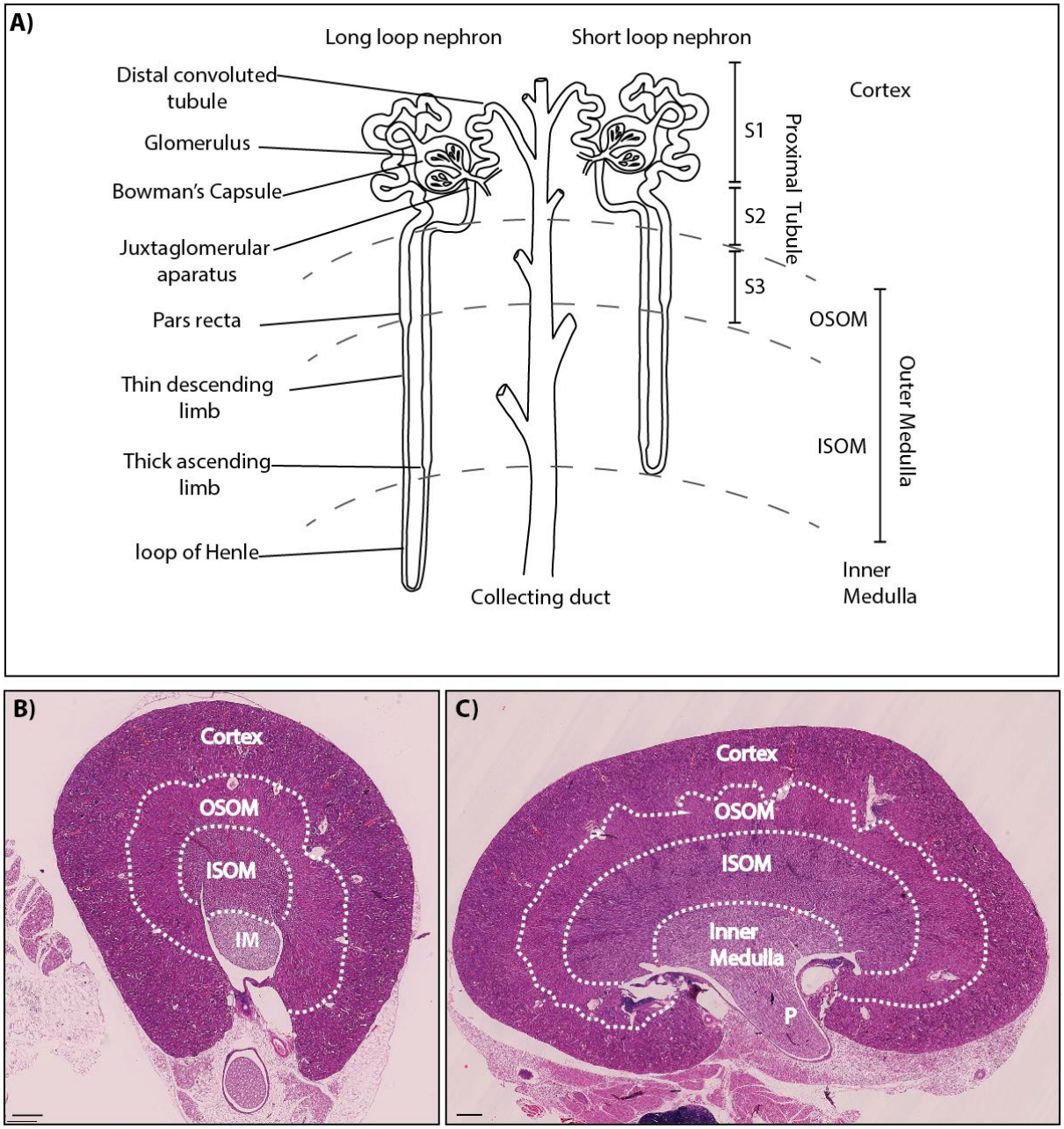

Figure 4.1: Nephron structure and kidney regions

The Nephron is a complicated structure made up of tubular segments which are highly specialised for filtrate resorption. A) A schematic of the nephron details the segments of the glomerulus, proximal tubule (S1, S2 and S3), distal tubule and collecting duct and reflects where the segments lie within the kidney. Long loop nephrons project into the inner medulla whereas short loop nephrons make their turn in the ISOM. This reduction of tubular segments in the inner medulla gives rise to its tapering shape, seen in C) (Jamison, 1987). B) Transverse and C) Sagittal sections through the kidney reveal the cortex where the glomeruli lie; the outer medulla, divided up into the outer stripe and inner stripe; and the inner medulla (IM) which leads into the pelvis. Scale bar 500µm. Diagram in A) adapted from (Fujiwara et al., 2009) P= renal pelvis.

4.1.2 Kap-iCre is expressed in the proximal tubule

Pkd2$^{lrm4/lrm4}$ embryonic kidneys develop cysts, however the fully penetrant embryonic lethality made assessment of the homozygotes after birth impossible. While the heterozygote adult mice did not progress to end-stage renal failure, low numbers of microcysts and liver cysts were evident. Therefore, *Pkd2*^{lrm4} was attractive as a cystogenic allele to assess over a null allele in the kidney. The embryonic lethality was likely to be linked to cardiac defects; therefore to avoid the effects of global mutation of *Pkd2* a spatially restricted deletion of a floxed allele was performed, allowing the heart to develop normally. A kidney specific Cre driver was selected in order to conditionally delete *Pkd2*^{flox} in the proximal tubule, leaving only the *lrm4* allele of *Pkd2* in proximal tubule cells. This enables the investigation of the cellular recessive effect of the *Pkd2*^{lrm4} allele in the adult kidney without the effect of the Wt protein.

A Cre driver line, Tg(Kap-iCre)29066/2Sig, here referred to as Kap-iCre, was obtained from the MRC Clinical Sciences Centre in London (**MM:1.1.3**). This line expresses an improved Cre recombinase (iCre) that has been codon optimised for mammalian cells, reducing CpG content which in turn reduces the likelihood of epigenetic silencing (Shimshek et al., 2002). Kap-iCre is controlled by the mouse kidney androgen regulated protein (*Kap*) promotor and *Kap* expression is tightly regulated by hormones in the proximal tubule. KAP is synthesised at a high level in male mouse kidneys and at a 10 fold lower level in female kidneys; castrated males express 200 fold reduced levels when compared with normal males. Administration of testosterone has been shown to raise expression levels in both females and castrated males to normal male levels (Toole et al., 1979).

The *Kap* gene is the most highly expressed gene in the proximal tubule of the mouse kidney and is the second most abundantly expressed transcript in the entire kidney (Virlon et al., 1999). The *Kap* promoter sequence contains response elements to a number of hormones including androgen response element (ARE), oestrogen response element (ERE) and Thyroid hormone response elements (TRE), which allow the gene's expression to be regulated. Assessment of *Kap* expression by in situ hybridisation has defined specific areas of the proximal tubule in which *Kap* expression is induced. Expression in S3 of the proximal tubule, the portion furthest from the glomerulus, appears to be the strongest (Tzortzaki et al., 2002)

and is under the control of pituitary hormone, thyrotropin and oestrogen (Meseguer and Catterall, 1992b). S1 and S2 segmental expression of *Kap* is controlled by androgenic stimulation. This leads to a sexually dimorphic spatial expression of the protein in the kidney. Females express the gene in the S3 segment alone, whereas males exhibit a wider expression pattern, in all three segments of the proximal tubule. Tzortzaki et al report age related decline in endogenous *Kap* expression in proximal tubules which is reported to be linked to a reduction in circulating hormone levels with age (Tzortzaki et al., 2002).

Kap-iCre is a transgenic construct made up of the *Kap* promotor and the iCre sequence that is inserted into exon 2 of a cloned genomic region of the human angiotensinogen gene (*hAGT*). The *Kap* promoter alone is not sufficient to confer proximal tubule specific expression (Fan et al., 2010), therefore exons 3-5 of *hAGT* which conveyed specific spatial expression in the renal proximal tubule, were included in the construct (**Fig 4.2**). This sequence does not produce any protein. Both the *hAGT* and *Kap* loci are tightly spatially regulated by hormones. Angiotensinogen is modulated by androgens, oestrogens, glucocorticoids, thyrotropin, cytokines and angiotensin-II (Ding and Sigmund, 2001). These hormones control the tissue specific expression of AGT; androgen administration causes a significant increase of AGT expression in the kidney yet only a slight increase in the liver. Similarly, oestrogens increase AGT levels in the liver and kidneys yet do not affect aorta and adipose expression levels. Hormone response elements (HRE) in the 5' flanking region of the gene, similar to the *Kap* gene, are responsible for the hormonal regulation (Ding and Sigmund, 2001).

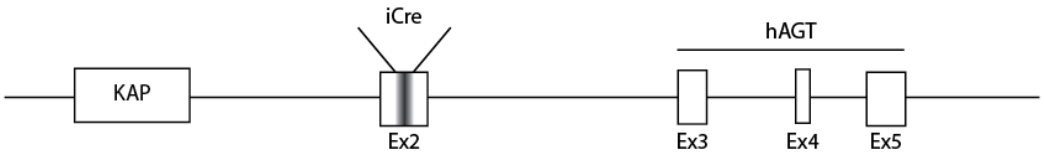

Figure 4.2: Schematic of transgenic Kap-iCre construct.

The *Kap* promotor is upstream of exons2-5 of the human angiotensinogen (hAGT) gene. The i0 coding sequence is inserted into exon 2 of hAGT and is under control of the *Kap* promoter. Exons 3-5 convey proximal tubule specific expression but are non-protein coding.

The expression pattern of this construct was tested in order to assure that it would be suitable to drive deletion of the floxed allele in the kidney.

4.2 Results

4.2.1 Kap-iCre has a sexually dimorphic expression pattern

When crossed with a floxed allele, Kap-iCre-mediated recombination results in deletion of the targeted gene in the proximal tubule cells of the kidney. We assessed endogenous activation of the recombinase by crossing the Kap-iCre recombinase to the Gt(ROSA)26Sor^{tm1Sor} (R26R) mouse line harbouring the ROSA26-lacZ reporter. iCre-mediated recombination removes a floxed region of DNA which prevents lacZ expression. Once activated, the lacZ gene expresses β-galactisidase, that when combined with X-gal yields an insoluble blue compound. Therefore, cells where iCre was expressed, under the control of the *Kap* promoter, were able to activate the expression of the LacZ reporter construct and produce blue-stained cells. As this modifies the genome, the lineage of daughter cells originating from a blue cell will also be blue.

Male and female mice were assessed in two age groups, 4-5 months and 8-9 months, for LacZ expression. Mice carrying Kap-iCre and R26R, along with controls which did not carry the recombinase but expressed R26R, and controls which carried neither the recombinase nor R26R were assessed. These mice are detailed in **Table 4.1.**

Table 4.1: Table detailing genotypes of mice used in R26R lineage tracing.

Kidneys were harvested and stained in two time-points; 4-5 months and 8-9 months. The 8 mice from each age group were stained at the same time, in a batch with the same stain. The purpose column described why each genotype was used.

Genotype	Age	Female	Male	Purpose
R26R$^{lacZ/+}$; Kap::iCre	4-5m	2	2	To assess cells in which Kap-iCre is active
	8-9m	2	2	
R26R$^{lacZ/+}$; Kap::Wt	4-5m	1	1	To assess the propensity of R26R transgene recombination without Cre
	8-9m	2	0	
R26R$^{+/+}$; Kap::Wt	4-5m	1	1	To assess background staining
	8-9m	1	1	

Mice were terminally anesthetised then perfused with 4% PFA and kidneys dissected out. Perfusion reduces the non-specific staining of red blood cells. Each kidney was cut in half transversely; one half of each kidney was embedded for cryosectioning and the other was

LacZ stained as described in materials and methods. Briefly, kidneys were submerged in 30% sucrose for 24-48 hrs, rinsed in PBS and incubated in X-gal stain solution for 24-48 hours at 37°C. After rinsing in PBS, the kidneys were post fixed with 4% PFA, taken through a glycerol series and imaged in 50% glycerol.

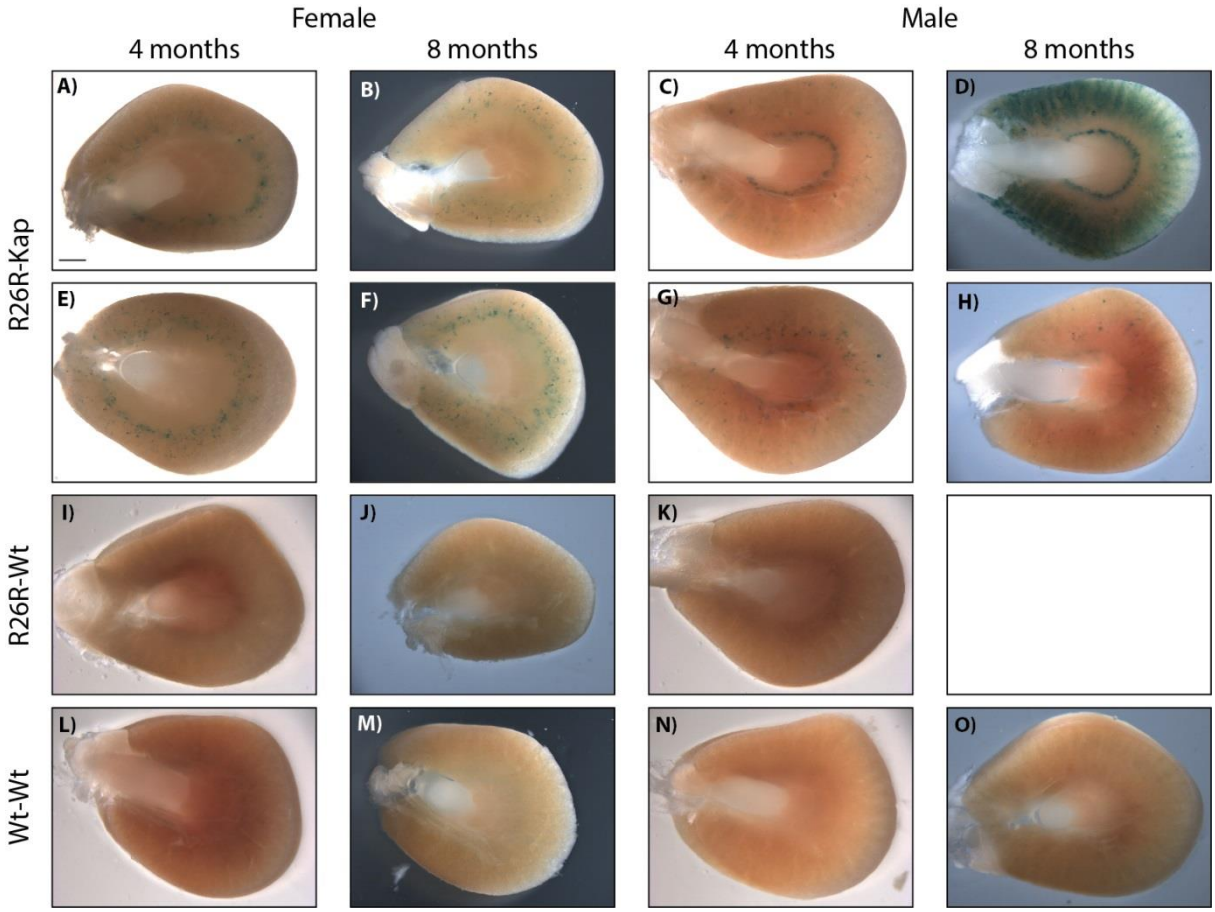

Figure 4.3: LacZ staining showing the activity pattern of Kap-iCre in male and female mice of 4-8 months old.

Female mice carrying R26R and Kap-iCre at 4 months. A) and E) and 8 months B) and F) exhibit blue staining throughout the cortex. Male mice carrying R26R and Kap-iCre at 4 months C) and G) exhibit a band of staining in the OSOM and speckles throughout the cortex. Older males of the same genotype D) and H) seemed variable. D) exhibited the dark band in the OSOM as previously seen but also a striated staining pattern in the cortex. H) more closely resembled the 4 month old mice, with a ring in the OSOM and speckles in the cortex. None of the mice that did not carry Kap-iCre exhibited staining. I)-K) show R26R-Wt mice and L)-O) show Wt-Wt mice. Scale bar=1mm.

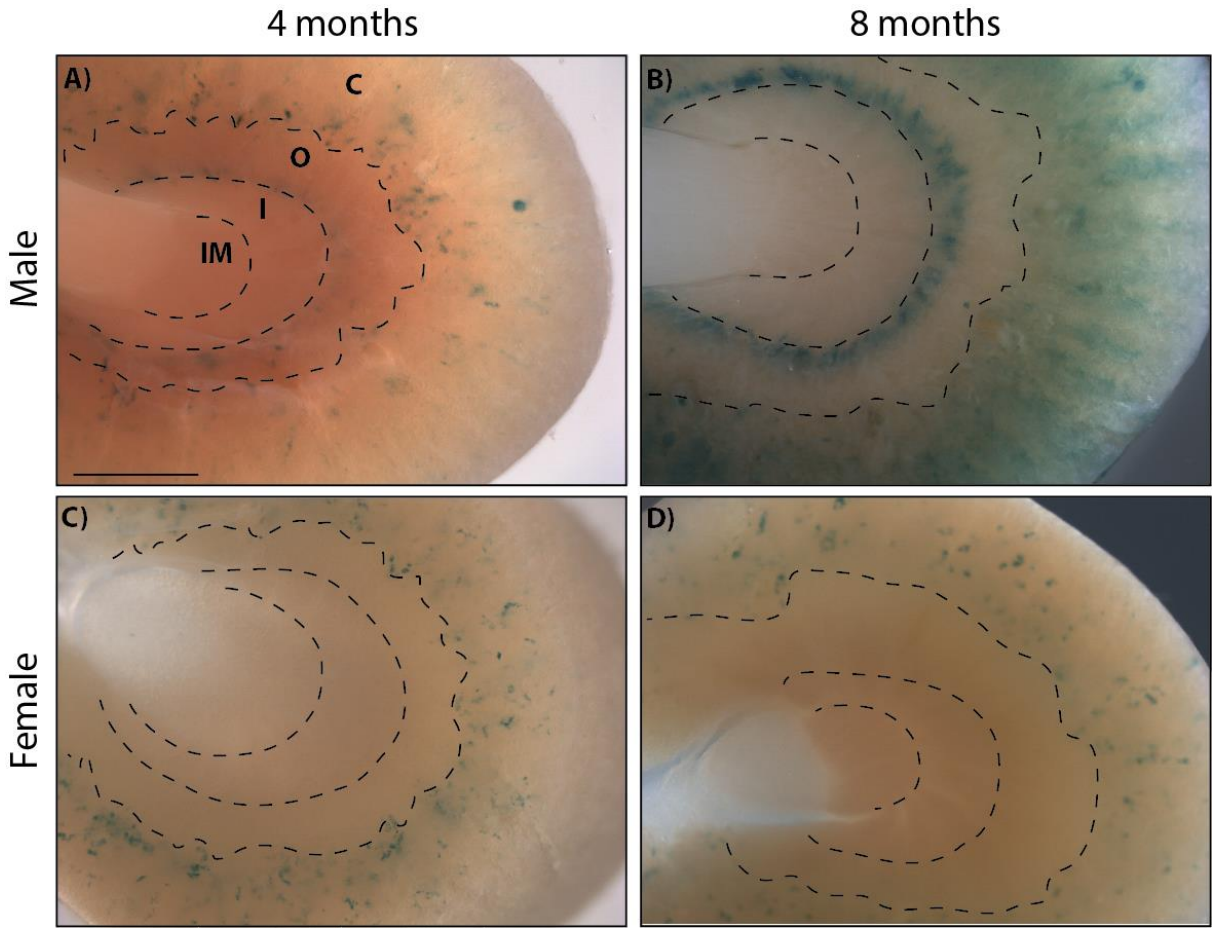

Figure 4.4: Close up of staining pattern of lacZ stained R26R-Kap kidneys.

A) at 4 months, the male exhibits a band of staining at the border between the OSOM and ISOM and a speckled pattern in the cortex. B) by 8 months, the strong OSOM/ISOM band is still evident and one of two males exhibited a striated pattern in the cortex. C) –D) females of both ages only expressed blue cells in the cortex. IM=inner medulla, I=ISOM. O=OSOM, C=Cortex. Scale bar =1mm.

Staining was observed in all *R26R*$^{lacZ/+}$; *Kap*::*iCre* kidneys but was absent from the *R26R*$^{lacZ/+}$; *Kap*::Wt and *R26R*$^{+/+}$; *Kap*::*Wt* kidneys, indicating that the expression pattern was specific to the Kap-iCre recombinase activity in combination with R26R. Distinct patterns of staining were seen in males and females in both groups. In the 4 month group, female staining was more diffuse and restricted to the cortex where S1 and S2 of the proximal tubule lie (see **Fig 4.1 A**). The male pattern is strong at the boundary between the OSOM and ISOM, which corresponds to the point at which S3 transitions to the thin descending limb. Expression appears more intense here, reflecting the density of the tubule in the outer medulla; this is consistent with the same number of tubules being stained in males and females.

In the older group of mice, another pattern of expression arises in the male. Of the two pairs of male kidneys assessed at 8-9m, one had a low level of expression in the OSOM similar to the younger males and the other presented strong expression here and additional expression in the cortex. Both males in this older group exhibit a striated pattern of staining in the cortex; the gap between striations is consistent with unstained vasculature, cortical distal tubule and collecting duct segments. It is known that testosterone levels in group housed male mice differ, with the dominant male producing the most testosterone (Giammanco et al., 2005). The more extensively stained kidneys could therefore be from a dominant male, with higher testosterone levels increasing expression in the cortex. The female pattern of staining does not appear to change with age.

Tzortzaki et al observed an age related decline in endogenous *Kap* expression in proximal tubules between 1-3 months of age, which is suggested to be linked to a reduction in circulating hormone levels with age (Tzortzaki et al., 2002). We do not observe a change in lacZ staining between 4-8 months however; since LacZ expression is binary, changes of levels of expression cannot be assessed in this way.

These staining patterns are summarised in **Table 4.2**.

Table 4.2: LacZ staining patterns seen in mice carrying R26R and Kap-iCre.

The three main staining patterns seen in male and female mice are shown with n numbers in middle column and a description of the pattern in the final column.

	Sex and n numbers	**Pattern**
	Female 2/2 at 4 months 2/2 at 8 months	S1 and S2 in cortex Same pattern expressed bilaterally and in both mice
	Male 2/2 at 4 months 1/2 at 8 months	Boundary of OSOM and ISOM, end of S3. Some expression in cortex Same pattern expressed bilaterally and in each mouse
	Male 1/2 at 8 months	Strong striated staining in S1 and S2 in cortex And at the boundary of OSOM and ISOM, end of S3

Contrary to Fan et al, who report that the transgene is not induced in females and that endogenous androgen activates the transgene (Fan et al., 2010), we found that Kap-iCre was activated in females and it seems likely that this is regulated by oestrogen induction of the ERE. This pattern is consistent in all females carrying both R26R and Kap-iCre and

therefore is attributed to the action of Kap-iCre rather than non-specific staining. Assessment of KAP expression in androgen-receptor deficient (Meseguer and Catterall, 1990), castrated and hypothyroid (Solé et al., 1996) mice has defined the spatial activation of *Kap*. Expression in the cortical segments (S1 and S2) is regulated by androgens (Meseguer and Catterall, 1990) and the expression in S3 is regulated by oestrogen and thyroid hormone (Meseguer and Catterall, 1992a). **Table 4.3** summarises this and compares our result.

Table 4.3: Summary of expected hormonal regulation and the expression pattern observed and expected

Segment	Reported regulation	Observed	Expected
S1 and S2	Androgens	Stronger in females at 4 months, increases in males with age	Only in males
S3	Oestrogens and thyrotropin	Male specific activation at bottom of OSOM	In both sexes, throughout whole OSOM

Staining in S1 and S2 is observed in both sexes. This could be related to testosterone in both sexes or could indicate that oestrogens or thyrotropin can activate Kap-iCre in the cortex. The literature suggests that KAP is most highly expressed in S3 (Tzortzaki et al., 2002) and that expression in this segment is seen in both sexes, however we observe a consistent male specific expression pattern here, in both age groups. Our expression data advocate a different expression pattern to that seen in the literature; S1 and S2 are activated in both sexes suggesting a non-sex hormone related factor (e.g. thyrotropin) and S3 is activated in males suggesting a sex hormone (e.g. androgen). The pattern of two non-contiguous areas of expression is not seen in the literature. We observe a clear gap in staining between the stained cortex regions and the staining in the male OSOM. This gap in staining corresponds to the majority of the OSOM in all kidneys. It appears that only the bottom portion of S3 is activated in our mice.

The difference in expression between our observation and that reported in the literature could be due to a number of factors. The expression of endogenous *Kap* was assessed by mRNA expression pattern with in situ hybridisation (Meseguer and Catterall, 1990, Tzortzaki et al., 2002, Solé et al., 1996). This provided evidence of the specific hormone regulated zones. Our assessment in transgenic mice using a LacZ reporter reflects the lineage of cells

in which the lacZ reporter has been activated. It is important to consider the effect of the hormone regulation of the *hAGT* exons which also direct the expression of the transgene. Assessment of the Kap-iCre construct with respect to androgen regulation of the *hAGT* portion concluded that an ARE is located within intron II of the *hAGT* gene (Fan et al., 2010). Intron II directly follows exon 2, the site where iCre sequence is inserted. However, this study did not assess the tubule specificity conveyed ARE induction. We have established that the Kap-iCre transgene is expressed in a different pattern to *Kap* mRNA and suggest that this is the result of elements within the Kap-iCre construct, most likely the *hAGT* portion.

To further pinpoint expression patterns, comparisons to other work with Kap-iCre were made. Li et al also assessed the expression pattern of Kap-iCre using R26R (Li et al., 2008). However, they reported that Kap::Wt mice exhibited staining, which may indicate that their perfusions were not effective leading to significant non-specific staining (Li et al., 2008). LacZ expression was seen in male cortical proximal tubules, co-localizing with AQP1 antibody labelling. AQP1 is a water permeable channel which localizes along all segments of the proximal tubules and in the thin ascending limb of the loop of Henle, throughout the cortex into the inner medulla (Maunsbach et al., 1997). In males, staining was observed more strongly at the base of the OSOM, similar to our male specific expression pattern (Li et al., 2008). However, assessment of females was inconclusive due to background staining. Our lacZ reporter assay is cleaner and stronger than the Li assay (Li et al., 2008); we have no expression in the Cre negative controls and can detect faint staining well.

There are consistent differences in male and female Kap-iCre expression patterns, yet both sexes appear to induce significant recombination in the proximal tubule. Kap-iCre is a proximal tubule recombinase which is able to produce specific expression patterns in the male and female kidney. Importantly, there is no activation in the Wt kidney. Therefore, this line fulfilled our requirements to use as a proximal tubule specific driver to delete our floxed allele.

4.2.2 Conditional deletion of the floxed allele causes cyst development

The Kap-iCre mice were crossed to *Pkd2*$^{lrm4/+}$ mice producing double heterozygotes carrying both Kap-iCre and *Pkd2*^{lrm4}. These *Pkd2*$^{lrm4/+}$*;Kap::iCre* mice were then crossed to *Pkd2*$^{flox/flox}$ mice to produce the experimental cohort. This cross produced *Pkd2*$^{flox/lrm4}$*;Kap::iCre* experimental mice; *Pkd2*$^{flox/+}$*;Kap::iCre* and *Pkd2*$^{flox/lrm4}$*;Kap::Wt* mice which were used as controls. All mice were congenically B6J. Preliminary analysis of a cohort of ten litters aged between postnatal day 10 (P10) and postnatal day 76 (P76) were assessed for the development of renal cysts, these are detailed in **Table 4.4**. For ease, a shorthand for the genotype will be used to refer to the mice, this is detailed in **Table4.4**. These mice were sacrificed and their kidneys removed. The mice were sexed by identification of internal anatomy post mortem and separated by sex. Ear and tail biopsies were collected for genotyping and the kidneys were dissected, weighed and fixed in formal saline.

Table 4.4: Genotypes, ages and numbers examined in the preliminary cohort.

Ten litters were examined between P10 and P76. Sexes were separated and analysed before being placed by genotypes. The table shows the number of mice, with age in brackets of each genotype that was studied. In the genotype column, the shorthand for each genotype is recorded in brackets.

Genotype (referred to as)	**Female**	**Male**
Pkd2$^{lrm4/flox}$:Kap::iCre (lrm4-Kap)	3 (P18), 2 (P73)	1 (P15), 1 (P18), 2 (P26), 1(P52), 2(P62)
Pkd2$^{+/flox}$;Kap::iCre (Wt-Kap)	3(P10), 1 (P15), 1 (P26), 1 (P61)	2(P10),1 (P15), 1 (P18) 1(P62), 1(P75)
Pkd2$^{lrm4/flox}$;Kap::Wt (lrm4-Wt)	1 (P10), 2 (P18), 2(P26), 1(P76)	1(P10), 1 (P15), 1(P18),1 (P26), 2(P52), 1(P62), 2(P76)
Pkd2$^{+/flox}$;Kap::Wt (Wt-Wt)	1 (P10), 1 (P15), 2(P52), 2(P73)	1 (P15), 3(P52),2(P75)

External kidney morphology was examined and 6/24 kidneys assessed between P50-75 presented with externally visible cysts which protruded through the capsule of the kidney (**Fig 4.5**). Kidneys were photographed before being embedded in paraffin for sectioning. Six to eight sections per kidney were cut to a thickness of 7µm with 56µm intervals and H&E stained. Stained sections were imaged on the Hamamatsu slide scanner with a 20X lens and assessed, blind to genotype for development of cysts (**Fig 4.6**).

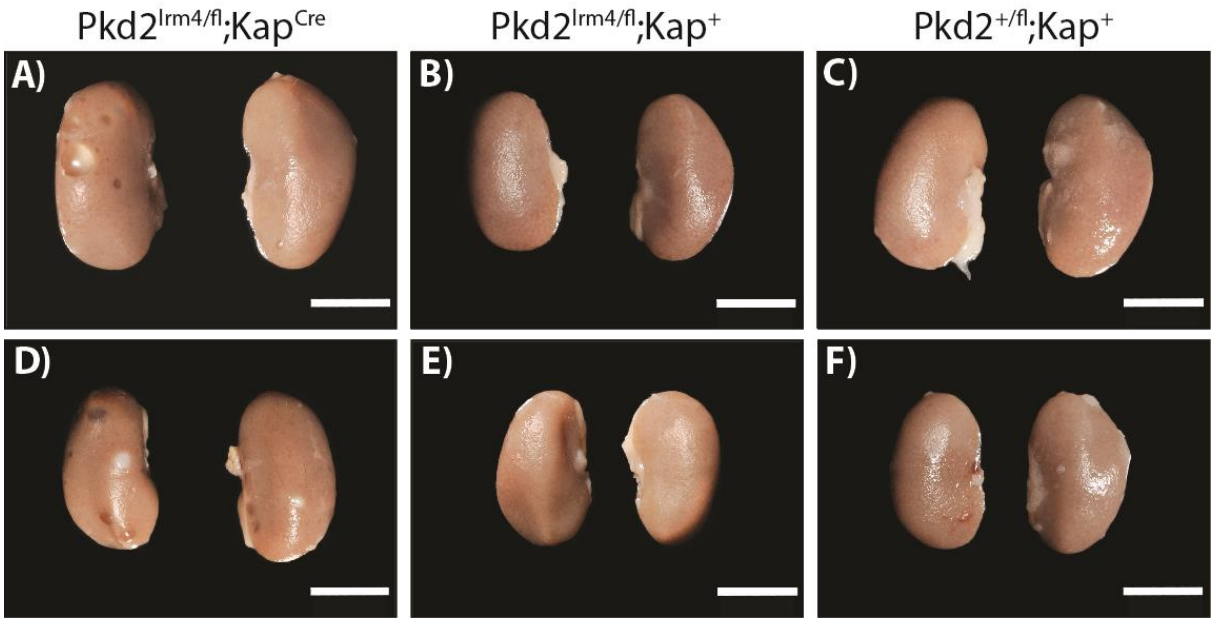

Figure 4.5: External images of kidneys from preliminary cohort.

Displayed are representative kidneys from three genotypes of the preliminary cohort of mice. Cysts are evident protruding through the capsule in the Pkd2$^{lrm4/flox}$;Kap::iCre kidneys A) and D), but not in B), C), E) nor F). A) and B) are males aged P52. C) and F) are males aged P76. D) and E) are females, D) is P73 and E) is P52. Scale bar 0.5 cm.

Figure 4.6: Analysis of cyst diameters in preliminary cohort.

The table (below) details the numbers of males (m) and females (f) assessed for each genotype. Cyst classes between micro and macro2 are detailed in the table. Overleaf; A)-D) show representative lrm4-Kap kidneys. A) a female and B) a male at P18, C) shows a female at P73 and D) a male at P62. E)-H) depict cysts from lrm4-Kap kidneys. E) shows a large cortical cyst 1070µm. the point at the base of the cyst could indicate that two tubules have merged into one cyst .F) and G) contain a proteinaceous substance.

I) represents cyst diameters from all genotypes. Each point is a cyst, kidneys pooled by sex. The dotted horizontal lines mark off size categories, µ=micro, M=macro, M2=macro2. J) represents only lrm4-Kap mice, divided by sex and age. Scale bar in A) 500um, in E) is 100um.

	lrm4-wt	**wt-Kap**	**lrm4-Kap**	**Wt-Wt**
	5F:7M	2F:3M	5F:6M	5F:5M
Micro (116.1-193.5 µm)	0:2	4:1	14:9	2:2
Macro (193.5-500 µm)	1:2	0:0	12:21	0:0
Macro2 (>500 µm)	0:1	0:0	10:9	0:0
hydronephrosis	1:1	0:1	2:0	3:2

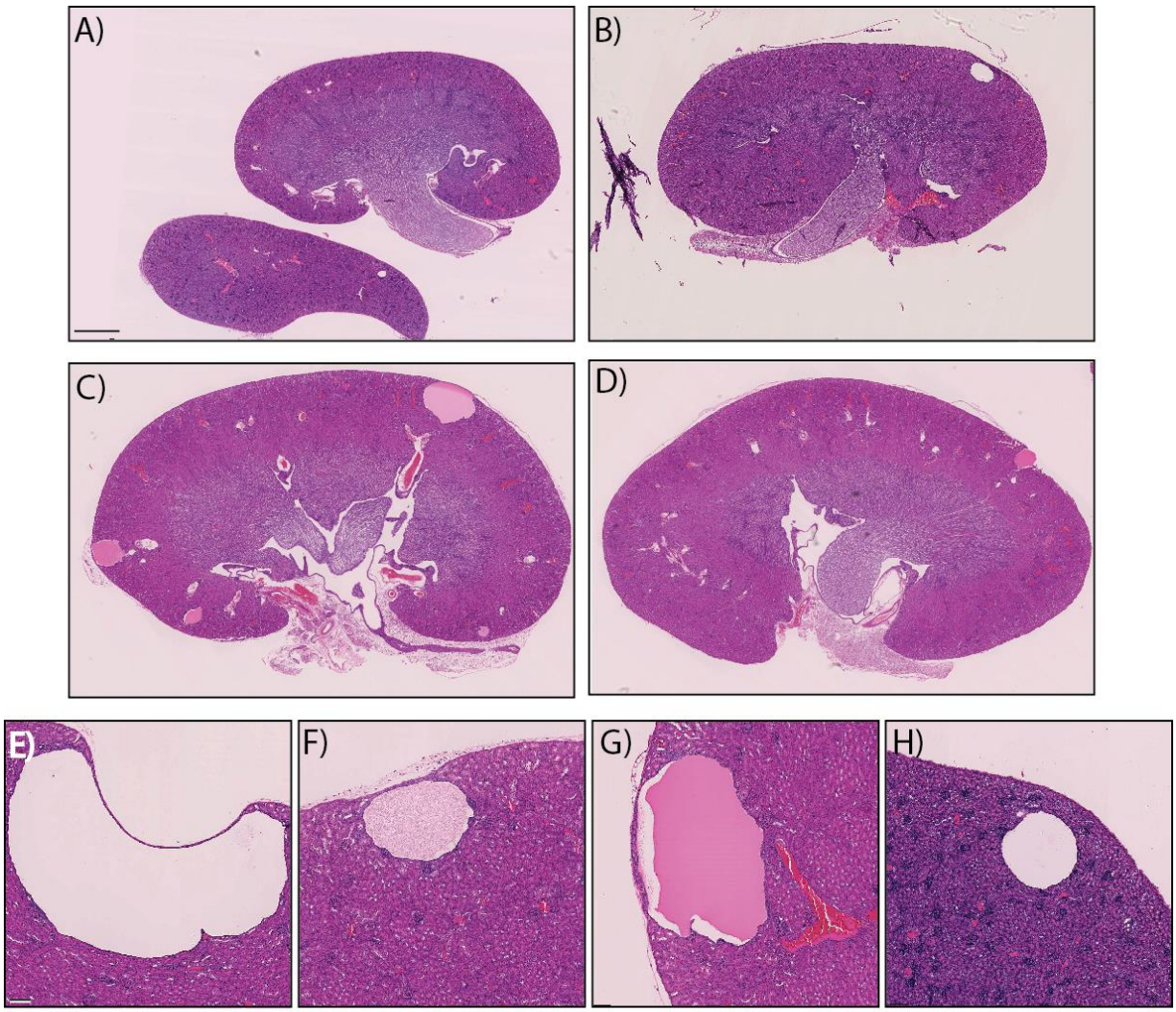
A)
B)
C)
D)
E)
F)
G)
H)

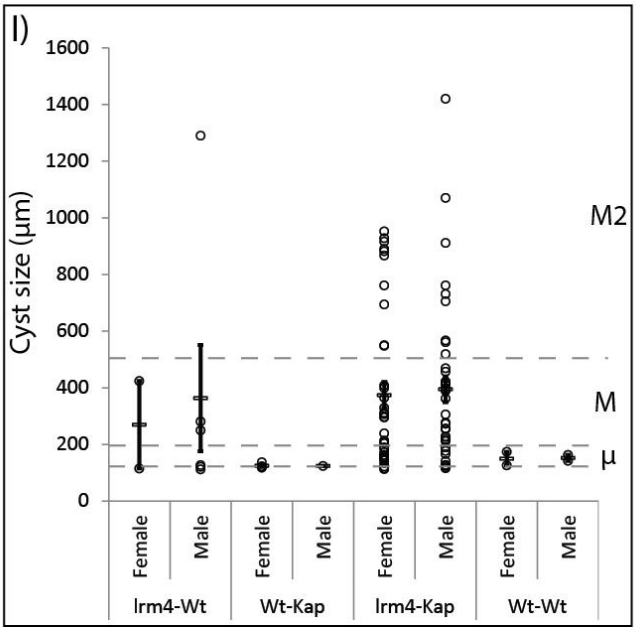
I)
Cyst size (µm)
1600
1400
1200
1000
800
600
400
200
0
M2
M
µ
Female
Male
Female
Male
Female
Male
Female
Male
Irm4-Wt
Wt-Kap
Irm4-Kap
Wt-Wt

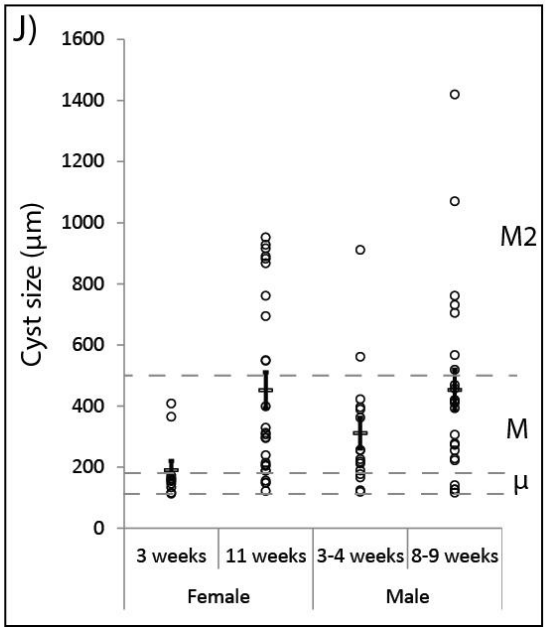
J)
Cyst size (µm)
1600
1400
1200
1000
800
600
400
200
0
M2
M
µ
3 weeks
11 weeks
3-4 weeks
8-9 weeks
Female
Male

Cysts were scored using the definitions set out in the previous chapter (see table in **Fig 4.6**). An additional class was added to divide macrocysts; those between 193.5-500µm were denoted macrocysts, those above 500µm were denoted Macro2. The graph in I) represents all genotypes assessed. Significant differences were seen between cyst diameters from lrm4-Kap and Wt-Kap (P=0.043) and between Wt-Wt and Wt-Kap (P=0.034). lrm4-Kap and Wt-Kap are markedly different. Excluding one large macrocyst in lrm4-Wt, only lrm4-Kap exhibits cysts in the largest category. Mice carrying *Pkd2*^{lrm4} exclusively exhibit cysts greater than 174µm microcysts. Assuming *Pkd2*^{flox} is equivalent to *Pkd2*$^{+}$, lrm4-Wt mice are expected to exhibit a similar number of cysts to the Pkd2$^{lrm4/+}$ mice that were examined in the previous chapter. The presence of larger cysts in this group indicates that *Pkd2*^{fl} may be slightly hypomorphic. When assessing lrm4-Kap alone (graph J)), males and females exhibited similar numbers and sizes of cysts. A trend is evident of increased cyst development between the two age groups in both sexes; more cysts and a larger size are seen. Cyst size in females is significantly greater in the older group (p=0.0083). Although the trend of progressive cysts development is evident in males, the size of cysts was not significantly different between the two ages. This may be because, of the three younger males, only one was 3 weeks old, the others were slightly older (4 weeks).

Hydronephrosis was common across genotypes and particularly so in Wt-Wt mice. No mice exhibited bilateral hydronephrosis. Cyst diameters were scored in sagittal sections however the orientation of blood vessels complicates cyst identification in this orientation, therefore for further cohorts, kidneys were sectioned laterally.

4.2.3 After deletion of *Pkd2*^{flox}, cysts increase in size and number with age.

Since a clear increase in size and number of cysts was observed in both sexes with age in the preliminary cohort, a larger cohort of mice was planned so that kidney function and cyst development over a greater range of ages could be assessed. Male and female mice were aged to 6, 9, 12 and 15 months then urine and blood samples were collected. Mice were allowed to rest for at least a week after spending time in metabolism cages before terminal bleed and kidney dissection (**Fig 4.7**). Kidneys were fixed in formalin and embedded in paraffin wax. Twelve sections were cut per kidney at 7µm thickness with 56µm intervals, mounted and processed for H&E staining. One kidney from each pair was cut sagittally, the

other transversely. Stained sections were imaged on the Hamamatsu slide scanner at 40X and assessed for development of cysts (**Fig 4.8**).

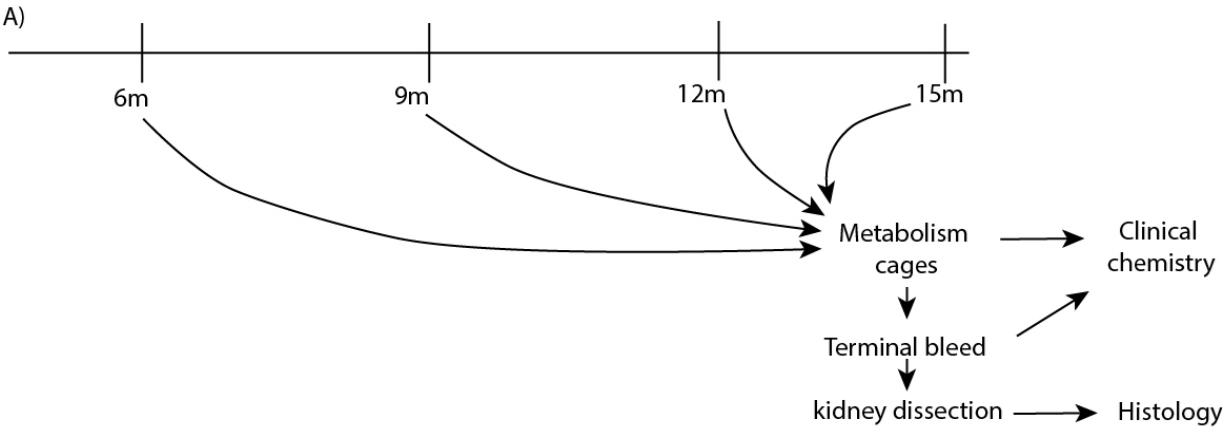

Genotype	Age	Female	Male
Pkd2$^{lrm4/flox}$;Kap::iCre (lrm4-Kap)	6m	3	2
	9m	3	3
	12m	3	3
	15m	3	3
Pkd2$^{+/flox}$;Kap::Wt (Wt-Wt)	6m	3	1
	9m	3	2
	12m	3	3
	15m	3	3
Pkd2$^{lrm4/flox}$;Kap::Wt (lrm4-Wt)	6m	3	2
	9m	3	3
	12m	3	3
	15m	3	3
Pkd2$^{+/flox}$;Kap::iCre (Wt-Kap)	6m	3	3
	9m	3	3
	12m	3	3
	15m	3	3

Figure 4.7: Schematic of the experimental pipeline undertaken with the conditional cohort.

A) details mice aged to 6, 9, 12 and 15 months and at each time point urine is collected in metabolism cages, terminal blood samples were collected and kidneys were dissected. Blood and urine were analysed and kidney sections were cut and stained.

The table details the genotypes and numbers of the mice used.

As the mice were bred and genotyped, experimental mice were assigned an age group. Mice were sacrificed as they reached the age of the group they were assigned to. The urine and plasma sample analysis has been undertaken and is detailed in the following sections. For

each kidney, four lateral kidney sections were scored blindly for tubule dilations. **Fig 4.8** presents representative sections of kidneys from each genotype, aged to 15 months. At 15 months, cysts are not observed in Wt-Wt, lrm4-Wt or Wt-Kap kidneys of either sex. Cystic dilations are observed in lrm4-Kap kidneys at 15 months, with the male being more strongly affected.

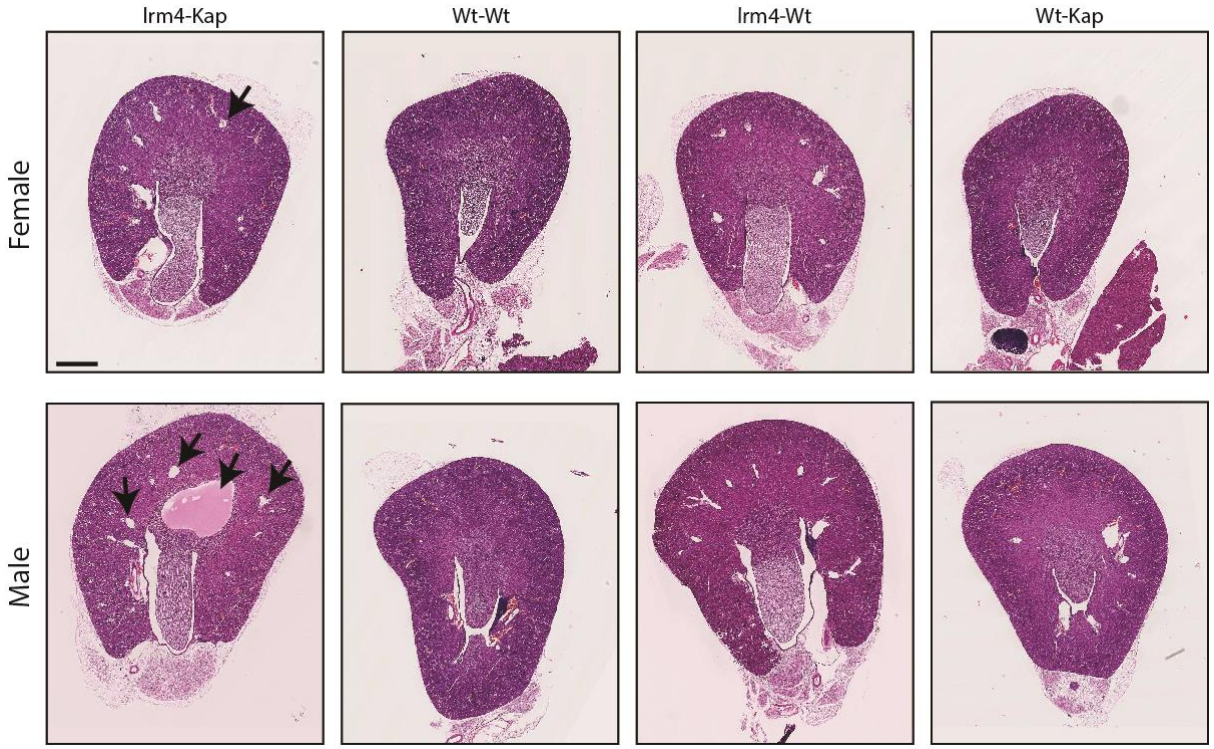

Figure 4.8: kidneys from 15 month old male and female mice from all genotypes

A representative kidney from each genotype is presented. The female and male lrm4-Kap kidneys contain cysts (arrow), the male being more severely affected. Scale bar 500 µm.

Fig 4.9 represents kidneys from lrm4-Kap mice from both sexes, across the age groups. Cysts were observed originating throughout the cortex in both male and female lrm4-Kap mice. Cyst development appears to be variable in both sexes. There is bilateral cyst development in both male and female kidneys but the extent of cyst development and growth is variable across ages in both sexes. The male kidneys exhibit a stronger phenotype with larger and more frequent cysts originating in the cortex. This is consistent with the analysis of the younger mice of the preliminary cohort. The female mice appear to exhibit a milder phenotype than the males, both in this group of mice and in the preliminary cohort which were assessed at a younger age. When comparing the average diameter of cysts across age groups, there does not appear to be a trend to indicate that either male or female kidney

cysts diameters increase with age. However, when cyst diameters were averaged from cysts that were classed as microcysts (μ) or larger, the size of cysts in female kidneys appears to decrease with age across the age groups, whereas male kidneys appear to have a more varied average of cyst diameters. It is possible that a trend relating to progression of cyst development with age may arise if higher numbers of kidneys were assessed. Currently, it is difficult to discern whether there is a linear relationship between cyst size and age as is suggested by the preliminary cohort.

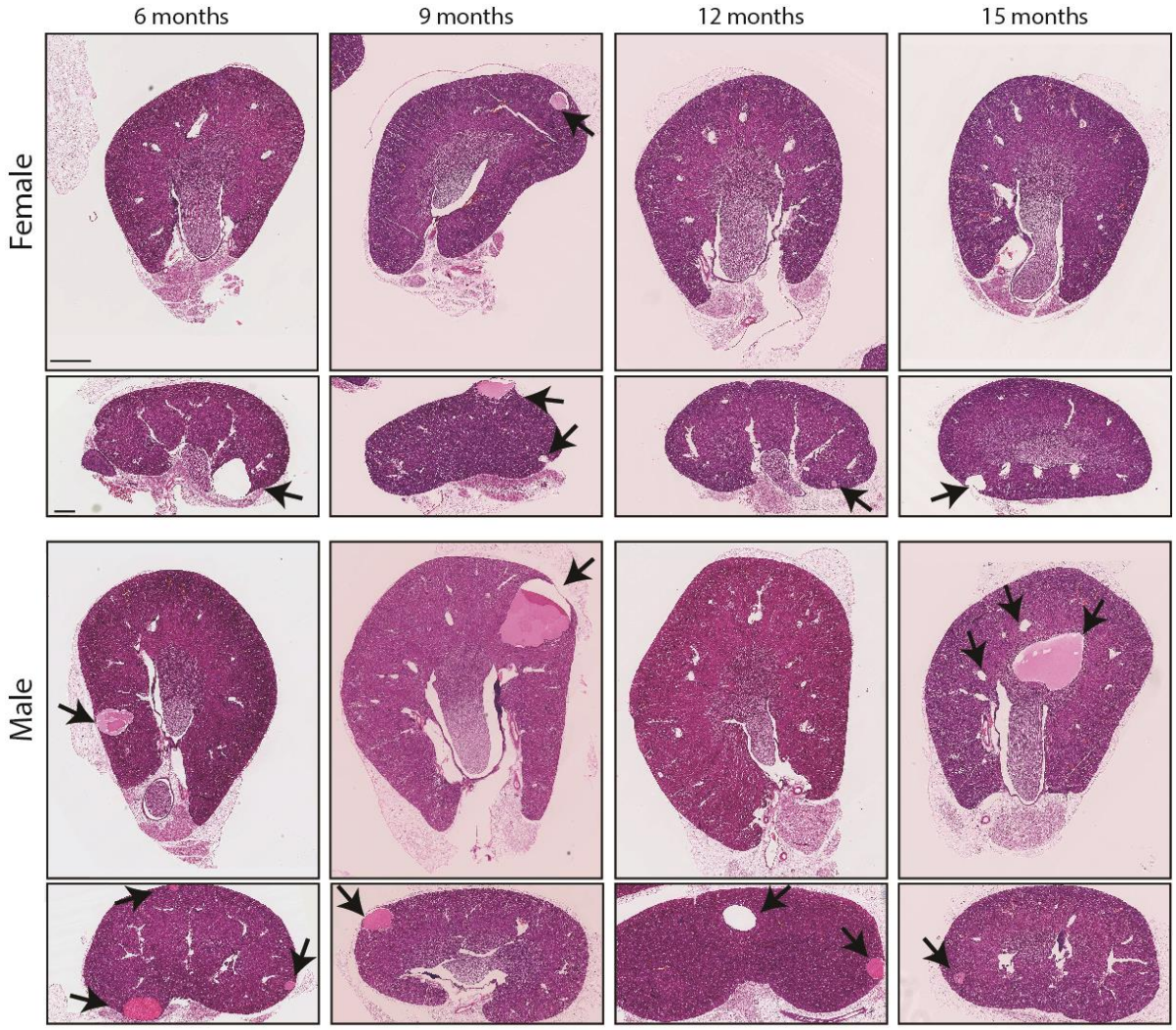

Figure 4.9: Female and male lrm4-Kap kidneys from all age groups

The panels show representative kidneys from 6-15 month age groups. The top row shows female kidneys cut transversely. Below each transverse section, the sagittal section from the pair can be seen. The second row of transverse sections are from males, below these are the male sagittal sections. Arrows indicate cysts. Scale bars are 500µm.

Cyst diameters were measured using the definitions set out in the previous chapter (see table in **Fig 4.6**), with the additional class of macrocysts, denoted Macro2 (>500µm), that was used for the preliminary investigation in this chapter (**4.2.2**). Four transverse sections per mouse were assessed (from one kidney per mouse) for tubule dilations. The graph in **Fig 4.10** represents cyst diameters scored from mice across 4 age groups and 4 genotypes.

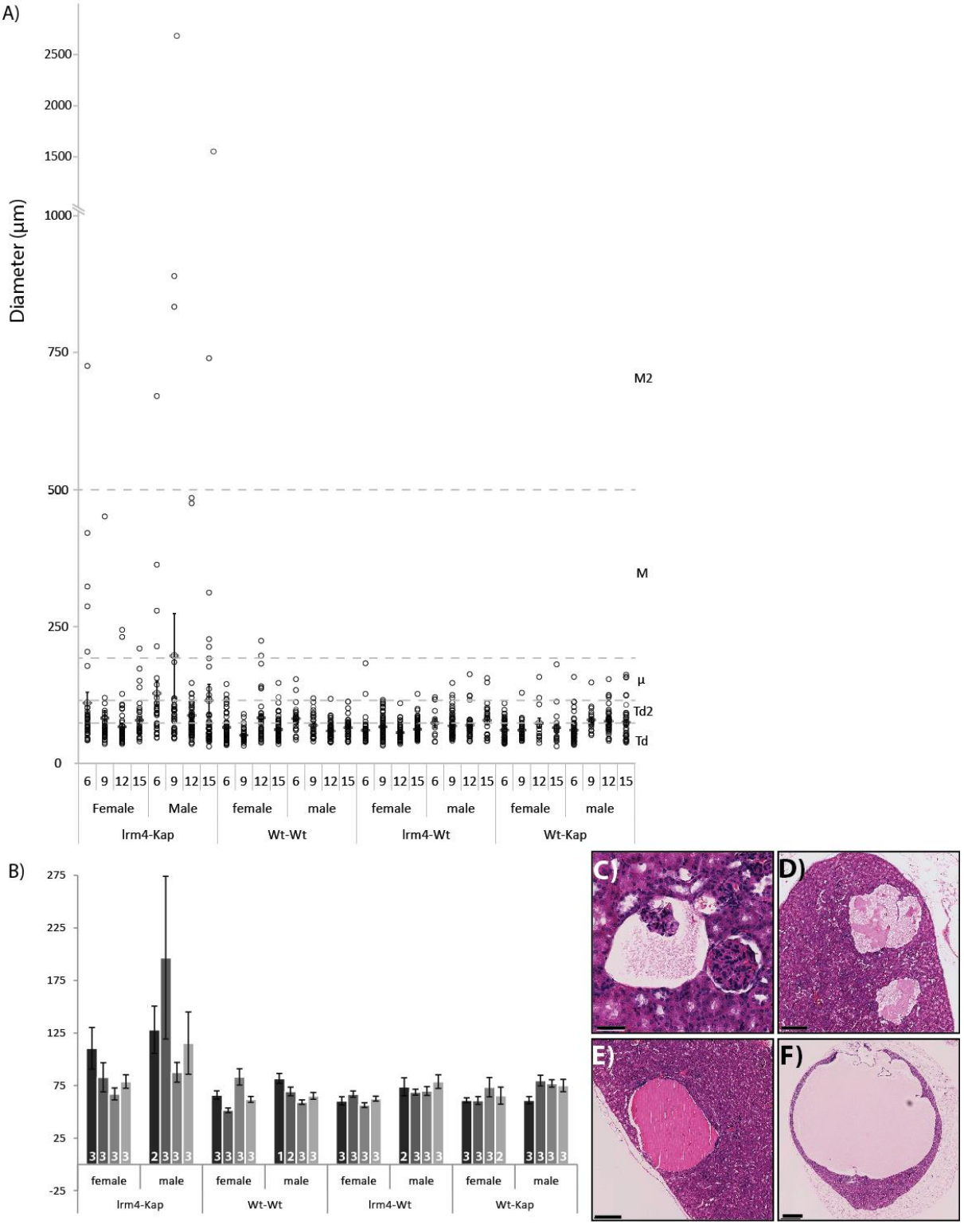

Figure 4.10: Analysis of cyst diameters in Kap-iCre mice

The graph in A) shows cyst diameters for all genotypes for males and females, from 6-15 months. Each point represents a single measurement. The rectangular point in each group represents the average size of dilations. Error bars show SEM. Up to 3 mice were assessed for each group. The graph is divided horizontally into size categories, Td=small dilation, Td2=larger dilation, µ=microcyst, M=macrocyst and M2=larger Macrocyst. The dimensions

for which are recorded in **Fig 4.6.** B) graph represents the average cyst size for each group. Error bars represent SEM. The darkest column in each set shows the value for the 6 months group, the second darkest for the 9 months group, the third for the 12 month group and the lightest column shows the data for the 15 month group. C)-F) show images of cysts from lrm4-Kap kidneys. C) shows an uncommon glomerular cyst, recognisable by the glomerular tuft in the centre. Next to this cyst is a normal glomerulus. D) shows a pair of cysts that have developed in the cortex. E) shows a cortical cyst which is filled with a proteinaceous substance. F) shows the largest cysts that was noted, the diameter of which is 2680µm this cyst was seen in a 9 month old male lrm4-Kap kidney. N numbers are recorded at the base of the columns in graph B). Scale bar in C-E is 200µm, the scale bar in F) is 400µm.

Although microcysts present fairly commonly in these mice across genotypes (**Fig 4.10 A**), only lrm4-Kap mice present with the largest class of cyst. Cysts greater than 500µm (M2) were seen in both sexes; in 6 month old females and in 6, 9 and 15 month old males. There were two Wt-Wt M cysts, both from the same 12 month old female mouse. These measured 197µm and 224µm, at the lower end of the M cyst category (193.5-500µm). Other than these two cysts, this class is also reserved for lrm4-Kap.

The largest cyst observed was 2680µm and is pictured in **Fig 4.10 F**. This could be confused with hydronephrosis if assessed alone due to its size overtaking the whole of the cortex of the section. However, other sections from the same kidney showed a normal renal pelvis and also exhibited other cysts in the cortex. Another section of the same kidney is presented as the 9 month old male transverse section of a kidney in **Fig 4.9**.

From this incomplete assessment of cyst diameters, it is possible to state that the deletion of the floxed allele using Kap-iCre in the context of *Pkd2*^{lrm4} is sufficient to cause cyst development in the cortex of the mouse kidney.

4.2.4 Plasma analysis shows evidence of altered kidney function

Biochemical analysis of plasma samples was undertaken as detailed in **chapter 3**. The results of the plasma samples are presented in **Fig 4.11.** A table of corresponding average values and standard deviations is available in **Appendix2:Table 2.4**

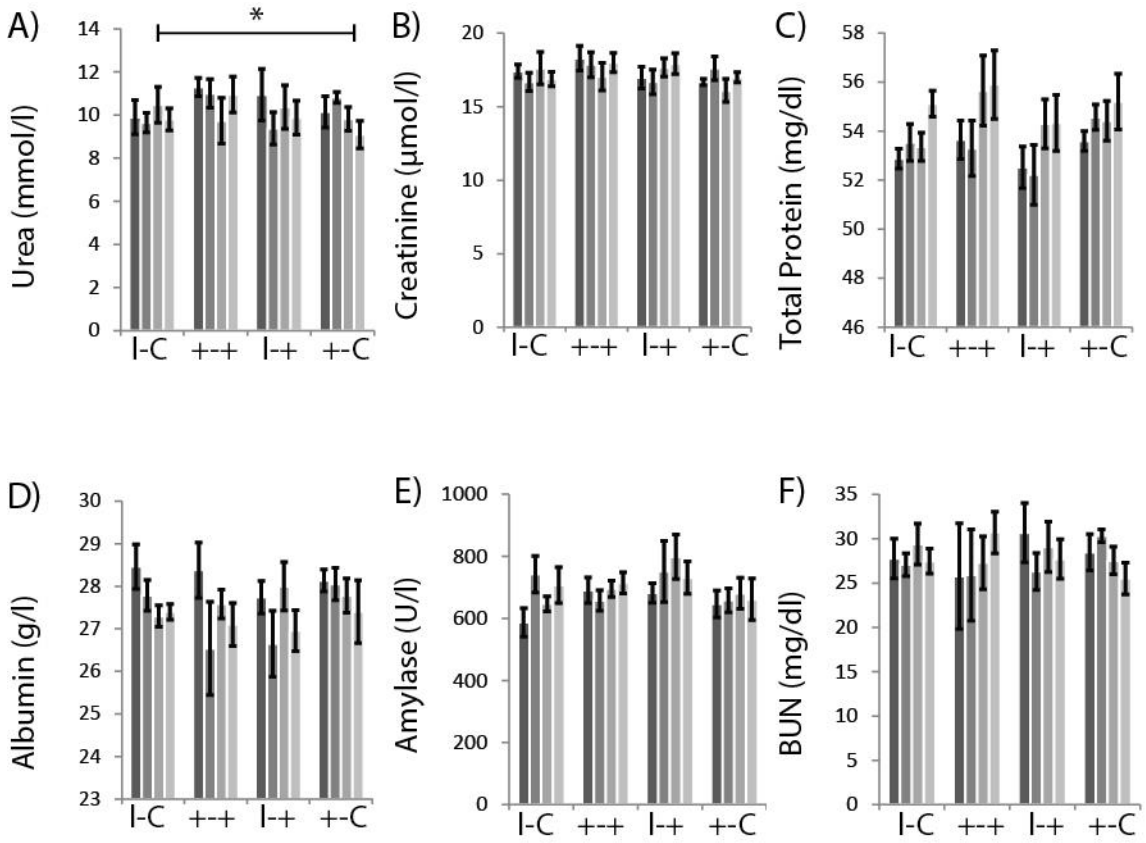

Figure 4.11: A comparison between plasma components from each of the four genotypes analysed male and females combined.

Each graph depicts the 4 genotypes over the 4 time-points. The first cluster in each case represents the lrm4-Cre [l-C] mice, the second represents Wt-Wt [+-+], the third lrm4-Wt [l-+] and the last Wt-Cre [+-C]. The darkest column in each cluster represents plasma assessed from the 6 month old mice, the next from 9 months, the next from 12 months and the last from 15 months. Each column represents an average (combined sexes) of 4-6 mice assessed for each component. Error bars represent SEM. *= $p<0.05$

When these plasma components were compared, age related decline towards renal failure was not detected in the serum components analysed. Student's T-tests were performed comparing all possible combinations of genotypes within each age group for every plasma component (**Appendix2:Table 2.6**). When sexes were pooled, one t-test was significant at $P<0.05$; urea levels were significantly lower ($P=0.049$) in lrm4-Kap mice compared to Wt-Wt at nine months. Lrm4-Wt urea was also similarly low but was not significant. This was not a consistent trend with age and is therefore unlikely to reflect declining renal function.

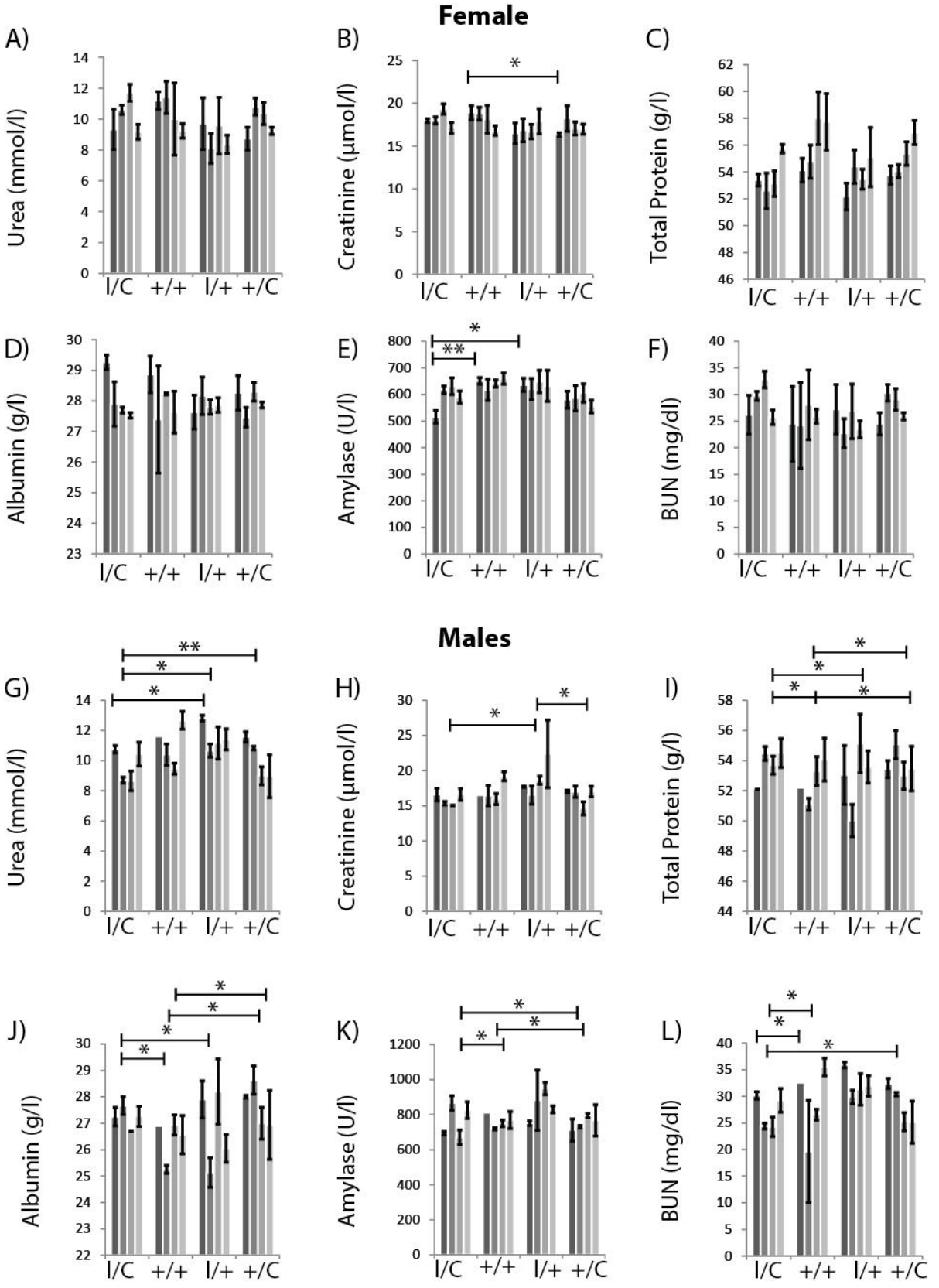

Figure 4.12: graphs representing Plasma analysis separated by sex

Each graph depicts the 4 genotypes over the 4 time-points. A)-F) show analysis of female samples. G)-L) show analysis of male samples. The first cluster in each case represents the

lrm4-Cre [l/C] mice, the second represents Wt-Wt [+/+], the third lrm4-Wt [l/+] and the last Wt-Cre [+/C]. The darkest column in each cluster represents plasma assessed from the 6 month old mice, the next from 9 months, the next from 12 months and the last from 15 months. Each column represents an average of up to 3 mice assessed for each component. Error bars represent SEM. *= p<0.05, **=p<0.01

When separating the mice by sex and age (**Fig 4.12**) (**Appendix2:Table 2.7-8**), the female comparisons produced three significant results and the males produced 19 significant comparisons. The significant female comparisons were seen for creatinine between Wt-Wt and Wt-Kap at six months (P=0.042) and for amylase between lrm4-Kap and Wt-Wt (P=0.007) and between lrm4-Kap and Wt-Kap (p=0.0077) at six months. The amylase level in Kap-Wt is lower than all other genotypes at 6 months but does not remain consistently low over time. As these results do not remain significant in subsequent age groups, it seems most likely that these results are amongst the 5% of data-points expected to randomly appear significant.

Since there was only one 6 month old male Wt-Wt, Student's T-tests could not be performed between Wt-Wt and other genotypes at six months. Nonetheless, two groups of the results were significant over two time periods. When comparing urea levels in lrm4-Kap and lrm4-Wt, lrm4-Kap was significantly lower at 6 months (P=0.024) and 9 months (p=0.015). Lrm4-Kap remained lower than all other genotypes at all ages except 15 months when Wt-Wt urea levels are lower. Lrm4-Kap and Wt-Wt urea levels were significantly different at 9 months (p=0.0008). Blood urea nitrogen (BUN) was calculated for these samples and although combined sexes and females alone were not significant, the male samples produced three significant comparisons. BUN T-tests were significant when lrm4-Kap was compared with lrm4-Wt at 6 (p=0.024) and 9 months (p=0.015). At 9 months lrm4-Kap was significantly different to lrm4-Wt (p=0.015) and Wt-Wt (p=0.0008). Reflecting the urea result, the lrm4-Kap BUN was significantly lower than other genotypes. In combination, these factors indicate that urea levels are significantly reduced in the plasma of lrm4-Kap male mice. Whereas increased urea is a marker of kidney disease, decreased serum urea is an indication of liver malfunction since urea is produced in the liver as a metabolite of protein.

4.2.5 Urinalysis shows evidence of altered kidney function

The urine was also assessed for markers of renal function in the same way as for the *Pkd2*$^{lrm4/+}$ mice. The urine sample results are recorded in graphs in **Fig 4.13** and a table of averages and standard deviations can be found in **Appendix2:Table 2.5.**

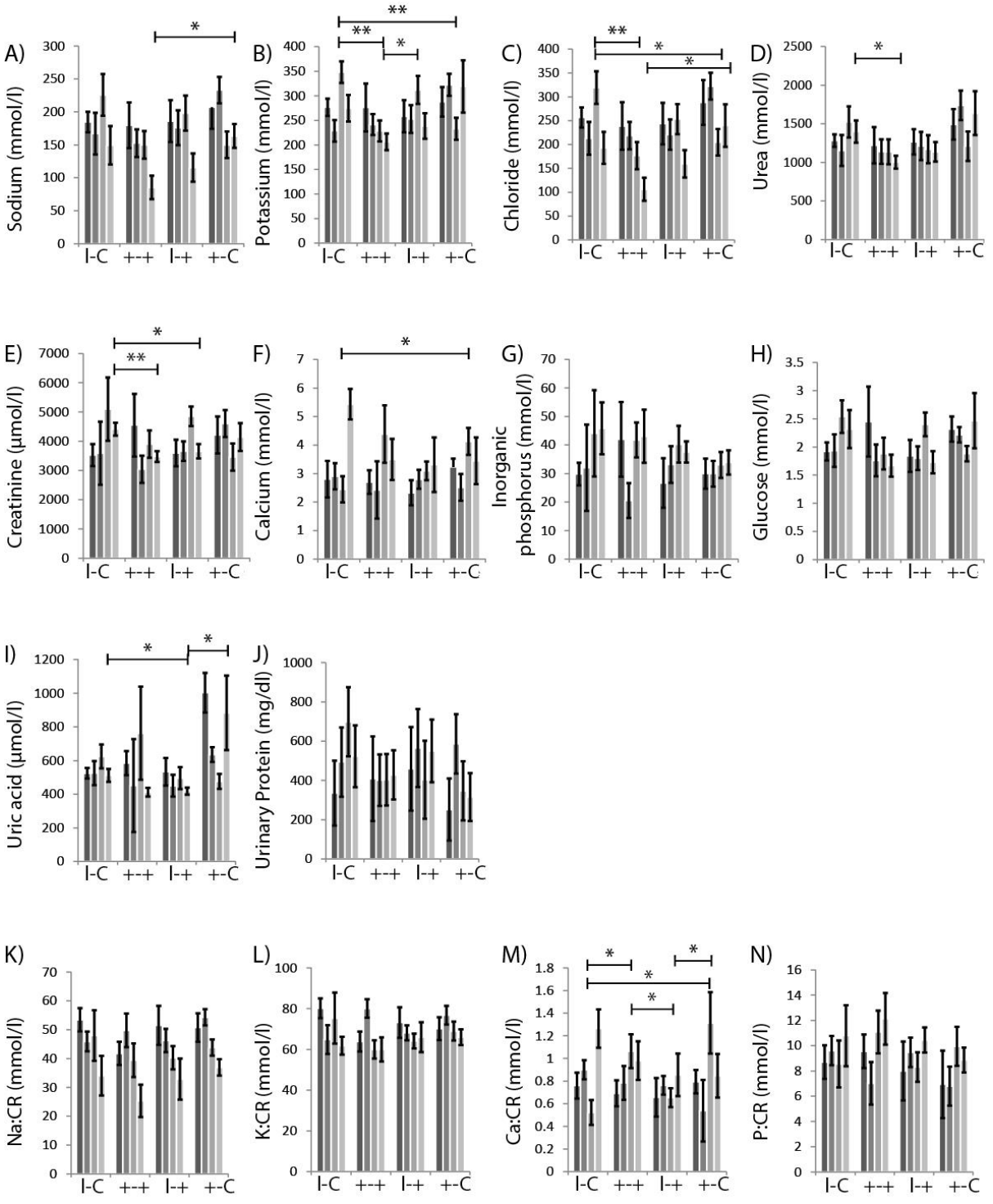

Figure 4.13: A comparison between urine components from each of the four genotypes analysed over 4 time points

Each graph depicts the 4 genotypes over the 4 time-points. The first cluster in each case represents the lrm4-Cre [l-C] mice, the second represents Wt-Wt [+-+], the third lrm4-Wt [l-+] and the last Wt-Cre [+-C]. The darkest column in each cluster represents urine assessed from the 6 month old mice, the next from 9 months, the next from 12 months and the last from 15 months. Each column represents an average (combined sexes) of 4-6 mice assessed

for each component. Error bars represent SEM. *= p<0.05, **=p<0.01 Na=sodium, K=potassium, Cl= chloride, Cr=creatinine, Ca=calcium, P= inorganic phosphorus.

Student's T-tests were undertaken to compare genotypes and age groups for male and female combined, males alone and females alone.

When assessed without separating by sex as previously, 17 tests were significant (**Appendix2:Table 2.9**). Notably, levels of potassium were significantly different when lrm4-Kap mice were compared with Wt-Wt *(p=0.0038)* and Wt-Kap (p=0.0063) at 12 months. Chloride levels were significantly higher in lrm4-Kap when compared to both Wt-Kap (p=0.010) and Wt-Wt (p=0.032) at 12 months but by 15 months were back down to a normal level, consistent with the other genotypes.

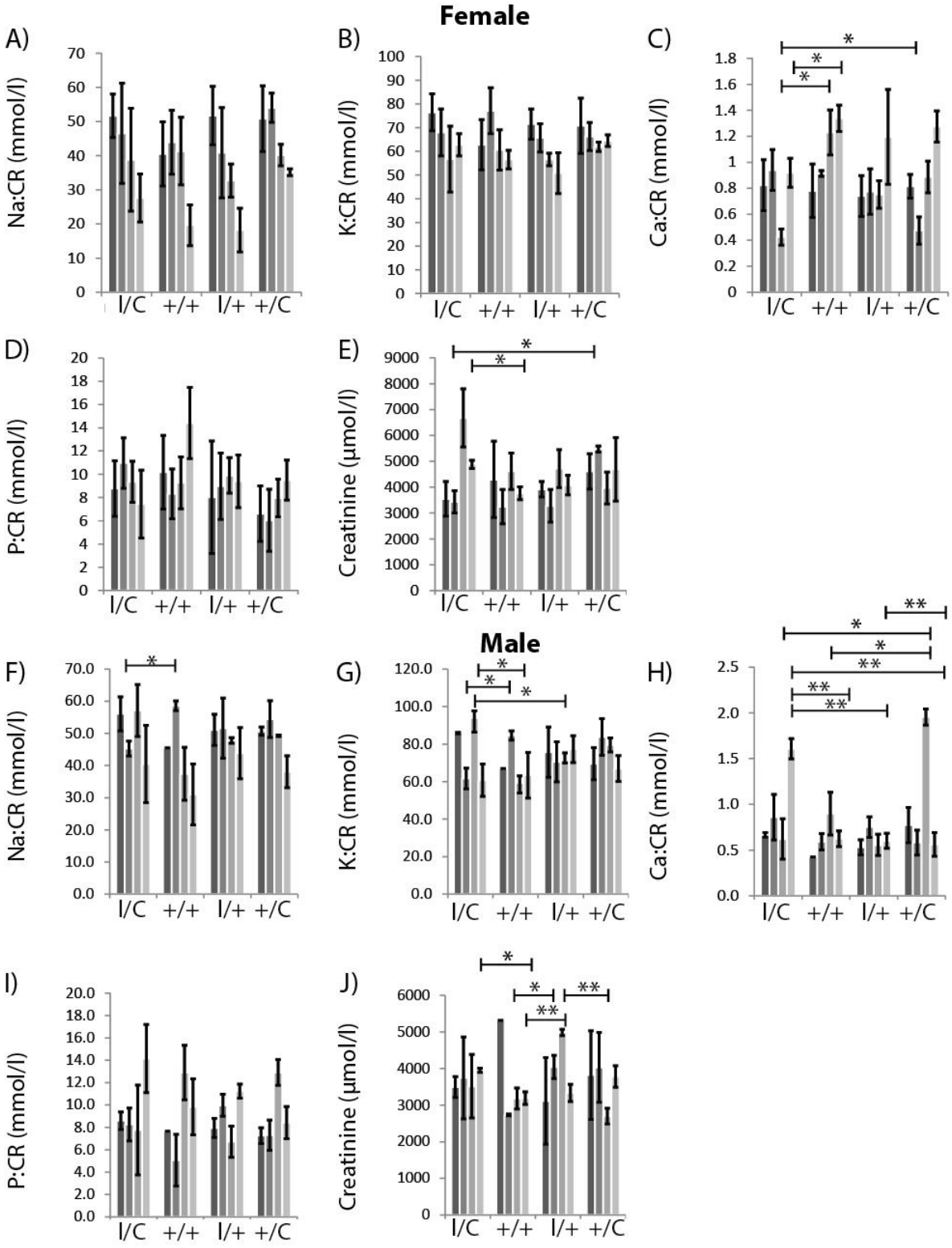

Figure 4.14: A comparison between urine components from each of the four genotypes analysed over 4 time points, sexes separated

Each graph depicts the 4 genotypes over the 4 time-points. A)-E) show analysis of female samples. F)-J) show analysis of male samples. The first cluster in each case represents the lrm4-Cre [I/C] mice, the second represents Wt-Wt [+/+], the third lrm4-Wt [I/+] and the last

Wt-Cre [+/C]. The darkest column in each cluster represents plasma assessed from the 6 month old mice, the next from 9 months, the next from 12 months and the last from 15 months. Each column represents an average of up to 3 mice assessed for each component. Error bars represent SEM. *= p<0.05, **=p<0.01 Na=sodium, K=potassium, Cl= chloride, Cr=creatinine, Ca=calcium, P= inorganic phosphorus.

Considering the differential expression of Kap-iCre in male and females, it is important to assess male and female phenotypes separately as well as in combination (**Fig 4.14**) (**Appendix2:Table 2.10-11**). For the graphs that are separated by sex, the creatinine ratios are represented. Potassium remained high in female lrm4-Kap mice when compared to Wt-Wt at both 12 (p=0.0056) and 15 months (p=0.0435), and when compared to Wt-Kap mice at 12 months (p=0.0470). Normalised calcium (Ca:Cr) was also elevated in lrm4-Kap females when compared to Wt-Wt at 12 (p=0.0385) and 15 months (p=0.0494). These increased levels in the experimental genotype which remained high at 12 and 15 months are indicators that kidney function is beginning to be affected by renal cyst development.

Assessment of plasma components indicated that lrm4-Kap male mice had decreased BUN which is an indicator of liver disease. However, of the comparisons made for urea levels in males, none were significant. At 15 months calcium levels were three fold higher in lrm4-Kap urine than in any other genotype (Wt-Kap (p=0.0007), lrm4-Wt *(p=0.0003), or* Wt-Wt (p=0.0012). Calcium levels were significantly lower in lrm4-Kap when compared to Wt-Wt at 12 months (p=0.0083). When calcium is expressed as a ratio of creatinine, this same pattern is observed. This could represent a disruption of calcium regulation as at 15 months all 3 males had significantly higher levels of calcium in the urine.

A number of plasma and urea components were significantly altered in lrm4-Kap mice. This may indicate a decline towards renal insufficiency. Often large changes are not observed in urea or plasma markers until a substantial proportion of kidney structure has been affected, however BUN is argued to be a marker of late stages of kidney disease in both humans and rodents (Scarfe et al., 2015). Therefore, this data likely represents a disruption of kidney function.

4.2.4 Liver cyst development

Assessment of pathology revealed that livers from both lrm4-Kap and lrm4-Wt mice exhibited externally visible cysts (**Fig 4.15**). Since Kap-iCre expression was only expected in the kidney, it seemed strange that there was a liver phenotype. It is possible that there was ectopic expression of Kap-iCre in the liver. Kap-iCre expression has been reported previously in the liver (Li et al., 2008), although less abundantly than the kidney. While this could explain the lrm4-Kap liver phenotype, it does not explain the liver cysts of lrm4-Wt mice. The aberrant recombination of the floxed allele could explain these liver cysts, perhaps the floxed allele was recombining in the absence of Cre. However, every genotype assessed carried $Pkd2^{fl}$ and liver cysts are only evident in those with $Pkd2^{lrm4}$. The liver cysts seen in these mice appear consistent with the phenotype seen in the $Pkd2^{lrm4/+}$ mice. This indicates that $Pkd2^{lrm4}$ is responsible for the liver phenotype; that *Pkd2* function in the liver is disrupted by the lrm4 mutation and that *Pkd2* is essential for maintenance of normal liver tubule architecture.

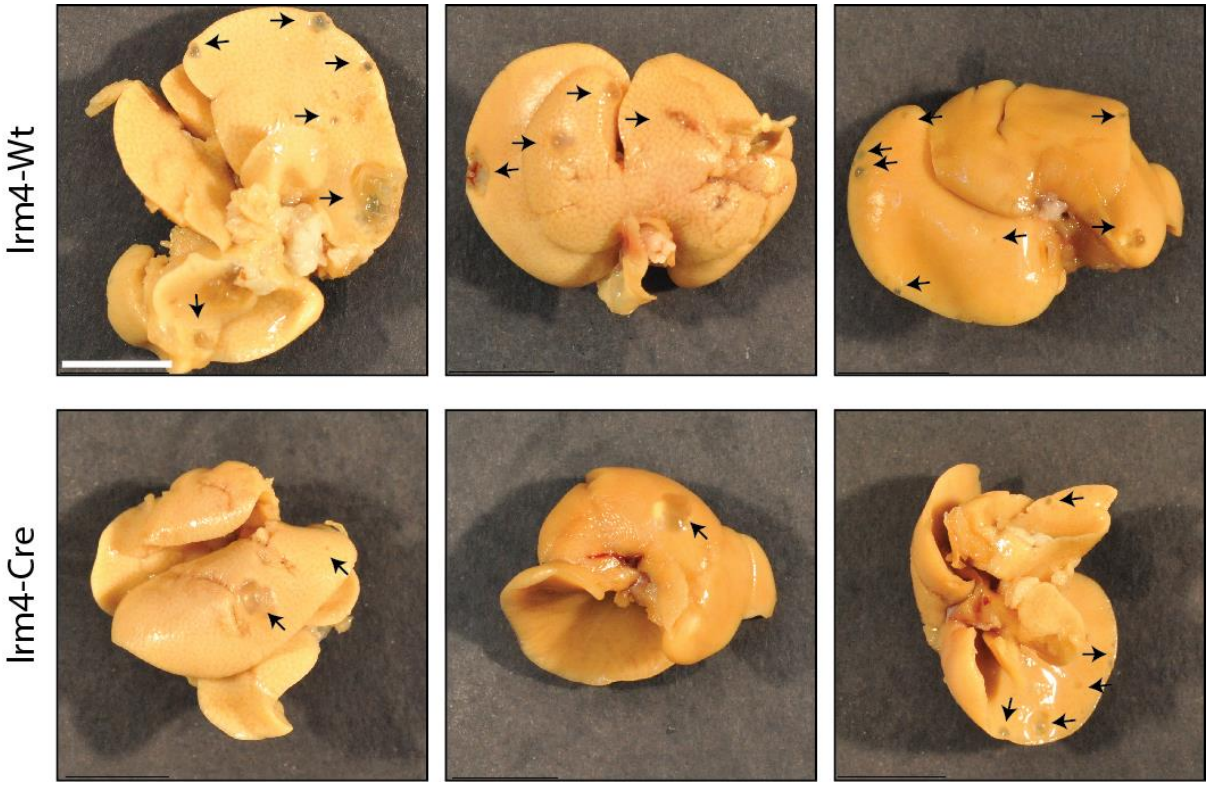

Figure 4.15: external images of livers collected from 15 month old mice.

The top row shows 3 livers from lrm4-Wt mice and the bottom row shows livers from three lrm4-Cre mice. Cysts are visible in both genotypes and throughout each liver (Arrows).

Assessment of serum components revealed significantly lower levels of serum urea and BUN in lrm4-Kap mice compared to other genotypes. Lowered serum urea is associated with liver dysfunction and reflects the cysts seen in the livers of these mice. Reduced serum urea was seen in the lrm4-Kap mice but not in lrm4-Wt mice, despite both groups displaying liver cysts. This indicates that other factors relating to the kap-iCre are responsible for significant reduction in liver function. The lowered urea and BUN was also not observed in *Pkd2*$^{lrm4/+}$ mice despite the liver cysts appearing equal. Perhaps this reflects different areas of the liver in which the cysts are forming or perhaps another undetected liver disease could be present in these mice. Since the liver phenotype was unexpected, only a small number of mice were assessed and few sections were analysed. Future assessment will require more extensive liver phenotyping to discern the differences between liver cyst development in these genotypes.

4.2.5 *Kap*-iCre expression can be induced with administration of exogenous hormone

A second cohort of mice was assessed concurrently with the conditional deletion cohort. As others have induced greater expression of Kap-iCre by administering exogenous hormones (Li et al., 2008), we assessed whether it would be possible to increase Kap-iCre activity and therefore increase cyst development. In the Li study, testosterone induction did not affect iCre mRNA levels in males but induced robust expression in females (Li et al., 2008). Before induction, female expression of LacZ was seen in the OSOM (of both Cre positive and negative mice) but a greater spatial expression was seen after induction, in S1 and S2 in the cortex (Li et al., 2008). In contrast to Li et al, our un-induced mice exhibit a high level of LacZ activity; upon LacZ staining female mice exhibit a staining pattern in cortical segments, whereas staining in the cortex and in a strong band in S3 is seen in males. We see an increase in LacZ staining in males with age, possibly due to dominance induced testosterone release. Therefore it seemed probable that induction with testosterone would produce increased Kap-iCre activity. This seemed likely to result in a greater proportion of tubules deleting the floxed allele and developing cysts.

Testosterone can be metabolised into androgenic and oestrogenic compounds, whereas Dihydrotestosterone (DHT), an active form of testosterone, is non-aromatizable. This means that DHT cannot be converted to oestrogenic products and only activates the *Kap* AREs whereas testosterone would activate both EREs and AREs. This allows for a more specific assessment of the differences between induced and non-induced mice. Induction with DHT was predicted to only increase Kap-iCre expression in S1 and S2 of the proximal tubule, increasing cyst formation in the cortex.

A 5mg/ml solution of DHT was prepared in a solution of HPβCD (H107-5G Sigma) and sterile injectable water. HPβCD is a cyclodextrin compound which enables solubilisation and stabilisation of steroid hormones (Albers and Muller, 1992). DHT was administered by subcutaneous injection into the nape of the neck, between the shoulder blades. Mice were injected with 25ug/g body weight DHT (5mg/ml DHT, 5% w/v EtOH, 53mg/ml HPβCD in 10ml injectable water) or vehicle (5% w/v EtOH, 53mg/ml HPβCD in 10ml injectable water) for three consecutive days. The level of circulating testosterone has been reported to drop to endogenous levels within a few days (Ding and Sigmund, 2001).

The developmental switch where cyst development transition from a rapid process of new cyst development to a slower, progressive growth of cysts, is reported to occur at around P13 (Piontek et al., 2007, Lantinga-van Leeuwen et al., 2007), therefore mice were treated at 1 month of age in order to avoid rapid and severe cyst development. Deletion of the floxed allele at this time is unlikely to cause a severe cystic phenotype, but it may act more like a second somatic hit. The germline *Pkd2*^{lrm4} mutation is the first hit and the DHT encourages a second hit to occur in the proximal tubules due to the recombination of *Pkd2*^{flox}. This is expected to produce progressive cyst development similar to that seen in adult ADPKD. As seen in the preliminary cohort of mice, by 1 month of age (P30) cysts will have already started to develop, indicating that Cre recombination has already occurred. DHT induction at this stage is predicted to provide a second round of deletion which is additional to the basal level; mopping up any floxed alleles that have yet to recombine.

4.2.6 DHT administration induces LacZ expression in Kap-iCre kidneys

Two cohorts of mice were bred for testosterone induction. First, a group of Kap-iCre carrying mice was bred with the R26R-lacZ mice, as before and injected with DHT or vehicle at six month old and perfused at 9 months. A second group expressing the Kap-iCre were bred with *Pkd2*^{lrm4} mice, with controls, for androgen induction experiments. Genotypes and treatments for both these groups are detailed in **Table 4.5.**

Table 4.5: Genotypes and treatments for testosterone induction cohorts.

The top two rows detail mice that carry the R26R^{LacZ} reporter and were used to assess the expression pattern of Kap-iCre after induction with DHT. The bottom three rows of mice carry Kap-iCre and combinations of *Pkd2^{lrm4}*, *Pkd2^{fl}* and *Pkd2^{+}* alleles. Mice were treated with DHT or vehicle injections to induce the transgene.

	DHT		**Vehicle**		**Purpose**
	Female	Male	Female	Male	
Kap::Wt; R26R$^{lacZ/+}$ (Wt-R26R)	1	1			Control for DHT effect of LacZ pattern
Kap::icre; R26R$^{lacZ/+}$ (Kap-R26R)	2	2		4	Assess LacZ pattern
Pkd2$^{lrm4/fl}$; Kap::iCre (lrm4-Kap)	6	4	2	0	Experimental mice- to assess effect of DHT
Pkd2$^{+/fl}$; Kap::iCre (Wt-Kap)	6	6	6	5	Control for effect of deleting Pkd2^{fl}
Pkd2$^{+/+}$; Kap::iCre (Kap)	3	3	3	3	Control for effect of DHT on Kap

To assess the expression pattern, kidneys from Kap-R26R and Wt-R26R mice were perfused, dissected and stained as described earlier. The same staining patterns were seen in these kidneys as in the previous R26R cohort, yet the intensities were different. Both DHT induced female and male Wt-R26R control kidneys were clear from LacZ staining (**Fig 4.16**). Male Kap-R26R kidneys consistently expressed the striated pattern in the cortex as well as the strong band in the S3 portions. The striated pattern does not occur in females to the same extent as is seen in the male, yet there does appear to be a faint striated pattern in in the cortex of these mice. Comparison between female kidneys from mice treated with DHT and those from the previous cohort that were untreated indicates that there may be a slight increase in staining with DHT treatment. However, considering the variation seen in the male, whether the difference in female staining is specifically due to DHT induction is inconclusive. This seems strange since the Kap-iCre HREs should be unaffected by sex, therefore induction with DHT should induce the male staining pattern to the same level in both sexes.

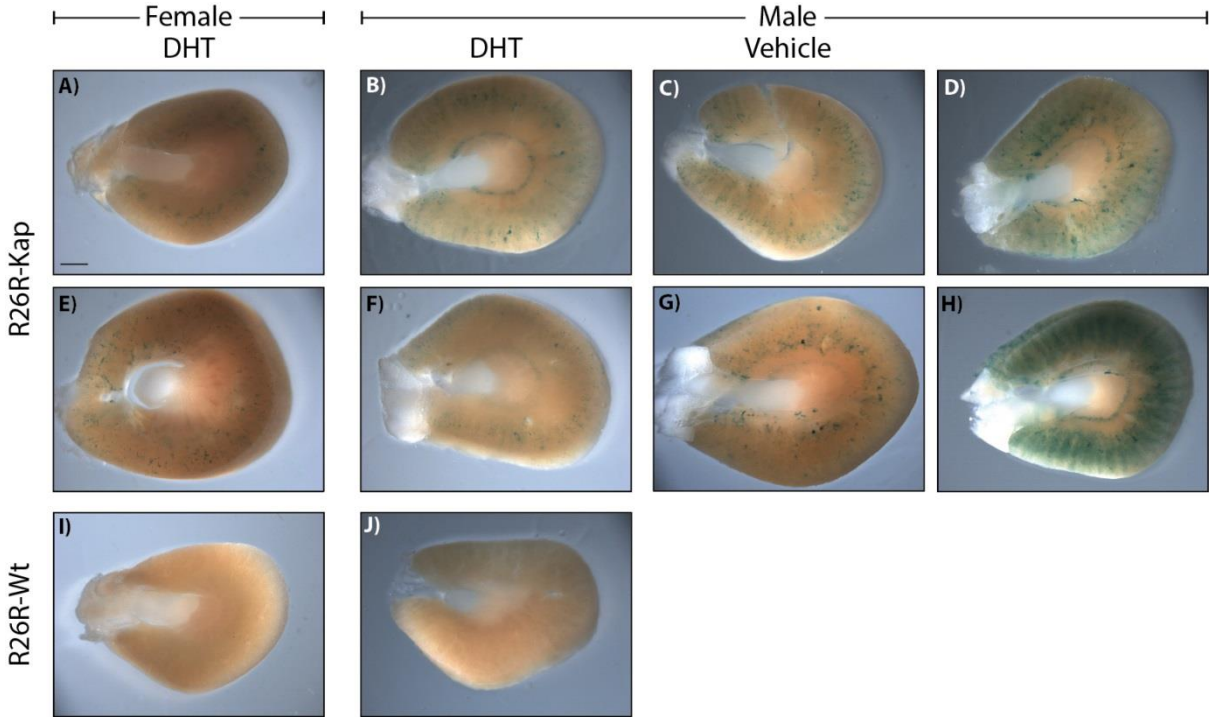

Figure 4.16: LacZ staining of 6 month old mice after DHT or vehicle injections

A) and E) show the lacZ staining pattern of female R26R-Kap kidneys injected with DHT. Staining can be seen in the cortex of both kidneys. B)-F) show male R26R-Kap kidneys injected with DHT. The consistent male OSOM band can be seen and a striated pattern is also seen in the cortex. C) ,D), G) and H) all show R26R-Kap kidneys injected with vehicle. Staining ranges in intensity in these kidneys. R26R-Wt kidneys, I) female and J) male both injected with DHT, both negative for lacZ stain. Scale bar=1mm.

The speckled expression in the female cortex (**Fig 4.16**) has been noted in female kidneys by Li et al. The pattern was present before testosterone induction and is observed to increase after induction (Li et al., 2008), indicating that female S1-S2 is responsive to testosterone. However, since Li et al used testosterone, the increased expression in S1-S2 could be due to oestrogenic metabolites of testosterone. Li et al induced their mice at 6-8 months of age with a subcutaneous testosterone pellet for 5days (Li et al., 2008). Our LacZ mice were injected at 6 months of age; therefore both cohorts were likely to have similar basal levels of expression before induction. The level of speckled expression we see in the female cortex is likely to be real and may be related to low levels of testosterone or oestrogen present in female mice. Since DHT increases the staining in the male S1-S2, the cortex expression of Kap-iCre is likely to be driven by androgens, but perhaps there is a mechanism blocking AREs in females which is stopping the increased upregulation of Kap-iCre in the female cortex.

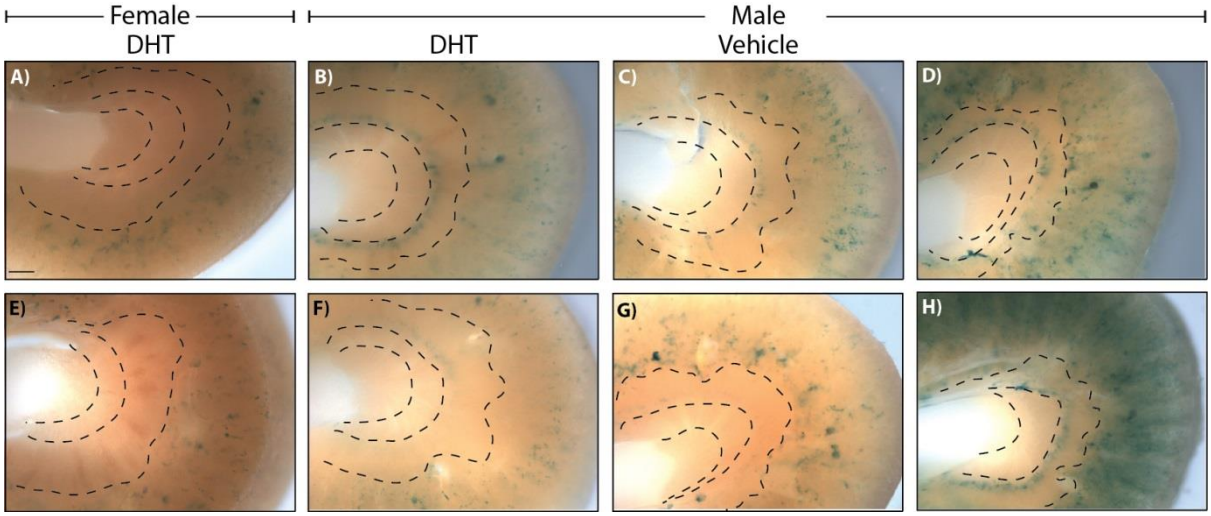

Figure 4.17: Regions of LacZ stained R26R-Kap kidneys after DHT or vehicle injections

A striated pattern of lacZ staining can be seen in the cortex of all kidneys examined. A) and E) are female kidneys treated with DHT. Staining is only observed in the cortex. B) and F) are male kidneys treated with DHT. In addition to the striated pattern in the cortex, a band of staining between the OSOM and ISOM, observed in all male kidneys assessed, is observed. Male mice treated with vehicle C), D), G) and H) exhibited the same pattern of staining as was previously seen.

The male specific band of staining at the border between the OSOM and the ISOM was not induced in the females that were treated with DHT. This indicates that this region is not under the control of DHT. However, since it is consistently seen in all male kidneys and never in females, expression in this area of the kidney must be controlled by a male specific element.

The high level of expression we see in a male treated with the vehicle is similar to the higher level which we saw in one 8-9 month old male from the un-induced cohort. This level of expression in the uninduced mouse may be due to dominance induced testosterone increase which may also be the case with the vehicle treated mouse. This would indicate that the levels of androgen response we induce with this dose of DHT may be lower than it is possible to achieve naturally. However, this demonstrates that this dose is within a physiological range.

4.2.7 Effect of using DHT to increase deletion in the lrm4-Kap kidney

Table 4.5 details a second group of DHT treatment mice. These mice are two of the same genotypes as before: lrm4-Kap and Wt-Kap with the addition of a group which only carry Kap-iCre (referred to as Kap). The Kap mice carry two *Pkd2*$^{+}$ alleles, whereas the Wt-Kap are *Pkd2*$^{fl/+}$. Cells where the *Kap* is active in Wt-Kap mice will delete the floxed allele and these cells will then be *Pkd2*$^{-/+}$, whereas the Kap mice do not carry a floxed allele therefore all the cells with retain two Wt copies of *Pkd2*. This cohort of mice was administered with DHT or vehicle in order to assess the ability of the hormone to increase the deletion of the floxed allele of *Pkd2* and assess whether cyst development could be increased. **Fig 4.18** details the experimental pipeline for these mice. Three consecutive daily injections were carried out at 1 month. After a further month, urine was collected in metabolism cages, and mice were returned to home cages. After a final month, urine was collected a second time, mice were allowed to recover for a week and then necropsy was performed. Terminal bleeds and kidney dissections were undertaken. Urine and plasma were analysed for markers of decreased renal function and kidneys were processed for histological sectioning. This work is ongoing.

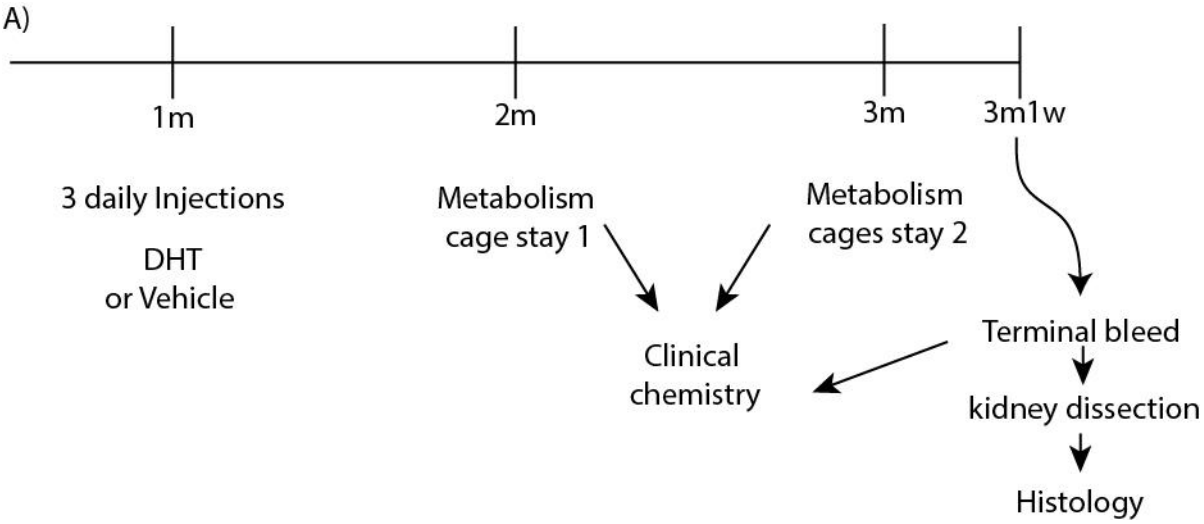

Figure 4.18: Experimental pipeline for mice induced with DHT

Mice are injected at 1m of age with three consecutive daily injections of either DHT or vehicle. A month later, mice spend 24 hrs in metabolism cages. After a further month, urine is collected a second time in metabolism cages. After a week of rest, the mice are sacrificed and blood and kidneys are collected.

At present, kidneys have been collected from 19 mice; 3 lrm4-kap males and 5 female treated with DHT, 4 male Wt-Kap mice treated with DHT, and 7 female Wt-Kap mice;6 treated with DHT and 1 treated with vehicle. The males appear to be more affected by DHT induction than females. As the LacZ staining would suggest, there appears to be varied expression of the transgene in the males. When the full data set is complied, it will be interesting to compare the uninduced male lrm4-Kap kidneys with the DHT treated kidneys.

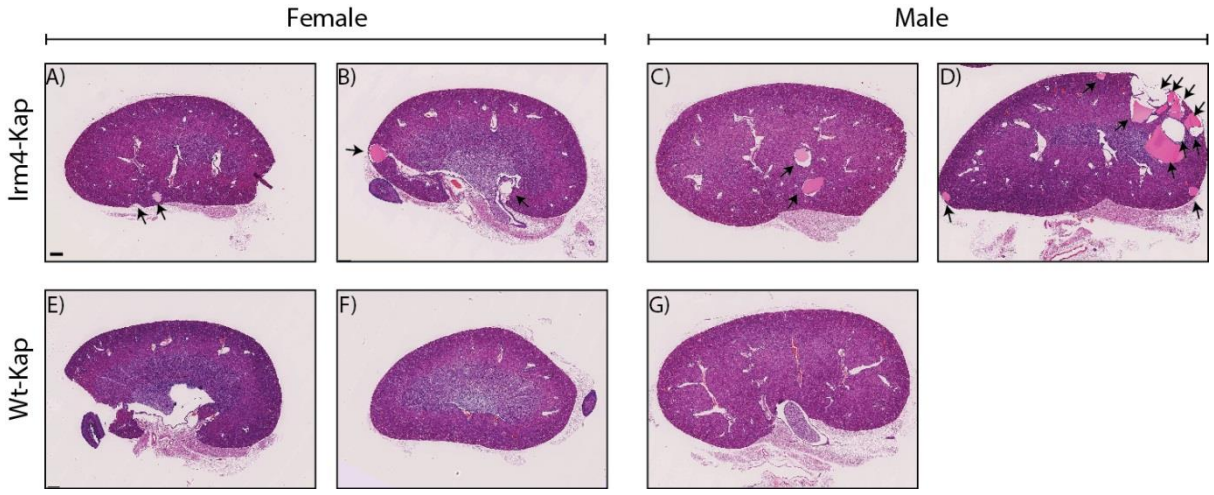

Figure 4.19: Kidneys from mice treated with DHT or Vehicle.

Kidneys dissected from three month old mice that were injected with either DHT or Vehicle at 1 month. The top row shows lrm4-kap mice. A) and B) are female mice induced with DHT which exhibit a small number of cysts in the cortex (arrows). C) and D) are male mice, both induced with DHT. C) exhibits similar levels of cysts as the females, the cysts imaged are in the cortex. D) exhibits a stronger cyst development. A large cluster of cysts can be seen. The largest is 1.01mm diameter. E) is a female Wt-Kap kidney, treated with DHT. No cysts are evident. F) is a female Wt-Kap which was treated with Vehicle. No cysts are evident. G) is a male Wt-Kap which was treated with DHT, no cysts are evident. Scale bar 500µm.

4.1 Results summary

A lrm4-Kap transgenic line was used to assess the *lrm4* allele over a null allele in specific tubules of the kidney. The deletion of $Pkd2^{fl}$ in lrm4-Kap mice led to the development of renal cysts. Cysts increased in number and size with age. Liver cysts were observed in these mice and also in the lrm4-Wt mice, suggesting a link between the $Pkd2^{lrm4}$ allele and disruption of liver development. This work provides a novel progressive model of ADPKD which offers the opportunity to assess cyst progression in a specific subset of cells in the kidney.

4.2 Discussion

4.4.1 Advantage of inducibility

Lrm4-Kap adult mice are distinctive in that they are semi-inducible. Kap-iCre activation is achieved by endogenous hormones and can be increased by exogenous delivery of hormones. Cyst development can be restricted to tubules of the cortex, the OSOM, or all three segments of the proximal tubule covering a larger proportion of the kidney. Hormone response elements within the Kap-iCre construct create an adaptive model which can be induced by hormones to control expression in specific portions of the proximal tubule. Here, expression in the proximal tubule has been induced with DHT, leading to cyst development predominantly in the cortex. The potential to delete the floxed allele in the whole proximal tubule, or specifically restricted portions remains and the use of different hormonal treatments would allow this. Since the transgene is activated in a proportion of tubules, cysts have time to enlarge and progress before renal failure is reached. This model has the potential to enable preclinical drug trials which alter the progression of cyst development.

The lrm4-Kap mouse line provides an adaptable model of progressive PKD in the adult mouse. The use of other hormones to induce the transgene across different segments of the proximal tubule would provide more insight into the specific cell types and nephron portions causing cyst development. In this case, a floxed allele of *Pkd2* is deleted to produce a null allele allowing the investigation of the point mutation $Pkd2^{lrm4}$ in the proximal tubule. Different combinations of Cre recombinase, floxed allele or mutated allele could be interchanged to allow further investigation of the characteristics of PKD development. $Pkd2^{flox}$ could be combined with a $Pkd2^{-}$ allele in the kidney to produce a complete knockout in the proximal tubule, or other mutations could be assessed in place of $Pkd2^{lrm4}$. In addition to Kap-iCre, several other transgenic lines express Cre in the proximal tubules or other areas of the kidney. Kap-iCre has the advantage of being inducible and more tissue restricted than many other Cre lines. Since PKD2 expression in the proximal tubules has been shown to be maintained throughout development and into the adult kidney (Markowitz et al., 1999), the proximal tubule is a relevant population of cells in which to assess the function of *Pkd2* and this particular combination is likely to be useful to increase the understanding of ADPKD development.

Assessment of deletion in other tubular segments may be interesting however the merit of this system is that the proximal tubule can be specifically subdivided. Since the proximal tubule makes up a large portion of the nephron and contains a variety of cell types which each serve a specific function, the specificity of Kap-iCre to these regions is advantageous.

4.4.2 LacZ staining

It is curious that the female mice showed little to no increase of LacZ staining with DHT treatment. The male specific band of staining in the OSOM is never seen in females and is not induced by DHT injection. The striated pattern in the cortex does appear to increase in females treated with testosterone however, since no females were treated with vehicle it is difficult to assess whether these would have had similar levels of cortex staining. Nonetheless, the increase in expression in the cortex is only minor in females treated with DHT compared to untreated females. This could be due to a number of factors: 1) perhaps the induction with DHT is not effective. 2) since the transgene is equivalent between male and female mice, it is expected that the ARE would also be equivalent and that both male and female mice would exhibit an increase in ARE related expression. It is possible that this region gains a protective mark from oestrogen in the female, providing a way for the transgene to determine that it is expressed in a female. Further work with other hormones and larger numbers of mice would clarify this.

The first option seems more likely. However, other labs (Li et al., 2008) have assessed induction of the transgene with DHT and found it to be successful. They do not report the OSOM/ISOM band. This band is fully penetrant in all our male mice and absent from all females. Therefore this clearly reflects a sexually dimorphic expression of Kap-iCre, combined with R26R, in these mice.

4.2.3 Two-hit hypothesis model

Kap-icre expression deletes the $Pkd2^{flox}$ allele in a proportion of cells so that $Pkd2^{lrm4/-}$ is expressed. This mimics the two-hit hypothesis where $Pkd2^{lrm4}$ acts as a first hit, the germline mutation, and the deleted flox allele models a second hit. Similar to other models of the two-hit hypothesis, the second hit only occurs in a proportion of cells. Restricting the second hit to a certain cell type or portion of the tubule as we have done allows us to model a slow

progressing disease. The administration of DHT allows us to mop up any floxed alleles that have not recombined, thus inducing a higher level of second hits. This also helps to mimic a more progressive disease.

4.4.4 Biochemical analysis and the Floxed allele

Assessment of the kidney phenotype revealed that a substantial proportion of nephrons remained intact; indicating that kidney function was sustained. The biochemical analysis reflected the varied phenotype seen in the human disease; some urine and blood components were altered in a number of groups of mice however, larger sample groups may be required to reduce some of the variation between age groups. Since only one urine and blood sample was collected from each mouse, progression of renal disease could not be followed in an individual mouse. Collecting samples at multiple time points during each mouse's life would increase the power of the analysis.

The serum and urine analysis did produce a number of significant results. Notably, indicating that liver function was affected. According to Li and colleagues (Li et al., 2008), Kap-iCre is abundantly, though not exclusively expressed in the kidneys. Assessment of RNA showed that Kap-iCre expression was evident in the brain and liver, although to a lesser extent than in the kidney. Therefore, this could be an explanation for the cysts we see in the liver in lrm4-Kap mice but does not explain the liver phenotype of lrm4-Wt mice. Since the liver phenotypes are comparable with *Pkd2*$^{lrm4/+}$ aged mice, it is conceivable that *Pkd2*^{lrm4} is causing the liver phenotype. The serum analysis of the *Pkd2*$^{lrm4/+}$ mice however did not have low BUN nor urea levels, suggesting that the *Pkd2*$^{lrm4/+}$ livers cysts were either less severe or less common.

Despite PKD2^{fl} protein levels being equivalent to Wt levels in embryonic kidney lysate (**Fig 2.10**), it appears that *Pkd2*^{fl} is not acting equivalently in the adult liver. The function of the protein is unlikely to be affected by the insertion of loxP sites but it is possible that there was some aberrant recombination of the floxed allele leading to deletion. We know that Kap-iCre was not responsible for the recombination for two reasons: 1) these mice did not carry Kap-iCre and 2) the cysts occurred in areas outside the Kap-iCre expression pattern.

Although the reporter expression pattern indicated that the Kap-iCre transgene is active in a high proportion of proximal tubules, only a proportion of these tubules became cystic. This reflects the human development of cysts in ADPKD; although all cells in the kidney carry the mutated allele, only a proportion of tubules become cystic. The level of renal function remains high as the kidney compensates for the loss of the cystic tubules and only starts to fall after a high proportion of the kidney has been overtaken by cysts. Expressing the combination of mutant alleles in the proximal tubules alone allows these kidneys to reflect a more gradual and progressive phenotype which more closely models the slow development of cysts in the human kidney.

This chapter has confirmed that expressing the *Pkd2*^{lrm4} allele over a null allele is sufficient to cause cyst development in the kidneys and also leads to polycystic liver disease. This work has not however assessed the nature of the *Pkd2*^{lrm4} allele, the effect the mutation has on the protein or function of the protein within the cell. The following chapter therefore assesses these questions to establish the molecular characteristics of the mutation.

Chapter 5: Molecular phenotyping

5.1 Introduction

The previous chapters described the embryonic and adult phenotype of *Pkd2*^{lrm4} mice and assessed kidney cysts in the proximal tubule specific conditional mutant. *Pkd2*^{lrm4} causes cyst development in the homozygous embryonic kidney, microcyst development in the heterozygous adult kidney and large macrocysts in the adult kidney when expressed over a null allele. In this chapter the molecular phenotype of the mutant protein will be assessed.

5.1.1 Characterising the mutation

Genetic mutations can be characterised by the effect caused on protein function and described as gain-of-function (GOF) or loss-of-function (LOF) mutations. GOF mutations are defined by increased or additional protein function. These mutations exhibit the mutant phenotype in a dominant manner. A GOF can exhibit an entirely new function that is different from the Wt function or a dominant negative function which acts antagonistically towards the Wt protein, opposing the Wt function (Griffiths, 2000).

A LOF mutation involves the whole or partial inactivation of a gene, resulting in either complete loss or reduction of protein function (Griffiths, 2000). LOF mutations are often recessive since the Wt allele remains functional. A fully inactivated allele, or null allele, may either cause no effects because the Wt allele is enough to compensate for the lost allele, or may cause effects relating to reduced gene dosage. This is known as Haploinsufficiency. Haploinsufficiency describes a situation where a mutation reduces gene dosage below a critical point and the single functional copy is unable to produce enough protein to preserve the Wt phenotype. The majority of cases are recessive mutations where the Wt copy is sufficient. A smaller number of LOF mutations are haploinsuficient. A full null, with two LOF alleles will have a stronger phenotype than either of these on their own.

A mutation causing reduced gene function is known as a hypomorphic allele and reduces protein performance or lowers levels of protein production. An allele which presents as a null allele can be classified in three ways; 1) an mRNA-null has a disruption at the level of transcription, 2) a protein-null produces no protein due to disruption at the level of translation and 3) a functional-null renders the protein inactive despite protein being made.

To understand how a mutation perturbs gene function, genetic analysis of the mutation in different contexts is classically used. *Pkd2*^{lrm4} appears to be a recessive mutation since, unlike homozygotes, heterozygous survive to adulthood and do not develop embryonic renal cysts. However, the heterozygotes do develop renal microcysts and liver cysts as adults, therefore indicating that *Pkd2*^{lrm4} is a dominant allele. In humans, ADPKD is classified as dominant due to the inheritance pattern; only one affected parent is required to pass the disease on to a child at a rate of 50%. However, the disease is thought to be recessive at a cellular level (Qian et al., 1996) and may require a second mutational hit before cyst progression is observed.

Recessive mutations are likely to be LOF mutations. A hypomorphic mutation causes partial reduction of gene function and is more severe when combined with a null allele than when homozygous due to lower protein levels. A null allele elicits the same phenotype when homozygous and when expressed over a null allele. *Pkd2*$^{lrm4/-}$ embryos have a very similar phenotype to *Pkd2*$^{lrm4/lrm4}$ embryos, both in terms of cyst development, lethality and *situs* defects (**Chapter2, Fig 2.12**). This suggests that *Pkd2*^{lrm4} is a null allele rather than a hypomorphic allele.

Pkd2^{lrm4} was previously reported to be a null allele (Ermakov et al., 2009). However, assessment of *Pkd2*^{lrm4} by Yoshiba et al indicates that *lrm4* not only produces protein, but that the mutant protein retains calcium channel activity when assessed in a cell free system (Yoshiba et al., 2012). This suggests that a more complicated mechanism is in place.

5.1.2 Gene dosage is important in cystogenesis

Hypomorphic human alleles of *PKD1* have implicated gene dosage in initiation of cystogenesis. The incompletely penetrant pathogenic PKD1 mutation, Arg3277Cys (*PKD1*^{RC}), is a missence mutation which causes a mild and slow progressing phenotype (Rossetti et al., 2009). *PKD1*^{RC} was seen in a family with severe in utero cystic disease, however in this family *PKD1*^{RC} was inherited in combination with a strongly pathogenic *PKD1* allele *(Rossetti et al., 2009)*. In combination these two alleles produced a particularly aggressive form of the disease. When expressed in mice, *Pkd1*^{RC} was shown to be a modifying allele. *Pkd1*$^{+/-}$ mice (~50% reduction in protein levels) do not develop renal cysts whereas *Pkd1*$^{RC/-}$ (~80% reduction in protein levels) exhibited rapidly progressing cystic disease. *Pkd1*$^{RC/RC}$ mice

(~60% reduction in protein levels) develop a gradual progressive disease (Hopp et al., 2012). In contrast, patients with high levels of PKD1 and mice overexpressing PKD1 have been shown to develop rapid renal disease (Thivierge et al., 2006).

A hypomorphic allele of PKD2 is reported in the PKDdb (PKDb, 2016). The *PKD2* Leu656Trp (*PKD2*^{LW}) allele was homozygous in a proband with early onset ADPKD, who inherited two copies of the hypomorphic allele by uniparental disomy. The mother, carrying a single copy of *PKD2*^{LW} did not develop cysts, nor was there any family history of the disease (Losekoot et al., 2012). This is evidence that gene dosage is important in ADPKD caused by both PKD1 and PKD2.

5.1.3 Ciliary trafficking and localisation

ADPKD is a ciliopathy and both PKD1 and PKD2 have been shown to localise along the ciliary membrane. PKD1 and PKD2 interact and co-localise within renal epithelial cells, at the base of the cell, regulating cell-matrix interactions (Foggensteiner et al., 2000); between cells in cell-cell adherens sites, in the plasma membrane (PM) and in the ciliary membrane (Pazour et al., 2002, Yoder et al., 2002, Nauli et al., 2003). PKD2 also localises within the endoplasmic reticulum (ER) (Tsiokas et al., 2007, Cai et al., 1999).

A set of specific signalling peptides and trafficking proteins regulate the transport and maintenance of PKD2 in specific cellular compartments. The C-terminus is required for ER retention (Cai et al., 1999) and contains a signal peptide which ensures ER capture. Trafficking of PKD2 between the ER and PM is regulated by PACS proteins and may require PKD2 phosphorylation (Kottgen and Walz, 2005). Trafficking to the PM is reported to be by direct interaction with PACS-1 through an acidic motif in the C-terminus, whereas retention in the ER is associated with PACS-2 binding to the same motif. PACS proteins associate with different vesicular coat proteins and this may cause their distinct trajectories (Kottgen and Walz, 2005).

Trafficking of PKD2 to the ciliary membrane is argued to be distinct from the route taken by PKD2 to the PM (Hoffmeister et al., 2011). Since there is a substantial barrier between the cilium and the cytoplasm, specific mechanisms must exist for the transport of PKD2 into the ciliary membrane. Three possible mechanisms have been suggested to transport proteins

into the cilium: 1) vesicles dock at the base of the cilium and are loaded onto the IFT system before fusing with the ciliary membrane. 2) Proteins diffuse from the PM into the ciliary membrane. 3) Proteins dock at the base of the cilium and are then integrated into the ciliary membrane (Hoffmeister et al., 2011). The first is unlikely as this would require vesicle transport and membrane fusion machinery within the cilium. The second is improbable due to periciliary diffusion barrier, an area at the base of the cilium which restricts diffusion into the cilium. Indeed, the ciliary membrane has a distinct protein composition to that of the PM, arguing against passive diffusion. At present, the third possibility seems most likely.

A series of elegant experiments by Hoffmeister et al enabled the mechanisms of PKD2 transport to the PM and ciliary membrane to be disentangled (Hoffmeister et al., 2011). De-glycosylation experiments revealed that PKD2 targeted to the ciliary membrane does not travel through the golgi apparatus. Disruption of COPII-dependent budding from the ER greatly reduced ciliary PKD2 levels, arguing a role for COPII-dependant vesicle transport from the ER. Further disruption of the golgi apparatus inhibited all PKD2 from entering the cilium, implying that PKD2 must reach the golgi apparatus, but not travel through it, before entering the cilium.

Around the base of the ciliary membrane lies the ciliary pocket; this may act as a platform for vesicle trafficking allowing transport of proteins from the cell body into the cilium. The diffusion barrier at the base of the cilium may be made up of the structures within the transition zone. The transition zone incorporates the distal and sub-distal appendages which dock the base of the cilium to the membrane at the ciliary pocket (**Fig 5.1**) (Kee et al., 2012)**.** The transition zone has been compared to the nuclear pore complex and is thought to provide a restrictive barrier, allowing only molecules smaller than 41KDa to enter the cilium by diffusion (Kee et al., 2012). Convincing evidence of this diffusion barrier comes in the form of a black-hole. Vieira et al. use a membrane targeted fluorescent protein which was unable to diffuse from the apical plasma membrane into the ciliary membrane of MDCK cells. The protein left a black-hole devoid of fluorescence around the base of the cilium with a diameter of 1.2-1.8µm, indicating that the ciliary membrane encompasses a larger area than was previously thought (Vieira et al., 2006). The distal and sub-distal appendages act like a sieve trapping molecules larger than 60nm diameter (Nachury et al., 2010). The transition zone makes up part of the ciliary pore complex which provides a selective barrier

for sorting proteins that enter the cilium. A ring of septin proteins at the base of the cilium may also be involved (Hu et al., 2010).

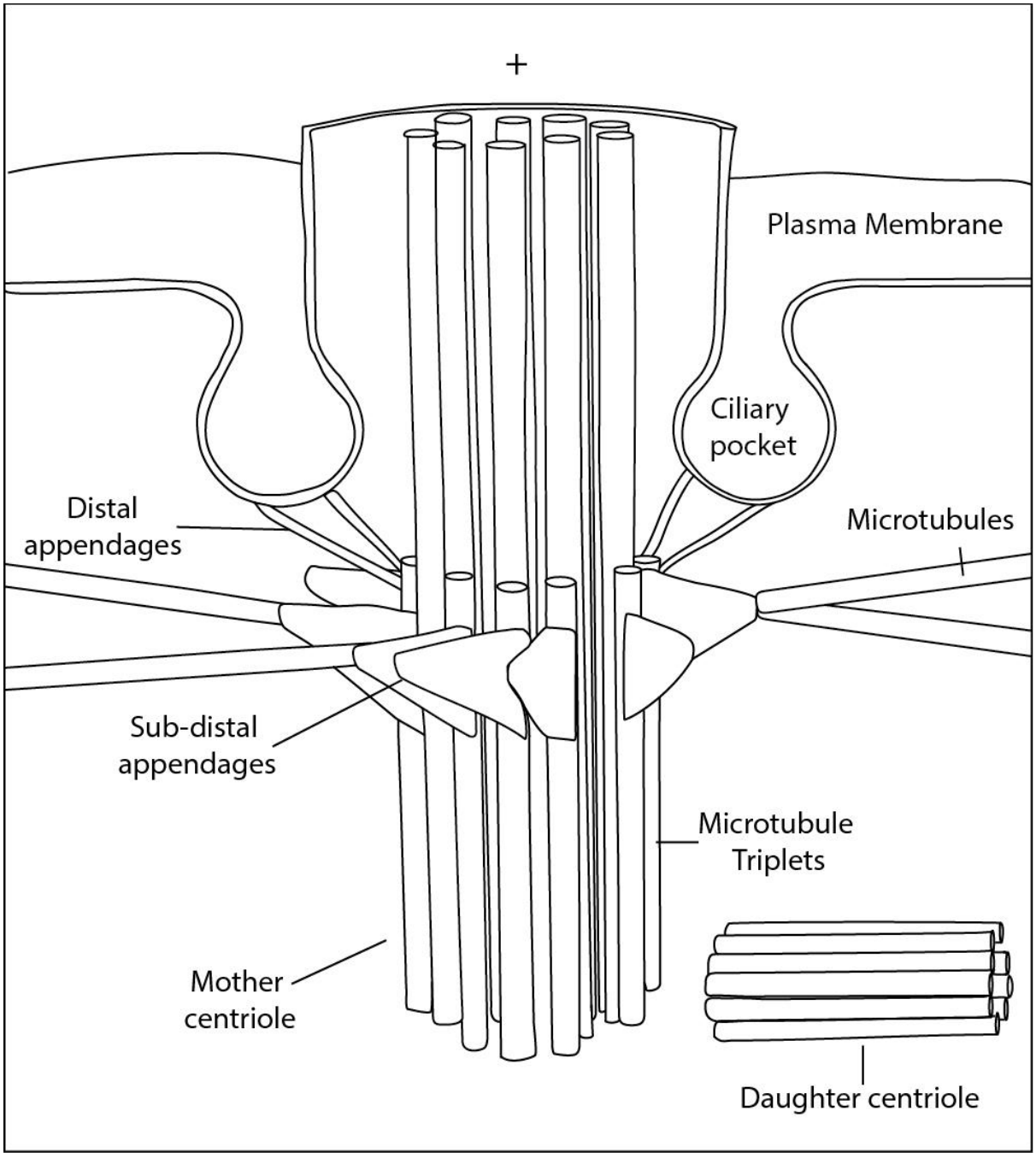

Figure 5.1: Structures at the base of the cilium.

At the base of the cilium sits the basal body; a cylindrical structure that is made up of the mother and daughter centrioles. The basal body is made up of nine sets of microtubule triplets and acts to anchor and pattern the ciliary axoneme. Just below the membrane, the sub-distal appendages on the mother centriole anchor the base of the cilium to the microtubule skeleton. Distal appendages or transitional fibres, attach the cilium to the

membrane at the ciliary pocket. Vesicles dock to the ciliary pocket. Diagram adapted from (Veleri et al., 2014).

PKD2 contain an N-terminal RVxP motif which acts as a ciliary targeting sequence (Geng et al., 2006). RVxP has been shown to be essential for PKD2 ciliary localisation and likely forms part of a protein interaction domain, but binding partners have not yet been identified.

Transport to the ciliary membrane may be through vesicles which dock at the distal appendages. Components such as the clathrin coat proteins and adaptors, small GTPases and SNARE proteins are thought to be involved in vesicle transport. Many of these components dock below the transition zone at the ciliary base. Clathrin coated vesicles have been shown to dock at the ciliary pocket (Molla-Herman et al., 2010) and along with other endocytic proteins, are enriched in the periciliary membrane.

An essential element in the selective entry of PKD1 or PKD2 into the cilium is the small GTPase, Rab8. Rab proteins are a group of proteins which are known to facilitate to the transport, docking and fusion of vesicles to the base of the cilium (Nachury et al., 2010, Nachury et al., 2007). Having discovered that trafficking of PKD2 to the ciliary membrane began with COP-II mediated budding from the ER, Hoffmeister et al showed that Rab8a is essential for PKD2 trafficking to the cilium (Hoffmeister et al., 2011). A cascade of proteins activates Rab8 allowing Rab8 mediated delivery and docking of the vesicle-bound PKD2 at the ciliary base. Vesicles may dock and unload at the distal appendages before proteins are carried into the cilium (Tanos et al., 2013). It is unclear how PKD2 passes the ciliary pore complex and diffusion barriers at the base of the cilium before entering the ciliary membrane.

5.2 Results

To understand the nature of the *lrm4* mutation, how it disrupts the function of *Pkd2* and causes the cyst phenotype, a number of possible hypotheses were considered and tested.

Hypotheses:

1) *Pkd2*^{lrm4} is a hypomorphic allele. Protein is produced at a lower level compared to Wt protein. This could mean that the protein levels in the *Pkd2*$^{lrm4/lrm4}$ embryos were not

high enough to prevent cyst development if the *Pkd2*^{lrm4} allele confers haploinsufficiency.

2) The *Pkd2*^{lrm4} allele is a complete protein or mRNA null. No protein is produced. This would mean that the cysts develop due to the absence of PKD2.
3) PKD2^{lrm4} is mis-folding and therefore being sent for degradation.
4) PKD2^{lrm4} is unable to traffic correctly within the cell and is therefore being accumulated inappropriately elsewhere in the cell and not able to reach the ciliary membrane.

These would all result in lowered or absent PKD2 levels within the cell as a whole or specifically within an essential cellular compartment.

5.2.1 *Pkd2*^{lrm4} produces protein in cultured cell lines

To assess protein levels and address the first and second hypotheses, Western blots were performed.

Embryos were harvested from *Pkd2*$^{lrm4/+}$ intercrosses in order to obtain litters containing Wt, *Pkd2*$^{lrm4/+}$ and *Pkd2*$^{lrm4/lrm4}$ embryos. To make Mouse Embryonic Fibroblasts (MEFs), E13.5 embryos were dissected; the head, limbs and internal organs were removed and the carcass placed in cold PBS. Embryonic tails were removed for lrm4 genotyping. In a cell culture hood, carcasses were minced to produce a fine suspension of cells as detailed in **MM:1.4.1**. Once the cells were confluent, they were immortalised by electroporation with largeT SV40 plasmid (**MM:1.4.2**).

To assess the level of protein produced by each allele of *Pkd2*; confluent plates of *Pkd2*$^{+/+}$, *Pkd2*$^{lrm4/+}$ and *Pkd2*$^{lrm4/lrm4}$ MEFs were lysed (**MM:1.3.1**). A Bradford protein quantification assay was undertaken and 50ug of protein was prepared for denaturing SDS-PAGE. The membranes were imaged using the Odyssey image studio system. Densitometry of bands was undertaken to quantify protein levels. The PKD2 band is seen at ~110KDa. Band intensities were measured and normalised against the Tubulin band loading control seen at 50KDa in each lane. These values were compared statistically (**Fig 5.2**).

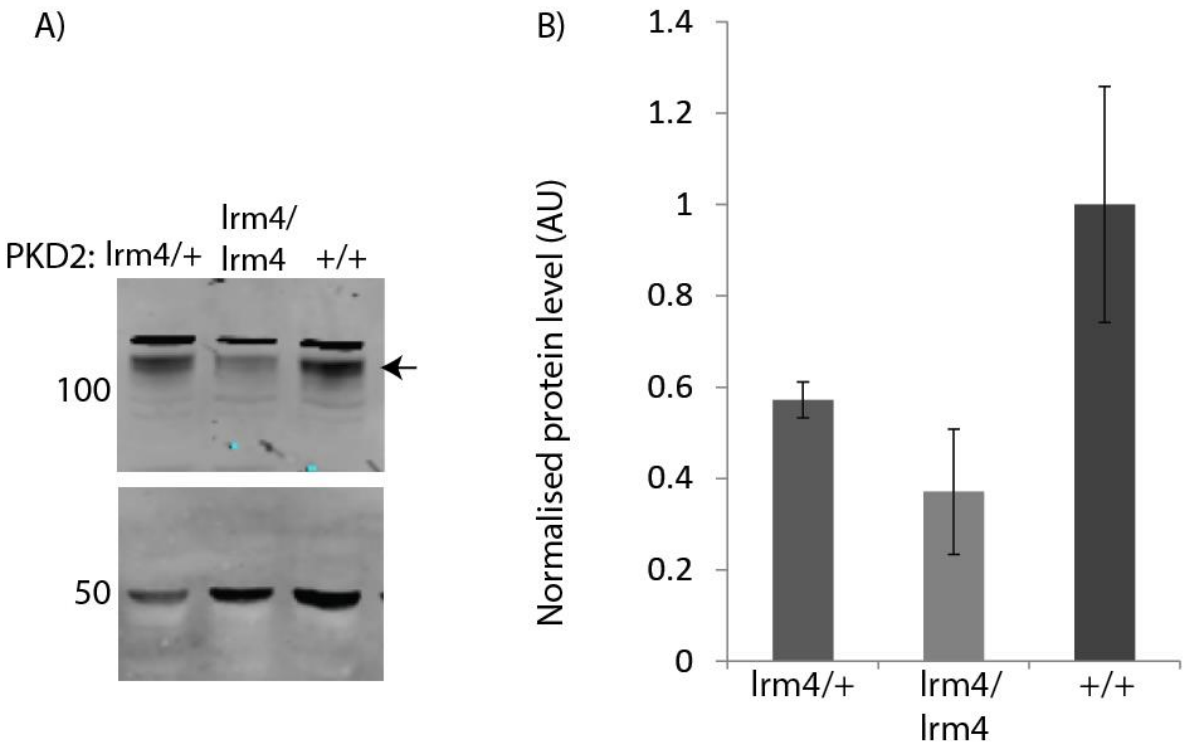

Figure 5.2: Western blot and densitometry of PKD2 protein from MEFs

A) shows a representative Western blot of PKD2; lane one lysate from *Pkd2*$^{lrm4/+}$ MEFs, lane two from *Pkd2*$^{lrm4/lrm4}$ MEFs and lane three from Wt MEFs. The arrow at ~110 KDa indicates the band which corresponds to PKD2. A non-specific band is seen above the PKD2 band at around 120KDa, this did not change across genotypes. The band at 50KDa corresponds to tubulin. B) Represents densitometry analysis of PKD2, showing the drop in protein levels between *Pkd2*$^{+/+}$ and *Pkd2*$^{lrm4/lrm4}$ samples. Here a drop to 37% of Wt levels is shown but this is varied between samples and across gels. (AU-arbitrary units).

Protein is evident in *Pkd2*$^{lrm4/lrm4}$ samples, indicating that *Pkd2*^{lrm4} is not a protein null. This refutes hypothesis 2, PKD2 protein is made. When Protein levels were compared in MEFs, it was clear that less PKD2^{lrm4} is present than the Wt protein. Densitometry indicated that PKD2^{lrm4} levels were ~37% of Wt. However this varied greatly between samples and experiments, between 12% and 51%. This variation may have been due to the method used to prepare the sample and the volume of lysis buffer used. Reducing the lysis volume and aspirating the cells efficiently to ensure that the lysis buffer was not diluted improved the levels of protein detected.

5.2.2 *Pkd2*^{lrm4} produces protein in embryonic kidneys

Analysis of protein levels in MEFs provided useful insight into the PKD2^{lrm4} protein levels however, assessment of protein levels in embryonic kidney lysates was performed to provide data from a second, more biologically relevant tissue. Kidneys were collected from E14.5 embryos; a stage before cysts have developed in the *Pkd2*$^{lrm4/lrm4}$ kidneys and when kidneys across genotypes are likely to contain a similar number of cells.

On dissection, embryonic kidneys were frozen in liquid nitrogen and tail samples were taken for genotyping. A preliminary study was undertaken to assess the number of kidneys required to produce a sufficient amount of protein. Pools of single pairs, two pairs, and three pairs were assessed, loading 20-50µm of sample. Three pair pools were selected as this provides sufficient protein for analysis whilst allowing for technical replicates to be performed. Pooling kidneys also reduces variation between samples. Samples were lysed in 45ul RIPA buffer with protease inhibitors and homogenised with a pestle on ice before centrifugation at 13000rpm for 10mins at 4°C **(MM:1.3.1)**. A Bradford protein quantification assay was performed and samples were prepared for Western blot as for MEFs. Five biological replicates and two technical replicates were performed for each genotype. After probing for PKD2 and Tubulin, the membranes were imaged on the Odyssey Image Studio (Li-COR) system. Band intensities were quantified and statistical tests undertaken (**Fig 5.3**).

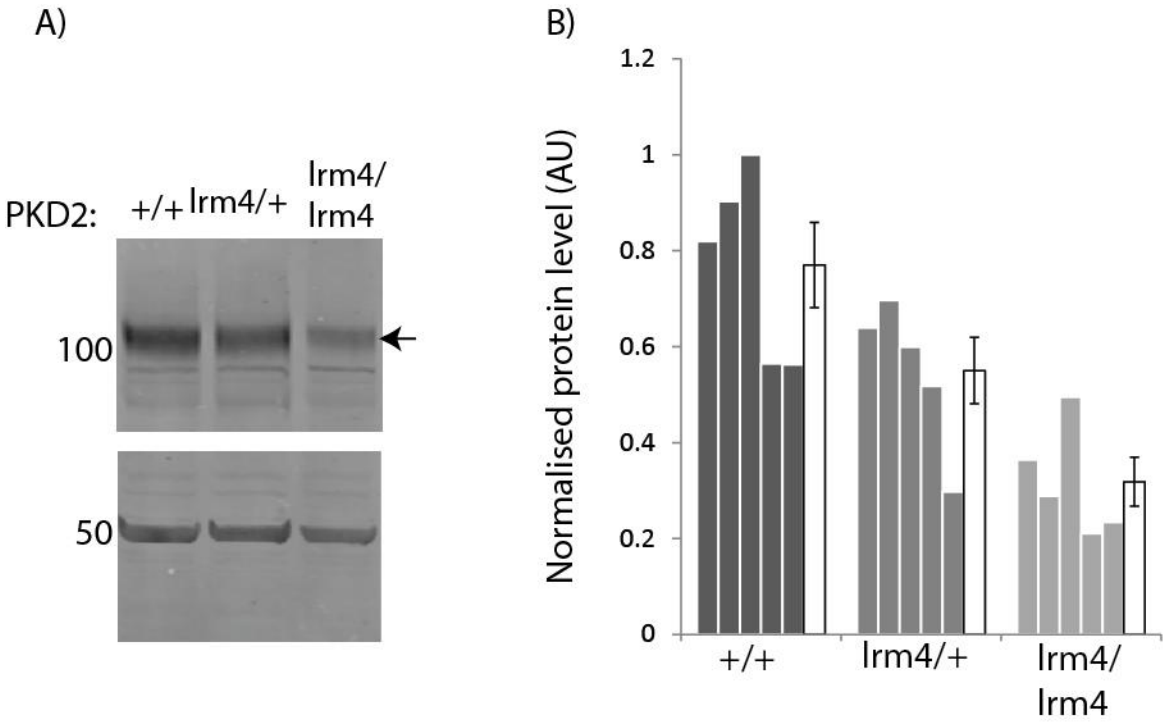

Figure 5.3: Western blot and densitometry of PKD2 protein from embryonic kidney lysate

A) shows a representative Western blot of PKD2 from E14.5 embryonic kidneys; lane one shows lysate from a pool of Wt kidneys, lane two from *Pkd2*$^{lrm4/+}$ kidneys and lane three from *Pkd2*$^{lrm4/lrm4}$ kidneys. The arrow at ~110 KDa indicates the band which corresponds to PKD2. The band at 50KDa corresponds to tubulin. B) presents densitometry analysis of PKD2, each column represents the PKD2 normalised to tubulin for a pool of three kidneys, the white column in each group represents the average for each genotype. Here, the average *Pkd2*$^{lrm4/lrm4}$ protein drops to 41% of the *Pkd2*$^{+/+}$ level.

Analysis of embryonic kidney lysate confirms that PKD2^{lrm4} protein is produced in *Pkd2*$^{lrm4/lrm4}$ kidneys, refuting the hypothesis that *Pkd2*^{lrm4} is a protein-null. PKD2^{lrm4} is expressed at a lower level than the Wt protein. The average PKD2 levels in *Pkd2*$^{lrm4/lrm4}$ kidney lysates were 41% of the WT level but again the values varied. The heterozygote protein level was intermediate between Wt and *Pkd2*$^{lrm4/lrm4}$, indicating that each *lrm4* allele causes protein levels to drop by ~30%.

This could argue that *Pkd2*^{lrm4} confers haploinsufficiency i.e. that the Wt copy does not produce enough protein to avoid cyst development as the first hypothesis argues. Classical genetic analysis argues that *Pkd2*^{lrm4} is not a hypomorphic allele; *Pkd2*$^{lrm4/-}$ and *Pkd2*$^{lrm4/lrm4}$ embryos exhibit indistinguishable phenotypes (**Fig 2.12** and **2.13**). However, it is known that gene dosage plays an important role in the pathogenesis of ADPKD, we therefore investigated whether levels of PKD2^{lrm4} were insufficient to maintain the Wt phenotype.

5.2.3 PKD2 is present at a similar level in *Pkd2*$^{lrm4/lrm4}$ and *Pkd2*$^{-/+}$

Pkd2^{lrm4} is not a protein null but could cause haploinsufficeincy. Further assessment of protein levels was undertaken to establish whether *Pkd2*^{lrm4} simply produces too little protein to prevent cyst formation.

We know that *Pkd2*$^{-/+}$ mice do not develop strong embryonic cysts (demonstrated in embryonic kidneys in **Chapter2**). In theory these mice produce 50% of the Wt protein levels. Therefore, PKD2 levels must be below those observed in *Pkd2*$^{-/+}$ mice in order for cysts to develop. It is possible that there could be compensatory mechanisms in place where the Wt allele increases protein production to compensate for the loss of the deleted allele.

To assess the possibility that *Pkd2*$^{lrm4/lrm4}$ mice produce protein below the threshold required to prevent renal cyst development, protein levels were quantified by Western blot. Embryonic kidneys dissected from E14.5 *Pkd2*$^{lrm4/lrm4}$, *Pkd2*$^{-/+}$ and *Pkd2*$^{+/+}$ embryos were frozen in liquid nitrogen before being pooled by genotype and lysed as before.

Four biological and two technical repeats were assessed per genotype. The whole experiment was repeated twice with separate samples. Densitometry analysis of the signal intensities of each band was undertaken. Using the Image Studio software, signal intensity of each band was normalised to tubulin for each sample.

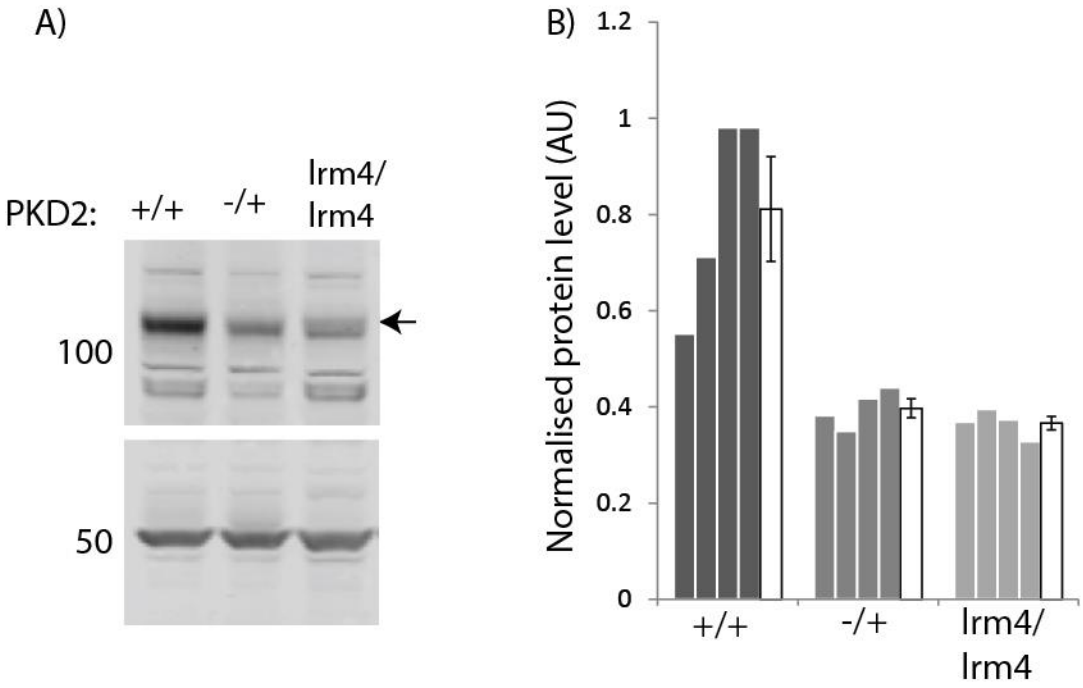

	Pkd2$^{+/+}$	**Pkd2$^{-/+}$**	**Pkd2$^{lrm4/lrm4}$**
Experiment1	0.80	0.18 (22.0%) **	0.26 (32.1%) **
Technical repeat 1	0.74	0.39 (53.0%)	0.41 (55.2%)
Experiment2	0.81	0.40 (49.0%) **	0.37 (45.2%) **
Technical repeat 2	0.79	0.43 (54.7%) **	0.32(40.8%) **

Figure 5.4: comparison of PKD2 protein from *Pkd2$^{lrm4/lrm4}$* and *Pkd2$^{-/+}$* embryonic kidney lysate.

A) shows a representative Western blot of PKD2 from E14.5 embryonic kidneys; lane one shows lysate from a pool of Wt kidneys, lane two from *Pkd2$^{-/+}$* kidneys and lane three from *Pkd2$^{lrm4/lrm4}$* kidneys. The arrow at ~110 KDa indicates the band which corresponds to PKD2. The band at 50KDa corresponds to tubulin. B) presents densitometry analysis of PKD2, each column represents the band intensity of PKD2 normalised to tubulin for a pool of three kidneys, the white column in each group represents the average for each genotype. Here, *Pkd2$^{lrm4/lrm4}$* and *Pkd2$^{-/+}$* can be observed at a similar level. The table represents average band intensities and % of Wt protein, scaled to the highest Wt value, for each experiment and technical repeat. Each experiment assessed 4 samples for each genotype which consisted of a pool of three pairs of kidneys. A technical replicate was loaded for each sample. A second experiment (experiment 2) repeated the first experiment with a fresh set of samples. T-Tests showed that Pkd2$^{-/+}$ and Pkd2$^{lrm4/lrm4}$ samples were significantly different from Wt but not from each other. **=p<0.01

The protein levels detected in *Pkd2$^{-/+}$* and *Pkd2$^{lrm4/lrm4}$* samples are very close, with values overlapping between the two data sets. The *Pkd2$^{-/+}$* samples ranged from 22-54.7% of Wt protein, the *Pkd2$^{lrm4/lrm4}$* samples ranged from 32.1-55.2% of Wt levels. In both experiments, both the *Pkd2$^{-/+}$* and *Pkd2$^{lrm4/lrm4}$* protein levels were significantly different from the Wt level but not from one another. The technical repeat of experiment 1 may have failed to be

significant because the variance between points was quite high. From these experiments, observing both averages and individual values, there is no obvious difference between *Pkd2*$^{-/+}$ and *Pkd2*$^{lrm4/lrm4}$ datasets and protein levels could not be statistically distinguished. The datasets for the two genotypes overlap and are not statistically distinct. The increase in detection of *Pkd2*^{lrm4} protein in these experiments, compared to previous experiments, is likely due to increasingly proficient lysate preparation technique.

Since *Pkd2*$^{-/+}$ kidneys express enough Wt protein to avoid the cystic phenotype and *Pkd2*$^{lrm4/lrm4}$ kidneys express an overlapping level of protein, it is unlikely that the levels of PKD2 in *Pkd2*$^{lrm4/lrm4}$ kidneys would be sufficient to prevent cyst formation. The mutation must be acting via a mechanism other than reduced protein levels to cause cyst development.

5.2.4 *PKD2*^{lrm4} is degraded by the proteasome

The level of protein in a cell is determined by both synthesis and degradation rate. The reduced protein levels in *Pkd2*$^{lrm4/lrm4}$ samples might reflect degradation of the mutant protein. To test this, proteasome inhibition experiments were performed in immortalised MEFs. In work-up experiments, cells were lysed at different time points to determine the optimum point for inhibition of the proteasome. Cells incubated for 24 or 48 hours were severely affected by the proteasome inhibitor and the majority died. Cells incubated for 10 hours had optimal time to inhibit protein production and had the fewest dead cells. Since the half-life of proteins within a cell is vastly variable, a long period of incubation (10 hrs) was chosen to ensure that a detectable level of degradation could be observed.

Six 10cm dishes each of *Pkd2*$^{lrm4/lrm4}$ and *Pkd2*$^{+/+}$ MEFs were grown to confluency. For each experiment, three plates of each genotype were treated with inhibitor and three were untreated. When confluent, cells were washed with warm PBS and the media was replaced. Half the plates received medium supplemented with 5µm/ml MG132, a potent proteasome inhibitor, the other half were given normal complete media. After 10 hours, the medium from each dish was collected and centrifuged in order to collect cells which had detached. Both detached and adherent cells were collected, pooled and analysed. The plates were lysed with RIPA as described in **MM:1.3.3**. Samples were then quantified by Bradford assay and prepared for Western Blot. The blots were imaged and analysed using the Image Studio

package and densitometry of the bands was performed. Each sample was normalised to Tubulin. There were three biological repeats and two technical repeats of each sample.

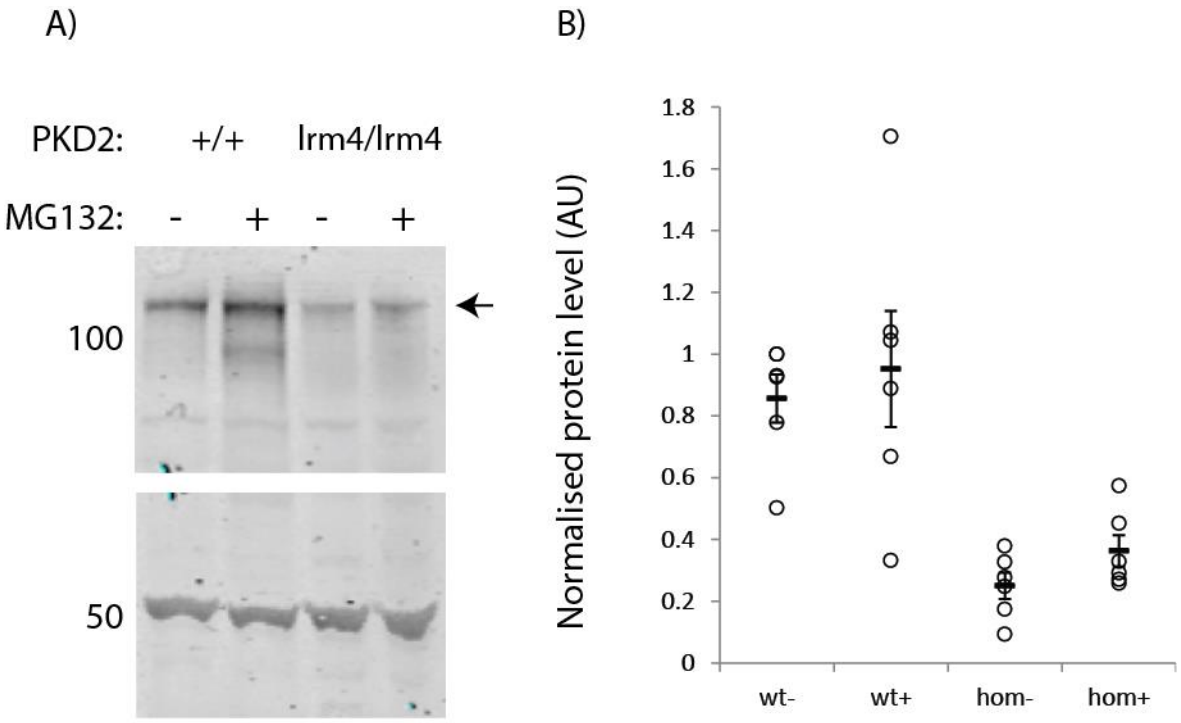

Figure 5.5: Proteasome inhibition in *Pkd2*$^{+/+}$ and *Pkd2*$^{lrm4/lrm4}$ MEFs.

A) shows a representative Western blot of protein from cells treated with MG132. In the first lane, *Pkd2*$^{+/+}$ cells have not been treated with the proteasome inhibitor. A slight rise in intensity can be seen in the second lane which has been treated with inhibitor. The third lane represents *Pkd2*$^{lrm4/lrm4}$ cells which have not been treated and the fourth lane, cells which have been treated with proteasome inhibitor. The band at ~110KDa corresponds to PKD2 (arrow) and the band at 50KDa corresponds with tubulin. B) shows the intensity of each lane and represents two experiments of 3 biological repeats each. An increase in protein levels can be seen in both Wt and *Pkd2*$^{lrm4/lrm4}$ samples when incubated with proteasome inhibitor.

As MG132 inhibits the proteasome, proteins that would be sent for degradation by the proteasome build up. If PKD2^{lrm4} is sent to the proteasome for degradation, an increase in PKD2^{lrm4} protein levels would be detected in the proteasome inhibition experiments. The average level of PKD2^{+} protein increase was 0.095AU when normalised to Wt, representing the increase between the average Wt- to Wt+ on the graph. This equates to an increase of ~11% (expressed as a percentage of Wt uninhibited level) when incubated with the proteasome inhibitor, indicating that Wt PKD2 is not turned over at a high rate over a 10 hour time period. However, the average PKD2^{lrm4} levels increase by 0.113 when normalised

to Wt, representing the increase between the average hom- to hom+ on the graph. This equates to an increase of ~45% (expressed as a percentage of PKD2^{lrm4} uninhibited level) with the addition of the proteasome inhibitor, indicating that PKD2^{lrm4} is degraded more readily than the Wt protein. Neither the percentage increase from uninhibited to inhibited, nor the overall increase in protein level were significantly different between the genotypes. However, there was a trend towards greater protein accumulation in the mutant samples. After several repeated experiments, the trend remained the same: PKD2^{lrm4} accumulated with proteasome inhibition, but not significantly more so than in the Wt samples. This is consistent with the proteasome being involved in the degradation of PKD2^{lrm4} but does not account for the whole drop in protein levels that we see. Therefore it is likely that another mechanism may also be involved in degrading PKD2^{lrm4} or that the protein is not made at the same level as the Wt protein.

Apart from the proteasome, other mechanisms within the cell exist which are involved in protein degradation. A protein that has a rapid turnover may contain a PEST domain. A PEST domain is a hydrophobic sequence rich in Proline (P), Glutamic acid (E), Serine (S) and Threonine (T) that acts as a signal to target the protein for degradation by the proteasome or calpain, a calcium dependent non-lysosomal cysteine protease (Rogers et al., 1986). In silico analysis of the PKD2 protein sequence revealed that it contains a potential PEST domain at position 61-80 of the intracellular N-terminus of the protein (Schuster, 2002). This could provide a mechanism for PKD2 degradation which does not occur via the proteasome and therefore would not be detected in the proteasome inhibition experiment.

5.2.5 PKD2^{lrm4} is glycosylated normally

To assess whether the protein could be misfolded or incorrectly targeted within the cell, experiments were undertaken to analyse glycosylation of PKD2 protein. Glycosylation of a protein is a posttranslational modification which occurs before the protein is targeted to the correct location in the cell. There are two main types of glycosylation in eukaryotes; N-linked where a glycan is attached to an asparagine (Asn), and O-linked where glycans are attached to the hydroxyl oxygen of serine or threonine residues (Varki A, 2009). N-acetyl-glucosamine (GlcNAc) is usually the first monosaccharide attached to the asparagine at the root of the sugar tree. Sugar moieties are added in a stepwise fashion by a host of enzymes

which have a specialised function. The extent of modifications that can be added by glycosylation greatly increases the diversity of proteins present within the cell (Taylor, 2011). We know that mislocalisation of proteins within the cell can cause them to be targeted to the proteasome for degradation, therefore experiments were undertaken to assess the localisation (in the next section) of the mutant protein.

De-glycosylation enzymes allow assessment of glycosylation in protein studies. Peptide-N-glycosidase F (PNGaseF) removes N-linked oligosaccharides, leaving the protein itself intact (**Fig 5.6**). PNGaseF cuts at the glycosidic bond between Asn and the first GlcNAc, providing it is unmodified or attached to α1-6 Fucose (Stanley, 2009). Endoglycosidade H (EndoH) cleaves between the two GlcNAcs, leaving one attached to the Asn residue.

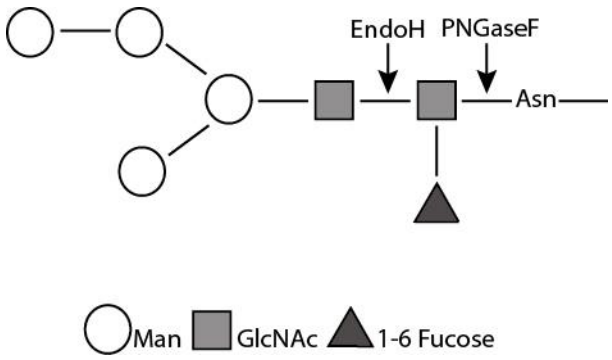

Figure 5.6: Schematic representing cleavage sites for deglycosylation enzymes, EndoH and PNGaseF.

The Asn to the right represents the portion of the protein that is on the cytoplasmic face of the ER and available for glycosylation. Squares are N-acetyl-glucosamine (GlcNAc) sites, the triangle represents modifications such as α1-6 Fucose and the circles represent other sugar moieties such as Manose. The arrows indicate the position at which the two enzymes cut.

PKD2 has five predicted external N-glycosylation sites (Cai et al., 1999), all of which are located in the first extracellular loop. These are on the luminal side of the ER membrane when PKD2 is in the ER. Since the *Pkd2*^{lrm4} mutation (E442G) is in this loop it is possible that the mutation may disrupt glycosylation of the protein by preventing the correct folding or presentation of amino acids to enzymes to receive sugar moieties. We therefore assessed the glycosylation state of the Wt and mutated protein. Similar de-glycosylation experiments of Wt PKD2 have been undertaken in a number of studies (Cai et al., 1999, Koulen et al., 2002, Hoffmeister et al., 2011) and comparing the mutated protein to the Wt glycosylation state reflects how the mutant protein may be being trafficked through the cell.

Proteins that are sensitive to EndoH are typically localised to the ER or cis-golgi since glycosylation marks are usually removed in the later portions of the golgi. PKD2 localises to the ER but is also thought to traffic to the cilium by a route which circumvents the mid-trans golgi (Hoffmeister et al., 2011). This would mean that ciliary PKD2 likely remains sensitive to EndoH cleavage.

To assess glycosylation, 10cm dishes of Wt and *Pkd2*$^{lrm4/lrm4}$ MEFs were grown to confluency and lysed, as previously described. In total, 16 dishes were lysed; eight samples were prepared for each genotype. Two biological repeats for each enzyme treatment: with and without PNGaseF, and with and without EndoH. Samples were prepared using NEB Glycoprotein denaturing kits for EndoH and PNGaseF incubations, described in **MM:1.3.4**.

Following enzyme digestion, samples were prepared for analysis by SDS-PAGE with appropriate protein molecular weight marker in reducing conditions and the gel was ran in denaturing conditions. The blot was probed for Pkd2 and tubulin (**Fig 5.7**).

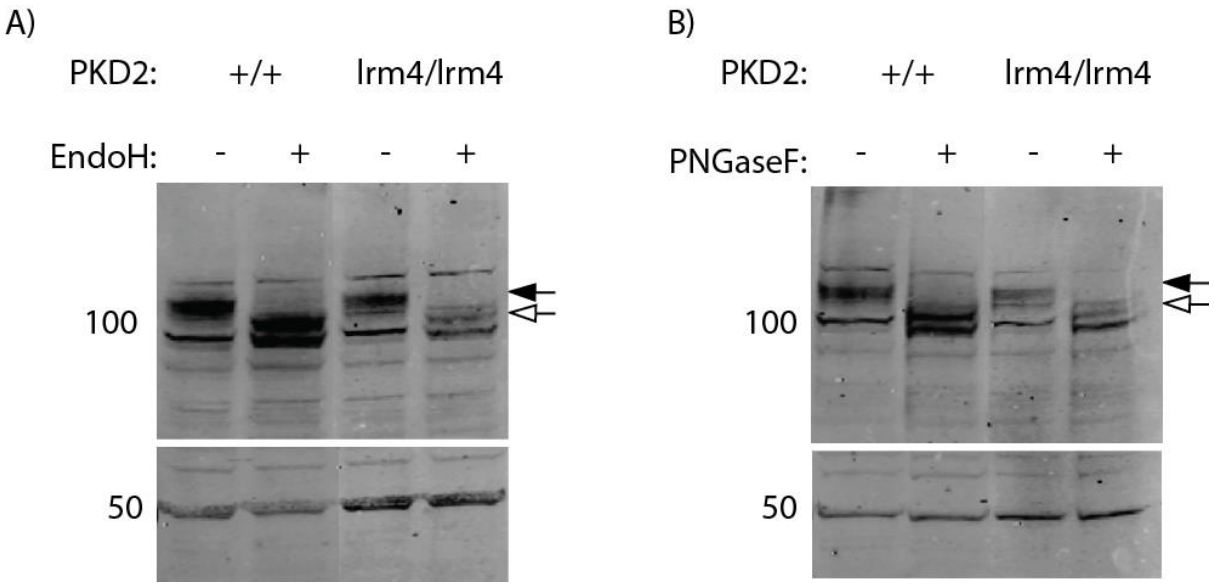

Figure 5.7: EndoH and PNGaseF deglycosylation

A) lysates incubated with EndoH (2nd and 4th lane) migrate further along the gel indicating that they have been deglycosylated by EndoH. Glycosylated PKD2 (black arrow) is ~110KDa (lane 1 and 3) whereas deglycosylated PKD2 (white arrow) migrates to around 100KDa. B) both Wt and PKD2^{lrm4} proteins remain sensitive to PNGaseF**.** In both cases, the lrm4/lrm4 lanes have been exposed further to make the band clearer.

The bands corresponding to untreated Wt and PKD2^{lrm4} were a similar size in both experiments, suggesting that the proteins are similarily glycosylated. When digested with both PNGaseF and EndoH, the Wt band clearly drops in size, indicating that PKD2^{+} is susceptible to PNGaseF and EndoH cleavage. The bands corresponding to PKD2^{lrm4} similarly drop in size, indicating that PKD2^{lrm4} remains sensitive to deglycosylation. *Pkd2^{lrm4}* does not appear to disrupt the glycosylation sites in the first extracellular loop of PKD2. The bands appear to correlate in size between the Wt and PKD2^{lrm4} samples consistent with the same number of sugar moieties being added to Wt and PKD2^{lrm4} proteins. Protein length and glycosylation state appears to be equivalent in both cases.

PKD2^{lrm4} remains sensitive to PNGaseF. PNGaseF is a generic protease that cleaves N-linked sugar moieties from the root Asn. This indicates that PKD2 is an N-linked glycoprotein. PKD2^{lrm4} remains sensitive to EndoH digestion, indicating that it does not pass through the mid-golgi, similar to the Wt protein.

5.2.6 *Pkd2^{lrm4}* does not localise to the ciliary membrane

Having established that protein is made in *Pkd2$^{lrm4/lrm4}$* kidneys and that protein levels were equivalent between *Pkd2$^{lrm4/lrm4}$* and *Pkd2$^{-/+}$* samples, making reduced protein levels unlikely to underpin the *lrm4* phenotype, the cellular localisation of PKD2^{lrm4} was assessed.

To address this final hypothesis and assess whether PKD2^{lrm4} is able to localise to the cilium and perform its function, antibody staining within cells was used to assess cellular localisation of the protein. Since no evident of disrupted glycosylation state was found, it is possible that PKD2^{lrm4} traffics normally in the cell and may be able to target to the cilium appropriately. Therefore, the localisation of the protein within the cell was assessed.

Yoshiba et al. demonstrated that a fluorescently tagged *Pkd2^{lrm4}* construct did not localise to node cilia (Yoshiba et al., 2012). This was recently confirmed by our lab with endogenous PKD2^{lrm4} (Grimes et al., 2016). Therefore it seemed possible that altered cellular localisation was responsible for the kidney phenotype, consequently the specific localisation of PKD2^{lrm4} was assessed in both MEFs and kidney cells.

Briefly, MEFs were seeded on to coverslips in a 6 well plate and grown to confluency before serum was removed to encourage cilia growth. Coverslips were probed with antibodies for the assessment of specific compartment of the cell (**MM:1.4.9**).

Kidney outgrowths from dissected from E14.5 embryos were similarly assessed. Kidneys were each cut into ~six pieces and left to settle on coverslips. When cells started to grow out from the main chunk of kidney, the coverslips were immunostained in the same way as for the MEFs.

Super-resolution structured illumination microscopy (SIM) was undertaken for samples of Wt and $Pkd2^{lrm4/lrm4}$ MEFs. Images of cilia were collected and analysed for seven Wt cilia, five $Pkd2^{lrm4/+}$ and five $Pkd2^{lrm4/lrm4}$ cilia with acetylated tubulin and PKD2 staining (**Fig 5.8**).

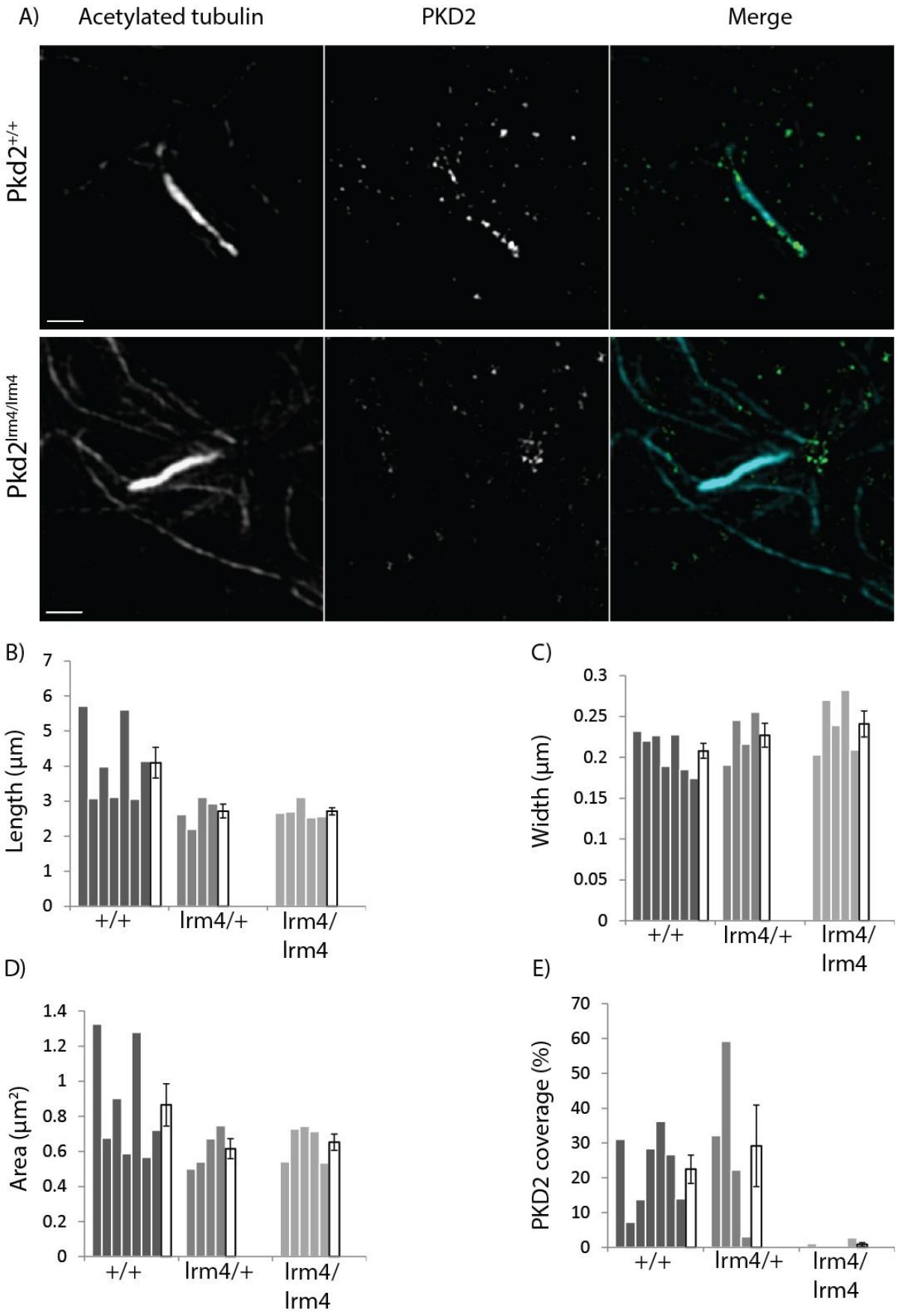

Figure 5.8: Super-resolution images and analysis of *Pkd2*$^{lrm4/lrm4}$ and *Pkd2*$^{+/+}$ cilia

A) shows representative images of *Pkd2*$^{+/+}$ (top row) and *Pkd2*$^{lrm4/lrm4}$ (bottom row) cilia. Ciliary axoneme is marked with acetylated tubulin in the first column and PKD2 is labelled by α-PKD2 in the centre column. PKD2 can be seen to localise along the length of the cilium whereas PKD2^{lrm4} is not within the cilium. The merge shows acetylated tubulin in blue and PKD2 in green. B) compares measurements of length for each genotype. The white column in each case is the average for the set. C) Compares the ciliary width normalised along the length of the cilium. D) represents the single plane area of each cilium and E) shows the percentage of cilium area that is covered by PKD2. Scale bar 1 µm.

Pkd2$^{lrm4/lrm4}$, *Pkd2*$^{lrm4/+}$ and *Pkd2*$^{+/+}$ cilia were compared by length, width, area as well as % of PKD2 coverage; the results are recoded in graphs in **Fig 5.8.** Wt PKD2 protein can be seen to localise along the length of the cilium. While PKD2^{lrm4} protein is observed in the cell, it is not seen within the ciliary axoneme. The area of PKD2 within the cilium was measured using image analysis software (ImageJ) and is presented as percentage coverage over the cilium area (**Fig 5.8 E**). PKD2^{lrm4} was unable to localise along the length of the cilium. One might expect *Pkd2*$^{lrm4/+}$ cilia to have an intermediate level of PKD2 coverage, between Wt and *Pkd2*$^{lrm4/lrm4}$; but there is in fact no difference between the levels of Wt protein in *Pkd2*$^{+/+}$ and *Pkd2*$^{lrm4/+}$ cilia (**Fig 5.8 E**). It is important to remember that ciliary PKD2 represents a small proportion of PKD2 in the cell and therefore may not reflect the overall change in protein levels. Indeed, since the cilium plays an important role in cell signalling, it is possible that a mechanism sensing PKD2 levels in the cilium could increase Wt PKD2 trafficking to the cilium in order to compensate for the PKD2^{lrm4} protein not entering.

PKD2 coverage is very variable, possibly reflecting the different stages of cell growth. Cells were serum starved to induce cilium growth but they were not synchronised, therefore cells may have established cilia at different times and therefore have different amounts of PKD2 in the cilia. These cells are also a mixed population of MEFs, they were not clonally expanded from a single cell and therefore are not genetically identical. Therefore there may be subtle differences in gene expression despite appearing morphologically similar.

Measurements of cilia length revealed, possibly due to two particularly long Wt cilia, that Wt cilia were significantly longer than both *Pkd2*$^{lrm4/+}$ (p=0.049) and *Pkd2*$^{lrm4/lrm4}$ (p=0.026) cilia. However, the width and area of these cilia was not significantly difference across genotypes. The significant difference in length may be due to a small sample size. These super-resolution images took a long time to capture, therefore a larger sample size of MEF

cilia was collected using an Axio-observeZ1 widefield microscope. Twenty frames of cilia were collected for Wt, *Pkd2*$^{lrm4/+}$ and *Pkd2*$^{lrm4/lrm4}$, images were then randomised and cilium length was scored blindly. Of the 142 cilia measured, 50 were *Pkd2*$^{lrm4/lrm4}$, 43 were *Pkd2*$^{lrm4/+}$ and 49 were Wt (**Fig 5.9**).

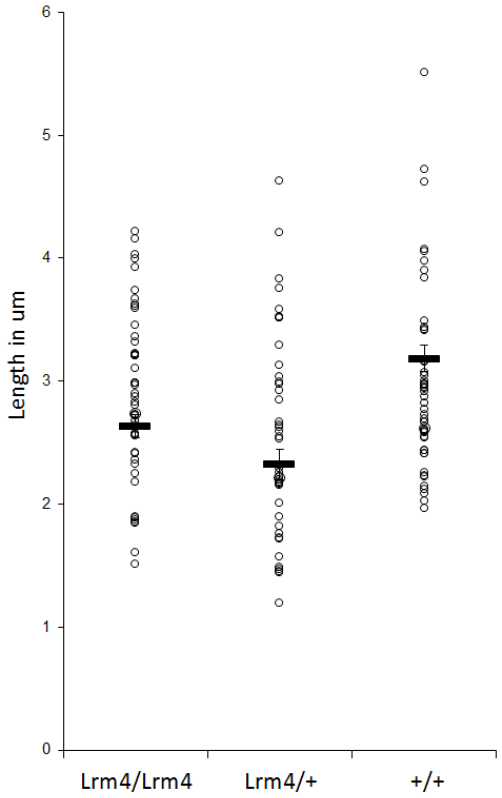

Figure 5.9: MEF cilium lengths

Each point represents the length of a single cilium the dark rectangle is the average value for each set and the error bars represent SEM.

The *Pkd2*$^{lrm4/lrm4}$ cilia length was not significantly different from Wt cilia. Supprisingly, the *Pkd2*$^{lrm4/+}$ cilia were significantly shorter than Wt (p=0.0074) and *Pkd2*$^{lrm4/lrm4}$ (p=0.0283). The cilium length varies more in this dataset than the other two; confounding factors which have not been assessed include differences in the density of the cells or the stage of the cell cycle. The *Pkd2*$^{lrm4/lrm4}$ cilia were similar in length to the Wt cilia, therefore it is unlikely that the shortness of *Pkd2*$^{lrm4/+}$ cilia is related to the *Pkd2*^{lrm4} allele.

Kidney cilia were also imaged using super-resolution microscopy and found to exhibit similar patterns to MEF cilia. PKD2^{lrm4} was unable to localise along the length of the cilium despite

being present in the cell. The Wt protein however, localised along the length of the cilium (**Fig 5.10**).

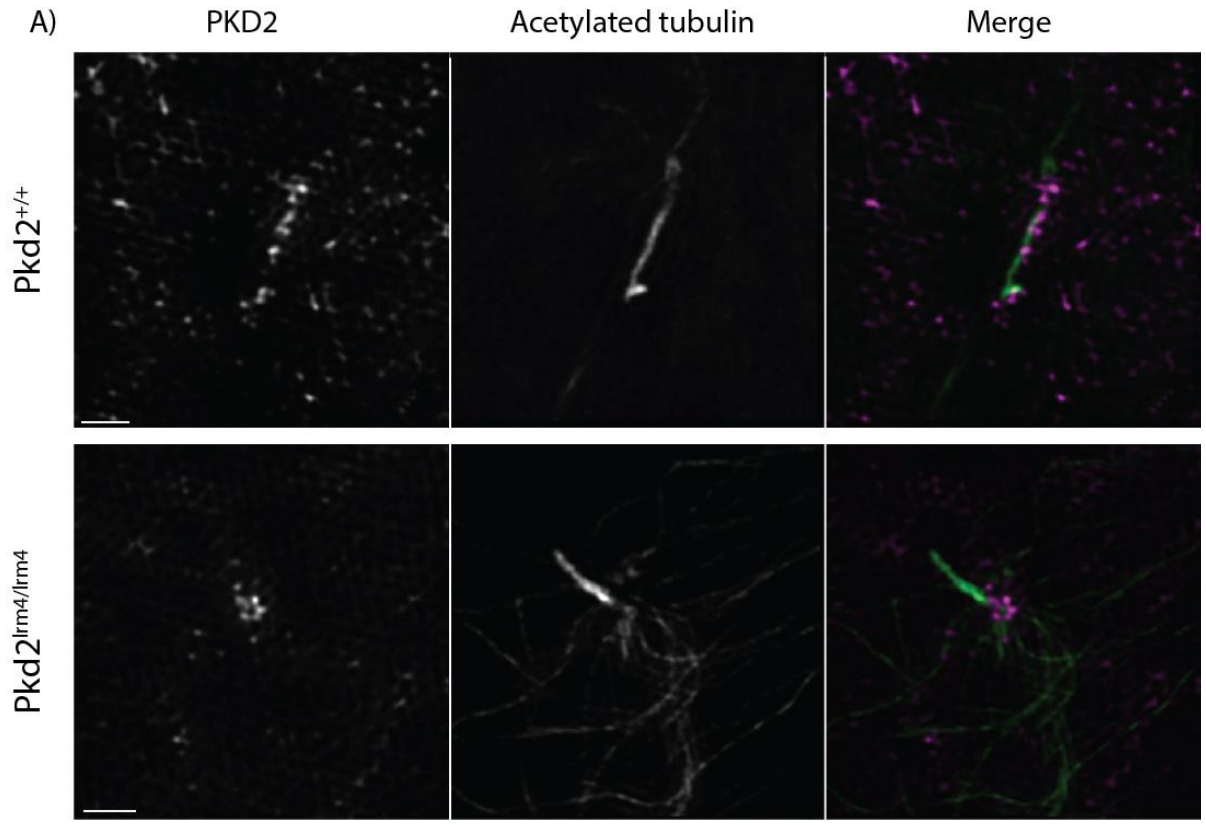

Figure 5.10: Structural illumination microscopy of cilia from kidney outgrowths

Representative images of *Pkd2*$^{+/+}$ (top row) and *Pkd2*$^{lrm4/lrm4}$ (bottom row) kidney outgrowth cilia. PKD2 is labelled in the first column and in the merge appears in purple. The ciliary axoneme is marked with acetylated tubulin in the centre column and in the merged panel appears green. PKD2 can be seen to localise along the length of the cilium whereas PKD2^{lrm4} is not within the cilium. Scale bar 1µm.

During assessment of these cilia, a distinct localisation pattern of PKD2 was observed at the base of the cilium. This pattern was also present in Wt samples, albeit at a much lower level, and was far stronger in *Pkd2*$^{lrm4/lrm4}$ samples, suggesting that the pattern represents a specific stage during the trafficking of PKD2 into the cilium. This may be the point at which *Pkd2*$^{lrm4/lrm4}$ encoded protein trafficking to the cilium arrests. To elucidate whether this ring structure corresponds to a specific structural component at the base of the cilium, further PKD2^{lrm4} localisation studies were undertaken. Initially, PKD2^{lrm4} was analysed with respect to gamma-tubulin, an antibody that recognises the basal body (**Fig 5.11**).

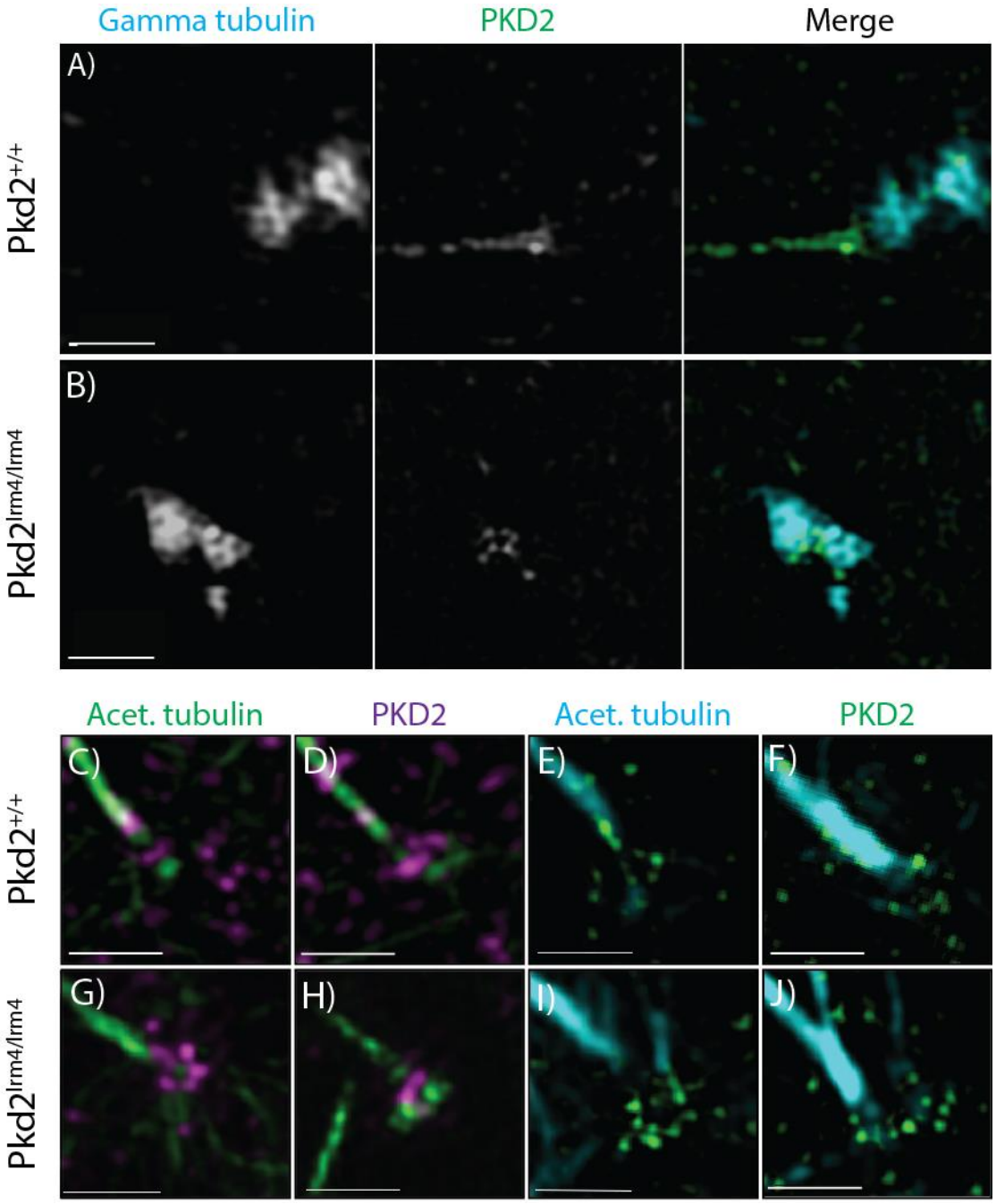

Figure 5.11: PKD2 at the base of the cilium

A) and B) show MEF cilia that are stained with gamma tubulin and PKD2. In the first column gamma-tubulin which recognises the basal body can be seen (blue in merge) and the central column shows PKD2 (green in merge). In A) the cilium is clearly filled with PKD2 but in B) the cilium cannot be distinguished. PKD2 cannot localise along the length of the cilium but is seen in a ring structure between the two centrioles of the basal body. C) and D) show the base of Wt kidney cilia, G) and H) show the base of *Pkd2*$^{lrm4/lrm4}$ kidney cilia. The cilium is marked with acetylated tubulin in green and PKD2 is marked in purple. E) and F) represent Wt MEF cilia and I) and J) show *Pkd2*$^{lrm4/lrm4}$ MEF cilia. The cilium is marked with acetylated tubulin in blue and PKD2 is marked in green. Each scale bar is 1µm long.

When assessing gamma tubulin staining, in combination with PKD2^{lrm4}, it becomes clear that PKD2 protein associates with one of the centrioles. The mother centriole docks to the plasma membrane and patterns the axoneme of the cilium. The more mature of the two centrioles, the mother centriole, can be distinguished from the daughter centriole by the distal and sub-distal appendages. Distal appendages are thought to be involved in anchoring the basal body and cilium to the membrane. The ring structure at the base of the cilium, seen in both kidney cilia and cilia from MEFs, appears to localise to a structure on the basal body. This is particularly evident in the kidney cilia, where a ring of PKD2 appears to encircle the acetylated tubulin at the base of the cilium. Several images appeared to have a ring of five puncta, this can be seen particularly well in B), E) and G) of **Fig 5.11**.

The fact that PKD2^{lrm4} persistently forms a structural pattern at the base of the cilium indicates that the protein is localising with a specific structure, therefore further antibodies were employed to discriminate between structures at the base of the cilium (**Fig 5.12**). It seemed probable that PKD2^{lrm4} is arresting at the mother centriole since the mother centriole is more decorated with structures than the daughter.

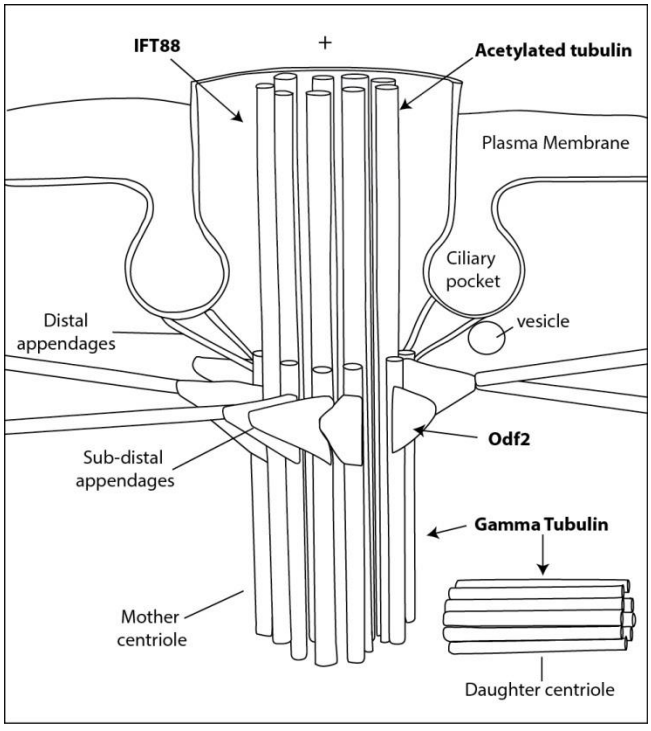

Figure 5.12: Schematic of the base of the cilium with antibodies markers labelled.

At the base of the cilium the perpendicular mother and daughter centrioles can be seen. The daughter is quite plain but the mother exhibits distal and sub-distal appendages for

docking to the ciliary membrane. Both centrioles are marked by gamma tubulin. The mother centriole is marked by Odf2 (outer dense fibre 2) at the subdistal appendages. The ciliary axoneme is marked by acetylated tubulin and by IFT88, which marks components of the IFT train.

Accumulation of protein at the base of the cilium can indicate that there are defects in IFT function. Defective IFT machinery, which causes the transport system to be unable to traffic proteins into or out of the cilium, normally result in absent, shortened or bulging cilia. Since *Pkd2*$^{lrm4/lrm4}$ cilia are a normal length and thickness, it seemed unlikely that defective IFT underlay the defect. However, we assessed the localisation of IFT88, a component of complex B, the anteriograde IFT raft; this appeared equivalent between Wt and *Pkd2*$^{lrm4/lrm4}$ cilia (**Fig 5.13**). IFT does not appear to be essential for transport of proteins into cilia, but may be involved in ciliary membrane protein regulation (Pazour et al., 2002). PKD2^{lrm4} again could not localise along the ciliary axoneme. A ring structure is seen at the base of both Wt and *Pkd2*$^{lrm4/lrm4}$ cilia, suggesting that the ring structure represents an area of the cilium where PKD2 normally interacts before entering the cilium. This could be a point at which vesicles dock before PKD2 enters the cilium. There is a clear distinction between PKD2 staining and IFT88 staining in *Pkd2*$^{lrm4/lrm4}$ cilia suggesting that PKD2^{lrm4} cannot interact with IFT88 and be trafficked along the axoneme.

Attempts to assess PKD2^{lrm4} localisation with the sub-distal appendage marker Odf2 were unsuccessful in *Pkd2*$^{lrm4/lrm4}$ cells, since the cells did not present with their characteristic ring pattern and PKD2 staining was weak. However in Wt cells (**Fig 5.13**), Odf2 can be seen at the base of the cilium, marking the sub-distal appendages of the mother centriole. Odf2 is therefore a potential marker which can be used in future to assess the specific localisation of PKD2^{lrm4}.

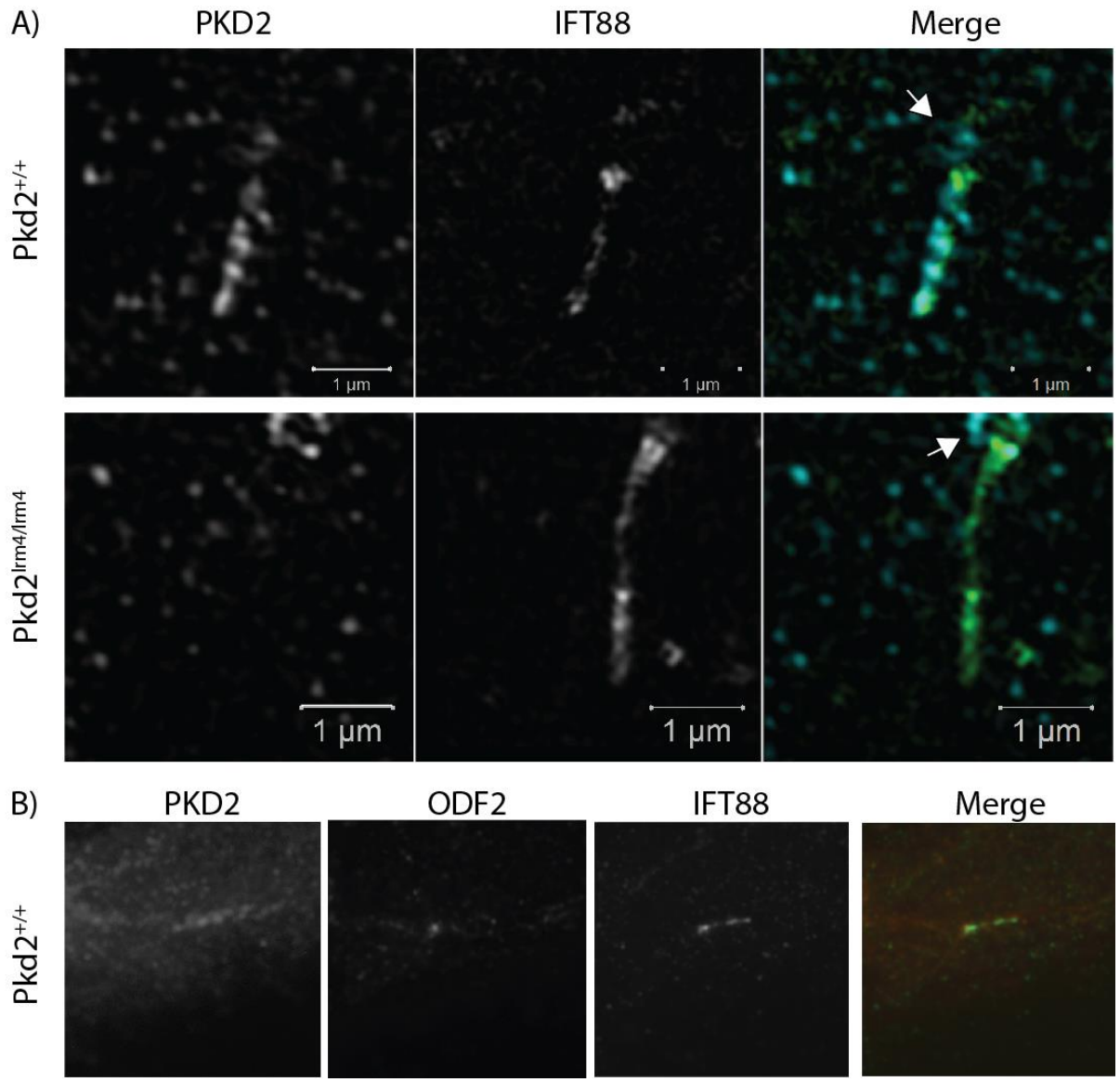

Figure 5.13: Super-resolution images of IFT88 staining in MEF cilia.

A) The top row represents a *Pkd2*$^{+/+}$ cilium. The first column shows PKD2 (blue in merge) and can be seen to localise along the cilium. IFT88 is in marking the axoneme in the central column (green in merge). The second row of panels represents a *Pkd2*$^{lrm4/lrm4}$ cilium. Pkd2 (blue in merge) cannot be seen in the cilium which is marked by IFT88 (green in merge). The white arrows in the merge panels point to the ring structure at the base of each cilium. The ring structure is evident in both genotypes but more intense at the base of the *Pkd2*$^{lrm4/lrm4}$ cilium. B) shows a Wt cilium, imaged by widefield microscope. The first panel shows PKD2 which weakly associates with the cilium, the second panel shows ODF2 which marks the sub-distal appendages of the mother centriole.IFT88 in the third panel localises to the ciliary axoneme. The final column shows the merge (Green for IFT88, Blue for ODF2 and Red for PKD2).

5.3 Results summary

The *Pkd2*^{lrm4} allele was assessed for expression levels, cellular degredation, glycosylation and cellular localisation. The *Pkd2*^{lrm4} allele was shown to produce protein in both MEFs and embryonic kidneys indicating that *lrm4* is not a protein-null. *Pkd2*$^{lrm4/lrm4}$ protein levels were found to be reduced when compared to Wt protein but were similar to those produced in *Pkd2*$^{-/+}$ kidneys. Since *Pkd2*$^{-/+}$ does not develop kidney cysts, it can be assumed that the levels of PKD2 in *Pkd2*$^{-/+}$ kidneys are sufficient to maintain the Wt phenotype. Since *Pkd2*$^{lrm4/lrm4}$ protein levels were similar to those seen in *Pkd2*$^{-/+}$, the reduction in protein levels observed in *Pkd2*$^{lrm4/lrm4}$ was not likely to be responsible for the cyst phenotype. The reduction in protein levels were assessed by experiments inhibiting the proteasome. Degradation by the proteasome does not seem to be wholly responsible for the reduced protein levels in *Pkd2*$^{lrm4/lrm4}$; however it is possible that other degradation mechanisms may be acting. A putative PEST domain has been identified within PKD2 which could signal for the protein to be degraded. Glycosylation experiments showed that PKD2^{lrm4} remains sensitive to both EndoH and PNGaseF, consistent with trafficking within the cell not being disrupted. De-glycosylation is controlled in the cell by specifically compartmentalising enzymes, therefore a glycoprotein that is sensitive to cleavage by a particular enzyme can be said to not have trafficked through that compartment. EndoH can cleave proteins that have travelled through the ER but not those that have entered the Golgi. PKD2^{lrm4} was shown to not be able to localise to the cilium but arrested at a structure which may be associated with the mother centriole. PKD2 docking to the mother centriole may be a normal process during its journey to the cilium since PKD2 and PKD2^{lrm4} are both seen to accumulate the base of the cilium.

5.4 Discussion

5.4.1 Pkd2^{lrm4}- A functional null allele

Assessment of PKD2 levels in the *Pkd2*$^{lrm4/lrm4}$ cells and kidney lysate has shown that *Pkd2*^{lrm4} is not a protein-null. Protein is produced and trafficked to the base of the cilium but is unable to enter the cilium to reach the final destination. This indicates that PKD2^{lrm4} is essentially a functional null, with respect to the cilium. Despite being reported to retain calcium channel function (Yoshiba et al., 2012) PKD2^{lrm4} is unable to reach the cilium and therefore cannot perform as a calcium channel in the cilium. This is consistent with PKD2 function in the cilium being specifically required to retain the Wt phenotype.

5.4.2 PKD2 channel location

Cellular compartmentalisation of PKD2 is associated with variable functionality of the protein. PKD2 localises to the PM where it is thought to act as a receptor-operated channel; to the ER, functioning as an intracellular Ca^{2+} release channel and to the ciliary membrane where it is likely to act as a mechanosensitive channel (Tsiokas et al., 2007). Shuttling between these compartments regulates the activity of PKD2 (Hidaka et al., 2004, Kottgen and Walz, 2005, Hanaoka et al., 2000).

The *Pkd2*^{lrm4} mutation (E442G) causes a single amino acid change within the first extracellular loop (FEL), between the first two transmembrane domains of PKD2. This mutation affects ciliary targeting, specifically entry into the cilium after docking at the base of the cilium has occurred. Since the putative ciliary localisation signal (RVxP) is reported to be at the N-terminus (Geng et al., 2006), on the cytoplasmic side of the ciliary membrane, the Pkd2^{lrm4} mutation is unlikely to interact with or disrupt this motif. Therefore, assessment of the domain architecture of the protein was undertaken, particularly of the FEL, in order to understand the effect of the mutation.

In the FEL of PKD2, there are two highly conserved polycystin domains, PC-A (310-331) (Venglarik et al., 2004) and PC-B (406-449) (Li et al., 2003, Knobel et al., 2008) (**Fig 5.14**). These have been recognised as highly conserved but have yet to be associated with a function. The whole FEL has been shown to be required for ciliary localisation of PKD2,

indicating the ciliary localisation is not conveyed by the RVxP signal alone (Knobel et al., 2008).

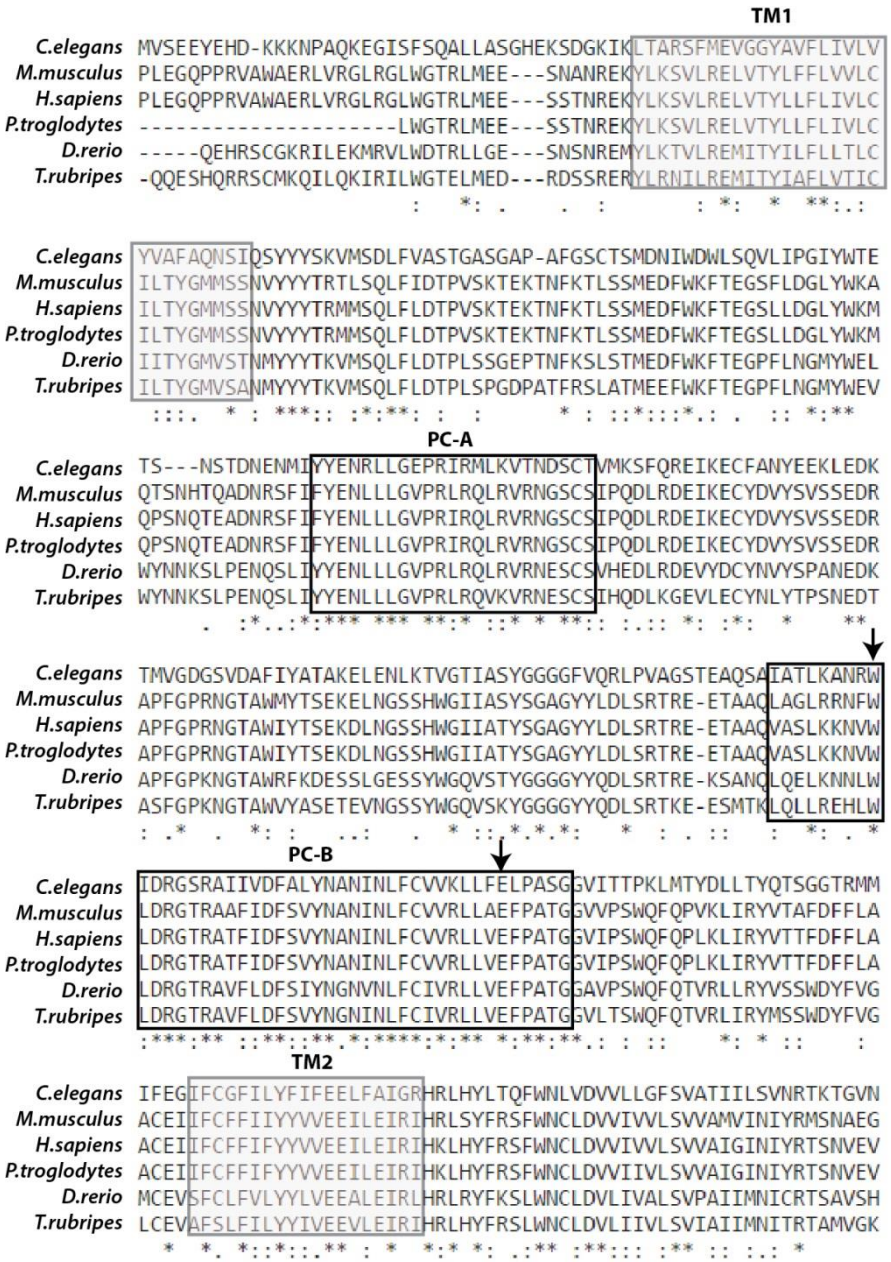

Figure 5.14: Multiple sequence alignment of the first extracellular loop of PKD2

Clustal Omega multiple sequence alignment (McWilliam et al., 2013). The light boxes highlight the transmembrane domains (TM1 and TM2) between these are the Polycystin domains. The first box, shows PC-A at residues 310-331. The second box shows PC-B at residues 469-487. Within PC-B, the position of the *lrm4* mutation is indicated with an arrow (E442G) and the position of W414G (Cai et al., 2014) is also indicated**.**

It is unclear whether these specific domains are required for ciliary localisation, however a number of single amino acid substitutions have been recorded within these domains, all of

which are reported to be pathogenic (PKDb, 2016). Notably, W414G a very similar allele to E442G is also localised in the PC-B domain and cannot localise to the cilium (Cai et al., 2014). Like PKD2^{lrm4} (Yoshiba et al., 2012), calcium channel activity was maintained in PKD2^{W414G}. Together these data strongly suggest that ciliary localisation is required to prevent ADPKD and that activity in the ER is not sufficient to do so.

Further assessment of these domains is required to determine whether PC-A, PC-B, both or neither is required for ciliary localisation. Site directed mutagenesis provides a useful tool to specifically mutate the protein within these domains and assess its localisation within the cell and to the cilium. Electroporated *Pkd2*$^{-/-}$ MEFs would allow efficient assessment of this in the absence of endogenous PKD2. Presently, attempts to assess ciliary localisation of exogenously expressed mutated forms of the human protein have been unsuccessful. Further experimentation, perhaps using the murine equivalents of the mutations, will provide further evidence as to the requirement of these domains for ciliary localisation.

5.4.3 Ring at the base of the cilium

We have identified a ring structure of PKD2^{lrm4} at the base of the cilium which may localise to a specific structural component of the mother centriole. Accumulation of PKD2 to the base of *C.elegans* dendrites has been previously reported (Peden and Barr, 2005) and related to transition zone docking. We have seen PKD2^{lrm4} associating with microtubules at the base of the cilium which organise at the basal body and particularly in a ring structure at the mother centriole. These positions are consistent with PKD2 filled vesicles travelling along the cytoskeleton and docking at the sub-distal or distal appendages. It seems likely that the ciliary pore complex prevents PKD2^{lrm4} trafficking into the cilium, but allows PKD2^{+} inside. This can be seen in Pkd2$^{lrm4/+}$ cilia, where the pore complex is likely sorting the mutant from the Wt protein at the base of the cilium.

Septin molecules have been reported to form a ring structure at the base of the cilium. Septins are GTPases that form a diffusion barrier in budding yeast. Septin2 (SEPT2) localises in a ring structure of ~500nm diameter to the base of the cilium between the ciliary and pericilary membrane. However, Hu et al. show that SEPT2 localises between the axoneme and distal appendages and that it may be associated with the periciliary membrane. SEPT2 may form a diffusion barrier to prevent molecules travelling from the PM to the ciliary

membrane. Proteins may be inserted into the ciliary membrane by IFT or BBSome components which may be responsible for carrying proteins over the diffusion barrier (Hu et al., 2010).

Further assessment of distal and subdistal appendage proteins will allow us to specifically pinpoint the point at which PKD2 is being retained. Vesicles dock at the distal appendages before proteins are released and trafficked into the cilium. Proteins of the distal and sub-distal appendages localise in a ring around the cilium and form the ciliary pore complex. Co-localisation studies with distal appendage proteins such as CEP83, SCLT1, FBF1, CEP89 and CEP164 and sub-distal appendage proteins ODF2 and Ninein will help to pinpoint PKD2^{lrm4} mislocalisation (Tanos et al., 2013).

5.4.4 Ciliary localisation is essential

In their review, Winyard and Jenkins argue that cilia are unlikely to be wholly responsible for cyst formation in ADPKD (Winyard and Jenkins, 2011). The literature is replete with evidence of a ciliary link to ADPKD cyst formation, including that PKD1, PKD2 and other ciliopathy genes: 1) localise to the cilium, and when disrupted cause abnormalities of the cilium structure or function; 2) regulate genetic cascades which are abnormal in cystic epithelia; and 3) inhibit cyst formation when expressed in abnormal ciliary related pathways. Nonetheless, a number of these experiments do not dissect the cellular spatial expression of the Polycystins. PKD2 localises to several areas of the cell, including cell–cell junctions (Wilson, 2001) and the plasma membrane, therefore it is possible that these functions are also essential to prevent cyst formation. The *Pkd2^{lrm4}* mutation enables this spatial dissection of the function of PKD2. PKD2^{lrm4} is unable to localise to the cilium, but still functions as a calcium channel. This indicates that the ciliary function of PKD2, and not other cellular functions, is essential for cyst prevention. The cilium and the Polycystins are indeed working together to prevent cyst formation in the renal tubule and disruption of this relationship causes cyst development.

Chapter 6: Summary and Conclusions

This thesis has examined the role of ciliary localisation of PKD2 in the prevention of polycystic kidney disease and has sought to deepen the understanding of the molecular characterises of ADPKD progression. This work has spatially dissected the requirement of PKD2 localisation within the cell and specifically underlined the importance of ciliary localisation.

6.1 Key findings

6.1.1 *Pkd2*^{lrm4} causes embryonic renal cysts

Having overcome the embryonic lethality by changing the genetic background on which the mice were analysed, phenotyping of *Pkd2*$^{lrm4/lrm4}$ embryos was undertaken. *Pkd2*$^{lrm4/lrm4}$ kidneys were found to develop cysts by E15.5. These cysts were indistinguishable from those seen in *Pkd2*$^{-/-}$ embryonic kidneys. *Pkd2*$^{lrm4/lrm4}$ embryos exhibited disrupted organ patterning and embryos exhibited situs defects. As such, we can now say that *Pkd2*^{lrm4} is a pathogenic mutation in the kidney.

6.1.2 *Pkd2*$^{lrm4/+}$ mice develop microcysts with age

Pkd2$^{lrm4/+}$ mice were aged to adulthood and found to develop renal microcysts. The mice also developed polycystic liver disease, modelling closely the extrarenal manifestations of ADPKD. This mimicked existing *Pkd2*$^{-/+}$ mouse models (Wu et al., 2000, Wu et al., 1998), therefore suggesting that *Pkd2*^{lrm4} could be a null allele.

6.1.3 *Pkd2*^{lrm4} expressed over a null allele in the kidney causes cyst development

Specific deletion of the Wt copy of *Pkd2* in the proximal tubule, in the context of the *Pkd2*^{lrm4} allele, led to the development of renal cysts. Cysts increased in size and number with age, modelling aspects of the progression of ADPKD. A kidney specific Cre recombinase (Kap-iCre) was characterised and found to recapitulate a sexually dimorphic expression pattern. The Kap-iCre transgene allowed deletion of a floxed allele of *Pkd2* in the proximal tubule in a spatially and temporally specific context. This provides a mechanism by which individual mutations can be assessed. *Pkd2*^{lrm4} was shown to cause cyst development in cells where the Wt copy of *Pkd2* had been deleted, supporting the two-hit hypothesis.

6.1.3 Pkd2^{lrm4} cannot localise to the cilium

The molecular characteristics of PKD2^{lrm4} were observed. PKD2^{lrm4} is detected at a lower level than the Wt protein, but at similar levels to PKD2 found in *Pkd2*$^{-/+}$ samples. Pkd2$^{-/+}$ mice do not develop cysts. Therefore the lower level of PKD2^{lrm4} in *Pkd2*$^{lrm4/lrm4}$ samples is likely to be at a sufficient level to avoid cyst development, indicating that another aspect of the mutation is responsible for the phenotype. This also indicated that *Pkd2*^{lrm4} is not a hypomorphic allele. PKD2^{lrm4} was shown to be similarly glycosylated to the Wt protein. PKD2^{lrm4} remained sensitive to EndoH and to PNGaseF cleavage and was cleaved to a similar extent to PKD2^{+}, indicating that the proteins carry a similar amount of glycans. PNGaseF digestion confirmed that PKD2 is an N-linked glycoprotein. EndoH sensitivity indicates that proteins pass through the ER but do not pass through the golgi, consistent with the proposed trafficking route to the cilium. The cleavage of PKD2 was consistent with cell trafficking being undisturbed by the *lrm4* mutation. When assessing cellular localisation, PKD2^{lrm4} was shown to be unable to localise to the ciliary membrane in embryonic kidney explants and mouse embryonic fibroblasts. It is this mislocalisation that we believe to be responsible for the phenotype. PKD2^{lrm4} arrests at the basal body and cannot move into the cilium.

Pkd2^{lrm4} is a new model of ADPKD which mimics aspects of several other models of the disease and is closely linked to the disease itself. Embryonically, *Pkd2*$^{lrm4/lrm4}$ models a rapid development of cysts, similar to that seen in established null mouse lines (Wu et al., 1998, Wu et al., 2000). Assessment of *Pkd2*^{lrm4} has provided evidence that convincingly shows that PKD2 is required in the cilium in order to function in the prevention of PKD.

Throughout this work, the question of the whether *Pkd2*^{lrm4} is a null allele has remained. The data presented in this thesis have shown, with some certainty that *Pkd2*^{lrm4} acts as a functional null. Despite PKD2^{lrm4} being detected at a lower level that Wt protein in MEF cell lines and embryonic kidney lysates, the levels detected were shown to be comparable and overlapping with PKD2 those seen in *Pkd2*$^{-/+}$ samples. This indicated that enough protein was present in *Pkd2*$^{lrm4/lrm4}$ samples to avoid cyst development. *Pkd2*^{lrm4} is not a hypomorphic or null allele and does not cause Haploinsufficiency. PKD2^{lrm4} was shown to be unable to localise along the length of the cilium in both kidney and MEF cell lines. The cilium

is therefore identified as an essential compartment for PKD2 function and ciliary localisation of PKD2 is required for prevention of the cystic phenotype. Despite retaining calcium channel activity (Yoshiba et al., 2012), *Pkd2*^{lrm4} is unable to prevent PKD due to its inability to localise to the cilium. This points to *Pkd2*^{lrm4} being a functional null allele.

6.2 The two-hit hypothesis

The data presented in **chapter 4** provide a good model for investigating the two-hit hypothesis. The recombinase (Kap-iCre) provides a mechanism by which a second mutation can be introduced into cells that are already carrying a germline mutation. In this case, *Pkd2*^{lrm4} acted as the first germline mutation whilst the second mutation, came in the form of the deleted *Pkd2*^{fl} allele. This is a useful model because unlike the unstable allele of Pkd2 (Wu et al., 1998), the second hit was directed to a specific population of cells and could provide insight specifically about the role of *Pkd2* in the proximal tubules. This makes it possible to assess whether there is a spread of cysts into other areas of the kidney, caused by damage from nearby enlarging cysts. Since the proximal tubule makes up a large proportion of the tubule segments in the cortex, a substantial area of the kidney can be targeted. However, the downside to this is that the effect of other segments of the nephron, which all become cystic in ADPKD, cannot be observed. The question of the clonal nature of the cyst development has not been assessed here, but with dissection of cyst linings, it would be possible to assess whether the cells were expanded clonally from a founder cell which deleted the *Pkd2* Wt allele. However, the question of why all such cells do not develop into cysts remains. A larger proportion of cells stained blue in the LacZ assessment of Kap-iCre activity than there were cysts in the adult mice. This indicates that not all cells that deleted the Wt allele became cystic. More investigation into the other factors involved in cyst development are required. One area of the tubule could be weaker or more susceptible to injury than other areas and this may be a factor in determining cyst development.

We endeavoured to address the timing of cyst development in these mice by dosing the mice with DHT. Dosing after the developmental switch enabled us to avoid a rapid development of cysts that we may expect from early deletion. The dose of DHT acted as a mechanism to mop up any cells that had not deleted the Wt copy when exposed to the

endogenous hormones. Other background conditions, such as assessment in castrated males, may provide insight into the development of cysts. In castrated males, the transgene could be activated by hormones at one specific time period and without the background endogenous hormone levels. This may provide insight into the timings of cyst development and progression.

When the deletion of the floxed allele was induced by endogenous hormones, cysts could be seen to develop in the cortex of the kidney. *Pkd2*$^{lrm4/+}$ mice slowly develop a sparse presentation of microcysts, similar to the mildest forms of ADPKD where patients, who may carry a hypormophic mutation, develop a small number of cysts late in life and do not suffer from renal failure. When in combination with a deletion of *Pkd2,* disease progression becomes much more severe. Since only a portion of the cells are affected by this second mutation, ESRF is not present in these mice; however some blood and plasma components are consistent with a decline in renal function.

The Kap-iCre recombinase is a valuable tool for altering renal phenotypes; the regulatory elements allow for fine tuning of the expression pattern. However, more characterisation of the transgene is required. The mechanism behind the sexually dimorphic expression pattern remains unclear. There must be some effector which modulates the transgene expression differently between sexes and this somehow prevents DHT from inducing the same expression pattern in male and female mice. The induction with DHT produced mixed results; previous studies have led to a greater increase in expression after induction than we have seen (Ding and Sigmund, 2001) and the expression pattern, as assessed by LacZ reporters, appears to be somewhat variable. It is unclear why the female expression pattern remains distinct from the male pattern when both sexes are induced with DHT, since the construct is equivalent in both sexes. Perhaps earlier induction with DHT would yield different results, modulating the expression of the transgene before the endogenous proteins have acted. In the future, further characterisation is required. The difficulty with undertaking such a characterisation lies in the high numbers of mice required, especially considering the levels of variation between mice. However, behind the cost of characterisation lies a great potential for a wealth of discoveries to be made. The construct does carry the potential for an array of finely tuned experiments. The timing of induction, target of deletion, spatial expression and genetic context could all be altered to provide an

array of information. Particularly of interest is the way that this system lends itself to the assessment of different combinations of mutations. Any mutation thought to be involved in cyst development through the two-hit mechanism could be investigated in combination with deletion of a floxed allele.

6.3 Ciliary localisation is essential

The function of PKD2 has been spatially dissected in this work. It is known that different glycoforms of PKD2 exist which target the protein to different areas of the cell (Hoffmeister et al., 2011) and that PKD2 is involved in a number of cellular pathways. This indicates that there may be other roles for PKD2 within the cell outside of maintaining tubule structure, or that PKD2 appears at several points in the pathway, playing different roles. For instance, one hypothetical pathway involves PKD2 in the cilium responding flow on the cilium and causing Ca^{2+} influx into the cilium; a signal which is then transferred to the ER and causes PKD2 in the ER to induce Ca^{2+} release into the cell (Nauli et al., 2003). Since, no difference in the glycosylation state of $PKD2^{lrm4}$ with respect to PNGaseF and EndoH cleavage was observed, it would appear that cellular targeting outside of the cilium is not disrupted and that the mutation does not affect these functions. This separates the function in the cilium from other possible functions throughout the cell, in the ER, between cells or in the cell plasma membrane (Chapin and Caplan, 2010).

Throughout this thesis, PKD2 has been assessed independently of PKD1. PKD1 and PKD2 are known to interact (Qian et al., 1997, Tsiokas et al., 1997) and function in the same cellular pathway (Lee and Somlo, 2014). Further assessment of $PKD2^{lrm4}$ function in terms of PKD1 cellular trafficking and function remain to be undertaken and a plethora of insight remains to be gained. Since PKD1 and PKD2 interact, it is possible that they form a complex before trafficking to the cilium (Hanaoka et al., 2000, Nauli et al., 2003), indeed PKD2 is thought to be required for PKD1 to traffic to the cilium (Chapin et al., 2010). It is thought that PKD2 binds and enable the maturation of PKD1 and that this maturation is required before PKD1 can localise to the cilium (Chapin et al., 2010, Gainullin et al., 2015). PKD2 is thought to be able to localise independently of PKD1 (Hoffmeister et al., 2011). This may indicate that there may be cases where PKD2 is acting in the cilium independently of PKD1 or that, if there are more PKD2 subunits than PKD1 units in the complex, perhaps the complex forms

in the cilium as PKD2 subunits join. Since PKD2^{lrm4} cannot localise to the cilium, the *Pkd2*$^{lrm4/lrm4}$ mice provide a good model for testing whether PKD1 can localise to the cilium independently of PKD2. It is likely that PKD1 localisation is also disrupted in *Pkd2*$^{lrm4/lrm4}$ cells, yet this remains to be assessed. PKD1 may also arrest at the base of the cilium with PKD2^{lrm4}.

Both these proteins localise to the primary cilium yet the mechanism of how this localisation comes about is poorly understood. Two different ciliary targeting sequences appear to be involved in targeting PKD1 (Ward et al., 2011) and PKD2 to the cilium (Geng et al., 2006). PKD2 has an N-terminal RVxP peptide tag but it appears that this alone is not sufficient to target PKD2 to the cilium since mutations outside of this domain, such as *Pkd2*^{lrm4} and *Pkd2*^{W414G} (Cai et al., 2014) abrogate ciliary localisation. Knobel et al. identified that the transmembrane region (aa74-541), incorporating half the N-terminal tail, the first three transmembrane domains and part of the second extracellular transmembrane loop, is required for ciliary localisation in *C.elegans (Knobel et al., 2008).* Human PKD2 fused to GFP failed to localise to the cilium however, a chimeric construct replacing the human TM region with the corresponding *C.elegans* TM region was able to localise to the cilium. This showed that the N- and C- termini of *C.elegans* PKD2 homolog are not required for ciliary targeting but that the TM domain contains a region which effectively targets proteins to the cilium. The human TM domain, as part of the full length fusion protein, could not target the protein to the cilium in *C.elegans,* this region has 43% sequence identity between the two species. Geng et al. show that this region alone is unable to localise PKD2 to cilia in mammalian cells and that the N-terminal RVxP sequence is necessary (Geng et al., 2006). We have shown that mutation in this region does affect ciliary localisation. This provides more evidence that a domain, likely residing within the first extracellular loop of PKD2, modulates ciliary targeting.

6.4 Future directions

6.4.1 Localisation domains

Two domains were identified which may be essential for ciliary localisation. The highly conserved polycystin domains, PC-A and PC-B, may represent the regions in the TM domain identified by Kobel et al. as important for localisation to *C.elegans cilia (Knobel et al., 2008)*. These regions have high sequence identity between human and *C.elegans* (**Fig 5.13**). Further investigation of these domains will provide essential understanding of the mechanism behind ciliary localisation of the protein. It will be interesting to investigate how this region interacts with the N-terminal RVxP sequence and whether both Polycystin domains are required for ciliary localisation. If only one of the Polycystin domains is sufficient for ciliary targeting along with the RVxP, this begs the question of the other regions function, since its high conservation across species indicates that it is a functional domain.

6.4.2 *Pkd2*$^{lrm4/-}$

The murine model of ADPKD described in **chapter 4** provides an appealing model for therapeutic testing. These mice model the disease with both a progressive development of renal cysts and the development of polycystic liver disease, a common extrarenal complication seen in ADPKD. Currently, murine models of cyst development can be categorised into two classes; the first are those that have mutations in *Pkd1* or *Pkd2*, since these are the genes which cause ADPKD, these are models of ADPKD. The second are those that have mutations in other genes. These are models of polycystic kidney disease (PKD), the development of renal cysts in these cases is often related to defects of the cilium or ciliary genes.

A number of mouse models of ADPKD exist and these model aspects of the disease such as renal cyst development, liver and pancreatic cysts, as well as molecular pathways and aspects of cyst progression (Stypmann et al., 2007, Wu et al., 1998, Wu et al., 2000, Lu et al., 1997, Kim et al., 2000, Boulter et al., 2001). Our mice add to these models by modelling the slow cyst development of ADPKD in adult mice as well as underlining the importance of the primary cilium as an important functional niche of PKD2 in cyst prevention. So far, Pkd2^{lrm4} has revealed a slow development of renal cysts which do not progress to ESRF. However, the Kap-iCre model allows for a variety of permutations to be made, for instance earlier

deletion of the floxed allele may allow for a more severe progression of the disease to be observed. Therefore, *Pkd2*^{lrm4} provides a close model of ADPKD which will allow for features that are specific to ADPKD disease progression to be untangled.

Models of PKD, those with mutations in genes other than *Pkd1* and *Pkd2* have provided great and valuable insight into the development of renal cystic disease. Among these, mutations in *Ift88* (Moyer et al., 1994, Pazour et al., 2000, Taulman et al., 2001, Pazour et al., 2002), *Invs* (Yokoyama et al., 1993, Watanabe et al., 2003) and *Nek8* (Manning et al., 2012) have provided evidence that cilium growth, maintenance and signalling is essential in the prevention of PKD.

6.5 Closing remarks

This thesis has examined the role of PKD2 localisation to the cilium concentrating on its function in the prevention of ADPKD. The data described herein strongly suggest that the cilium is a specific niche in which PKD2 functions to prevent cyst development. There exist localisation mutants of PKD2, mutated in regions other than the RVxP motif, which prevent ciliary localisation of the protein and these are predicted to be pathogenic (Cai et al., 2014). Ciliary localisation is critical for PKD2 function in prevention of ADPKD and it is unlikely that channel activity elsewhere in the cell is sufficient to prevent cyst development. This adds to the evidence that a functional protein can be rendered a functional null by mislocalisation.

The mouse models described here provide a close and representative pastiche of the human condition, modelling a number of aspects of the disease, which will be invaluable for further elucidation of the mechanisms underlying the development of the disease.

Having produced a plethora of discoveries in the past several decades, this field does not show signs of slowing down. With the first successful drug being prescribed to patients we see a beginning of new insights into factors which can modify the disease in such a way as to improve patient health. Basic science is essential to the understanding of the functional aspects of disease progression and is therefore vital to the progression of the field.

Soli Deo Gloria

REFERENCES

ABOUALAIWI, W. A., TAKAHASHI, M., MELL, B. R., JONES, T. J., RATNAM, S., KOLB, R. J. & NAULI, S. M. 2009. Ciliary polycystin-2 is a mechanosensitive calcium channel involved in nitric oxide signaling cascades. *Circ Res,* 104**,** 860-9.

ACEVEDO-AROZENA, A., WELLS, S., POTTER, P., KELLY, M., COX, R. D. & BROWN, S. D. 2008. ENU mutagenesis, a way forward to understand gene function. *Annu Rev Genomics Hum Genet,* 9**,** 49-69.

AL-AWQATI, Q. & GOLDBERG, M. R. 1998. Architectural patterns in branching morphogenesis in the kidney. *Kidney Int,* 54**,** 1832-42.

AL-AWQATI, Q. & OLIVER, J. A. 2002. Stem cells in the kidney. *Kidney Int,* 61**,** 387-95.

ALBERS, E. & MULLER, B. W. 1992. Complexation of steroid hormones with cyclodextrin derivatives: substituent effects of the guest molecule on solubility and stability in aqueous solution. *J Pharm Sci,* 81**,** 756-61.

BAERT, L. 1978. Hereditary polycystic kidney disease (adult form): a microdissection study of two cases at an early stage of the disease. *Kidney Int,* 13**,** 519-25.

BASTOS, A. P., PIONTEK, K., SILVA, A. M., MARTINI, D., MENEZES, L. F., FONSECA, J. M., FONSECA, II, GERMINO, G. G. & ONUCHIC, L. F. 2009. Pkd1 haploinsufficiency increases renal damage and induces microcyst formation following ischemia/reperfusion. *J Am Soc Nephrol,* 20**,** 2389-402.

BATAILLE, S., DEMOULIN, N., DEVUYST, O., AUDREZET, M. P., DAHAN, K., GODIN, M., FONTES, M., PIRSON, Y. & BURTEY, S. 2011. Association of PKD2 (polycystin 2) mutations with left-right laterality defects. *Am J Kidney Dis,* 58**,** 456-60.

BAYLIS, C. 2012. Sexual Dimorphism: The Aging Kidney, Involvement of Nitric Oxide Deficiency, and Angiotensin II Overactivity. *The Journals of Gerontology Series A: Biological Sciences and Medical Sciences,* 67**,** 1365-1372.

BERTRAM, J. F. 2013. Estimating glomerular number: why we do it and how. *Clin Exp Pharmacol Physiol,* 40**,** 785-8.

BERTRAM, J. F., DOUGLAS-DENTON, R. N., DIOUF, B., HUGHSON, M. D. & HOY, W. E. 2011. Human nephron number: implications for health and disease. *Pediatr Nephrol,* 26**,** 1529-33.

BIREWAR, S. & ZAWADA, E. T., JR. 2003. Early onset polycystic kidney disease: how early is early? *S D J Med,* 56**,** 465-8.

BISSLER, J. J., SIROKY, B. J. & YIN, H. 2010. Glomerulocystic kidney disease. *Pediatric Nephrology (Berlin, Germany),* 25**,** 2049-2059.

BLUM, M., FEISTEL, K., THUMBERGER, T. & SCHWEICKERT, A. 2014a. The evolution and conservation of left-right patterning mechanisms. *Development,* 141**,** 1603-13.

BLUM, M., SCHWEICKERT, A., VICK, P., WRIGHT, C. V. & DANILCHIK, M. V. 2014b. Symmetry breakage in the vertebrate embryo: when does it happen and how does it work? *Dev Biol,* 393**,** 109-23.

BOEHLKE, C., KOTSIS, F., PATEL, V., BRAEG, S., VOELKER, H., BREDT, S., BEYER, T., JANUSCH, H., HAMANN, C., GODEL, M., MULLER, K., HERBST, M., HORNUNG, M., DOERKEN, M., KOTTGEN, M., NITSCHKE, R., IGARASHI, P., WALZ, G. & KUEHN, E. W. 2010. Primary cilia regulate mTORC1 activity and cell size through Lkb1. *Nat Cell Biol,* 12**,** 1115-22.

BOIVIN, F. J., SARIN, S., EVANS, J. C. & BRIDGEWATER, D. 2015. The Good and Bad of beta-Catenin in Kidney Development and Renal Dysplasia. *Front Cell Dev Biol,* 3**,** 81.

BOSOMWORTH, M. P., APARICIO, S. R. & HAY, A. W. 1999. Urine N-acetyl-beta-D-glucosaminidase--a marker of tubular damage? *Nephrol Dial Transplant,* 14**,** 620-6.

BOULTER, C., MULROY, S., WEBB, S., FLEMING, S., BRINDLE, K. & SANDFORD, R. 2001. Cardiovascular, skeletal, and renal defects in mice with a targeted disruption of the Pkd1 gene. *Proceedings of the National Academy of Sciences of the United States of America,* 98**,** 12174-12179.

BOWEN, S. E., WATT, C. L., MURAWSKI, I. J., GUPTA, I. R. & ABRAHAM, S. N. 2013. Interplay between vesicoureteric reflux and kidney infection in the development of reflux nephropathy in mice. *Dis Model Mech,* 6**,** 934-41.

BRASIER, J. L. & HENSKE, E. P. 1997. Loss of the polycystic kidney disease (PKD1) region of chromosome 16p13 in renal cyst cells supports a loss-of-function model for cyst pathogenesis. *J Clin Invest,* 99**,** 194-9.

BRAYTON, C. 2009. Spontaneous Diseases in Commonly Used Mouse Strains / Stocks.

BRAYTON, C. F., TREUTING, P. M. & WARD, J. M. 2012. Pathobiology of aging mice and GEM: background strains and experimental design. *Vet Pathol,* 49**,** 85-105.

CAI, Y., FEDELES, S. V., DONG, K., ANYATONWU, G., ONOE, T., MITOBE, M., GAO, J. D., OKUHARA, D., TIAN, X., GALLAGHER, A. R., TANG, Z., XIE, X., LALIOTI, M. D., LEE, A. H., EHRLICH, B. E. & SOMLO, S. 2014. Altered trafficking and stability of polycystins underlie polycystic kidney disease. *J Clin Invest,* 124**,** 5129-44.

CAI, Y., MAEDA, Y., CEDZICH, A., TORRES, V. E., WU, G., HAYASHI, T., MOCHIZUKI, T., PARK, J. H., WITZGALL, R. & SOMLO, S. 1999. Identification and characterization of polycystin-2, the PKD2 gene product. *J Biol Chem,* 274**,** 28557-65.

CAIN, J. E., DI GIOVANNI, V., SMEETON, J. & ROSENBLUM, N. D. 2010. Genetics of Renal Hypoplasia: Insights Into the Mechanisms Controlling Nephron Endowment. *Pediatr Res,* 68**,** 91-98.

CALVET, J. P. 1994. Injury and development in polycystic kidney disease. *Curr Opin Nephrol Hypertens,* 3**,** 340-8.

CARTWRIGHT, J. H., PIRO, N., PIRO, O. & TUVAL, I. 2008. Fluid dynamics of nodal flow and left-right patterning in development. *Dev Dyn,* 237.

CEBRIAN, C., BORODO, K., CHARLES, N. & HERZLINGER, D. A. 2004. Morphometric index of the developing murine kidney. *Dev Dyn,* 231**,** 601-8.

CHAMPY, M. F., SELLOUM, M., ZEITLER, V., CARADEC, C., JUNG, B., ROUSSEAU, S., POUILLY, L., SORG, T. & AUWERX, J. 2008. Genetic background determines metabolic phenotypes in the mouse. *Mamm Genome,* 19**,** 318-31.

CHAPIN, H. C. & CAPLAN, M. J. 2010. The cell biology of polycystic kidney disease. *J Cell Biol,* 191**,** 701-10.

CHAPIN, H. C., RAJENDRAN, V. & CAPLAN, M. J. 2010. Polycystin-1 surface localization is stimulated by polycystin-2 and cleavage at the G protein-coupled receptor proteolytic site. *Mol Biol Cell,* 21**,** 4338-48.

CHAPMAN, A. B., TORRES, V. E., PERRONE, R. D., STEINMAN, T. I., BAE, K. T., MILLER, J. P., MISKULIN, D. C., RAHBARI OSKOUI, F., MASOUMI, A., HOGAN, M. C., WINKLHOFER, F. T., BRAUN, W., THOMPSON, P. A., MEYERS, C. M., KELLEHER, C. & SCHRIER, R. W. 2010. The HALT polycystic kidney disease trials: design and implementation. *Clin J Am Soc Nephrol,* 5**,** 102-9.

CHEA, S. W. & LEE, K. B. 2009. TGF-beta mediated epithelial-mesenchymal transition in autosomal dominant polycystic kidney disease. *Yonsei Med J,* 50**,** 105-11.

CHEN, D., NORRIS, D. & VENTIKOS, Y. 2014. Chemosignalling, mechanotransduction and ciliary behaviour in the embryonic node: Computational evaluation of competing theories. *Proc Inst Mech Eng H,* 228**,** 465-476.

CHERTOW, G. M., LAZARUS, J. M., PAGANINI, E. P., ALLGREN, R. L., LAFAYETTE, R. A. & SAYEGH, M. H. 1998. Predictors of mortality and the provision of dialysis in patients with acute tubular necrosis. The Auriculin Anaritide Acute Renal Failure Study Group. *J Am Soc Nephrol,* 9**,** 692-8.

COLE, B. R., CONLEY, S. B. & STAPLETON, F. B. 1987. Polycystic kidney disease in the first year of life. *J Pediatr,* 111**,** 693-9.

COLLIGNON, J., VARLET, I. & ROBERTSON, E. J. 1996. Relationship between asymmetric nodal expression and the direction of embryonic turning. *Nature,* 381**,** 155-8.

CORNEC-LE GALL, E., AUDREZET, M. P., LE MEUR, Y., CHEN, J. M. & FEREC, C. 2014. Genetics and pathogenesis of autosomal dominant polycystic kidney disease: 20 years on. *Hum Mutat,* 35**,** 1393-406.

CURTHOYS, N. P. & MOE, O. W. 2014. Proximal Tubule Function and Response to Acidosis. *Clinical Journal of the American Society of Nephrology : CJASN,* 9**,** 1627-1638.

DELL, K. M. 2011. The Spectrum of Polycystic Kidney Disease in Children. *Advances in chronic kidney disease,* 18**,** 339-347.

DELL, K. M., MATHESON, M., HARTUNG, E. A., WARADY, B. A., FURTH, S. L., MUÑOZ, A., DART, A., GREENBAUM, L., GOEBEL, J., MITSNEFES, M., FLYNN, J., WONG, C., FATHALLAH, S., SALUSKY, I., YADIN, O., MORGENSTERN, B., BLYDT-HANSEN, T., DAVIS, K., PAN, C., AL-UZRI, A., JENKINS, R., PORTALE, A., SEIKALY, M., TURMAN, M., WONG, C., ALEXANDER, S., HASTINGS, C., JENKINS, R., RODIG, N., HARMON, W., BARTOSH, S., BENADOR, N., MAK, R., WOOD, E., JENKINS, R., LERNER, G., MASSENGILL, S., HIDALGO, G., ATKINSON, M., GIPSON, D., SRIVATHS, P., SAMUELS, J., KASKEL, F., MATTOSIAN, D., CAI, Y., ANDREOLI, S., SALAND, J., PATEL, H., NORWOOD, V., PAREKH, R., ROBINSON, L., MENDLEY, S., LANDE, M., SCHWARTZ, G., BROPHY, P., JOHN, E., UPADHYAY, K., FERRIS, M., MATOO, T., KUPFERMAN, J., WEISS, L., LANGMAN, C., SEO-MAYER, P., KHER, K. & SAMSONOV, D. 2016. Kidney Disease Progression in Autosomal Recessive Polycystic Kidney Disease. *The Journal of Pediatrics,* 171**,** 196-201.e1.

DELLING, M., DECAEN, P. G., DOERNER, J. F., FEBVAY, S. & CLAPHAM, D. E. 2013. Primary cilia are specialized calcium signalling organelles. *Nature,* 504**,** 311-4.

DELLING, M., INDZHYKULIAN, A. A., LIU, X., LI, Y., XIE, T., COREY, D. P. & CLAPHAM, D. E. 2016. Primary cilia are not calcium-responsive mechanosensors. *Nature,* 531**,** 656-60.

DEVENPORT, D. 2014. The cell biology of planar cell polarity. *J Cell Biol,* 207**,** 171-9.

DING, Y. & SIGMUND, C. D. 2001. Androgen-dependent regulation of human angiotensinogen expression in KAP-hAGT transgenic mice. *Am J Physiol Renal Physiol,* 280**,** F54-60.

DOME, J. S. & HUFF, V. 1993. Wilms Tumor Overview. *In:* PAGON, R. A., ADAM, M. P., ARDINGER, H. H., WALLACE, S. E., AMEMIYA, A., BEAN, L. J. H., BIRD, T. D., FONG, C. T., MEFFORD, H. C., SMITH, R. J. H. & STEPHENS, K. (eds.) *GeneReviews(R).* Seattle (WA): University of Washington, Seattle University of Washington, Seattle. All rights reserved.

DU, J. & WILSON, P. D. 1995. Abnormal polarization of EGF receptors and autocrine stimulation of cyst epithelial growth in human ADPKD. *Am J Physiol,* 269**,** C487-95.

ELLIOT, S. J., KARL, M., BERHO, M., POTIER, M., ZHENG, F., LECLERCQ, B., STRIKER, G. E. & STRIKER, L. J. 2003. Estrogen Deficiency Accelerates Progression of Glomerulosclerosis in Susceptible Mice. *The American Journal of Pathology,* 162**,** 1441-1448.

ERMAKOV, A., STEVENS, J. L., WHITEHILL, E., ROBSON, J. E., PIELES, G., BROOKER, D., GOGGOLIDOU, P., POWLES-GLOVER, N., HACKER, T., YOUNG, S. R., DEAR, N., HIRST, E., TYMOWSKA-LALANNE, Z., BRISCOE, J., BHATTACHARYA, S. & NORRIS, D. P. 2009. Mouse mutagenesis identifies novel roles for left–right patterning genes in pulmonary, craniofacial, ocular, and limb development. *Developmental Dynamics,* 238**,** 581-594.

FAN, L.-Q., HARDY, D. O., CATTERALL, J. F., ZHAO, J. & LI, S.-X. 2010. Identification and Characterization of an Androgen-responsive Kap Promoter Enhancer Located in the Intron II Region of human Angiotensinogen Gene. *The Journal of steroid biochemistry and molecular biology,* 119**,** 135-140.

FENG, S., OKENKA, G. M., BAI, C. X., STREETS, A. J., NEWBY, L. J., DECHANT, B. T., TSIOKAS, L., OBARA, T. & ONG, A. C. 2008. Identification and functional characterization of an N-terminal oligomerization domain for polycystin-2. *J Biol Chem,* 283**,** 28471-9.

FERREIRA, F. M., OLIVEIRA, L. C., GERMINO, G. G., ONUCHIC, J. N. & ONUCHIC, L. F. 2011. Macromolecular assembly of polycystin-2 intracytosolic C-terminal domain. *Proc Natl Acad Sci U S A,* 108**,** 9833-8.

FERREIRA, F. W., EH; ONUCHIC, LF. 2015. Polycystins and Molecular Basis of Autosomal Dominant Polycystic Kidney Disease. *In:* X, L. (ed.) *Polycystic Kidney Disease [Internet].* Brisbane (AU): Codon Publications.

FIELD, S., RILEY, K. L., GRIMES, D. T., HILTON, H., SIMON, M., POWLES-GLOVER, N., SIGGERS, P., BOGANI, D., GREENFIELD, A. & NORRIS, D. P. 2011. Pkd1l1 establishes left-right asymmetry and physically interacts with Pkd2. *Development,* 138**,** 1131-42.

FISCHER, E., LEGUE, E., DOYEN, A., NATO, F., NICOLAS, J. F., TORRES, V., YANIV, M. & PONTOGLIO, M. 2006. Defective planar cell polarity in polycystic kidney disease. *Nat Genet,* 38**,** 21-3.

FOGGENSTEINER, L., BEVAN, A. P., THOMAS, R., COLEMAN, N., BOULTER, C., BRADLEY, J., IBRAGHIMOV-BESKROVNAYA, O., KLINGER, K. & SANDFORD, R. 2000. Cellular and subcellular distribution of polycystin-2, the protein product of the PKD2 gene. *J Am Soc Nephrol,* 11**,** 814-27.

FRAZIER, K. S., SEELY, J. C., HARD, G. C., BETTON, G., BURNETT, R., NAKATSUJI, S., NISHIKAWA, A., DURCHFELD-MEYER, B. & BUBE, A. 2012. Proliferative and nonproliferative lesions of the rat and mouse urinary system. *Toxicol Pathol,* 40**,** 14s-86s.

FUJIWARA, K., SHIN, M., MATSUNAGA, H., SAITA, T. & LARSSON, L. I. 2009. Light-microscopic immunocytochemistry for gentamicin and its use for studying uptake of the drug in kidney. *Antimicrob Agents Chemother,* 53**,** 3302-7.

GABOW , P. A. 1993. Autosomal Dominant Polycystic Kidney Disease. *New England Journal of Medicine,* 329**,** 332-342.

GAINULLIN, V. G., HOPP, K., WARD, C. J., HOMMERDING, C. J. & HARRIS, P. C. 2015. Polycystin-1 maturation requires polycystin-2 in a dose-dependent manner. *The Journal of Clinical Investigation,* 125**,** 607-620.

GARCIA-GONZALEZ, M. A., MENEZES, L. F., PIONTEK, K. B., KAIMORI, J., HUSO, D. L., WATNICK, T., ONUCHIC, L. F., GUAY-WOODFORD, L. M. & GERMINO, G. G. 2007. Genetic Interaction Studies Link Autosomal Dominant And Recessive Polycystic Kidney Disease In A Common Pathway. *Human molecular genetics,* 16**,** 1940-1950.

GARCIA-GONZALEZ, M. A., OUTEDA, P., ZHOU, Q., ZHOU, F., MENEZES, L. F., QIAN, F., HUSO, D. L., GERMINO, G. G., PIONTEK, K. B. & WATNICK, T. 2010. Pkd1 and Pkd2 are required for normal placental development. *PLoS One,* 5.

GENG, L., OKUHARA, D., YU, Z., TIAN, X., CAI, Y., SHIBAZAKI, S. & SOMLO, S. 2006. Polycystin-2 traffics to cilia independently of polycystin-1 by using an N-terminal RVxP motif. *J Cell Sci,* 119**,** 1383-95.

GIAMMANCO, M., TABACCHI, G., GIAMMANCO, S., DI MAJO, D. & LA GUARDIA, M. 2005. Testosterone and aggressiveness. *Med Sci Monit,* 11**,** Ra136-45.

GIFFORD, J. L., WALSH, M. P. & VOGEL, H. J. 2007. Structures and metal-ion-binding properties of the Ca2+-binding helix-loop-helix EF-hand motifs. *Biochem J,* 405**,** 199-221.

GONDO, Y., FUKUMURA, R., MURATA, T. & MAKINO, S. 2010. ENU-based gene-driven mutagenesis in the mouse: a next-generation gene-targeting system. *Exp Anim,* 59**,** 537-48.

GRIFFITHS, A., ; MILLER, JH,; SUZUKIM DT; 2000. An Introduction to Genetic Analysis. 7th edition ed. New York: W. H. Freeman.

GRIMES, D. T., KEYNTON, J. L., BUENAVISTA, M. T., JIN, X., PATEL, S. H., KYOSUKE, S., VIBERT, J., WILLIAMS, D. J., HAMADA, H., HUSSAIN, R., NAULI, S. M. & NORRIS, D. P. 2016. Genetic Analysis Reveals a Hierarchy of Interactions between Polycystin-Encoding Genes and Genes Controlling Cilia Function during Left-Right Determination. *PLoS Genet,* 12**,** e1006070.

GUAY-WOODFORD, M. L., GALLIANI, A. C., MUSULMAN-MROCZEK, E., SPEAR, S. G., GUILLOT, P. A. & BERNSTEIN, J. 1998. Diffuse renal cystic disease in children: morphologic and genetic correlations. *Pediatric Nephrology,* 12**,** 173-182.

HANAOKA, K. & GUGGINO, W. B. 2000. cAMP regulates cell proliferation and cyst formation in autosomal polycystic kidney disease cells. *J Am Soc Nephrol,* 11**,** 1179-87.

HANAOKA, K., QIAN, F., BOLETTA, A., BHUNIA, A. K., PIONTEK, K., TSIOKAS, L., SUKHATME, V. P., GUGGINO, W. B. & GERMINO, G. G. 2000. Co-assembly of polycystin-1 and -2 produces unique cation-permeable currents. *Nature,* 408**,** 990-4.

HAPPÉ, H., DE HEER, E. & PETERS, D. J. M. 2011. Polycystic kidney disease: The complexity of planar cell polarity and signaling during tissue regeneration and cyst formation. *Biochimica et Biophysica Acta (BBA) - Molecular Basis of Disease,* 1812**,** 1249-1255.

HAPPE, H. & PETERS, D. J. 2014. Translational research in ADPKD: lessons from animal models. *Nat Rev Nephrol,* 10**,** 587-601.

HARRIS, P. C. & ROSSETTI, S. 2010. Molecular diagnostics for autosomal dominant polycystic kidney disease. *Nature reviews. Nephrology,* 6**,** 197-206.

HARRIS, P. C. & TORRES, V. E. 2009. Polycystic kidney disease. *Annu Rev Med,* 60.

HARRIS, P. C. & TORRES, V. E. 2014. Genetic mechanisms and signaling pathways in autosomal dominant polycystic kidney disease. *J Clin Invest,* 124**,** 2315-24.

HARRIS, P. C., WARD, C. J., PERAL, B. & HUGHES, J. 1995. Polycystic kidney disease. 1: Identification and analysis of the primary defect. *J Am Soc Nephrol,* 6**,** 1125-33.

HARTMAN, H. A., LAI, H. L. & PATTERSON, L. T. 2007. Cessation of renal morphogenesis in mice. *Developmental Biology,* 310**,** 379-387.

HASSANE, S., LEONHARD, W. N., VAN DER WAL, A., HAWINKELS, L. J., LANTINGA-VAN LEEUWEN, I. S., TEN DIJKE, P., BREUNING, M. H., DE HEER, E. & PETERS, D. J. 2010. Elevated TGFbeta-Smad signalling in experimental Pkd1 models and human patients with polycystic kidney disease. *J Pathol,* 222**,** 21-31.

HATEBOER, N., V DIJK, M. A., BOGDANOVA, N., COTO, E., SAGGAR-MALIK, A. K., SAN MILLAN, J. L., TORRA, R., BREUNING, M. & RAVINE, D. 1999. Comparison of phenotypes of polycystic kidney disease types 1 and 2. European PKD1-PKD2 Study Group. *Lancet,* 353**,** 103-7.

HEWITSON, T. D., ONO, T. & BECKER, G. J. 2009. Small animal models of kidney disease: a review. *Methods Mol Biol,* 466**,** 41-57.

HIDAKA, S., KONECKE, V., OSTEN, L. & WITZGALL, R. 2004. PIGEA-14, a novel coiled-coil protein affecting the intracellular distribution of polycystin-2. *J Biol Chem,* 279**,** 35009-16.

HIROKAWA, N., TANAKA, Y., OKADA, Y. & TAKEDA, S. 2006. Nodal flow and the generation of left-right asymmetry. *Cell,* 125**,** 33-45.

HOFFMEISTER, H., BABINGER, K., GURSTER, S., CEDZICH, A., MEESE, C., SCHADENDORF, K., OSTEN, L., DE VRIES, U., RASCLE, A. & WITZGALL, R. 2011. Polycystin-2 takes different routes to the somatic and ciliary plasma membrane. *J Cell Biol,* 192**,** 631-45.

HOGAN, M. C., ABEBE, K., TORRES, V. E., CHAPMAN, A. B., BAE, K. T., TAO, C., SUN, H., PERRONE, R. D., STEINMAN, T. I., BRAUN, W., WINKLHOFER, F. T., MISKULIN, D. C., RAHBARI-OSKOUI, F., BROSNAHAN, G., MASOUMI, A., KARPOV, I. O., SPILLANE, S., FLESSNER, M., MOORE, C. G. & SCHRIER, R. W. 2015. Liver involvement in early autosomal-dominant polycystic kidney disease. *Clin Gastroenterol Hepatol,* 13**,** 155-64.e6.

HOPP, K., WARD, C. J., HOMMERDING, C. J., NASR, S. H., TUAN, H. F., GAINULLIN, V. G., ROSSETTI, S., TORRES, V. E. & HARRIS, P. C. 2012. Functional polycystin-1 dosage governs autosomal dominant polycystic kidney disease severity. *J Clin Invest,* 122**,** 4257-73.

HU, Q., MILENKOVIC, L., JIN, H., SCOTT, M. P., NACHURY, M. V., SPILIOTIS, E. T. & NELSON, W. J. 2010. A septin diffusion barrier at the base of the primary cilium maintains ciliary membrane protein distribution. *Science,* 329**,** 436-9.

HUANG, L., SCARPELLINI, A., FUNCK, M., VERDERIO, E. A. & JOHNSON, T. S. 2013. Development of a chronic kidney disease model in C57BL/6 mice with relevance to human pathology. *Nephron Extra,* 3**,** 12-29.

HUGHES, J., WARD, C. J., PERAL, B., ASPINWALL, R., CLARK, K., SAN MILLAN, J. L., GAMBLE, V. & HARRIS, P. C. 1995. The polycystic kidney disease 1 (PKD1) gene encodes a novel protein with multiple cell recognition domains. *Nat Genet,* 10**,** 151-60.

IGARASHI, P. & SOMLO, S. 2002. Genetics and pathogenesis of polycystic kidney disease. *J Am Soc Nephrol,* 13**,** 2384-98.

INACIO, J. M., MARQUES, S., NAKAMURA, T., SHINOHARA, K., MENO, C., HAMADA, H. & BELO, J. A. 2013. The dynamic right-to-left translocation of Cerl2 is involved in the regulation and termination of Nodal activity in the mouse node. *PLoS One,* 8**,** e60406.

ISHOLA, D. A., JR., VAN DER GIEZEN, D. M., HAHNEL, B., GOLDSCHMEDING, R., KRIZ, W., KOOMANS, H. A. & JOLES, J. A. 2006. In mice, proteinuria and renal inflammatory responses to albumin overload are strain-dependent. *Nephrol Dial Transplant,* 21**,** 591-7.

JAMISON, R. L. 1987. Short and long loop nephrons. *Kidney Int,* 31**,** 597-605.

KAIMORI, J. Y. & GERMINO, G. G. 2008. ARPKD and ADPKD: first cousins or more distant relatives? *J Am Soc Nephrol,* 19**,** 416-8.

KALLIOKOSKI, O., JACOBSEN, K. R., DARUSMAN, H. S., HENRIKSEN, T., WEIMANN, A., POULSEN, H. E., HAU, J. & ABELSON, K. S. 2013. Mice do not habituate to metabolism cage housing--a three week study of male BALB/c mice. *PLoS One,* 8**,** e58460.

KEE, H. L., DISHINGER, J. F., BLASIUS, T. L., LIU, C. J., MARGOLIS, B. & VERHEY, K. J. 2012. A size-exclusion permeability barrier and nucleoporins characterize a ciliary pore complex that regulates transport into cilia. *Nat Cell Biol,* 14**,** 431-7.

KIM, I., DING, T., FU, Y., LI, C., CUI, L., LI, A., LIAN, P., LIANG, D., WANG, D. W., GUO, C., MA, J., ZHAO, P., COFFEY, R. J., ZHAN, Q. & WU, G. 2009. Conditional mutation of Pkd2 causes cystogenesis and upregulates beta-catenin. *J Am Soc Nephrol,* 20**,** 2556-69.

KIM, J. A., BLUMENFELD, J. D., CHHABRA, S., DUTRUEL, S. P., THIMMAPPA, N. D., BOBB, W. O., DONAHUE, S., RENNERT, H. E., TAN, A. Y., GIAMBRONE, A. E. & PRINCE, M. R. 2016. Pancreatic Cysts in Autosomal Dominant Polycystic Kidney Disease: Prevalence and Association with PKD2 Gene Mutations. *Radiology***,** 151650.

KIM, K., DRUMMOND, I., IBRAGHIMOV-BESKROVNAYA, O., KLINGER, K. & ARNAOUT, M. A. 2000. Polycystin 1 is required for the structural integrity of blood vessels. *Proc Natl Acad Sci U S A,* 97**,** 1731-6.

KIM, S. & DYNLACHT, B. D. 2013. Assembling a primary cilium. *Curr Opin Cell Biol,* 25**,** 506-11.

KNOBEL, K. M., PEDEN, E. M. & BARR, M. M. 2008. Distinct protein domains regulate ciliary targeting and function of C. elegans PKD-2. *Experimental Cell Research,* 314**,** 825-833.

KOPTIDES, M., HADJIMICHAEL, C., KOUPEPIDOU, P., PIERIDES, A. & CONSTANTINOU DELTAS, C. 1999. Germinal and somatic mutations in the PKD2 gene of renal cysts in autosomal dominant polycystic kidney disease. *Hum Mol Genet,* 8**,** 509-13.

KOPTIDES, M., MEAN, R., DEMETRIOU, K., PIERIDES, A. & DELTAS, C. C. 2000. Genetic evidence for a trans-heterozygous model for cystogenesis in autosomal dominant polycystic kidney disease. *Hum Mol Genet,* 9**,** 447-52.

KOTTGEN, M. & WALZ, G. 2005. Subcellular localization and trafficking of polycystins. *Pflugers Arch,* 451**,** 286-93.

KOULEN, P., CAI, Y., GENG, L., MAEDA, Y., NISHIMURA, S., WITZGALL, R., EHRLICH, B. E. & SOMLO, S. 2002. Polycystin-2 is an intracellular calcium release channel. *Nat Cell Biol,* 4**,** 191-7.

LANTINGA-VAN LEEUWEN, I. S., DAUWERSE, J. G., BAELDE, H. J., LEONHARD, W. N., VAN DE WAL, A., WARD, C. J., VERBEEK, S., DERUITER, M. C., BREUNING, M. H., DE HEER, E. & PETERS, D. J. 2004. Lowering of Pkd1 expression is sufficient to cause polycystic kidney disease. *Hum Mol Genet,* 13**,** 3069-77.

LANTINGA-VAN LEEUWEN, I. S., LEONHARD, W. N., VAN DER WAL, A., BREUNING, M. H., DE HEER, E. & PETERS, D. J. 2007. Kidney-specific inactivation of the Pkd1 gene induces rapid cyst formation in developing kidneys and a slow onset of disease in adult mice. *Hum Mol Genet,* 16**,** 3188-96.

LASCANO, M. E., SCHREIBER, M. J., NURKO, S. 2010. *Chronic Kidney Disease* [Online]. [Accessed 27/08/16].

LEE, S. H. & SOMLO, S. 2014. Cyst growth, polycystins, and primary cilia in autosomal dominant polycystic kidney disease. *Kidney Research and Clinical Practice,* 33**,** 73-78.

LEHMAN, J. M., MICHAUD, E. J., SCHOEB, T. R., AYDIN-SON, Y., MILLER, M. & YODER, B. K. 2008. The Oak Ridge Polycystic Kidney mouse: modeling ciliopathies of mice and men. *Dev Dyn,* 237**,** 1960-71.

LENNERZ, J. K., SPENCE, D. C., ISKANDAR, S. S., DEHNER, L. P. & LIAPIS, H. 2010. Glomerulocystic Kidney: One Hundred–Year Perspective. *Archives of Pathology & Laboratory Medicine,* 134**,** 583-605.

LEONHARD, W. N., KUNNEN, S. J., PLUGGE, A. J., PASTERNACK, A., JIANU, S. B., VERAAR, K., EL BOUAZZAOUI, F., HOOGAARS, W. M., TEN DIJKE, P., BREUNING, M. H., DE HEER, E., RITVOS, O. & PETERS, D. J. 2016. Inhibition of Activin Signaling Slows Progression of Polycystic Kidney Disease. *J Am Soc Nephrol*.

LI, A., TIAN, X., SUNG, S. W. & SOMLO, S. 2003. Identification of two novel polycystic kidney disease-1-like genes in human and mouse genomes. *Genomics,* 81**,** 596-608.

LI, H., ZHOU, X., DAVIS, D. R., XU, D. & SIGMUND, C. D. 2008. An androgen-inducible proximal tubule-specific Cre recombinase transgenic model. *Am J Physiol Renal Physiol,* 294**,** F1481-6.

LIN, F., HIESBERGER, T., CORDES, K., SINCLAIR, A. M., GOLDSTEIN, L. S., SOMLO, S. & IGARASHI, P. 2003. Kidney-specific inactivation of the KIF3A subunit of kinesin-II inhibits renal ciliogenesis and produces polycystic kidney disease. *Proc Natl Acad Sci U S A,* 100**,** 5286-91.

LITTLE, M. H. & MCMAHON, A. P. 2012. Mammalian kidney development: principles, progress, and projections. *Cold Spring Harb Perspect Biol,* 4.

LIU, B., CHEN, S.-C., YANG, Y.-M., YAN, K., QIAN, Y.-Q., ZHANG, J.-Y., HU, Y.-T., DONG, M.-Y., JIN, F., HUANG, H.-F. & XU, C.-M. 2015. Identification of novel PKD1 and PKD2 mutations in a Chinese population with autosomal dominant polycystic kidney disease. *Scientific Reports,* 5**,** 17468.

LIU, D., WANG, C. J., JUDGE, D. P., HALUSHKA, M. K., NI, J., HABASHI, J. P., MOSLEHI, J., BEDJA, D., GABRIELSON, K. L., XU, H., QIAN, F., HUSO, D., DIETZ, H. C., GERMINO, G. G. & WATNICK, T. 2014. A Pkd1-Fbn1 genetic interaction implicates TGF-beta signaling in the pathogenesis of vascular complications in autosomal dominant polycystic kidney disease. *J Am Soc Nephrol,* 25**,** 81-91.

LOSEKOOT, M., RUIVENKAMP, C. A., THOLENS, A. P., GRIMBERGEN, J. E., VIJFHUIZEN, L., VERMEER, S., DIJKMAN, H. B., CORNELISSEN, E. A., BONGERS, E. M. & PETERS, D. J. 2012. Neonatal onset autosomal dominant polycystic kidney disease (ADPKD) in a patient homozygous for a PKD2 missense mutation due to uniparental disomy. *J Med Genet,* 49**,** 37-40.

LOWE, L. A., SUPP, D. M., SAMPATH, K., YOKOYAMA, T., WRIGHT, C. V., POTTER, S. S., OVERBEEK, P. & KUEHN, M. R. 1996. Conserved left-right asymmetry of nodal expression and alterations in murine situs inversus. *Nature,* 381**,** 158-61.

LU, S. Y., JIN, Y., LI, X., SHEPPARD, P., BOCK, M. E., SHEIKH, F., DUCKWORTH, M. L. & CATTINI, P. A. 2010. Embryonic survival and severity of cardiac and craniofacial defects are affected by genetic background in fibroblast growth factor-16 null mice. *DNA Cell Biol,* 29**,** 407-15.

LU, W., FAN, X., BASORA, N., BABAKHANLOU, H., LAW, T., RIFAI, N., HARRIS, P. C., PEREZ-ATAYDE, A. R., RENNKE, H. G. & ZHOU, J. 1999. Late onset of renal and hepatic cysts in Pkd1-targeted heterozygotes. *Nat Genet,* 21**,** 160-1.

LU, W., PEISSEL, B., BABAKHANLOU, H., PAVLOVA, A., GENG, L., FAN, X., LARSON, C., BRENT, G. & ZHOU, J. 1997. Perinatal lethality with kidney and pancreas defects in mice with a targetted Pkd1 mutation. *Nat Genet,* 17**,** 179-181.

MA, L. J. & FOGO, A. B. 2003. Model of robust induction of glomerulosclerosis in mice: importance of genetic background. *Kidney Int,* 64**,** 350-5.

MA, M., TIAN, X., IGARASHI, P., PAZOUR, G. J. & SOMLO, S. 2013. Loss of cilia suppresses cyst growth in genetic models of autosomal dominant polycystic kidney disease. *Nat Genet,* 45**,** 1004-12.

MAIUOLO, J., OPPEDISANO, F., GRATTERI, S., MUSCOLI, C. & MOLLACE, V. 2016. Regulation of uric acid metabolism and excretion. *International Journal of Cardiology,* 213**,** 8-14.

MANGOLINI, A., DE STEPHANIS, L. & AGUIARI, G. 2016. Role of calcium in polycystic kidney disease: From signaling to pathology. *World Journal of Nephrology,* 5**,** 76-83.

MANNING, D. K., SERGEEV, M., VAN HEESBEEN, R. G., WONG, M. D., OH, J. H., LIU, Y., HENKELMAN, R. M., DRUMMOND, I., SHAH, J. V. & BEIER, D. R. 2012. Loss of the Ciliary Kinase Nek8 Causes Left-Right Asymmetry Defects. *J Am Soc Nephrol,* 24**,** 100-12.

MARKOWITZ, G. S., CAI, Y., LI, L., WU, G., WARD, L. C., SOMLO, S. & D'AGATI, V. D. 1999. Polycystin-2 expression is developmentally regulated. *American Journal of Physiology - Renal Physiology,* 277**,** F17-F25.

MARQUES, S., BORGES, A. C., SILVA, A. C., FREITAS, S., CORDENONSI, M. & BELO, J. A. 2004. The activity of the Nodal antagonist Cerl-2 in the mouse node is required for correct L/R body axis. *Genes Dev,* 18**,** 2342-7.

MAUNSBACH, A. B., MARPLES, D., CHIN, E., NING, G., BONDY, C., AGRE, P. & NIELSEN, S. 1997. Aquaporin-1 water channel expression in human kidney. *J Am Soc Nephrol,* 8**,** 1-14.

MCDILL, B. W., LI, S.-Z., KOVACH, P. A., DING, L. & CHEN, F. 2006. Congenital progressive hydronephrosis (cph) is caused by an S256L mutation in aquaporin-2 that affects its phosphorylation and apical membrane accumulation. *Proceedings of the National Academy of Sciences of the United States of America,* 103**,** 6952-6957.

MCGRATH, J., SOMLO, S., MAKOVA, S., TIAN, X. & BRUECKNER, M. 2003. Two populations of node monocilia initiate left-right asymmetry in the mouse. *Cell,* 114**,** 61-73.

MCWILLIAM, H., LI, W., ULUDAG, M., SQUIZZATO, S., PARK, Y. M., BUSO, N., COWLEY, A. P. & LOPEZ, R. 2013. Analysis Tool Web Services from the EMBL-EBI. *Nucleic Acids Research,* 41**,** W597-W600.

MENO, C., SAIJOH, Y., FUJII, H., IKEDA, M., YOKOYAMA, T., YOKOYAMA, M., TOYODA, Y. & HAMADA, H. 1996. Left-right asymmetric expression of the TGF[beta]-family member lefty in mouse embryos. *Nature,* 381**,** 151-155.

MESEGUER, A. & CATTERALL, J. F. 1990. Cell-specific expression of kidney androgen-regulated protein messenger RNA is under multihormonal control. *Mol Endocrinol,* 4**,** 1240-8.

MESEGUER, A. & CATTERALL, J. F. 1992a. Effects of pituitary hormones on the cell-specific expression of the KAP gene. *Mol Cell Endocrinol,* 89**,** 153-62.

MESEGUER, A. & CATTERALL, J. F. 1992b. Effects of pituitary hormones on the cell-specific expression of the KAP gene. *Molecular and Cellular Endocrinology,* 89**,** 153-162.

MOCHIZUKI, T., WU, G., HAYASHI, T., XENOPHONTOS, S. L., VELDHUISEN, B., SARIS, J. J., REYNOLDS, D. M., CAI, Y., GABOW, P. A., PIERIDES, A., KIMBERLING, W. J., BREUNING, M. H., DELTAS, C. C., PETERS, D. J. & SOMLO, S. 1996. PKD2, a gene for polycystic kidney disease that encodes an integral membrane protein. *Science,* 272**,** 1339-42.

MOLLA-HERMAN, A., GHOSSOUB, R., BLISNICK, T., MEUNIER, A., SERRES, C., SILBERMANN, F., EMMERSON, C., ROMEO, K., BOURDONCLE, P., SCHMITT, A., SAUNIER, S., SPASSKY, N., BASTIN, P. & BENMERAH, A. 2010. The ciliary pocket: an endocytic membrane domain at the base of primary and motile cilia. *J Cell Sci,* 123**,** 1785-95.

MOYER, J. H., LEE-TISCHLER, M. J., KWON, H. Y., SCHRICK, J. J., AVNER, E. D., SWEENEY, W. E., GODFREY, V. L., CACHEIRO, N. L., WILKINSON, J. E. & WOYCHIK, R. P. 1994. Candidate gene associated with a mutation causing recessive polycystic kidney disease in mice. *Science,* 264**,** 1329-33.

MURAWSKI, I. J., MAINA, R. W. & GUPTA, I. R. 2010a. The relationship between nephron number, kidney size and body weight in two inbred mouse strains. *Organogenesis,* 6**,** 189-194.

MURAWSKI, I. J., MAINA, R. W., MALO, D., GUAY-WOODFORD, L. M., GROS, P., FUJIWARA, M., MORGAN, K. & GUPTA, I. R. 2010b. The C3H/HeJ inbred mouse is a model of vesico-ureteric reflux with a susceptibility locus on chromosome 12. *Kidney Int,* 78**,** 269-78.

MURCIA, N. S., RICHARDS, W. G., YODER, B. K., MUCENSKI, M. L., DUNLAP, J. R. & WOYCHIK, R. P. 2000. The Oak Ridge Polycystic Kidney (orpk) disease gene is required for left-right axis determination. *Development,* 127**,** 2347-55.

MURCIA, N. S., SWEENEY, W. E., JR. & AVNER, E. D. 1999. New insights into the molecular pathophysiology of polycystic kidney disease. *Kidney Int,* 55**,** 1187-97.

NACHURY, M. V., LOKTEV, A. V., ZHANG, Q., WESTLAKE, C. J., PERÄNEN, J., MERDES, A., SLUSARSKI, D. C., SCHELLER, R. H., BAZAN, J. F., SHEFFIELD, V. C. & JACKSON, P. K. 2007. A Core Complex of BBS Proteins Cooperates with the GTPase Rab8 to Promote Ciliary Membrane Biogenesis. *Cell,* 129**,** 1201-1213.

NACHURY, M. V., SEELEY, E. S. & JIN, H. 2010. Trafficking to the Ciliary Membrane: How to Get Across the Periciliary Diffusion Barrier? *Annual review of cell and developmental biology,* 26**,** 59-87.

NAULI, S. M., ALENGHAT, F. J., LUO, Y., WILLIAMS, E., VASSILEV, P., LI, X., ELIA, A. E., LU, W., BROWN, E. M., QUINN, S. J., INGBER, D. E. & ZHOU, J. 2003. Polycystins 1 and 2 mediate mechanosensation in the primary cilium of kidney cells. *Nat Genet,* 33**,** 129-37.

NAYLOR, R. W. & DAVIDSON, A. J. 2016. Pronephric tubule formation in zebrafish: morphogenesis and migration. *Pediatr Nephrol*.

NEUGARTEN, J., KASISKE, B., SILBIGER, S. R. & NYENGAARD, J. R. 2002. Effects of sex on renal structure. *Nephron,* 90**,** 139-44.

NIE, X. & AREND, L. J. 2014. Novel roles of Pkd2 in male reproductive system development. *Differentiation,* 87**,** 161-171.

NISHIO, S., TIAN, X., GALLAGHER, A. R., YU, Z., PATEL, V., IGARASHI, P. & SOMLO, S. 2010. Loss of Oriented Cell Division Does not Initiate Cyst Formation. *Journal of the American Society of Nephrology : JASN,* 21**,** 295-302.

NONAKA, S., TANAKA, Y., OKADA, Y., TAKEDA, S., HARADA, A., KANAI, Y., KIDO, M. & HIROKAWA, N. 1998. Randomization of left-right asymmetry due to loss of nodal cilia generating leftward flow of extraembryonic fluid in mice lacking KIF3B motor protein. *Cell,* 95**,** 829-37.

NORMAN, J. 2011. Fibrosis and progression of autosomal dominant polycystic kidney disease (ADPKD). *Biochim Biophys Acta,* 1812**,** 1327-36.

NORRIS, D. P. & JACKSON, P. K. 2016. Cell biology: Calcium contradictions in cilia. *Nature,* 531**,** 582-3.

O'BRIEN, L. E., ZEGERS, M. M. P. & MOSTOV, K. E. 2002. Building epithelial architecture: insights from three-dimensional culture models. *Nat Rev Mol Cell Biol,* 3**,** 531-537.

OBIALO, C. I., CROWELL, A. K. & OKONOFUA, E. C. 2002. Acute renal failure mortality in hospitalized African Americans: age and gender considerations. *J Natl Med Assoc,* 94**,** 127-34.

OHATA, S., HERRANZ-PEREZ, V., NAKATANI, J., BOLETTA, A., GARCIA-VERDUGO, J. M. & ALVAREZ-BUYLLA, A. 2015. Mechanosensory Genes Pkd1 and Pkd2 Contribute to the Planar Polarization of Brain Ventricular Epithelium. *J Neurosci,* 35**,** 11153-68.

OKADA, Y., NONAKA, S., TANAKA, Y., SAIJOH, Y., HAMADA, H. & HIROKAWA, N. 1999. Abnormal Nodal Flow Precedes Situs Inversus in iv and inv mice. *Molecular Cell,* 4**,** 459-468.

OKADA, Y., TAKEDA, S., TANAKA, Y., IZPISUA BELMONTE, J. C. & HIROKAWA, N. 2005. Mechanism of nodal flow: a conserved symmetry breaking event in left-right axis determination. *Cell,* 121**,** 633-44.

ONG, A. C., DEVUYST, O., KNEBELMANN, B. & WALZ, G. 2015. Autosomal dominant polycystic kidney disease: the changing face of clinical management. *Lancet,* 385**,** 1993-2002.

ONG, A. C. & HARRIS, P. C. 1997. Molecular basis of renal cyst formation--one hit or two? *Lancet,* 349**,** 1039-40.

OTTO, E., HOEFELE, J., RUF, R., MUELLER, A. M., HILLER, K. S., WOLF, M. T., SCHUERMANN, M. J., BECKER, A., BIRKENHAGER, R., SUDBRAK, R., HENNIES, H. C., NURNBERG, P. & HILDEBRANDT, F. 2002. A gene mutated in nephronophthisis and retinitis pigmentosa encodes a novel protein, nephroretinin, conserved in evolution. *Am J Hum Genet,* 71**,** 1161-7.

OTTO, E. A., SCHERMER, B., OBARA, T., O'TOOLE, J. F., HILLER, K. S., MUELLER, A. M., RUF, R. G., HOEFELE, J., BEEKMANN, F., LANDAU, D., FOREMAN, J. W., GOODSHIP, J. A., STRACHAN, T.,

KISPERT, A., WOLF, M. T., GAGNADOUX, M. F., NIVET, H., ANTIGNAC, C., WALZ, G., DRUMMOND, I. A., BENZING, T. & HILDEBRANDT, F. 2003. Mutations in INVS encoding inversin cause nephronophthisis type 2, linking renal cystic disease to the function of primary cilia and left-right axis determination. *Nat Genet,* 34**,** 413-20.

OUTEDA, P., HUSO, DAVID L., FISHER, STEVEN A., HALUSHKA, MARC K., KIM, H., QIAN, F., GERMINO, GREGORY G. & WATNICK, T. 2014. Polycystin Signaling Is Required for Directed Endothelial Cell Migration and Lymphatic Development. *Cell Reports,* 7**,** 634-644.

PARK, E. Y., SUNG, Y. H., YANG, M. H., NOH, J. Y., PARK, S. Y., LEE, T. Y., YOOK, Y. J., YOO, K. H., ROH, K. J., KIM, I., HWANG, Y.-H., OH, G. T., SEONG, J. K., AHN, C., LEE, H.-W. & PARK, J. H. 2009. Cyst Formation in Kidney via B-Raf Signaling in the PKD2 Transgenic Mice. *The Journal of Biological Chemistry,* 284**,** 7214-7222.

PARK, K. M., CHO, H. J. & BONVENTRE, J. V. 2005. Orchiectomy reduces susceptibility to renal ischemic injury: a role for heat shock proteins. *Biochemical and Biophysical Research Communications,* 328**,** 312-317.

PATEL, V., CHOWDHURY, R. & IGARASHI, P. 2009. Advances in the Pathogenesis and Treatment of Polycystic Kidney Disease. *Current opinion in nephrology and hypertension,* 18**,** 99.

PAUL, B. M. & VANDEN HEUVEL, G. B. 2014. Kidney – Polycystic Kidney Disease. *Wiley interdisciplinary reviews. Developmental biology,* 3**,** 465-487.

PAUL, M., POYAN MEHR, A. & KREUTZ, R. 2006. Physiology of local renin-angiotensin systems. *Physiol Rev,* 86**,** 747-803.

PAZOUR, G. J., DICKERT, B. L., VUCICA, Y., SEELEY, E. S., ROSENBAUM, J. L., WITMAN, G. B. & COLE, D. G. 2000. Chlamydomonas IFT88 and its mouse homologue, polycystic kidney disease gene tg737, are required for assembly of cilia and flagella. *J Cell Biol,* 151**,** 709-18.

PAZOUR, G. J., SAN AGUSTIN, J. T., FOLLIT, J. A., ROSENBAUM, J. L. & WITMAN, G. B. 2002. Polycystin-2 localizes to kidney cilia and the ciliary level is elevated in orpk mice with polycystic kidney disease. *Current Biology,* 12**,** R378-R380.

PEDEN, E. M. & BARR, M. M. 2005. The KLP-6 Kinesin Is Required for Male Mating Behaviors and Polycystin Localization in Caenorhabditis elegans. *Current Biology,* 15**,** 394-404.

PEI, Y., WATNICK, T., HE, N., WANG, K., LIANG, Y., PARFREY, P., GERMINO, G. & ST GEORGE-HYSLOP, P. 1999. Somatic PKD2 mutations in individual kidney and liver cysts support a "two-hit" model of cystogenesis in type 2 autosomal dominant polycystic kidney disease. *J Am Soc Nephrol,* 10**,** 1524-9.

PENNEKAMP, P., KARCHER, C., FISCHER, A., SCHWEICKERT, A., SKRYABIN, B., HORST, J., BLUM, M. & DWORNICZAK, B. 2002. The ion channel polycystin-2 is required for left-right axis determination in mice. *Curr Biol,* 12**,** 938-43.

PETERS, D. J., SPRUIT, L., SARIS, J. J., RAVINE, D., SANDKUIJL, L. A., FOSSDAL, R., BOERSMA, J., VAN EIJK, R., NORBY, S., CONSTANTINOU-DELTAS, C. D. & ET AL. 1993. Chromosome 4 localization of a second gene for autosomal dominant polycystic kidney disease. *Nat Genet,* 5**,** 359-62.

PIONTEK, K., MENEZES, L. F., GARCIA-GONZALEZ, M. A., HUSO, D. L. & GERMINO, G. G. 2007. A critical developmental switch defines the kinetics of kidney cyst formation after loss of Pkd1. *Nat Med,* 13**,** 1490-5.

PKDB. 2016. *Pkdb.mayo.edu. (2016).* [Online]. [Accessed Accessed 18 Jul. 2016].

QIAN, F., GERMINO, F. J., CAI, Y., ZHANG, X., SOMLO, S. & GERMINO, G. G. 1997. PKD1 interacts with PKD2 through a probable coiled-coil domain. *Nat Genet,* 16**,** 179-83.

QIAN, F., WATNICK, T. J., ONUCHIC, L. F. & GERMINO, G. G. 1996. The molecular basis of focal cyst formation in human autosomal dominant polycystic kidney disease type I. *Cell,* 87**,** 979-87.

RAYER, P. F. O. 1839. *Traité Des Maladies Des Reins Et Des Altérations de la Sécrétion Urinaire, Étudiées en Elles-mêmes Et Dans Leurs Rapports Avec Les Maladies Des Uretères, de la Vessie ... Avec Un Atlas, Etc*.

RECKELHOFF, J. F., YANES, L. L., ILIESCU, R., FORTEPIANI, L. A. & GRANGER, J. P. 2005. Testosterone supplementation in aging men and women: possible impact on cardiovascular-renal disease. *Am J Physiol Renal Physiol,* 289**,** F941-8.

REYNOLDS, D. M., FALK, C. T., LI, A., KING, B. F., KAMATH, P. S., HUSTON III, J., SHUB, C., IGLESIAS, D. M., MARTIN, R. S., PIRSON, Y., TORRES, V. E. & SOMLO, S. 2000. Identification of a Locus for Autosomal Dominant Polycystic Liver Disease, on Chromosome 19p13.2-13.1. *The American Journal of Human Genetics,* 67**,** 1598-1604.

ROGERS, K. A., MORENO, S. E., SMITH, L. A., HUSSON, H., BUKANOV, N. O., LEDBETTER, S. R., BUDMAN, Y., LU, Y., WANG, B., IBRAGHIMOV-BESKROVNAYA, O. & NATOLI, T. A. 2016. Differences in the timing and magnitude of Pkd1 gene deletion determine the severity of polycystic kidney disease in an orthologous mouse model of ADPKD. *Physiological Reports,* 4**,** e12846.

ROGERS, S., WELLS, R. & RECHSTEINER, M. 1986. Amino acid sequences common to rapidly degraded proteins: the PEST hypothesis. *Science,* 234**,** 364-8.

ROSENBAUM, J. L. & WITMAN, G. B. 2002. Intraflagellar transport. *Nat Rev Mol Cell Biol,* 3**,** 813-825.

ROSSETTI, S. & HARRIS, P. C. 2007. Genotype-phenotype correlations in autosomal dominant and autosomal recessive polycystic kidney disease. *J Am Soc Nephrol,* 18**,** 1374-80.

ROSSETTI, S., KUBLY, V. J., CONSUGAR, M. B., HOPP, K., ROY, S., HORSLEY, S. W., CHAUVEAU, D., REES, L., BARRATT, T. M., VAN'T HOFF, W. G., NIAUDET, P., TORRES, V. E. & HARRIS, P. C. 2009. Incompletely penetrant PKD1 alleles suggest a role for gene dosage in cyst initiation in polycystic kidney disease. *Kidney Int,* 75**,** 848-55.

ROY, S., DILLON, M. J., TROMPETER, R. S. & BARRATT, T. M. 1997. Autosomal recessive polycystic kidney disease: long-term outcome of neonatal survivors. *Pediatr Nephrol,* 11**,** 302-6.

SANTOS, N. & REITER, J. F. 2010. Tilting at Nodal Windmills: Planar Cell Polarity Positions Cilia to Tell Left from Right. *Developmental Cell,* 19**,** 5-6.

SCARFE, L., RAK-RASZEWSKA, A., GERACI, S., DARSSAN, D., SHARKEY, J., HUANG, J., BURTON, N. C., MASON, D., RANJZAD, P., KENNY, S., GRETZ, N., LEVY, R., KEVIN PARK, B., GARCIA-FINANA, M., WOOLF, A. S., MURRAY, P. & WILM, B. 2015. Measures of kidney function by minimally invasive techniques correlate with histological glomerular damage in SCID mice with adriamycin-induced nephropathy. *Sci Rep,* 5**,** 13601.

SCHNEIDER, M. C., RODRIGUEZ, A. M., NOMURA, H., ZHOU, J., MORTON, C. C., REEDERS, S. T. & WEREMOWICZ, S. 1996. A Gene Similar to PKD1 Maps to Chromosome 4q22: A Candidate Gene for PKD2. *Genomics,* 38**,** 1-4.

SCHUSTER, M. K. G., M. ; ROGERS, S. ; RECHSTEINER, M. 2002. *e-PEST find* [Online]. [Accessed 6/09/16].

SCUDAMORE, C. L. 2014. *A practical guide to the histology of the mouse*, Wiley.

SERRA, A. L., POSTER, D., KISTLER, A. D., KRAUER, F., RAINA, S., YOUNG, J., RENTSCH, K. M., SPANAUS, K. S., SENN, O., KRISTANTO, P., SCHEFFEL, H., WEISHAUPT, D. & WUTHRICH, R. P. 2010. Sirolimus and kidney growth in autosomal dominant polycystic kidney disease. *N Engl J Med,* 363**,** 820-9.

SHARMA, N., LI, L. & ECELBARGER, C. M. 2015. Sex differences in renal and metabolic responses to a high-fructose diet in mice. *American Journal of Physiology - Renal Physiology,* 308**,** F400-F410.

SHARP, C. K., BERGMAN, S. M., STOCKWIN, J. M., ROBBIN, M. L., GALLIANI, C. & GUAY-WOODFORD, L. M. 1997. Dominantly transmitted glomerulocystic kidney disease: a distinct genetic entity. *J Am Soc Nephrol,* 8**,** 77-84.

SHILLINGFORD, J. M., MURCIA, N. S., LARSON, C. H., LOW, S. H., HEDGEPETH, R., BROWN, N., FLASK, C. A., NOVICK, A. C., GOLDFARB, D. A., KRAMER-ZUCKER, A., WALZ, G., PIONTEK, K. B., GERMINO, G. G. & WEIMBS, T. 2006. The mTOR pathway is regulated by polycystin-1, and its inhibition reverses renal cystogenesis in polycystic kidney disease. *Proc Natl Acad Sci U S A,* 103**,** 5466-71.

SHIMSHEK, D. R., KIM, J., HUBNER, M. R., SPERGEL, D. J., BUCHHOLZ, F., CASANOVA, E., STEWART, A. F., SEEBURG, P. H. & SPRENGEL, R. 2002. Codon-improved Cre recombinase (iCre) expression in the mouse. *Genesis,* 32**,** 19-26.

SHIRATORI, H., SAKUMA, R., WATANABE, M., HASHIGUCHI, H., MOCHIDA, K., SAKAI, Y., NISHINO, J., SAIJOH, Y., WHITMAN, M. & HAMADA, H. 2001. Two-Step Regulation of Left–Right Asymmetric Expression of Pitx2: Initiation by Nodal Signaling and Maintenance by Nkx2. *Molecular Cell,* 7**,** 137-149.

SHORT, K. M. & SMYTH, I. M. 2015. A morphological investigation of sexual and lateral dimorphism in the developing metanephric kidney. *Sci Rep,* 5**,** 15209.

SIMMS, R. J. 2016. Autosomal dominant polycystic kidney disease. *BMJ,* 352.

SOHARA, E., LUO, Y., ZHANG, J., MANNING, D. K., BEIER, D. R. & ZHOU, J. 2008. Nek8 Regulates the Expression and Localization of Polycystin-1 and Polycystin-2. *J Am Soc Nephrol,* 19**,** 469-76.

SOLÉ, E., CALVO, R., OBREGÓN, M. J. & MESEGUER, A. 1996. Effects of thyroid hormone on the androgenic expression of KAP gene in mouse kidney. *Molecular and Cellular Endocrinology,* 119**,** 147-159.

SPANI, D., ARRAS, M., KONIG, B. & RULICKE, T. 2003. Higher heart rate of laboratory mice housed individually vs in pairs. *Lab Anim,* 37**,** 54-62.

STANLEY, P., SCHACHTER, H., TANIGUCHI, N. 2009. . N-Glycans. *Essentials of Glycobiology.* . 2nd edition. ed.: Cold Spring Harbor (NY): Cold Spring Harbor Laboratory Press.

STECHMAN, M. J., AHMAD, B. N., LOH, N. Y., REED, A. A., STEWART, M., WELLS, S., HOUGH, T., BENTLEY, L., COX, R. D., BROWN, S. D. & THAKKER, R. V. 2010. Establishing normal plasma and 24-hour urinary biochemistry ranges in C3H, BALB/c and C57BL/6J mice following acclimatization in metabolic cages. *Lab Anim,* 44**,** 218-25.

STYPMANN, J., ENGELEN, M. A., ORWAT, S., BILBILIS, K., ROTHENBURGER, M., ECKARDT, L., HAVERKAMP, W., HORST, J., DWORNICZAK, B. & PENNEKAMP, P. 2007. Cardiovascular characterization of Pkd2+/LacZ mice, an animal model for the autosomal dominant polycystic kidney disease type 2 (ADPKD2). *International Journal of Cardiology,* 120**,** 158-166.

SWEENEY WE, A. E. S. W., AVNER ED. 2016. *Polycystic Kidney Disease, Autosomal Recessive,* Seattle (WA): University of Washington, Seattle; 1993-2016.

TABIN, C. J. & VOGAN, K. J. 2003. A two-cilia model for vertebrate left-right axis specification. *Genes Dev,* 17**,** 1-6.

TAKASATO, M. & LITTLE, M. H. 2015. The origin of the mammalian kidney: implications for recreating the kidney in vitro. *Development,* 142**,** 1937-47.

TAN, Y.-C., BLUMENFELD, J. & RENNERT, H. 2011a. Autosomal dominant polycystic kidney disease: Genetics, mutations and microRNAs. *Biochimica et Biophysica Acta (BBA) - Molecular Basis of Disease,* 1812**,** 1202-1212.

TAN, Y. C., BLUMENFELD, J., MICHAEEL, A., DONAHUE, S., BALINA, M., PARKER, T., LEVINE, D. & RENNERT, H. 2011b. Aberrant PKD2 splicing due to a presumed novel missense mutation in autosomal-dominant polycystic kidney disease. *Clin Genet,* 80**,** 287-92.

TANAKA, Y., OKADA, Y. & HIROKAWA, N. 2005. FGF-induced vesicular release of Sonic hedgehog and retinoic acid in leftward nodal flow is critical for left-right determination. *Nature,* 435**,** 172-7.

TANOS, B. E., YANG, H.-J., SONI, R., WANG, W.-J., MACALUSO, F. P., ASARA, J. M. & TSOU, M.-F. B. 2013. Centriole distal appendages promote membrane docking, leading to cilia initiation. *Genes & Development,* 27**,** 163-168.

TAO, Y., KIM, J., SCHRIER, R. W. & EDELSTEIN, C. L. 2005. Rapamycin markedly slows disease progression in a rat model of polycystic kidney disease. *J Am Soc Nephrol,* 16**,** 46-51.

TAULMAN, P. D., HAYCRAFT, C. J., BALKOVETZ, D. F. & YODER, B. K. 2001. Polaris, a protein involved in left-right axis patterning, localizes to basal bodies and cilia. *Mol Biol Cell,* 12**,** 589-99.

TAYLOR, D. M. & FRASER, H. 1973. Hydronephrosis in inbred strains of mice with particular reference to the BRVR strain. *Lab Anim,* 7**,** 229-36.

TAYLOR, M. E., AND DRICKAMER, K. 2011. *Introduction to Glycobiology*, Oxford University Press.

THIVIERGE, C., KURBEGOVIC, A., COUILLARD, M., GUILLAUME, R., COTE, O. & TRUDEL, M. 2006. Overexpression of PKD1 causes polycystic kidney disease. *Mol Cell Biol,* 26**,** 1538-48.

TOOLE, J. J., HASTIE, N. D. & HELD, W. A. 1979. An abundant androgen-regulated mRNA in the mouse kidney. *Cell,* 17**,** 441-8.

TORRES, V. E., ABEBE, K. Z., CHAPMAN, A. B., SCHRIER, R. W., BRAUN, W. E., STEINMAN, T. I., WINKLHOFER, F. T., BROSNAHAN, G., CZARNECKI, P. G., HOGAN, M. C., MISKULIN, D. C., RAHBARI-OSKOUI, F. F., GRANTHAM, J. J., HARRIS, P. C., FLESSNER, M. F., MOORE, C. G. & PERRONE, R. D. 2014. Angiotensin Blockade in Late Autosomal Dominant Polycystic Kidney Disease. *The New England journal of medicine,* 371**,** 2267-2276.

TORRES, V. E., CHAPMAN, A. B., DEVUYST, O., GANSEVOORT, R. T., GRANTHAM, J. J., HIGASHIHARA, E., PERRONE, R. D., KRASA, H. B., OUYANG, J. & CZERWIEC, F. S. 2012. Tolvaptan in patients with autosomal dominant polycystic kidney disease. *N Engl J Med,* 367**,** 2407-18.

TORRES, V. E. & HARRIS, P. C. 2009. Autosomal dominant polycystic kidney disease: the last 3 years. *Kidney international,* 76**,** 149-168.

TORRES, V. E. & WATSON, M. L. 1998. Polycystic kidney disease: antiquity to the 20th century. *Nephrol Dial Transplant,* 13**,** 2690-6.

TROF, R. J., DI MAGGIO, F., LEEMREIS, J. & GROENEVELD, A. B. 2006. Biomarkers of acute renal injury and renal failure. *Shock,* 26**,** 245-53.

TSIOKAS, L., KIM, E., ARNOULD, T., SUKHATME, V. P. & WALZ, G. 1997. Homo- and heterodimeric interactions between the gene products of PKD1 and PKD2. *Proc Natl Acad Sci U S A,* 94**,** 6965-70.

TSIOKAS, L., KIM, S. & ONG, E. C. 2007. Cell biology of Polycystin-2. *Cellular signalling,* 19**,** 444-453.

TZORTZAKI, E. G., GLASS, D., YANG, M., EVAN, A. P., BLEDSOE, S. B., STAMBROOK, P. J., SAHOTA, A. & TISCHFIELD, J. A. 2002. Gender- and age-dependent changes in kidney androgen protein mRNA expression in a knockout mouse model for nephrolithiasis. *J Histochem Cytochem,* 50**,** 1663-9.

URUSHIHARA, M. & KAGAMI, S. 2016. Role of the intrarenal renin–angiotensin system in the progression of renal disease. *Pediatric Nephrology***,** 1-9.

VARKI A, S. N. 2009. *Essentials of Glycobiology. 2nd edition.* , Cold Spring Harbor (NY): Cold Spring Harbor Laboratory Press.

VELERI, S., MANJUNATH, S. H., FARISS, R. N., MAY-SIMERA, H., BROOKS, M., FOSKETT, T. A., GAO, C., LONGO, T. A., LIU, P., NAGASHIMA, K., RACHEL, R. A., LI, T., DONG, L. & SWAROOP, A. 2014. Ciliopathy-associated gene Cc2d2a promotes assembly of subdistal appendages on the mother centriole during cilia biogenesis. *Nat Commun,* 5**,** 4207.

VENGLARIK, C. J., GAO, Z. & LU, X. 2004. Evolutionary conservation of Drosophila polycystin-2 as a calcium-activated cation channel. *J Am Soc Nephrol,* 15**,** 1168-77.

VIEIRA, O. V., GAUS, K., VERKADE, P., FULLEKRUG, J., VAZ, W. L. & SIMONS, K. 2006. FAPP2, cilium formation, and compartmentalization of the apical membrane in polarized Madin-Darby canine kidney (MDCK) cells. *Proc Natl Acad Sci U S A,* 103**,** 18556-61.

VIRLON, B., CHEVAL, L., BUHLER, J.-M., BILLON, E., DOUCET, A. & ELALOUF, J.-M. 1999. Serial microanalysis of renal transcriptomes. *Proceedings of the National Academy of Sciences,* 96**,** 15286-15291.

WALKIN, L., HERRICK, S. E., SUMMERS, A., BRENCHLEY, P. E., HOFF, C. M., KORSTANJE, R. & MARGETTS, P. J. 2013. The role of mouse strain differences in the susceptibility to fibrosis: a systematic review. *Fibrogenesis & Tissue Repair,* 6**,** 1-12.

WALZ, G., BUDDE, K., MANNAA, M., NURNBERGER, J., WANNER, C., SOMMERER, C., KUNZENDORF, U., BANAS, B., HORL, W. H., OBERMULLER, N., ARNS, W., PAVENSTADT, H., GAEDEKE, J., BUCHERT, M., MAY, C., GSCHAIDMEIER, H., KRAMER, S. & ECKARDT, K. U. 2010. Everolimus in patients with autosomal dominant polycystic kidney disease. *N Engl J Med,* 363**,** 830-40.

WANG, S., ZHANG, J., NAULI, S. M., LI, X., STARREMANS, P. G., LUO, Y., ROBERTS, K. A. & ZHOU, J. 2007. Fibrocystin/polyductin, found in the same protein complex with polycystin-2, regulates calcium responses in kidney epithelia. *Mol Cell Biol,* 27**,** 3241-52.

WARD, C. J., HOGAN, M. C., ROSSETTI, S., WALKER, D., SNEDDON, T., WANG, X., KUBLY, V., CUNNINGHAM, J. M., BACALLAO, R., ISHIBASHI, M., MILLINER, D. S., TORRES, V. E. & HARRIS, P. C. 2002. The gene mutated in autosomal recessive polycystic kidney disease encodes a large, receptor-like protein. *Nat Genet,* 30**,** 259-69.

WARD, C. P., B.; HUGHES, J.: THOMAS, S.; GAMBLE, V.; MACCARTHY, A.B.; SLOANE-STANLEY, J.; BUCKLE, V.J; KEARNEY,L.; HIGGS, D.R.; RATCLIFFE, P.J; HARRIS, P.C.; ROELFSEMA, J.H; SPRUIT,L.;. SARIS, J.J.; DAUWERSE, H.G.; PETERS, D.J.M.; BREUNING, M.H.; NELLIST, M.; BROOK-CARTER,1P.T.; MAHESHWAR, M.M.; CORDEIRO, I.; SANTOS,H.; CABRAL, P.; J.R. SAMPSON.; JANSSEN,B.; HESSELING-JANSSEN, A.L.W.; VAN DEN OUWELAND, A.M.W.; EUSSEN,B.; VERHOEF,S.; LINDHOUT, D.; HALLEY, D.J.J. 1994. The polycystic kidney disease 1 gene encodes a 14 kb transcript and lies within a duplicated region on chromosome 16. The European Polycystic Kidney Disease Consortium. *Cell,* 77**,** 881-94.

WARD, H. H., BROWN-GLABERMAN, U., WANG, J., MORITA, Y., ALPER, S. L., BEDRICK, E. J., GATTONE, V. H., 2ND, DERETIC, D. & WANDINGER-NESS, A. 2011. A conserved signal and GTPase complex are required for the ciliary transport of polycystin-1. *Mol Biol Cell,* 22**,** 3289-305.

WATANABE, D., SAIJOH, Y., NONAKA, S., SASAKI, G., IKAWA, Y., YOKOYAMA, T. & HAMADA, H. 2003. The left-right determinant Inversin is a component of node monocilia and other 9+0 cilia. *Development,* 130**,** 1725-34.

WATNICK, T., HE, N., WANG, K., LIANG, Y., PARFREY, P., HEFFERTON, D., ST GEORGE-HYSLOP, P., GERMINO, G. & PEI, Y. 2000. Mutations of PKD1 in ADPKD2 cysts suggest a pathogenic effect of trans-heterozygous mutations. *Nat Genet,* 25**,** 143-4.

WILLS, E. S., ROEPMAN, R. & DRENTH, J. P. H. 2014. Polycystic liver disease: ductal plate malformation and the primary cilium. *Trends in Molecular Medicine,* 20**,** 261-270.

WILSON, P. D. 2001. Polycystin: new aspects of structure, function, and regulation. *J Am Soc Nephrol,* 12**,** 834-45.

WILSON, P. D. 2004. Polycystic Kidney Disease. *New England Journal of Medicine,* 350**,** 151-164.

WINYARD, P. & JENKINS, D. 2011. Putative roles of cilia in polycystic kidney disease. *Biochimica et Biophysica Acta (BBA) - Molecular Basis of Disease,* 1812**,** 1256-1262.

WOO, D. 1995. Apoptosis and loss of renal tissue in polycystic kidney diseases. *N Engl J Med,* 333**,** 18-25.

WU, B., SAHOO, D. & BROOKS, J. D. 2013. Comprehensive Gene Expression Changes Associated with Mouse Postnatal Kidney Development. *The Journal of Urology,* 189**,** 2385-2390.

WU, G., D'AGATI, V., CAI, Y., MARKOWITZ, G., PARK, J. H., REYNOLDS, D. M., MAEDA, Y., LE, T. C., HOU, H., JR., KUCHERLAPATI, R., EDELMANN, W. & SOMLO, S. 1998. Somatic inactivation of Pkd2 results in polycystic kidney disease. *Cell,* 93**,** 177-88.

WU, G., MARKOWITZ, G. S., LI, L., D'AGATI, V. D., FACTOR, S. M., GENG, L., TIBARA, S., TUCHMAN, J., CAI, Y., PARK, J. H., VAN ADELSBERG, J., HOU, H., JR., KUCHERLAPATI, R., EDELMANN, W. & SOMLO, S. 2000. Cardiac defects and renal failure in mice with targeted mutations in Pkd2. *Nat Genet,* 24**,** 75-8.

WU, G., TIAN, X., NISHIMURA, S., MARKOWITZ, G. S., D'AGATI, V., PARK, J. H., YAO, L., LI, L., GENG, L., ZHAO, H., EDELMANN, W. & SOMLO, S. 2002. Trans-heterozygous Pkd1 and Pkd2 mutations modify expression of polycystic kidney disease. *Hum Mol Genet,* 11**,** 1845-54.

WU, Y., DAI, X. Q., LI, Q., CHEN, C. X., MAI, W., HUSSAIN, Z., LONG, W., MONTALBETTI, N., LI, G., GLYNNE, R., WANG, S., CANTIELLO, H. F., WU, G. & CHEN, X. Z. 2006. Kinesin-2 mediates physical and functional interactions between polycystin-2 and fibrocystin. *Hum Mol Genet,* 15**,** 3280-92.

XIONG, H., CHEN, Y., YI, Y., TSUCHIYA, K., MOECKEL, G., CHEUNG, J., LIANG, D., THAM, K., XU, X., CHEN, X. Z., PEI, Y., ZHAO, Z. J. & WU, G. 2002. A novel gene encoding a TIG multiple domain

protein is a positional candidate for autosomal recessive polycystic kidney disease. *Genomics,* 80**,** 96-104.

YABUKI, A., TANAKA, S., MATSUMOTO, M. & SUZUKI, S. 2006. Morphometric study of gender differences with regard to age-related changes in the C57BL/6 mouse kidney. *Exp Anim,* 55**,** 399-404.

YODER, B. K., HOU, X. & GUAY-WOODFORD, L. M. 2002. The polycystic kidney disease proteins, polycystin-1, polycystin-2, polaris, and cystin, are co-localized in renal cilia. *J Am Soc Nephrol,* 13**,** 2508-16.

YOKOYAMA, T., COPELAND, N. G., JENKINS, N. A., MONTGOMERY, C. A., ELDER, F. F. & OVERBEEK, P. A. 1993. Reversal of left-right asymmetry: a situs inversus mutation. *Science,* 260**,** 679-82.

YOSHIBA, S., SHIRATORI, H., KUO, I. Y., KAWASUMI, A., SHINOHARA, K., NONAKA, S., ASAI, Y., SASAKI, G., BELO, J. A., SASAKI, H., NAKAI, J., DWORNICZAK, B., EHRLICH, B. E., PENNEKAMP, P. & HAMADA, H. 2012. Cilia at the node of mouse embryos sense fluid flow for left-right determination via Pkd2. *Science,* 338**,** 226-31.

ZHANG, M. Z., MAI, W., LI, C., CHO, S. Y., HAO, C., MOECKEL, G., ZHAO, R., KIM, I., WANG, J., XIONG, H., WANG, H., SATO, Y., WU, Y., NAKANUMA, Y., LILOVA, M., PEI, Y., HARRIS, R. C., LI, S., COFFEY, R. J., SUN, L., WU, D., CHEN, X. Z., BREYER, M. D., ZHAO, Z. J., MCKANNA, J. A. & WU, G. 2004. PKHD1 protein encoded by the gene for autosomal recessive polycystic kidney disease associates with basal bodies and primary cilia in renal epithelial cells. *Proc Natl Acad Sci U S A,* 101**,** 2311-6.

ZHELEZNOVA, N. N., WILSON, P. D. & STARUSCHENKO, A. 2011. Epidermal growth factor-mediated proliferation and sodium transport in normal and PKD epithelial cells. *Biochimica et Biophysica Acta (BBA) - Molecular Basis of Disease,* 1812**,** 1301-1313.

ZHONG, J., PERRIEN, D. S., YANG, H.-C., KON, V., FOGO, A. B., ICHIKAWA, I. & MA, J. 2012. Maturational Regression of Glomeruli Determines the Nephron Population in Normal Mice. *Pediatric research,* 72**,** 241-248.

7. Appendix

Appendix 1: Materials and Methods

This section contains information regarding mouse strains, molecular biology, protein biochemistry, cell media and chemicals, antibodies and general protocols for laboratory procedures.

More specific information concerning protocols will be given in the appropriate sections.

1.1 Mouse strains

Animals were maintained according to the Medical Research Council's guidance in 'Responsibility in the Use of Animals for Medical Research' (July 1993), and in accordance with the Animals (Scientific Procedures) Act, 1986.

Ethical approval for all studies involving mouse work was obtained as part of the application for the UK Home Office Project Licence and all mice were kept in accordance with UK Home Office welfare guidance and Home Office project licence restrictions. Mice were maintained in controlled light with a 12 hour light/dark cycle, with controlled temperature (21 ± 2°C) and humidity (55 ± 10%). Mice had free access to water (10–12 ppm [parts per million] chlorine) and were fed ad libitum on a commercial diet (5.3% fat [corn oil], 21.2% protein, 57.4% carbohydrate, 4.6% fibre; Rat and Mouse Diet No. 3 [RM3], Special Diet Services, Essex, UK). All mice were socially housed in groups of 2–5 mice until the start of study.

1.1.1 Background strains

All mice were maintained on a C57BL/6J background with back crossing until congenic. With the exception of the $Pkd2^{lrm4}$ line which was crossed to several strains to assess survival, this is detailed below.

1.1.2 $Pkd2^{lrm4}$

Left-right mutant 4 (lrm4) mice carry an A-to-G transversion in exon 7 of Pkd2 (Ermakov et al., 2009). The line, having been maintained on a C3H/HeH, was outcrossed to CD1 to assess survival, then finally crossed to C57BL/6J, the strain on which they were maintained. $Pkd2^{lrm4}$ was backcrossed to C57BL/6J to produce a congenic line.

The mutation was genotyped by a PCR-pyrosequencing method. 125bp flanking the mutation at nucleotide 1408 was amplified by PCR using the biotinylated forward primer lrm4_F_Biotin and the reverse primer lrm4_R.

The PCR set-up was as follows: 10 µl MasterMix (Qiagen); 0.2 µl 100 µM lrm4_F_Biotin and lrm4_R primers; 1 µl genomic DNA; 8.6µl ddH_2O.

PCR protocol: 95°C for 5 mins followed by 44 cycles of 95°C 15 s, 60°C 30 s, and 72°C 15 s with a final extension 72°C for 5 mins. Pyrosequencing of the PCR product was performed using the reverse sequencing primer lrm4_seqR.

1.1.3 Kap-iCre

Mice exhibiting the transgene KAP2-iCre; Tg(Kap-cre)29066/2Sig were obtained from the Jackson laboratory repository (the donating investigator being Dr. Curt Sigmund, University of Iowa College of Medicine). These mice express the improved Cre recombinase (iCre) under the control of the mouse kidney androgen regulated protein (Kap). Improved Cre has been codon optimised so that the sequence is more similar to the eukaryotic genome. The KAP chimera vector with proximal end of human angiotensinogen (hATG) gene confers proximal tubular specificity for Cre expression. Exon 2 of hATG is deleted resulting in termination of protein production. Transgene induction occurs with endogenous testosterone and can be increased with exogenous hormone treatment.

These mice were supplied by the Dr J. Leiper (Nitric Oxide Signalling group, MRC clinical sciences centre London) who, having obtained the Tg(Kap-cre)29066/2Sig mice, crossed to a line containing a dimethylarginine dimethylaminohydrolases, DDAH1 floxed allele. It was therefore necessary to segregate the Cre before proceeding with the experimental cross. This was achieved by breeding the Cre carrying mice with *Pkd2*$^{lrm4\ /+}$ mice and selecting for Cre and lrm4 positive but DDAH1 negative mice. After segregation of the DDAH1 allele, the mice were crossed with R26R –LacZ in order to assess the activity of the cre allele.)

Genotyping was carried out for icre, DDAH1 and PKD2^{lrm4} using the primers in the primer table.

1.1.4 Pkd2-flox

Mice carrying Lox-p sites flanking exons 11 and 13 of the *Pkd2* gene were obtained from the Jax laboratory under stock code Pkd2tm1.1Tjwt/J. The Donating investigator was David Huso, John Hopkins University PKD Core Center. The inserted cassette is not reported to cause a functional change. When bred to a line carrying a cre recombinase, exons 11-13 of the *Pkd2* gene are deleted, this leads to the production of a null allele. These mice were maintained as a homozygous colony on a C57BL/6J background.

Genotyping detects the presence of the downstream loxP site. The forward primer, Pkd2floxF is situated in exon 13 whilst the reverse primer is situated in the intron, after the loxP site. The wt band is 382bp whereas the mutant band is 499bp long. The sequence of these primers can be found in the primer table.

The PCR set-up was as follows: 10 µl MasterMix (Qiagen); 1 µl each 10 µM Forward and reverse primers; 1 µl genomic DNA; 8 µl ddH_2O.

1.1.5 Pkd2-del

These mice are offspring from a pkd2-flox cross with a line harbouring Actin-cre recombinase. This recombines the LoxP sites flanking exon 11-13 in the pkd2-flox line causing the intermediate sequence to be deleted. This line was bred with C57BL/6J wildtype mice to segregate the cre and then maintained as a heterozygous colony, which we call pkd2-del.

The PCR set-up was as follows: 10 µl MasterMix (Qiagen); 1 µl each 10 µM Forward and reverse primers; 1 µl genomic DNA; 8 µl ddH_2O.

PCR protocol: 95°C for 5 mins followed

1.1.6 $Pkd2^{fl/lrm4}$; $Kap^{cre/+}$

Pkd2-flox mice were bred with Pkd2-lrm4 mice and maintained as a colony of $Pkd2^{lrm4/fl}$ mice, these mice are viable since the floxed allele does not alter gene function before cre recombination. These $Pkd2^{lrm4/fl}$ mice were bred with mice carrying a cre recombinase under the control of a Kap promoter. The cre recombinase is driven by the kidney androgen protein promotor specifically in the proximal tubules of the renal cortex. The resulting cross produced mice with $Pkd2^{lrm4/-}$ in the proximal tubules but left the $Pkd2^{fl}$ allele intact elsewhere.

These mice were genotyped using the lrm4 pyrosequencing assay, the icre and pkd2-flox assays described elsewhere.

1.1.8 R26R mice

B6;129S4-Gt(ROSA)26Sor^{tm1Sor}/J mice were obtained from Jax laboratory, further information of which can be found here https://www.jax.org/strain/003309 . In the text, these mice are referred to as R26R-reporter mice

1.2 Molecular biology

1.2.1 Polymerase Chain reaction

Polymerase chain reaction is performed in order to amplify fragments of DNA for analysis. Reactions mixes were prepared according to manufactures instructions using Qiagen Taq mastermix (Cat No:201445) and performed on a Gstorm thermocycler.

1.2.2 Genotyping

Genomic DNA was crudely extracted for genotyping from ear biopsies and embryonic material, by heating to 95°C for 1 hour in 90 µl of 50mM NaOH. The reaction was cooled, neutralised with 10 µl of 1 M Tris-HCl pH4.5 and diluted with ddH_2O. This DNA preparation was used for genotyping PCRs the primer sequences given in the table below.

Primer Table:

Genotyping assay	Forward Primer 5'-3'(Melting temp)	Reverse Primer (Melting temp)	Annealing Temp
Lrm4	BIO-GAACACGGAACAAGGGTCAG	NNNGGTTTGCTACTGGAACTATCAAGA	60
Kap-icre	AGATGCCAGGACATCAGGAACCTG	ATCAGCCACACCAGACACAGAGATC	
DDAH1	TCAGTTGGAGTGTAGTGACGA	CCTCCCATTGCTAATGAAACGGA	65

	GG	GC	
Pkd1del-deleted exons	18F : TGTGCCTCAATCCGCCTCTC (56)	19R : CACCATCTTCTGCATCACGC (56)	54
Pkd1del-IRES	TAACGTTACTGGCCGAAG (52)	GTCGCTACAGACGTTGTT (52)	54
Pkd2-Flox	Pkd2floxF: GGGGTTTCCTATGAAGAGTTCCAAG	Pkd2floxR: CTGACAGGCACCTACAGAACAGTG	54
Pkd2-del	TAAACAAGCCATTGCTGCTG	CTGCCCTTTCCTCTGTGTTC	51

1.2.3 Agarose gel electrophoresis

1% agarose, TBE gels were submerged in TBE buffer with 0.5% ethidium Bromide. TAE gels were used for cloning, with TAE buffer. Samples mixed with 20% w/v Ficol OrangeG and DNA ladders (1kb plus, New England Biolabs) were loaded into wells. A constant voltage of 80-100V was applied across the gel for 30-60 mins to separate the linear DNA fragments by size. Fluorescence under UV light was achieved by the use of the DNA intercalatant, Ethidium Bromide and visualised using a Gel Doc system (BioRad).

1.2.4 Purification of PCR products

PCR products were purified using a QIAquick PCR Purification kit or the QIAquick gel extraction kit according to manufactures instructions.

1.2.5 DNA sequencing

Purified DNA was sequenced by GATC biotech using primers targeted to the sequence of interest. Samples prepared according to GATX guidelines.

1.2.6 Restriction enzyme digestion

Restriction endonucleases purchased from NEB were used with the recommended buffer and incubation temperature. 1 unit of restriction enzyme is defined as the activity required to fully cleave 1µg of lambda DNA in a 50µl reaction in 1 hour.

Digests were routinely performed with the following set-up: 1µg purified DNA, 5 µl 10 x restriction enzyme buffer (NEB), 10U restriction enzyme, and ddH_2O to final volume 50 µl. The success of restriction digestion was determined by DNA gel electrohoresis.

1.2.7 x-gal staining

For assessment of LacZ expression, embryo and kidney sections were stained with X-gal staining solution (1 mg/ml X-Gal in DMF, 5 mM potassium ferricyanide, and 5 mM potassium ferrocyanide, 2mM $MgCl_2$, 0.02% IGEPAL, 0.01% Na deoxycholate in PBS). Dissected embryos

or kidneys were fixed in 4% PFA for 1 hour at room temperature, washed three times (PBS, 5 minutes) and desiccated with 30% sucrose overnight at 4^{o}C before being embedded in OCT. Sections were cut at 7 um and frozen at -80^{o}C until staining. All solutions for staining were applied cold, fresh and at pH8.

Slides were allowed to thaw then fixed in 4% PFA for 10imns. Slides were then washed three times for 5mins each in PBS before incubation in X-gal stain solution (5 mM K3Fe(CN)6, 5 mM K4Fe(CN)6, 2 mM MgCl2, 0.01% deoxycholate, 0.02% NP-40, 1 mg/ml X-gal in PBS) at 37^{o}C until colour developed sufficiently.

At this point the reaction was stopped with a rinse in PBS and post-fixing in 4% PFA for 10 mins. Slides were rinsed in water before being dehydrated through a series of MeOH washes before cover slipping using DPX mountant.

For whole adult kidney staining, after perfusion, kidneys were bisected. One half was embedded for frozen sectioning and the other half was stained whole. Following perfusion, the whole half was fixed in 4% PFA for 1 hour at room temperature, washed three times (PBS, 5 minutes) and desiccated with 30% sucrose overnight at 4^{o}C. These were submerged in X-gal staining solution (1 mg/ml X-Gal in DMF, 5 mM potassium ferricyanide, and 5 mM potassium ferrocyanide, 2mM $MgCl_{2'}$ 0.02% IGEPAL, 0.01% Na deoxycholate in PBS) for 24-48 hours. Following this kidneys were rinsed in PBS (3x 5mins) and post-stain-fixed in 4% PFA for 1 hour. PFA was rinsed off with PBS (3x 5mins) and submerged in 30% sucrose. All solutions for staining were applied cold, fresh and at pH8.

1.3 Protein biochemistry

1.3.1 Sample lysis and protein extraction

Cell plates (10cm Nunc) were placed on ice and washed with ice cold PBS. Cells were dried well by aspiration with a pipette before addition of 100ul ice cold 1X RIPA (radioimmunoprecipitation assay) buffer *(150 mM NaCl, 1.0% IGEPAL® CA-630, 0.5% sodium deoxycholate, 0.1% SDS, and 50 mM Tris-HCL, pH 8.0. with protease inhibitors).* Plates were scraped and then moved into a cooled Eppendorf tube and agitated at 4°C for 20mins before being spun at 13000rpm for 10mins at 4°C. The supernatant was collected and used for protein studies or stored at -80°C.

Embryonic kidneys were collected on ice, dried and snap frozen in liquid Nitrogen and stored at -80°C before being lysed. For lysis, kidneys were homogenised in 45 µl 1xRIPA buffer on ice over a period 30mins. The cell suspension was then agitated for a further 20mins at 4°C before centrifugation 13000rpm for 10mins at 4°C.

1.3.2 Bradford assay

A Bradford assay was used to quantify the protein concentration of the samples before proceeding with the analysis. A protein standard was prepared with BSA between 0-1.4mg/ml in 10% RIPA lysis buffer. Samples were diluted 1:10. To a 95well plate, 5ul diluted sample and 5ul protein standards were mixed with 250ul room temperature Bradford reagent. These were incubated on a rocker in the dark at room temperature for 5 mins. Sample absorbance was measured at 595nm and sample concentrations recorded.

1.3.3 Proteasome inhibition assay

Cells were grown to 90% confluency in 10cm dishes. A stock solution of 10mM MG132 in DMSO was thawed. 5µm/m of the proteasome inhibitor, MG132 (Sigma) was added to cell media at a final concentration of 50µM (1.06um per 10ml). A batch of inhibitor medium is made up for all plates requiring inhibition in order to reduce pipetting error. This was added to the cells. Cells were harvested 10 hrs after this.

The medium from each dish was collected, the plates were washed gently with PBS and this was added to the collected medium before being centrifuged for 5mins at 800rpm at room temperature. Dishes were thoroughly dried before being lysed in 100ul RIPA with protease inhibitors. The medium was removed from the cell pellet of collected cells and the pellets were washed with PBS. Dishes were scraped on ice and the lysate added to the cell pellet. The lysate was mixed with the pellet to ensure all cells were lysed and this was transferred to microcentrifuge tubes before being agitated in a rotator at 4°C for 10 mins. Samples were centrifuged for 10mins at 13000 rpm at 4°C and the supernatant was collected. These samples were then assessed for protein levels by Bradford assay and then prepared for analysis by Western Blot.

1.3.4 Deglycosylation: digestion with PNGaseF and EndoH

EndoH (P0702S) and PNGaseF (P0704S) kits were purchased from NEB and digestion was undertaken according to manufacturer's instructions.

Cells were grown to confluency in 10cm plates and lysed in RIPA buffer with protease inhibitors. Fresh lysate was used for digestion; do not freeze samples before digestion.

EndoH: 1-20µg of glycoprotein, 1µl of 10X Glycoprotein Denaturing Buffer and H_2O were combined to make a 10µl total reaction volume. The protein was denatured by heating at 100°C for 10 minutes. Reactions were chilled on ice and spun down in centrifuge briefly. The total volume was brought to 20µl by adding 2µl of 10X GlycoBuffer 3, H_2O and 1µl EndoH, or 1µl H_2O to non-digested controls. Samples were incubated at 37°C for 1 hour.

Samples were then were reduced and denatured by boiling at 90°C for 10mins in 4xLDS sample buffer and 10X reducing agent (invitrogen). Samples were loaded onto 4-12% Bis-Tris SDS-PAGE gel (Novex) for Western blot analysis

PNGaseF: Denaturing Reaction Conditions:

1-20µg of glycoprotein, 1µl of Glycoprotein Denaturing Buffer (10X) and H_2O were combined to make a 10µl total reaction volume. The protein was denatured by heating at 100°C for 10 minutes. Reactions were chilled on ice and spun down in centrifuge briefly. The total volume was brought to 20µl by adding 2µl GlycoBuffer 2 (10X), 2µl 10% NP-40 and 6µl H_2O. Next, 1µl PNGaseF or 1µl of H_2O (for controls) was added. Reactions were incubated at 37°C for 1 hour.

Samples were then were reduced and denatured by boiling at 90°C for 10mins in 4xLDS sample buffer and 10X reducing agent (invitrogen). Samples were loaded onto 4-12% Bis-Tris SDS-PAGE gel (Novex) for Western blot analysis

N.B. PNGaseF is inhibited by SDS, therefore it is essential to have NP-40 in the reaction mixture under denaturing conditions.

1.3.5 Western blotting

Samples were reduced and denatured by boiling at 90°C for 10mins in 4xLDS sample buffer and 10X reducing agent (invitrogen). Samples were cooled and quickly spun down before being loaded into a 4-12% Bis-Tris SDS-PAGE gel (Novex), along with molecular weight marker (precision plus protein dual colour standard, BioRad). The centre of the tank was filled with 500ml MOPs buffer and 500ul of antioxidant (Invitrogen). Gels were run for 1hr at 200 V constant.

Gels were blotted using an iBlot transfer stack containing a nitrocellulose membrane and an iBlot Gel Transfer Device as per manufacturer's instructions. The nitrocellulose membrane was then blocked for 1hr in Milk block (5% skimmed milk, 0.1% Tween in PBS) with gentle rocking. Membranes were incubated with primary antibodies (rabbit-α-PKD2, H280, sc-25749, Santa Cruz, used at 1mg/ml; and mouse-α- acetylated tubulin) overnight with rocking at 4°C. The following day, membranes were washed 4x5mins in PBS+0.1%tween before the addition of the secondary antibody. Membranes were incubated with secondary antibodies for 1 hour at room temperature in the dark. Another 4x5mins in PBS+0.1%tween washes followed by a 5min wash in PBS and the membrane was dried in preparation for imaging.

1.4 Cell culture/ Tissue culture

Stringent aseptic technique is maintained throughout

1.4.1 Making Mouse Embryonic Fibroblasts (MEFs)

Mouse embryos were harvested from a pregnant mother at 13.5-14.5dpc. The head, limbs and organs were removed and the tail retained for genotyping. Each carcass was washed thoroughly with sterile PBS to remove blood cells. To each carcass, 200µl of 25% Trypsin was added before mincing finely. This was further broken down by pipetting up and down with 5 ml medium (DMEM + glutamax-1, 4.5g/L D-glucose, 10% FBS and 1% Penstrep) using a 5ml stripette 16 times before adding to a 10 cm dish of medium. Volume was increased to 10ml with complete medium. Cells were allowed to settle and incubated at 37°C with 5% CO_2. Medium was changed regularly.

1.4.2 Electroporation

A BioRad Gene Pulser Xcell was used with 0.4cm cuvettes operating the preset programme for Mammalian cells (0.2kV, 960µF; *tau* 20-25).

Cells were trypsinised to give a single cell suspension and the trypsin was neutralised with serum. After counting, cells were spun into a pellet of known cell number ($5x10^6$) and resuspended in 200µl Optimem (thermos fisher 11058021). To this, 10-50µg/ml Plasmid

DNA was added and the cuvette was placed in the ShockPod. Immediately after pulsing, cells were plated into 2ml growth media in 6 well plates and incubated at 37°C with 5% CO_2.

1.4.3 Immortalising MEFs

The SV40 large-T antigen plasmid was electroporated into primary MEFs to produce stable cell lines. Post electroporation, cells were allowed to grow and observed until untransfected cells had died. Cells were passaged a number of times before being frozen.

1.4.4 Freezing cells

Cells were expanded by seeding as many plates as possible from a founder plate. When confluent, cells were washed with warm PBS and 1-1.5mls 5%Trypsin was added. Once cells had completely detached, trypsin was neutralised and cells were pelleted by centrifugation at 800rpm for 5mins. The supernatant was aspirated away and the pellet resuspended in 1 ml Freezing medium (40% FBS, 50%DMEM, 10% DMSO). Cells were divided between cryo-tubes and transferred to Mr Frosty (freeze down box) before placing at -80°C. After a week a -80°C cells were transferred to liquid nitrogen storage.

1.4.5 Cells Thawing

Vials to be thawed were removed from liquid nitrogen stores and kept frozen on dry ice before thawing. Each vial was swirled in 37°C water bath and removed with a slither remaining frozen. Cells were then added dropwise to 10cm dish with 14mls pre-warmed MEF medium. Medium was exchanged as soon as cells settle.

1.4.6 Splitting cells

Cells were washed with warm PBS and 1-1.5mls 5%Trypsin was added. Once cells had completely un-adhered, trypsin was neutralised with three volumes of medium and then divided generally 1:3 and 1:10 into new plates. Cells were incubated at 37°C, 4% CO_2 until confluency was reached.

1.4.7 Counting cells

Trypsinised cells were pelleted by centrifugation at 800rpm for 5mins. The supernatant was aspirated away and the pellet re-suspended in 10ml medium. After preparing a haemocytometer, 10ul of cells were added to the chamber by capillary action. Cells were counted when inside the grid or touching the left or bottom wall. A $1mm^2$ square with a volume of 100nL is counted and an average was taken of 3 counts. This number is multiplied by 10^4 and corrected for the dilution factor (10 in this case), this number is the number of cell/ml in the original suspension.

1.4.8 Collagen coating

Type I Collagen (C8919) was purchased from Sigma at a concentration of 1mg/ml. A 1:10 dilution was made in PBS. 13mm coverslips were placed in a 6well plate and 950ul of collagen solution was added per well. The plate was incubated at 37°C for several hours

before the excess liquid was removed and the plate allowed to dry in the hood overnight. Cells were seeded the next day, after washing with PBS. Collagen was used at 10ug/Cm^2. Collagen was used when HEK cell were seeded onto coverslips for immunofluorescence.

1.4.9 Transfection of constructs

The day before transfection, $4X10^5$ were plated into 6well plates containing coverslips. Lipfectamine 2000 transfection reagent (ThermoFisher) was used according to manufacturer's instructions. DNA to be transfected was previously purified with the PureYield Maxiprep system kit (Promega). Cells were incubated overnight before media change to serum free medium to induce cilium growth.

1.4.9 Immunocytochemistry

Cells were seeded onto coverslips in a 6 well plate and allowed to grow to confluency. Cells were serum starved in order to induce cilium growth. The coverslips were washed with ice cold PBS and fixed with Ice cold MeOH for 5mins. Tilting the dish to align the cilia during fixation. Cells were washed 3x with PBS and permeabilised with 1% NP40 in PBS for no longer than 3mins. Cells were washed 2x with PBS and blocked in 4% BSA in PBS for 30mins at room temperature. Primary antibodies were diluted in 4% BSA in PBS and 50µl per coverslip was dotted onto parafilm in a humidified chamber. Coverslips were dried gently and placed face down onto the primary antibody solution for 1hr at room temperature. Cells were washed 3x 5mins in PBS and then incubated on parafilm with the secondary antibody in 4% BSA for 30 mins at room temperature in the dark. Coverslips were washed 3x 10 mins in PBS before mounting.

Antibodies used for immunocytochemistry:

Name (cat no)	recognises	dilution	Raised in	Uses
H280 (sc-25749)	aa 689-968 of Pkd2	1:200 (1µg/ml)	Rabbit	WB, IF

1.5 Dissection

1.5.1 Embryonic kidney dissection

Using a light microscope, the head is removed and the thoracic cavity opened. Lungs and heart are removed for situs assessment. Lung lobes (Wt 4:1, R:L) and heart situs (Wt apex L) were scored. Open the abdominal cavity and remove the liver and intestines. The kidneys lie on the back of the embryos. Fix the kidneys in 4% PFA for 2-3 hours at room temperature.

1.6 Clinical chemistry

BUN is calculated from urea as follows:

Urea (mmol/L) = BUN (mg/dL) x10 (dl/L)/14X2 (mg N/mmol urea)

BUN (mg/dl) = urea(mg/dL)/2.14

The 2.14 quotient is calculated by MW of urea=60/ MW of urea nitrogen 2(14) = 60/28=2.14

Creatinine ratios were calculated by dividing sodium, potassium, Calcium and inorganic phosphorus values by creatinine.

1.7 Administration of testosterone

One gram of Dihydrotestosterone (DHT) powder (5α-Androstan-17β-ol-3-one, A8380 Sigma) was dissolved in 10ml of pure EtOH to make a 100mg/ml stock solution, store at -20°C. To make a 5mg/ml solution for injections, add 500ul DHT solution to 530.9mg HPβCD (H107-5G Sigma) then dissolved in sterile injectable water (95289 Sigma) to a volume of 10ml.

2 HPβCD:1 DHT molar ratio (5mg/ml DHT is 17.22µM, 34.44µm of HPβCD gives 53mg/ml)

HPβCD is preferred to corn oil as a mode for injection as the mice exhibit skin reactions to corn oil. HPβCD enables steroid hormones to dissolve in water.

The vehicle is made with 530.9mg HPβCD, 500ul pure ethanol, and made up to 10ml with sterile injectable water.

Appendix 2: Data tables

This section contains data tables for chapters 3 and 4, detailing averages, standard deviations and T-tests undertaken for the clinical chemistry data.

2.1 Chapter 3 clinical chemistry

2.1.1 Plasma analysis for C3H- and B6- $Pkd2^{lrm4/+}$ mice

Table 2.1: C3H and B6J Plasma analysis, average and SD.
An average of the mice compared for each genotype, plasma component and age. Standard deviation= (SD). T-tests were performed to compare Wt and $Pkd2^{lrm4/+}$ mice in the same age group (in the same row of the table) for both cohorts. Mice with a significant results are signified by **= significant P=0.001 or *=significant P=0.05

		C3H/HeH		C57BL/6J	
	Age	**$Pkd2^{+/+}$**	**$Pkd2^{lrm4/+}$**	**$Pkd2^{+/+}$**	**$Pkd2^{lrm4/+}$**
Urea (mmol/l)	4-8m	9.1 (0.80)	13.1 (3.67)	13.2 (1.11)	12.7 (0.72)
	9-13m	10.2 (0.75)	12.0 (1.55)	10.3 (1.61)	10.1 (0.79)
	14-18m	11.3 (2.25)	11.94 (4.69)	12.8 (2.68)	11.5 (1.67)
Creatinine (µmol/l)	4-8m	17.9 (1.51)	20.7 (2.33)	17.0 (1.43)	17.3 (0.47)
	9-13m	17.2 (1.84)	18.7 (1.63)	18.1 (2.44)	17.4 (1.53)
	14-18m	19.6 (2.56)	16.46 (2.12)	16.7 (1.40)	17.9 (1.54)
Total protein (g/l)	4-8m	57.7 (4.56)	57.7 (6.64)	51.5 (1.99)	47.5 (0.68) **
	9-13m	62.7 (12.04)	56.3 (2.31)	50.0 (1.28)	49.0 (2.79)
	14-18m	64.8 (8.25)	65.14 (13.75)	52.4 (2.86)	51.5 (2.75)
Albumin (g/l)	4-8m	31.2 (2.45)	28.1 (1.57) *	27.3 (0.75)	25.5 (0.66) **
	9-13m	31.4 (6.98)	28.8 (1.65)	26.7 (1.16)	25.5 (1.46)
	14-18m	32.1 (4.28)	32.26 (6.71)	27.7 (2.38)	26.8 (1.51)
Amalyse (U/l)	4-8m	711.0 (128.2)	646.8 (57.50)	729.6 (72.86)	673.8 (27.15)
	9-13m	755.1 (181.89)	765.6 (85.27)	968.3 (307.70)	807.3 (145.33)
	14-18m	781.4 (167.38)	817.2 (314.91)	974.3 (199.00)	1046.5 (153.29)
BUN	4-8m	25.4 (2.25)	36.7 (10.28)	35.5 (2.02)	37.0 (3.12)

(mg/dL)	9-13m	28.7 (2.10)	33.5 (4.35)	28.2 (2.23)	28.9 (4.52)
	14-18m	31.7 (6.30)	33.5 (13.16)	32.3 (3.28)	36.0 (7.53)

2.1.1 Urinalysis for C3H- and B6- *Pkd2*$^{lrm4/+}$ mice

Table 2.2: C3H cohort urinalysis results.

An average of the Wt and *Pkd2*$^{lrm4/+}$ mice compared for each urine component and age. Standard deviation= (SD). T-tests were performed to compare Wt (grey columns) and *Pkd2*$^{lrm4/+}$ mice in the same age group (in the same row of the table). The shaded area at the bottom of the table contains results normalised to creatinine Mice with a significant results are signified by **= significant P=0.001 or *=significant P=0.05

	C3H/HeH					
	Pkd2$^{+/+}$	**Pkd2$^{lrm4/+}$**	**Pkd2$^{+/+}$**	**Pkd2$^{lrm4/+}$**	**Pkd2$^{+/+}$**	**Pkd2$^{lrm4/+}$**
	4-8 months		**9-13 months**		**14-18 months**	
Sodium (mmol/l)	195.5 (39.97)	133.8 (69.85)	137.5 (47.98)	165.71 (44.58)	140.6 (86.49)	99.2 (43.70)
Potassium (mmol/l)	252 (48.53)	247 (103.95)	250.25 (64.08)	269.71 (72.48)	198.6 (90.53)	183 (63.62)
Chloride (mmol/l)	242.8 (57.49)	176.4 (101.1)	189.25 (73.90)	224.57 (72.55)	175.8 (111.23)	123 (45.78)
Urea (mmol/l)	1087 (244.7)	1144 535.1)	1042.25 (306.43)	1151.86 (311.23)	841 (380.68)	805.8 (303.51)
Creatinine (µmol/l)	2865 (467.87)	2844.4 (1159.8)	3006 (1006.71)	2933.29 (666.65)	2244.4 (1069.49)	2410.4 (1195.43)
Calcium (mmol/l)	1.50 (0.54)	1.37 (0.66)	1.16 (0.57)	1.42 (0.47)	0.94 (0.49)	0.92 (0.48)
Inorganic phosphate (mmol/l)	19.55 (4.62)	39.72 (21.56)	28.73 (15.63)	21.94 (7.18)	18.92 (10.13)	28.68 (19.17)
Glucose (mmol/l)	0.85 (0.60)	1.26 (0.80)	0.73 (0.74)	0.83 (0.75)	0.54 (0.80)	0.6 (0.52)
Uric acid (µmol/l)	440.98 (119.14)	518.13 (31.45)	850.725 (422.41)*	454.1 (119.14)	542.42 (270.17)	584.15 (237.64)
Urinary protein (mg/dl)	722.6 (85.29)	770.32 (158.23)	662.9 (455.07)	786.67 (271.35)	448.68 (253.33)	491.38 (235.98)

Na:CR (mmol/L)	68.16 (8.42)	54.56 (32.03)	46.52 (7.12)	57.11 (12.86)	60.81 (8.11)	46.98 (19.91)
K:CR (mmol/L)	87.89 (8.73)	94.48 (35.13)	85.94 (11.00)	93.20 (22.13)	89.56 (7.06)	82.96 (19.42)
Ca:CR (mmol/L)	0.54 (0.27)	0.54 (0.27)	0.38 (0.12)	0.48 (0.12)	0.42 (0.08)	0.39 (0.06)
P: CR (mmol/L)	6.89 (1.65)	14.29 (5.05) *	9.58 (3.95)	7.96 (3.33)	9.03 (5.09)	10.53 (4.25)

Table 2.3: B6J cohort urinalysis results.

An average of the Wt and *Pkd2*$^{lrm4/+}$ -B6J mice compared for each urine component and age. Standard deviation= (SD). T-tests were performed to compare Wt and *Pkd2*$^{lrm4/+}$ mice in the same age group (in the same row of the table). Mice with a significant results are signified by **= significant P=0.001 or *=significant P=0.05

	C57BL/6J					
	Pkd2$^{+/+}$	**Pkd2$^{lrm4/+}$**	**Pkd2$^{+/+}$**	**Pkd2$^{lrm4/+}$**	**Pkd2$^{+/+}$**	**Pkd2$^{lrm4/+}$**
	4-8 months		**9-13 months**		**14-18 months**	
Sodium (mmol/l)	211.8 (48.35)	201.8 (57.71)	178.3 (38.31)	111.8 (44.33)	127.5 (25.68)	99.3 (53.5)
Potassium (mmol/l)	296.8 (46.56)	389.5 (99.68)	227.3 (43.92)	168.5 (40.54)	204.0 (17.22)	179.8 (60.82)
Chloride (mmol/l)	293.6 (52.57)	321.3 (109.44)	231.3 (49.61)	129.0 (69.46)	156.0 (30.80)	120.5 (71.19)
Urea (mmol/l)	1322.4 (194.60)	1464.3 (172.06)	1014.0 (175.4)	749.0 (214.93)	884.3 (67.10)	796.0 (261.53)
Creatinine (µmol/l)	3560.2 (436.35)	3934.7 (596.80)	3192.3 (503.60)	2955.3 (806.57)	3033.0 (729.18)	2866.8 (574.33)
Calcium (mmol/l)	2.7 (0.569)**	1.4 (0.29)	1.5 (0.25)	1.4 (0.34)	2.4 (0.56)	2.4 (1.23)
Inorganic phosphate	13.7 (14.17)**	54.3 (11.40)	20.1 (13.44)	28.4 (7.56)	25.8 (14.04)	32.6 (3.49)

(mmol/l)						
Glucose (mmol/l)	1.8 (0.22)	2.4 (0.88)	1.5 (0.24)	1.1 (0.24)	1.5 (0.50)	1.3 (0.48)
Uric acid (µmol/l)	543.7 (116.72)	605.2 (108.64)	859.6 (880.00)	402.2 (82.77)	483.3 (39.11)	451.8 (142.75)
Urinary protein (mg/dl)	663.8 (134.12)*	901.2 (19.58)	615.3 (306.59)	754.5 (140.55)	580.8 (104.68)	549.3 (41.72)
Na:CR (mmol/L)	59.4 (9.62)*	44.9 (3.23)	55.6 (5.91)*	37.3 (11.59)	44.6 (14.80)	33.1 (13.67)
K:CR (mmol/L)	83.1 (3.79)	87.7 (4.32)	71.0 (5.30)*	57.6 (7.00)	69.6 (13.72)	61.4 (9.07)
Ca:CR (mmol/L)	0.8 (0.24)*	0.4 (0.02)	0.5 (0.08)	0.5 (0.11)	0.8 (0.15)	0.8 (0.41)
P: CR (mmol/L)	3.9 (3.67)**	13.8 (1.58)	6.2 (4.50)	10.0 (3.24)	8.2 (2.40)	1.3 (3.74)

2.2 Chapter 4 clinical chemistry

2.2.1 Plasma analysis for conditional mice

Table 2.4: A comparison between plasma components from each of the four genotypes analysed

Average values (not divided by sex) of the mice compared for each genotype, plasma component and age. Standard deviation=(SD). T-tests were performed to compare between each combination of genotypes for each age and plasma component. *= p< 0.05. the graph below shows the male BUN data for each age group and genotype. Error bars represent SEM.

	Age	Lrm4-Kap	Wt-Wt	Lrm4-Wt	Wt- Kap
Urea (mmol/l)	6m	9.9 (1.78)	11.3 (0.84)	10.9 (2.66)	10.2 (1.79)
	9m	9.7 (1.11)*	11.0 (1.49)	9.4 (1.82)	10.8 (0.62)
	12m	10.5 (1.86)	9.7 (2.06)	10.4 (2.18)	9.8 (1.24)
	15m	9.8 (1.23)	11.0 (2.05)	9.9 (1.93)	9.1 (1.57)
Creatinine (µmol/l)	6m	17.4 (1.01)	18.3 (1.69)	17.0 (1.63)	16.7 (0.52)
	9m	16.7(1.53)	17.9(1.88)	16.7 (2.06)	17.6 (1.99)
	12m	17.6 (2.46)	17.1 (2.30)	17.7 (1.55)	16.1 (1.75)
	15m	16.9 (1.18)	18.0 (1.60)	17.9 (1.71)	17.0 (0.84)
Total protein (g/l)	6m	52.9 (0.90)	53.7 (1.58)	52.5 (1.90)	53.6 (1.00)
	9m	53.5 (1.85)	53.3 (2.53)	52.2 (3.00)	54.6 (1.27)
	12m	53.4 (1.28)	55.7 (3.51)	54.3 (2.45)	54.4 (1.80)
	15m	55.1 (1.30)	55.9 (3.43)	54.3 (2.80)	55.2 (2.78)
Albumin (g/l)	6m	28.5 (1.17)	28.4 (1.17)	27.7 (0.85)	28.1 (0.64)
	9m	27.8 (0.88)	26.5 (2.46)	26.7 (1.90)	28.1 (0.93)
	12m	27.3 (0.56)	27.6 (0.83)	28.0 (1.39)	27.8 (0.91)
	15m	27.4 (0.46)	27.1 (1.24)	27.0 (1.18)	27.4 (1.81)
Amalyse (U/l)	6m	587.6 (102.07)	691.0 (82.09)	682.2 (70.93)	646.3 (106.54)
	9m	742.7 (143.79)	658.0 (73.91)	751.5 (240.75)	658.7 (95.22)
	12m	647.0 (53.25)	695.7 (64.63)	798.7 (175.19)	680.8 (112.07)

	15m	707.8 (141.84)	714.5 (84.01)	731.2 (127.68)	661.5 (163.83)

2.2.2 Urinalysis for conditional mice

Table 2.5: A comparison between urine components from each of the four genotypes analysed

Average values (not divided by sex) of the mice compared for each genotype, plasma component and age. Standard deviation= (SD). T-tests were performed to compare between each combination of genotypes for each age and plasma component. The second table contains urinary sodium, potassium, calcium and inorganic phosphorus normalised to creatinine and expressed as creatinine ratios. Na=sodium, K=potassium, Cl= chloride, Cr=creatinine, Ca=calcium, P= inorganic phosphorus.

Pkd2:	lrm4-Kap	Wt-Wt	lrm4-Wt	Wt-Kap	lrm4-Kap	Wt-Wt	lrm4-Wt	Wt-Kap	lrm4-Kap	Wt-Wt	lrm4-Wt	Wt-Kap	lrm4-Kap	Wt-Wt	lrm4-Wt	Wt-Kap
	6 months				**9 months**				**12 months**				**15 months**			
Na (mmol/l)	184.6 (34.5)	179.7 (69.3)	186 (71.2)	207 (68.7)	167 (79.4)	152.6 (65.4)	175.8 (88.8)	233.2 (79.5)	225.8 (70.4)	149.8 (51.3)	198.2 (65.0)	150 (44.9)	149.2 (71.2)	85.3 (43.3)	115.4 (56.2)	163.5 (44.1)
K (mmol/l)	276.6 (39.0)	276.3 (97.7)	258.4 (73.4)	287.7 (91.1)	228.8 (75.2)	241.4 (68.4)	252.7 (83.2)	322.5 (74.0)	348 (49.1)	228.7 (52.2)	312 (69.9)	232.8 (50.2)	274.7 (66.2)	206.2 (41.3)	238. 6 (68.8)	319.2 (130.2)
Cl (mmol/l)	256.8 (47.0)	238.8 (99.7)	243.8 (97.5)	288.2 (103.3)	213 (108.7)	218.4 (93.8)	220.7 (116.2)	322.3 (115.4)	319.2 (76.6)	176.7 (70.2)	253.2 (77.6)	204.8 (62.4)	192.8 (81.8)	106.2 (58.9)	159.3 (76.1)	239.8 (109.3)
Urea (mmol/l)	1281.8 (180.9)	1267.0 (563.1)	1266.2 (368.2)	1492.0 (581.0)	1152.8 (436.3)	1139.0 (431.4)	1126.0 (350.9)	1678.3 (486.7)	1603.3 (450.8)	1136.7 (392.0)	1270.5 (72.8)	1208.2 (425.4)	1398.7 (349.0)	1001.7 (201.0)	1136.1 (333.4)	1637.0 (694.9)
Cr (µmol/l)	3526.8 (844.0)	4551.8 (2145.9)	3597.8 (1013.3)	4215.8 (1582.0)	3588.8 (1323.2)	3040.2 (855.8)	3660.2 (879.7)	4605.8 (1409.9)	5097.0 (2160.1)	3901.3 (1143.7)	4852.5 (818.6)	3460.0 (1035.5)	4415.8 (540.2)	3476.0 (454.2)	3655.0 (643.0)	4144.0 (1062.7)
Ca	2.8 (1.4)	2.7 (0.8)	2.3 (1.0)	3.2 (1.4)	2.9 (0.5)	2.4 (1.1)	2.8 (1.1)	2.5 (0.7)	2.4 (0.9)	4.4 (2.5)	3.1 (0.8)	4.1 (1.1)	5.4 (1.3)	3.5 (1.8)	3.3 (2.5)	3.4 (2.0)

(mmol/l)																
P (mmol/l)	29.8 (8.8)	42.0 (26.2)	26.7 (19.4)	29.9 (18.6)	32.0 (7.6)	20.5 (9.5)	33.2 (9.9)	29.9 (11.8)	44.1 (30.3)	41.8 (15.0)	40.3 (15.8)	33.0 (10.1)	45.9 (22.3)	43.1 (22.8)	37.6 (9.8)	33.9 (10.4)
Glucose (mmol/l)	1.9 (0.4)	2.5 (1.2)	1.8 (0.6)	2.3 (0.8)	1.9 (0.8)	1.8 (1.0)	1.8 (0.5)	2.2 (0.5)	2.5 (0.6)	1.9 (0.7)	2.4 (0.5)	1.9 (0.3)	2.3 (0.8)	1.7 (0.5)	1.7 (0.5)	2.5 (1.2)
Uric acid (µmol/l)	524.3 (69.4)	584.1 (143.2)	533.7 (182.4)	1003.3 (843.8)	525.4 (201.7)	451.2 (99.4)	450.6 (134.7)	635.2 (262.8)	624.2 (142.8)	762.1 (677.0)	495.2 (159.8)	476.1 (98.5)	511.8 (94.2)	412.0 (63.8)	417.9 (55.8)	883.5 (541.3)
protein (mg/dl)	335.7 (368.9)	408.6 (430.9)	459.1 (475.9)	252.1 (301.3)	286.2 (261.5)	402.1 (332.1)	565.4 (488.4)	518.1 (368.3)	698.6 (352.6)	403.6 (320.4)	401.7 (544.3)	346.8 (337.0)	523.1 (386.5)	428.0 (306.6)	550.7 (421.5)	315.4 (299.2)

Pkd2: Kap::	lrm4-Kap	Wt-Wt	lrm4-Wt	Wt-Kap	lrm4-Kap	Wt-Wt	lrm4-Wt	Wt-Kap	lrm4-Kap	Wt-Wt	lrm4-Wt	Wt-Kap	lrm4-Kap	Wt-Wt	lrm4-Wt	Wt-Kap
	6 months				**9 months**				**12 months**				**15 months**			
Na:CR (mmol/L)	53.4 (9.0)	41.7 (13.6)	51.5 (11.0)	50.8 (10.6)	45.9 (16.3)	49.8 (14.0)	46.2 (18.7)	54.3 (7.6)	39.4 (14.3)	40.3 (9.9)	48.0 (17.5)	43.8 (6.3)	34.1 (16.8)	25.3 (13.8)	32.9 (18.9)	36.9 (6.3)
K:CR (mmol/L)	80.2 (10.9)	63.8 (15.1)	73.2 (12.5)	70.2 (15.9)	64.8 (12.9)	80.1 (12.7)	68.1 (13.6)	76.8 (15.9)	75.3 (25.1)	60.0 (11.1)	64.1 (8.9)	68.9 (10.3)	61.8 (10.8)	60.0 (14.5)	66.0 (19.4)	66.0 (8.8)
Ca:CR (mmol/L)	0.8 (0.3)	0.7 (0.3)	0.7 (0.2)	0.8 (0.2)	0.9 (0.3)	0.8 (0.2)	0.8 (0.2)	0.5 (0.2)	0.5 (0.2)	1.1 (0.4)	0.7 (0.2)	1.3 (0.6)	1.3 (0.4)	1.0 (0.4)	0.9 (0.5)	0.8 (0.4)
P: CR (mmol/L)	8.7 (3.0)	9.5 (4.7)	8.0 (6.0)	6.9 (2.8)	9.6 (3.2)	7.0 (3.6)	9.5 (3.4)	6.8 (2.6)	8.6 (3.7)	11.1 (4.1)	8.3 (2.9)	9.9 (3.5)	10.8 (5.9)	12.1 (5.0)	10.4 (2.6)	8.9 (2.2)

2.2.3 Tables of Student T-test results for comparisons between conditional mice.

Table 2.6: T-tests of plasma components comparing all age groups, genotypes and plasma components. Both sexes p<0.05, p<0.01

Plasma both sexes							
Age (months)	**Plasma component**	**Lrm4-Kap vs Wt-Kap**	**Lrm4-Kap vs lrm4-Wt**	**Lrm4-Kap vs Wt-Wt**	**Wt-Kap vs lrm4-Wt**	**Wt-Kap vs Wt-Wt**	**lrm4-Wt vs Wt-Wt**
6	urea	0.194605173	0.48858542	0.822497938	0.804410404	0.27115183	0.571417
9		0.118627835	0.766474103	0.049065032	0.147513792	0.788383034	0.09917
12		0.60558235	0.934778493	0.527351543	0.675348798	0.947423769	0.665903
15		0.267042172	0.930848229	0.411116497	0.376117821	0.110346623	0.459106
6	**Creatinine**	0.361615975	0.622081287	0.56922241	0.273157869	0.054335156	0.681021
9		0.281904057	0.987616687	0.383640559	0.359268113	0.840714641	0.450762
12		0.700740785	0.970227629	0.292948006	0.597695951	0.467946119	0.149314
15		0.200008356	0.248388953	0.847821783	0.939171727	0.206258899	0.262668
6	**Total Protein**	0.384885746	0.712050284	0.24454208	0.312276296	0.952012823	0.255666
9		0.863360366	0.380327971	0.284850188	0.538006644	0.307352191	0.106801
12		0.203006002	0.46133955	0.322158573	0.458151122	0.498560418	0.929769
15		0.61244049	0.552864294	0.94826752	0.409358637	0.705996461	0.606114
6	**Albumin**	0.920574027	0.920574027	0.56922241	0.404722167	0.701870365	0.537582
9		0.274472275	0.274472275	0.621983937	0.93490689	0.428132254	0.135714
12		0.760035189	0.322158573	0.559341972	0.542908379	0.716051283	0.227929
15		0.590139387	0.411910806	1	0.843267281	0.744450256	0.62712
6	**Amylase**	0.145161161	0.127197957	0.377873949	0.867696048	0.500548641	0.537582
9		0.266240816	0.940019302	0.260382898	0.428132254	0.990111467	0.400386
12		0.212115491	0.09719828	0.559341972	0.542908379	0.788647739	0.227929
15		0.923050679	0.770705495	0.611879034	0.794815192	0.496832966	0.430478
6	**BUN**	0.194605173	0.48858542	0.822497938	0.804410404	0.27115183	0.571417
9		0.118627835	0.766474103	0.766474103	0.147513792	0.788383034	0.09917
12		0.60558235	0.934778493	0.527351543	0.675348798	0.947423769	0.665903
15		0.267042172	0.930848229	0.411116497	0.376117821	0.110346623	0.459106

Table 2.7: T-tests of plasma components comparing all age groups, genotypes and plasma components. Females p<0.05, p<0.01

Plasma Female							
Age (months)	**Plasma component**	**Lrm4-Kap vs Wt-Kap**	**Lrm4-Kap vs lrm4-Wt**	**Lrm4-Kap vs Wt-Wt**	**Wt-Kap vs lrm4-Wt**	**Wt-Kap vs Wt-Wt**	**lrm4-Wt vs Wt-Wt**
6	**urea**	0.260097311	0.870943874	0.709530082	0.443826656	0.058927117	0.625063
9		0.505680549	0.069740389	0.767643915	0.082670522	0.641070786	0.073416
12		0.517719132	0.327147615	0.217414466	0.890974592	0.888078071	0.705508
15		0.926070464	0.348641139	0.903906951	0.309569947	1	0.226763
6	**Creatinine**	0.340227507	0.300132861	0.178060697	0.179647494	0.042032752	0.899469
9		0.401134311	0.465842628	0.887825625	0.278486975	0.752373199	0.535079

12		0.525818614	0.065823483	0.079441679	0.476577874	0.581892953	0.762797
15		0.712173605	0.654023786	0.813764287	0.517973439	0.788529767	0.558549
6	**Total Protein**	0.500866773	0.321620471	0.681250047	0.13740951	0.760812343	0.257714
9		0.297059461	0.377405676	0.3562366	0.844326504	0.624917388	0.814733
12		0.089806784	0.796239558	0.71139367	0.097145355	0.288229011	0.173382
15		0.401160486	0.790123643	0.360931723	0.436436745	0.754306623	0.499388
6	**Albumin**	0.568530803	0.568530803	0.178060697	0.206041526	0.50780973	0.242167
9		0.805428293	0.805428293	0.611685709	0.701797995	0.960087638	0.370466
12		0.924645725	0.71139367	0.613051585	0.136852441	0.838877775	0.473686
15		0.892460623	0.252400549	0.73281353	0.764391577	0.847583186	1
6	**Amylase**	0.007686913	0.025679537	0.17972934	0.622834211	0.109148583	0.242167
9		0.97611791	0.970621801	0.549810844	0.960087638	0.642413579	0.614143
12		0.777215725	0.754258988	0.613051585	0.136852441	0.390038332	0.473686
15		0.090610535	0.534394829	0.595105668	0.683279755	0.153430319	0.391636
6	**BUN**	0.260097311	0.870943874	0.709530082	0.443826656	0.058927117	0.625062905
9		0.505680549	0.069740389	0.069740389	0.082670522	0.641070786	0.073416341
12		0.517719132	0.327147615	0.217414466	0.890974592	0.888078071	0.7055084
15		0.926070464	0.348641139	0.903906951	0.309569947	1	0.226763053

Table 2.8: T-tests of plasma components comparing all age groups, genotypes and plasma components. Males p<0.05, p<0.01

Plasma Male							
Age (months)	**Plasma component**	**Lrm4-Kap vs Wt-Kap**	**Lrm4-Kap vs lrm4-Wt**	**Lrm4-Kap vs Wt-Wt**	**Wt-Kap vs lrm4-Wt**	**Wt-Kap vs Wt-Wt**	**lrm4-Wt vs Wt-Wt**
6	**urea**		0.023532708	0.18393591			0.075525
9		0.061483604	0.015326896	0.000794251	0.752639687	0.484157618	0.733825
12		0.316781512	0.181089252	0.730569874	0.204310752	0.527858206	0.229035
15		0.087310623	0.411639696	0.417922945	0.236265799	0.073493808	0.197759
6	**Creatinine**		0.348416234	0.069898892			0.106527
9		0.406394351	0.426685941	0.126771724	0.969288158	0.739488786	0.775886
12		0.429843238	0.018210141	0.7150118	0.052552458	0.363078354	0.031336
15		0.070750513	0.303840042	0.738814982	0.547049834	0.091228317	0.333049
6	**Total Protein**		0.674296349	0.162746173			0.828571
9		0.015321467	0.019052695	0.594459694	0.504595104	0.048840982	0.023647
12		0.779413069	0.612718622	0.415954245	0.444069588	0.843889465	0.471142
15		0.812867804	0.557188598	0.589057641	0.798686218	0.784147002	0.951957
6	**Albumin**		0.493591898	0.069898892			0.669244
9		0.012703929	0.012703929	0.200625521	0.883575345	0.513925771	0.010637
12		0.795782759	0.415954245	0.10528298	0.382639172	0.926804008	0.045895
15		0.440297529	0.135507939	0.817765223	0.594149445	0.817277823	0.562829
6	**Amylase**		0.074607038	0.847260263			0.669244
9		0.068214694	0.932115866	0.030766227	0.513925771	0.366313894	0.427393
12		0.138919507	0.015610224	0.10528298	0.382639172	0.181059227	0.045895
15		0.454182879	0.942035545	0.596756483	0.316800121	0.990174895	0.53462

6	**BUN**		0.023532708	0.18393591			0.075525151
9		0.061483604	0.015326896	0.000794251	0.752639687	0.484157618	0.733824681
12		0.123667258	0.181089252	0.730569874	0.204310752	0.527858206	0.229034995
15		0.087310623	0.411639696	0.249112219	0.236265799	0.073493808	0.197759152

Table2.9: T-Test comparisons between all components, genotypes and ages for Urine samples- both sexes p<0.05, p<0.01

Urine both sexes							
Age (months)	**Urine component**	**Lrm4-Kap vs Wt-Kap**	**Lrm4-Kap vs lrm4-Wt**	**Lrm4-Kap vs Wt-Wt**	**Wt-Kap vs lrm4-Wt**	**Wt-Kap vs Wt-Wt**	**lrm4-Wt vs Wt-Wt**
6	**creatinine**	0.355035222	0.907143	0.406409	0.403647727	0.781508006	0.471787
9		0.446976339	0.914613	0.248914	0.269020738	0.066555722	0.2061
12		0.281027312	0.80351	0.174845	0.128624491	0.52307741	0.034086
15		0.008546017	0.043138	0.595111	0.58050757	0.193596093	0.341661
6	**calcium**	0.901583891	0.554937	0.354678	0.564005692	0.509987232	0.248401
9		0.351829598	0.833612	0.314011	0.569056654	0.868499993	0.595194
12		0.176010018	0.270283	0.040314	0.250347647	0.835065884	0.098256
15		0.05584007	0.092561	0.070189	0.884267308	0.965498007	0.918083
6	**phosphate**	0.356441704	0.750698	0.990355	0.284609987	0.415241717	0.783529
9		0.052477154	0.831527	0.730261	0.060869034	0.202179604	0.635492
12		0.873589331	0.797315	0.697781	0.869352726	0.296747722	0.400944
15		0.833962104	0.391054	0.261903	0.572583538	0.391756288	0.528184
6	**glucose**	0.386233385	0.386233	0.354678	0.366919206	0.843035758	0.256844
9		0.747396617	0.747397	0.475516	0.933110185	0.993218316	0.214768
12		0.774267402	0.697781	0.107259	0.172431776	0.992280463	0.821674
15		0.126498111	0.147485	0.806433	0.829715274	0.161659384	0.168441
6	**uric acid**	0.43442855	0.91689	0.241289	0.666213078	0.362628079	0.256844
9		0.475007168	0.467437	0.452107	0.993218316	0.181175137	0.165256
12		0.703956192	0.229818	0.107259	0.172431776	0.377612523	0.821674
15		0.057100973	0.047513	0.128538	0.861491124	0.060117611	0.043633
6	**protein**	0.792130881	0.659118	0.687902	0.873900196	0.51436169	0.40197
9		0.55681179	0.282887	0.304303	0.542640196	0.634700159	0.873905
12		0.2070554	0.379405	0.170996	0.994236571	0.781147476	0.852754
15		0.646915794	0.904767	0.322461	0.566787664	0.534176323	0.278323
6	**sodium**	0.894000895	0.96941	0.526835	0.898383886	0.557370953	0.631439
9		0.753717662	0.859465	0.179661	0.639766384	0.103862519	0.265724
12		0.068133962	0.515636	0.076863	0.183123653	0.995599783	0.195717
15		0.090084677	0.359816	0.683769	0.309582727	0.011289409	0.118671
6	**potassium**	0.994293952	0.637592	0.807082	0.762482188	0.854814264	0.577693
9		0.780439403	0.614033	0.054656	0.814484147	0.094036469	0.155499
12		0.003772891	0.359111	0.006341	0.041352029	0.897174705	0.063779
15		0.057069529	0.358014	0.472822	0.336424577	0.070321572	0.181096
6	**chloride**	0.727923577	0.795051	0.548729	0.941166522	0.474222376	0.485605
9		0.932468962	0.908376	0.122055	0.972815769	0.141091789	0.159383
12		0.010499515	0.191224	0.032223	0.103538321	0.504621826	0.291338
15		0.061519332	0.460102	0.418961	0.192813761	0.024879679	0.146634
6	**urea**	0.956585454	0.934328	0.45976	0.998106464	0.597804251	0.472906
9		0.959183065	0.914344	0.111987	0.959593752	0.121255735	0.08744

12		0.151212284	0.397643	0.258994	0.664086105	0.778277947	0.853062
15		0.036404346	0.193406	0.470094	0.408165896	0.056923426	0.117011
6	**Nacr**	0.163929953	0.768173	0.667256	0.271842504	0.272200344	0.912726
9		0.687570037	0.975708	0.321497	0.735653353	0.545636755	0.393708
12		0.418313591	0.395997	0.63257	0.901713329	0.540276292	0.511066
15		0.348443468	0.909077	0.729691	0.435060014	0.119037178	0.660614
6	**kcr**	0.098827675	0.370666	0.263093	0.340603447	0.545080616	0.73912
9		0.080979722	0.6763	0.201356	0.169682161	0.724521055	0.356106
12		0.21603119	0.333434	0.616679	0.495748742	0.202675044	0.425006
15		0.80728895	0.649426	0.502241	0.545054265	0.436327563	0.997804
6	**cacr**	0.740108351	0.518111	0.821497	0.855341104	0.58464073	0.352459
9		0.503427402	0.417241	0.056964	0.8691473	0.074755347	0.114146
12		0.03032253	0.359868	0.043979	0.037580994	0.419781313	0.03276
15		0.266133219	0.140022	0.13711	0.634571207	0.613616351	0.977213
6	**pcr**	0.749634968	0.817353	0.332624	0.68282377	0.29195725	0.705095
9		0.236836117	0.94377	0.151745	0.269592782	0.913692719	0.180502
12		0.353395148	0.909627	0.579236	0.206791465	0.636211473	0.413096
15		0.683032922	0.889869	0.509487	0.454684462	0.213034731	0.298542

Table 2.10: T-Test comparisons between all components, genotypes and ages for Urine samples- females p<0.05, p<0.01

Female urine							
Age (months)	**Urine component**	**Lrm4-Kap vs Wt-Kap**	**Lrm4-Kap vs lrm4-Wt**	**Lrm4-Kap vs Wt-Wt**	**Wt-Kap vs lrm4-Wt**	**Wt-Kap vs Wt-Wt**	**lrm4-Wt vs Wt-Wt**
6	**creatinine**	0.667861761	0.6382	0.328279	0.814491596	0.85567212	0.405212
9		0.823699611	0.849846	0.037369	0.972932606	0.080797603	0.076006
12		0.194145502	0.218501	0.10048	0.925675376	0.523811002	0.474927
15		0.019702054	0.125188	0.853409	0.520865973	0.408919501	0.598312
6	**calcium**	0.831973402	0.827992	0.219454	0.996677557	0.419913839	0.412486
9		0.828480121	0.580419	0.753624	0.734051647	0.967391203	0.742782
12		0.23242436	0.559145	0.541967	0.181134076	0.163412513	0.885116
15		0.552742205	0.791145	0.814587	0.979377871	0.891615988	0.920937
6	**phosphate**	0.545895889	0.96081	0.815961	0.521992369	0.736380429	0.827576
9		0.162635294	0.218326	0.783843	0.847800388	0.56397513	0.637308
12		0.437150794	0.472482	0.337639	0.857476951	0.454133118	0.303305
15		0.384908011	0.927567	0.996676	0.348046712	0.302551548	0.889341
6	**glucose**	0.624704803	0.624705	0.219454	0.858104666	0.773217584	0.404737
9		0.846962817	0.846963	0.34142	0.608924225	0.94820568	0.201443
12		0.441675132	0.337639	0.3964	0.956656575	0.409987606	0.496738
15		0.186213152	0.192468	0.735649	0.824942673	0.222651872	0.211895
6	**uric acid**	0.733625285	0.393919	0.092682	0.617344622	0.191676676	0.404737
9		0.868306798	0.845782	0.034848	0.94820568	0.027013574	0.062027
12		0.551480279	0.243643	0.3964	0.320083889	0.68488946	0.496738

15		0.019379549	0.034977	0.425769	0.998562497	0.197382923	0.199818
6	**protein**	0.761510472	0.637167	0.513143	0.979813792	0.40936936	0.22698
9		0.554428801	0.954925	0.192693	0.522099106	0.797009131	0.129709
12		0.297919903	0.246873	0.210908	0.307334311	0.131497839	0.289247
15		0.189194162	0.02932	0.446	0.287761559	0.833375053	0.317573
6	**sodium**	0.712422759	0.553854	0.090554	0.464991898	0.19936832	0.785746
9		0.805628634	0.810467	0.358898	0.982466098	0.233622455	0.282548
12		0.167117382	0.212403	0.182838	0.682107963	0.683209733	0.949495
15		0.204103757	0.293649	0.393414	0.866175992	0.034073382	0.066425
6	**potassium**	0.864630417	0.67177	0.10857	0.663626289	0.353097411	0.584321
9		0.894117973	0.858686	0.288395	0.767574398	0.367064752	0.25294
12		0.005572374	0.10099	0.047004	0.976764191	0.58969821	0.728754
15		0.043565418	0.171543	0.489865	0.98952346	0.132985759	0.172196
6	**chloride**	0.656627471	0.65582	0.065844	0.518249942	0.1631092	0.649922
9		0.90860105	0.736268	0.389744	0.81180003	0.310117833	0.234701
12		0.032206371	0.142203	0.144533	0.949485224	0.75617285	0.862579
15		0.123087194	0.245393	0.237586	0.779949139	0.083498322	0.11081
6	**urea**	0.891744714	0.417788	0.075072	0.690958704	0.302915356	0.356031
9		0.993576989	0.682967	0.093581	0.721111607	0.143784391	0.066171
12					0.357528825	0.843729018	0.746299
15		0.011832351	0.113308	0.451613	0.962736283	0.097778016	0.136028
6	**Na:cr**	0.382465904	0.994485	0.945262	0.426755178	0.486577205	0.946294
9		0.887320938	0.787092	0.722591	0.858625947	0.477688541	0.503188
12		0.890877217	0.668645	0.917073	0.478782659	0.914506279	0.26832
15		0.436004975	0.377609	0.470742	0.879108548	0.140372964	0.133126
6	**K:cr**	0.357048843	0.650835	0.706846	0.518456698	0.638804668	0.957946
9		0.545942336	0.855408	0.906713	0.373178518	0.472726043	0.956681
12		0.813145086	0.992425	0.661262	0.67648909	0.890583966	0.189463
15		0.358275739	0.289583	0.806288	0.582360249	0.231829141	0.31276
6	**Ca:cr**	0.889103213	0.758831	0.975406	0.883517126	0.883349322	0.698446
9		0.874741572	0.520265	0.121387	0.47467964	0.01296643	0.296879
12		0.038543711	0.108398	0.066491	0.078301172	0.179584738	0.45297
15		0.049421167	0.510374	0.125131	0.724849763	0.719745487	0.877005
6	**P:cr**	0.740377232	0.896519	0.557383	0.728222472	0.419717956	0.806689
9		0.43282187	0.607028	0.247239	0.863320769	0.55184748	0.534992
12		0.979868603	0.831762	0.615353	0.825577078	0.663517749	0.435441
15		0.175427239	0.623782	0.639935	0.258729368	0.324254361	0.975029

Table 2.11: T-Test comparisons between all components, genotypes and ages for Urine samples- Males only p<0.05, p<0.01

Male urine							
Age (months)	**Urine component**	**Lrm4-Kap vs Wt-Kap**	**Lrm4-Kap vs lrm4-Wt**	**Lrm4-Kap vs Wt-Wt**	**Wt-Kap vs lrm4-Wt**	**Wt-Kap vs Wt-Wt**	**lrm4-Wt vs Wt-Wt**
6	**creatinine**		0.784463	0.849649			0.720429
9		0.533131594	0.810074	0.854478	0.048523818	0.368562796	0.992028
12		0.684650001	0.111608	0.457275	0.003794755	0.315771194	0.001295
15		0.012920461	0.080914	0.591738	0.662232062	0.156030242	0.284894
6	**calcium**		0.182284	0.982919			0.158952
9		0.142113995	0.628017	0.230417	0.100127318	0.17194749	0.118906
12		0.479417634	0.360686	0.008312	0.88521964	0.129073375	0.036628
15		0.000707473	0.000272	0.001194	0.958410976	0.830696511	0.885014
6	**phosphate**		0.522429	0.64862			0.801394
9		0.105995358	0.050346	0.956369	0.026891007	0.172707124	0.117145
12		0.159320672	0.43379	0.239843	0.532888532	0.591245825	0.904717
15		0.136172105	0.157493	0.145893	0.386909344	0.8842556	0.457525
6	**glucose**		0.422649731	0.982919			0.428887
9		0.463455556	0.463456	0.962659	0.037469282	0.768762647	1
12		0.501181706	0.239843	0.175746	0.008160879	2.86972E-46	0.528906
15		0.144703999	0.67169	0.916365	0.188265522	0.148912638	0.752617
6	**uric acid**		0.219565	0.501884			0.428887
9		0.55189646	0.515661	0.570625	0.768762647	0.596221893	0.814629
12		0.662813232	0.711577	0.175746	0.502502418	0.509078864	0.528906
15		0.709136612	0.718404	0.287922	0.775793043	0.274978847	0.197125
6	**protein**		0.684755	0.668767			0.357913
9		0.463305708	0.063665	0.282561	0.12702746	0.60246858	0.178266
12		0.475003586	0.943687	0.047014	0.764732917	0.718774703	0.923867
15		0.194814875	0.937519	0.181798	0.179342726	0.356417883	0.118355
6	**sodium**		0.521541	0.956639			0.675638
9		0.926331734	0.488271	0.470178	0.372168171	0.451394886	0.852914
12		0.330791544	0.639511	0.440874	0.032948792	0.83290085	0.003748
15		0.358468034	0.74135	0.735655	0.290290291	0.29208354	0.956813
6	**potassium**		0.271703	0.754145			0.710466
9		0.86212008	0.354838	0.19858	0.385621047	0.251357597	0.544555
12		0.085694256	0.510212	0.185699	0.004877737	0.525872339	0.004569
15		0.497139428	0.7262	0.803987			0.970844
6	**chloride**		0.292602	0.885545			0.629634
9		0.694419994	0.510907	0.302023	0.748993111	0.479698383	0.581128
12		0.190357566	0.818439	0.291912	0.049192049	0.688683516	0.001298
15		0.304403736	0.838073	0.732403	0.181921364	0.22764949	0.791181
6	**urea**		0.254952	0.895005			0.693025
9		0.850380614	0.723171	0.620247	0.123609261	0.202995415	0.730826
12		0.117881828		0.290808		0.292728407	

15		0.451278173	0.93754	0.794793	0.352262701	0.378577658	0.814079
6	**Na:cr**		0.560839	0.297638			0.920855
9		0.026546302	0.545595	0.212843	0.606700137	0.620384924	0.809425
12		0.205353592	0.225173	0.432556	0.277341354	0.346862786	0.28062
15		0.569930317	0.814613	0.862514	0.344920634	0.545003808	0.598043
6	**K:cr**		0.526695	0.23794			0.709139
9		0.053450627	0.502305	0.119152	0.388131154	0.956868922	0.410403
12		0.031496901	0.034064	0.230809	0.098596739	0.076457252	0.106508
15		0.869043126	0.196938	0.603341	0.340929186	0.809450025	0.360341
6	**Ca:cr**		0.252304	0.697411			0.41227
9		0.472114621	0.710252	0.380869	0.387687586	0.9626271	0.388088
12		0.478438942	0.789984	0.030525	0.259592232	0.041729431	0.003407
15		0.002183544	0.000665	0.003553	0.852068863	0.706388409	0.798651
6	**P:cr**		0.629795	0.300486			0.57679
9		0.301148132	0.384466	0.656876	0.105816789	0.429079114	0.184596
12		0.321409986	0.786419	0.343432	0.092505142	0.999451274	0.053514
15		0.33562201	0.320876	0.164191	0.559530992	0.652384338	0.104086